Polymer stabilised phospholipid nanodiscs

Idini, Ilaria

Award date:
2014

Awarding institution:
University of Bath

Polymer Stabilised Phospholipid Nanodiscs

Ilaria Idini

A thesis submitted for the degree of Doctor of Philosophy

University of Bath

Chemistry Department

July 2014

To my Family

Acknowledgements

I would like to express my gratitude to all the people that, in different ways contributed to the completion of this thesis. Above all my deepest gratitude goes to my family; I am incredibly lucky to have you.

Thank you to University of Bath and Science and Technology Facilities Councils Biomed Network for founding the project. In particular I would like to express my gratitude to Stanley Botchway, for all his time and help.

I would like to thank my supervisor Karen Edler for her critical guide and consult during my Ph.D. and while writing my thesis. My sincere thanks goes also to my second supervisor Cameron Neylon and all the collaborators from the University of Birmingham, Tim Dafforn and Micheal Overduin for the illuminating discussions, Rosemary Parslow for her assistance and kindness in all my visits to their laboratory. A special thanks goes to Tim Knowles for his precious collaboration and to Mohammed Jamshad for all the help and support since the starting of our collaboration. Mohammed I will never forger all the gel filtration experiments at 3 am in the morning!

I am also very grateful for the constructive comments and stimulating discussions to Stephen Roser and Gareth Price. Thank you Gareth for allowed me to work in your laboratory.

I am also particularly grateful to John Lowe for all the help with the NMRs experiments and for always being available to discuss my data. My deepest appreciation goes also to all the instrument scientists that helped me and guided me on the numerous scattering experiments. Thank you to Ralph Schweins, Isabelle Grillo, Richard Heenan, Stephen King and Nick Terrill. A special thanks goes to Ann Terry, thanks for sharing your incredible passion for science and to Luke Clifton and Louise Hatter for their invaluable help and support.

Thank you to all the people in my group that made my time in the lab and in the long hours of scattering experiments enjoyable. Thank you to Robben for being always available for help and discussion.

Gavin, for always being so kind and positive! I feel the privilege to have met not only colleagues but also special people that shared their lives with me. Duygu I am very happy to have found you.

I am also deeply grateful to Amani El Fagui thanks for all the support during the inevitable dark moments, all the help with the thesis and for all the time spent together.

A special thanks to all my friends in Bath that made me feel at home since my first day here. A special thought to Lory, remember that even if we will probably be in different cities or maybe countries friendship doesn't have boundaries.

Least but not last, heartfelt thanks to my boyfriend Maisem for sharing with me the long hours of writing up and calming and supporting speeches when I needed the most.

Abstract

Membrane proteins are involved in several fundamental biological processes such as transport or signal transduction. Most of them are enzymes, receptors or other important biological macromolecules representing up to 70% of therapeutic targets. Despite the interest in understanding their structures and behaviour the scientific knowledge is still very limited due to several practical difficulties. In 2009 a new platform for membrane protein studies called SMALP (Styrene-Maleic Acid Lipid Particles) nanodiscs was introduced. SMALPs are self-assembled structures formed by a bilayer of phospholipids controlled in diameter by a polystyrene maleic acid (SMA) copolymer belt.

The purpose of this research project herein presented was to structurally characterise SMALPs, with analyses aimed to understand the role of both the polymeric and lipid parts in the self-assembly process. A series of investigations were carried out to elucidate the specific copolymer characteristics that allow the assembly into such well-defined, stable and reproducible structures. Experiments performed via small angle X-ray (SAXS) and neutron (SANS) scattering together with nuclear magnetic resonance (NMR), gel-filtration chromatography (GPC), dynamic light scattering (DLS), allowed identification of the specific polymeric characteristics of the copolymer architecture which were revealed to be crucial for the SMALPs assembly process.

Investigations performed also addressed the question whether it was possible to assemble nanodiscs with the use of different phospholipids (with different chain length and charged or non-charged heads) and what the impact of the different lipids had on the structures.

Finally, further analyses were made to test the physical chemical behaviour of the SMALPs when important environmental parameters such as temperature, pH and salt concentration of the buffer were changed.

Contents **Page**

List of Figures

List of Tables

List of Abbreviations

Symbol	*Definition*
AFM	Atomic Force Microscopy
AIBN	Azobis (isobutyronitril)
AMB	Atomic Mass Unit
AMU	Amphotericin B
Apo-A1	Apolipoprotein A1
ATRP	Atom Transfer Radical Polymerisation
CD	Circular Dichroism
CHAPS	3-[(3-Cholamidopropyl) dimethylammonio]-1-propane-sulfonate
^{13}C NMR	Carbon Nuclear Magnetic Resonance
CMC	Critical Micelle Concentration
CMT	Critical Micelle Temperature
CTA	Chain Transfer Agent
CTAB	Cetyl Trimethylammonium Bromide
Cryo-TEM	Cryogenic Transmission Electron Microscopy
DDMAT	2-(dodecylthicarbonolthiolylthiol)-2 –methylpropionic acid
DLS	Dynamic Light Scattering
DMF	Dimethylformamide
DMPC	1,2-dimyristoyl-sn-glycero-3-phosphocholine
DMPG	1,2-dimyristoyl-sn-glycero-3-phosphoglycerol
DP	Degree of Polymerisation
DPPC	1,2-dipalmitoyl-sn-glycero-3-phosphocholine
DSC	Differential Scanning Calorimetry
FTIR	Fourier Transform Infrared Spectroscopy
FID	Free Induction Decay
GPC	Gel Permeation Chromatography
GUVs	Giant Unilamellar Vesicles
HCl	Hydrochloric Acid
HDL	High-density lipoprotein
^{1}H NMR	Hydrogen Nuclear Magnetic Resonance

HVEM	High Voltage Electron Microscopy
ILL	Institute Lau Langevin
IUPAC	International Unit of Pure and Applied Chemistry
IR	Infrared Spectroscopy
LD	Linear Dichroism
LDLs	Low Density Lipoproteins
LUVs	Large Unilamellar Vesicles
LRP	Living Radical Polymerization
MA	Maleic Acid
MEK	Methyl Ethyl Ketone
MLVs	Multilamellar Vesicles
Monoolein	1-O-Octadecyl-2-O-methyl-sn-glycero-3-phosphorylcholine
M_n	Average Number Molecular Weight
M_w	Average Weight Molecular Weight
M_z	Average Z Molecular Weight
MSP	Membrane Scaffold Protein
NaCl	Sodium Chloride
NaOH	Sodium Hydroxide
NIST	National Institute of Standards and Technology
NNLS	Non Least Square Analysis
PCS	Photon Correlation Spectroscopy
PDI	Polydispersity Index
POPC	1-palmitoyl-2-oleoyl-sn-glycero-3-phosphocholine
PSMA	Poly (Styrene-Alt-Maleic Acid)
qELS	Quasi Elastic Scattering
RAFT	Reversible Addition Fragmentation chain Transfer
r-HDL	Reconstituted High Density Lipoprotein
SDS	Sodium Dodecyl Sulphate
SLD	Scattering Length Density
SMALP	Styrene Maleic Acid Lipid Particle
SMANS	Styrene-maleic anhydride neocarzinostatin
SUVs	Small Unilamellar Vesicles
SLD	Scattering Length Density

STY	Styrene
SAXS	Small Angle X-Ray Scattering
SANS	Small Angle Neutron Scattering
TEM	Transmission Electron Microscopy
THF	Tetra Hydrofuran
TM	Trans Membrane
UA	Uranyl Acetate
UV-Vis	Ultra Violet- Visible Spectroscopy
VLDLs	Very Low Density Lipoproteins

1

1 Phospholipid Bilayer Nanodiscs: Supports for Membrane Proteins Studies

1.1 Introduction

The aim of this first chapter was to provide a basic overview of membrane proteins and the reasons why in the past decades so much effort was put in order to solve their structures. A description of the cell membrane and its main characteristics is also provided for a clearer understanding of the natural environment of membrane proteins. Attention then moves onto a description of the lipid structures, elucidating their main properties and characteristics followed by an overview of the main physical properties of the membrane.

A number of different supports for purification and analysis of membrane proteins have been designed in the past decades. The advantages and disadvantages of the most common techniques are here discussed in order to introduce the membrane scaffold protein stabilised nanodiscs, to which the work presented in this thesis is closely connected. These new supports have proved to be extremely useful not only for membrane protein encapsulation but also for a number of alternative applications that are briefly discussed here. (Chapter 1)

Finally, the new copolymer stabilised nanodiscs formulation, the core of this project, is introduced. In this last section of the chapter the SMALP technology is presented highlighting the main differences and advantages in

comparison to the previous protein stabilised supports. A brief overview of the main questions addressed in this project and a link to each section is also presented.

1.2 Overview of Cell Components

1.2.1 Cell Membranes

Before describing some of the most common supports for membrane proteins, which have been created in the attempt to reproduce the cell membrane, this complex natural environment needs to be described. Generally, the basic unit of a biological membrane consists of a variety of lipid and non-lipid components, such as phospholipids, sphingolipids and sterols that determine the physical properties of the particular membrane, giving a wide variety of environments that surround membrane proteins. In Figure 1.1 the cell membrane and its components are illustrated in a cartoon representation.

For many years the accepted model for cell membrane was the fluid mosaic model [5, 6], which describes the cell membrane as a bilayer of lipids with their hydrophobic tails toward the interior part of the bilayer and the heads on the outside. Embedded in it, with their polar and non-polar components aligned with the lipids, are membrane proteins and cholesterol molecules. Despite the success of this model that has dominated for more than three decades it actually oversimplifies the structure and particularly the protein-protein [7, 8] and lipid–protein interactions [9-13] in the membrane. Furthermore this model does not take into account the wide variation in terms of lipid-protein composition [14] and the fact that many membranes have lipid-rich domains. This led to the introduction of the concept of raft domains [15-17] was introduced about ten years ago [17]. A lipid raft consists of a liquid ordered assembly within the membrane rich in sphingolipids and cholesterol. Cholesterol is part of the sterol family and consists mainly of hydrocarbons in the form of steroid ring

structures. Being composed of a high concentration of cholesterol molecules, the areas occupied by lipid raft are characterised by less fluidity compared to the surrounding plasma membrane [18]. Indeed cholesterol was shown to have important structural effects on the lipid bilayers, which are still under investigation [19-21]. In the biological relevant liquid crystalline state, cholesterol seems to reduce the rate of motion and increase the packing density of the phospholipids molecules [22, 23]. However, much uncertainty still exists about lipid rafts. It is known for instance, that inside lipid rafts a certain number of proteins exist [24] but it is still unclear whether clusters of proteins are randomly distributed between different rafts or if they are grouped in specialised rafts [17, 25]. Moreover the presence in the lipid raft of many membrane proteins involved in the cell signalling has led to the idea that lipid rafts play a crucial role in the process of signal transduction.

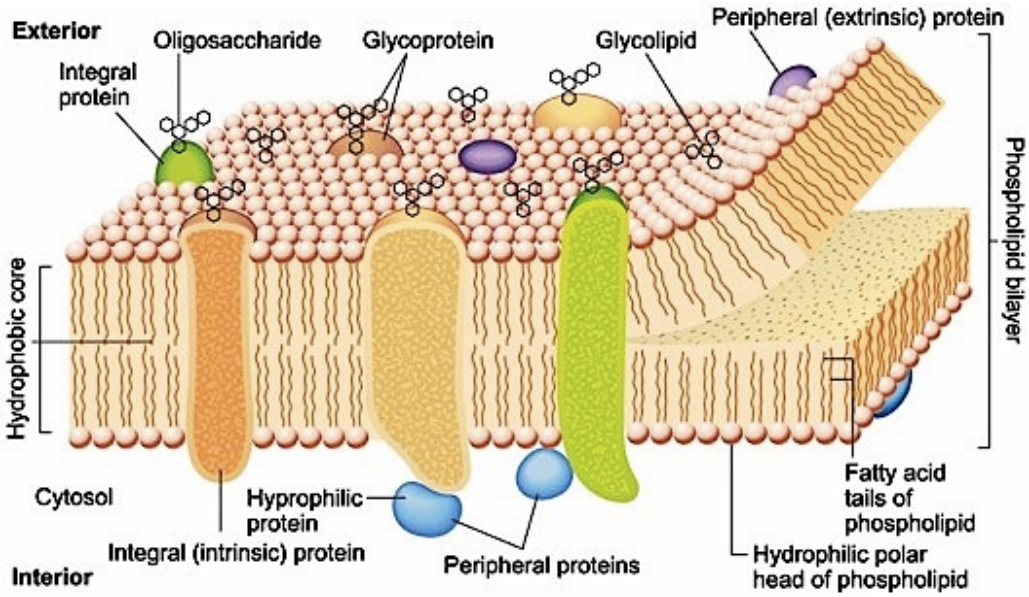

Figure 1.1. Cartoon representation of a cell membrane section. Picture reprinted with permission from [26].

It is evident from the complexity of the cell membrane that an accurate reproduction *in vitro* is almost impossible. However, much effort has been made to optimise lipid-based supports for membrane protein studies and the wide

variety facilitates studies of different proteins, which require different environmental conditions.

1.2.2 Lipid Bilayers: Components, Properties and Organisation

As already anticipated, biomembranes are made up of a variety of lipids. They can be composed of up to 100 different species of lipids, which vary in the acyl chains length, charge of the heads and in general structure. Lipids present in biomembranes fall mainly in three categories: the *sphingolipids*: a class of lipids containing a backbone of sphingoid bases namely a set of aliphatic amino alcohols that included sphyngosine. The *sterols:* a subgroup of the steroids compounds constituted of a characteristics arrangement of four cycloalkane rings joined together, most common sterol in the cell membrane is the molecule of cholesterol. Finally the class of *glycerophospholipids* (often simply called phospholipids).

Being one of the major components of the cell membrane, in this project attention was focused only on the phospholipid category. They are composed of two fatty acid tails, which together with glycerol form the hydrophobic part of the molecule, and a polar head formed of an amino alcohol attached to the phosphate group. A schematic illustration is given in Figure 1.2. They can further be classified into saturated phospholipids where the acyl chain domains contain no double bonds between the carbons, which means that as many hydrogen atoms as possible are attached to the carbon atoms. Or they can be part of the larger class of unsaturated phospholipids, where one or more double bonds are present. The presence of the double bond has an impact on the way the tail is spatially organised. Two different orientations are possible for each double bond. They are classified as *cis* configuration when hydrogen atoms lay both on the same side of the double bond whereas in case of *trans* configuration they are on opposite side with respect to the double bond. The *cis* configuration induces bends into the fatty acid chains whereas the *trans* configuration does not substantially change the spatial arrangement.

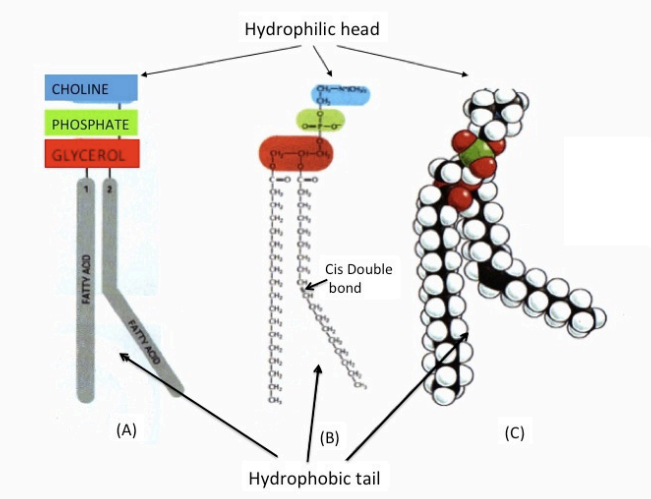

Figure 1.2. Example of a phospholipid molecule (phosphatidylcholine) represented A) schematicall; B) highlighting chemical elements; C) through a model used for molecular simulation. Picture adapted and reprinted with permission from [27].

1.2.3 Lipids Polymorphism

Phospholipids are amphiphilic molecules that, when dispersed in water can form a variety of different self-assembled structures that can be classified according to three basic features: the long range organisation related to the lattice type, the chain order and the curvature.

According to the nomenclature proposed by Luzzati [28], an upper case Latin letter characterises the long- range order. The three general categories for lipid phases are: the one dimensional lamellar (L) phase that can be visualised as a set of bilayers sheets arranged one on top of each other. The two dimensional hexagonal phase (H) composed of cylindrical micelles as the elementary repeating units, spatially arranged as a hexagonal structure. Finally the cubic phase (Q), which is a tridimensional structure of lipid channels inter-penetrated by water channels. A lower case Greek letter is used to characterise the chain status: α for disordered (fluid) phase; β for ordered and non-tilted chains and

finally *β'* for ordered tilted chains both *β* phases are also known as gel phases [29].

Another important parameter to be considered is the curvature. Indeed the role of the curvature in biological systems has been extensively explored together with its implication in the membrane structure and functions [30-33]. According to the convention in sign adopted the curvature can be positive, negative or zero as illustrated in Figure 1.3 [34].

A lipid monolayer in the lamellar phase is essentially flat which means zero curvature due to the equilibrium reached between the repulsive forces operating between the hydrocarbon chains and the hydration i.e. the head-water interactions, whereas in the hexagonal phase the lipid sheet is rolled into cylinders. This is due to the competing forces acting in the transition resulting in the system going from lamellar to hexagonal phase to lower the total free energy.

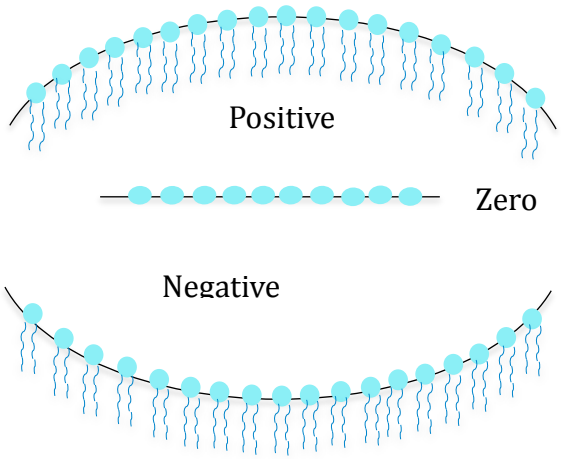

Figure 1.3. Schematic representation of lipid curvatures.

The major forces that govern the self-assembly process of lipids into well-defined structures such as micelles or bilayers are the hydrophobic effect on the lipid chains and the hydrophilic attraction at the heads-water interface.
The structure that a particular lipid may assume depends on the packing parameter, S defined by Israelachvili et al. [35].

$$S = \frac{V}{a_0 \, l_c} \qquad \text{Equation 1.1}$$

Where: V indicates the volume; a_0 the optimum surface area of the headgroups and l_c indicates the maximum length of the chains.

As illustrated in Figure 1.4, the shape of aggregates formed in water is qualitatively related to the packing parameter. Although these geometrical considerations offer a pretty straightforward way to analyse the packing properties of lipid structures, they are nevertheless incomplete due to the fact that curvature effects are not taken into consideration.

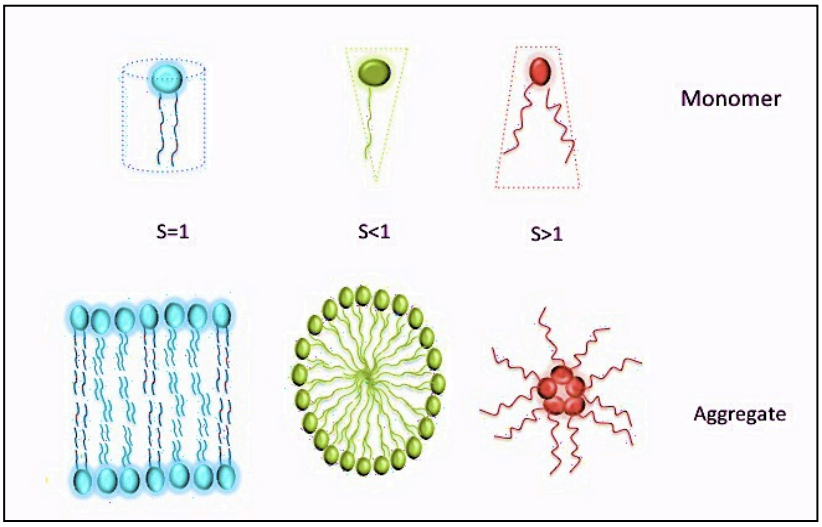

Figure 1.4. C*artoon representation of lipids self-assembled structures in solution in relation to their packing parameter S.*

A more rigorous approach was therefore taken [36] in a new model where the free energy is defined to be formed by the contribution of four factors: the membrane curvature elasticity, the hydrocarbon packing energies, the hydration and the electrostatic contribution.

1.2.4 Lipids Phase Transitions

Phospholipids not only assemble into different structures but they can also adopt different phases, where they possess different motional freedom. Moreover, they can transform from one to another when solution conditions are changed, due to changes in pH, temperature, or the ion concentration present in solution [37]. For the purpose of the work presented here, attention is focused on the effect of temperature, pH and salt concentration on lipid bilayers.

The normal organisation for a lipid bilayer, as seen before, is the lamellar sheet and the commonly observed structures are called $L_{\alpha,}$ referring to the lamellar liquid crystalline phase also known as L_d (*liquid disordered phase*), formed at high temperatures, the L_β lamellar gel phase also known as L_o (*liquid ordered phase*) formed at low temperatures, and the lamellar crystalline phase L_c formed at very low temperatures. Finally, the P_β phase known as *ripple phase* found during phase transitions between gel and liquid phase. Transition can be induced from one phase to the other operating on the temperature of the system.

Particularly interesting for the work here performed is the transition from the gel to fluid phase, which involves the chain melting transition. As the transition takes place, the packing area of the lipids increases as the acyl chain of the lipids become more disordered. The increase in temperature induces some of the carbon-carbon single bonds in the lipid chains to change from a state of *trans* to *gauche* isomerisation. This change requires the rotation around a single bond. At low temperature most of the carbon-carbon single bonds are in the *trans* configuration where the chains are fully extended, whereas in the gauche configuration there is a deviation from the linear direction [29].

1.2.5 Membrane Proteins

Proteins are a class of macromolecules composed of a long chain of single units, called amino acids, assembled together [1]. In nature a total of twenty different amino acids exist. The general structure of an amino acid consists a central carbon atom connected to an amino group ($-NH_2$), a carboxyl group ($-COOH$), a hydrogen atom and a variable group that is commonly indicated by the letter *R*. This group determines the characteristics of each single amino acid. A schematic representation is illustrated in Scheme 1.1.

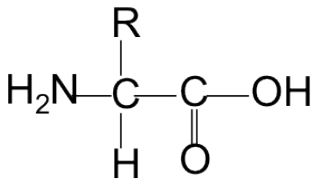

Scheme 1.1. Schematic representation of the general structure of an amino acid. R represents the variable group which will give the characteristic of a hydrophobic, hydrophilic, amphoteric or, in the particular case of an amino acid called cysteine, the ability to form covalent bonds between two sulphur atoms on another cysteine, changing the shape of the protein chain.

Proteins are molecules characterised by a complex spatial organization. Four levels of organisation can be identified:

- Primary Structure: indicates the particular sequence of the amino acids in a protein chain.
- Secondary Structure: when a protein chain is formed, each amino acid subunit keep the–C=O part of the carboxyl group and the −N−H part of the amine group (able to form hydrogen bonds) and gives the protein different shapes identified as secondary structures. The most common are known as “alpha helix” and “beta sheet” structures. In the alpha helix structure, hydrogen bonds are formed between the oxygen of the carbonyl group and the hydrogen of the third successive amino acid on the chain. These ligands force the chain to assume a spiral-like shape,

where the *R groups* are directed toward the exterior. In the beta sheet structure, the chains are disposed side to side and the configuration is kept due to the hydrogen bonds between peptides. This time the *R groups* are arranged on the top and bottom of the sheet.

- *Tertiary Structure:* It is rare that proteins only keep the simple folding due to the hydrogen bonds. Generally, they have much more complex tridimensional structures due to the nature of the single amino acids present in the chain causing mutual interactions (including hydrophobic interactions and pi-stacking interactions) and interactions with the external medium.
- *Quaternary Structure:* refers to the case when different peptide chains combine with each other while keeping their tertiary organization forming "super protein" structures [2].

Membrane proteins are a class of proteins linked to the cell membrane, as opposed to soluble proteins, which have active conformations while being surrounded by solvent. Membrane proteins can be classified into integral proteins, and peripheral proteins. Integral proteins, also known as trans-membrane proteins (TM), penetrate the hydrophobic core of the membrane and are often connected to a trans-membrane segment interacting with lipids and other proteins into the membrane. In order to extract integral proteins, the lipid bilayer needs to be disrupted. Peripheral proteins have a weak ionic interaction with the surface of the membrane. Therefore they can easily be removed by changing the ionic strength of the solution. Membrane proteins are incredibly important since they are involved in several crucial biological processes, such as transport (creating channels in the cell membrane, allowing selective transport of nutrients and other important molecules in and out of the cell). They can also be enzymes, in some cases a group of proteins with enzymatic function act as a team contributing to the metabolic pathway, and they are involved in signal transduction and cell-to-cell communication. Indeed, a membrane protein may have a binding site with a specific link for a particular receptor that can deliver its message to the cell [3].

Hence, being involved in so many important functions, constituting approximately 30% of the proteome and representing up to 70% of therapeutic targets, it is crucial to understand as much as possible about membrane protein structures, dynamic properties, lipid-proteins and proteins-proteins interactions [4]. Unfortunately, membrane protein studies are difficult for several reasons, including the lack of optimal supports, as it will be explained later in the text.

1.3 Overview of Supports for Membrane Protein Studies

1.3.1 Introduction

Studies of membrane proteins have been hampered by many practical difficulties. Firstly a considerable challenge is represented by the isolation of the protein of interest. It is rare to find a single peptide species as the major protein constituent of a cell membrane, although there are exceptions such as the *bacteriorhodopsin* found in great quantity in the *Halobacteria salinaria* [38] in which case proteins have been extensively studied. However, in the majority of cases it is difficult to obtain a sufficient high concentration of the membrane protein of interest from membranes abundance. Therefore, the tendency is to overexpress them in genetically engineered cells; however this comes with the risk of formation of protein aggregates [38].

Secondly, the complexity of the natural environment and the fact that for most of the techniques in use for protein characterisation (such as X-ray crystallography or nuclear magnetic resonance) proteins need to be extracted and successively reconstituted through several steps often leads to instability and/or denaturation [39]. In addition, purification procedures that work for one protein might not be suitable even for closely related proteins [39]. It is difficult to state which substrate type is a good model and which is not. However, there are some general features that a membrane model should possess, such as the

capability to incorporate the protein without leading to denaturation, aggregation or modification. It also should be possible to use different lipids within the support in order to accommodate the specific requirements of each protein.

The next section presents an overview of the different supports in use for membrane protein studies during the past decades.

1.3.2 Supports in Use for Membrane Proteins Analysis

Surfactants are amphiphilic molecules (which means that they possess a hydrophilic and a lipophilic part) constituted by a polar head and a hydrophobic tail. In aqueous solution, their polar heads form hydrogen bonds with water molecules while the hydrophobic chains can aggregates spontaneously in a roughly spherical self-assembled structure called micelles. In this structure the hydrophobic tails are oriented toward the interior and the hydrophilic heads stay exposed to the water medium.

An important parameter in micelles formation is the Critical Micelle Concentration (CMC), which represents the minimum amount of detergent that needs to be added to an aqueous solvent in order to start the aggregation into micelle structures. The size of micelles is usually described in terms of the aggregation number (N), which indicates the average number of detergent molecules per micelle. The aggregation number can be obtained using the formula reported in Equation 1.2, where the total micelle molecular weight (M_w) is divided by the molecular weight of the detergent molecule.

Equation 1.2

$$\mathrm{N} = \frac{M_w}{\mathrm{Monomeric}\ M_w}$$

Sometimes also the hydrodynamic radius or molecular weight is indicated. Knowing the CMC, the aggregation number and the bulk concentration C_s, it is

possible to calculate the concentration of micelles (in moles per litre) using the formula:

$$[\text{Micelles}] = \frac{C_s - CMC}{N}$$

Equation 1.3

Another important parameter governing these structures is the temperature. Surfactants can exist in different phases (crystalline, monomers and micelles), which are in equilibrium at the so-called Krafft Point.

From the graph in Figure 1.5, at low temperatures and low concentrations surfactants are in an insoluble crystalline state with some monomers in solution. As the temperature rises more and more monomers dissolve in solution until they reach the Critical Micellar Temperature (CMT), after that micellar structures are present in solution. For most surfactants, the Krafft point is equal to the CMT and micelles form spontaneously as the solid crystals dissolve [40, 41].

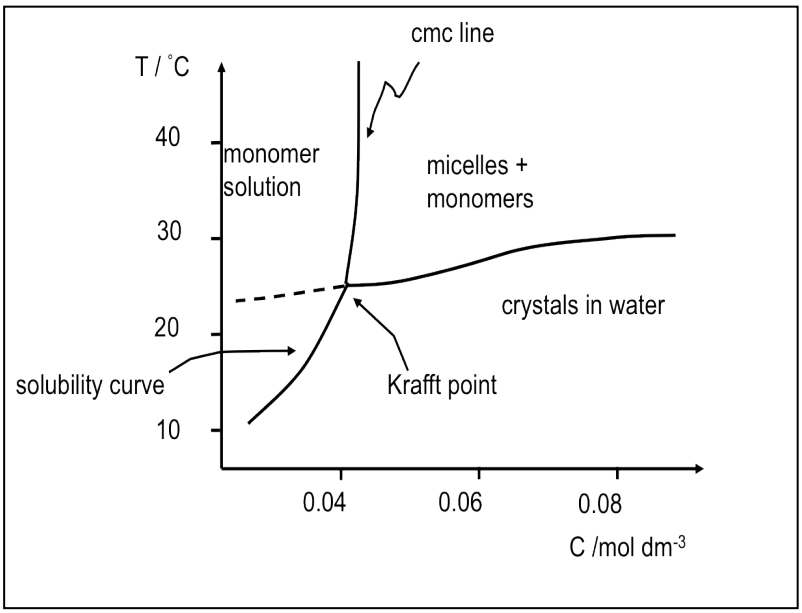

Figure 1.5. Phase diagram for surfactant solutions.

In vitro studies of membrane proteins, such as crystallization are based on the successful reconstitution of the protein itself, which involves several difficult steps to isolate, purify and crystallise them in order to obtain well-ordered 3D

crystals required for X-ray crystallography. Use of the appropriate detergent has been shown to be vital in protein extraction and reconstitution; Figure 1.6 reproduces with a schematic representation of the general mechanism of membrane solubilisation by use of a detergent. From top to bottom: at low detergent concentration some detergent molecules penetrate into the lipid bilayer surrounding the protein (in yellow) but do not disrupt the membrane completely. Increasing the concentration of detergent results in the formation of protein-lipid-detergent complexes and in the final stage at higher concentration of detergent, lipids are almost completely removed from the protein with the creation of lipid-detergent and protein-detergent complexes.

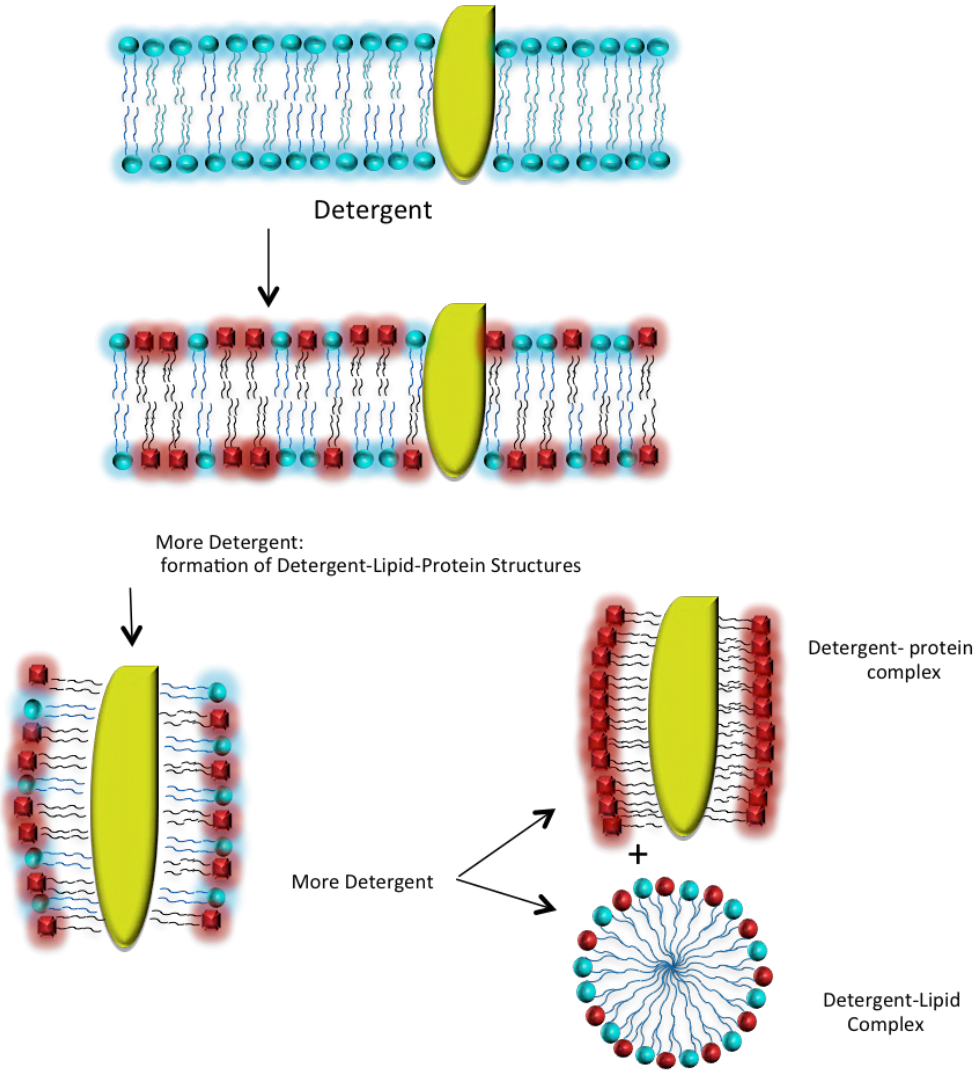

Figure 1.6. Schematic illustration of membrane solubilisation process. Picture after [3].

There are three main classes of surfactants, which have been summarised in Table 1.1. They have been classified according to their composition [42] into different categories:

Ionic Surfactants are characterised by a hydrophobic hydrocarbon chain and a permanent net charged head group that can be either anionic such as in sodium dodecyl sulphate (SDS), or cationic like in the case of cetyltrimethylammonium bromide (CTAB). The CMC of an ionic detergent is determined by the combined effect of repulsive interactions between the charged head groups and the hydrophobic action of the tails. The length of the tails is also crucial in the size of the micellar structure; the longer the chain the larger the micelle formed [43]. Ionic surfactants such as SDS are very useful in the solubilisation process but they sometimes lead to protein denaturation. In this case proteins can be reactivated via several processes [44] for instance SDS can be removed via organic solvent precipitation but with the high risk of aggregation and precipitation of proteins.

Bile Salts, they also belong to the ionic surfactant class with the difference that they contain a backbone consisting of rigid steroidal hydrophobic groups, such as sodium salt of cholic acid, in addition they also possess a hydroxyl group at the end of the short acyl chain. As a result of their rigid structure they form small kidney shaped aggregates different from the well-defined micelles formed by linear-chain ionic surfactants [45]

Non-Ionic Surfactants are considered to be mild amphiphiles due to the absence of electrostatic interactions with proteins. Their structure is constituted of uncharged hydrophilic head groups and hydrophobic tails. A very commonly used non-ionic detergent is Triton X-100. This molecule has a neutral head group containing polyoxyethylene and conjugated aromatic rings, which are often a disadvantage as they absorb light in the ultraviolet region interfering with eventual analysis of the proteins made with this technique. Other popular choices are the alkyl-sugar surfactants such as n-dodecyl-D-maltoside (DDM), which possess good optical properties [43].

Zwitterionic Surfactants combine properties of both ionic and non-ionic surfactants, like non-ionic surfactants, zwitterionic molecules do not possess a net charge and do not have electrophoretic properties but similar to ionic surfactants they are very efficient in breaking protein-protein interactions. An example is the 3-[(3-Cholamidopropyl) dimethylammonio]-1-propane-sulfonate (CHAPS), a detergent that has been shown to possess a lower rate of denaturation compared to other zwitterionic surfactants [120].

Even though commonly used in protein purification processes, surfactants present many problems. There have been many reported cases where the lipid removal process leaded to protein inactivation with consequent loss of functionality. A simplistic and unrealistic representation of this system is their assembly as an almost spherical structure. In reality micelles aggregate in a much more disorganised but more compact way [41]. Furthermore micelles of small detergent molecules exhibit fluctuations in shape and size and can deform, split and fuse over time. These mutations can occur with pure detergent but are even more common when the system includes lipids, proteins or other types of surfactants, resulting in an unstable support.

Ionic Surfactants	*Non-Ionic Surfactants*	*Zwitterionic*
Examples: Anionic: Sodium dodecyl sulfate (SDS) Cationic: Cetyltrimethyl ammonium bromide (CTAB)	Examples: Triton X-100	Examples: CHAPS; ZWITTERGENT® detergent 3-X series.
	Characteristics and properties	
Contain head group with a net charge. Charge could be either anionic (- charged) or cationic (+ charged). Micelle size is determined by the combined effect of hydrophobic attraction of the side chain and the repulsive force of the ionic head group. Useful for dissociating protein-protein interactions.	Uncharged hydrophilic head group. Better suited for breaking lipid-lipid and lipid-protein interactions. Salts have minimal effect on micellar size.	Offer combined properties of ionic and non-ionic surfactants. Suited for breaking protein-protein interactions.
The CMC of an ionic detergent is reduced by increasing the ionic strength of the medium, but is relatively unaffected by changes in temperature.	The CMC of a non-ionic detergent is relatively unaffected by increasing ionic strength, but increases substantially with rising temperature.	

Table 1.1. Principal types of surfactants and their main features. Table adapted from ***[42]***

Mixture of Surfactants and Lipids

As an alternative to the detergent-only systems, a mixture of surfactants and lipids has proven to be useful in NMR and crystallisation studies, and to limit the protein deactivation. When certain lipids and surfactants are mixed together (such as DMPC and CHAPS) at the right composition, they give rise to disc-like structures known as bicelles. These structures are formed with a lower amount of detergent and can help stabilize membrane proteins for experimental studies

[46]. For example the bicelle system made of DMPC and CHAPS allowed the study of rhodopsin, a protein which was very unstable in a detergent-only system [47]. The downside of this system is the restriction in the choice of lipids and stoichiometry. This can be a problem if the membrane protein requires a specific lipid environment to function. In addition they cannot be formed directly from biological membranes but need a solubilisation step of the protein with the use of surfactants.

Vesicles or Liposomes

These structures are spherical closed lipid bilayers with an aqueous solution inside [48] which makes the inner core inaccessible although they can be preloaded with various components. When proteins are incorporated in liposomes the resulting structures are called proteoliposomes. Depending on the method and the composition used, one can have unilamellar vesicles (UVs) constituted by a single layer of lipids and multilamellar vesicles (MLVs) made of up to twenty concentric spheres of lamellae. Unilamellar vesicles are also classified according to their size.

Small unilamellar vesicles (SUVs) have a diameter between 20 nm and 50 nm. Vesicle size influences the curvature of these objects and SUVs in particular possess a curvature that makes it difficult to incorporate proteins [49].

Large unilamellar vesicles (LUVs) possess a diameter between 50 nm and 100 μm. Advantages of these structures are the large volume available for encapsulation although they suffer from instability and non-uniform size distribution [50].
Giant unilamellar vesicles (GUVs) have a diameter from 5 μm up to 300 μm and are very large structures of the size of a cell, where a microelectrode can be inserted and optical microscopy analysis can be easily done [51]. One feature that can be a disadvantage in all vesicle structures is that when the experiment performed involves activities or events that are dependent on the orientation of the protein, in this case there is no way to ensure an absolute directionality of the protein within the lipid bilayer.

Monolayers: when amphiphilic molecules possessing a good portion of hydrophobic area are brought to the air-water interface they align themselves with the hydrophobic parts facing the air. These monolayers are usually obtained using the so-called Langmuir trough, the monolayer is created dissolving the desired amount of lipids in appropriate solvents such as chloroform or chloroform/ethanol mixture spreading the solution on the air water interface and while the solvent evaporates the lipids self-assemble vertically at the air/water interface with the hydrophilic head immersed in the water and the tails pointing to the air. The instrument consists of a mobile barrier on one side that allows the investigation of monolayers of known composition by controlling the pressure and the surface area. One of the great advantages of using Langmuir monolayer is the possibility to precisely control parameters such as thickness, surface pressure and molecular area. This method has been extensively used for membrane proteins studies for the past decades [52-55], during which many different characterisation techniques have been applied such as X-ray reflectivity [56] and rheology [57]. However, a limitation of this technique is the non-accurate reproducibility of the natural membrane environment constituted by a lipid bilayer and also the high surface tension of water that can cause proteins at the air-water interface to unfold or denature.

Amphipols are amphipathic polymers composed of a hydrophobic backbone with hydrophilic side chains. They possess the ability to hypercoil around the transmembrane region of proteins keeping their stability and retaining their functions [58-60]. They have been successfully used to maintain membrane solubility after treatment with a non-denaturing detergent [61] and to maintain the catalytic functionality of integral membrane enzymes [61]. However amphypols can interfere with the proteins activity and tend to aggregate when in acidic solution or when an inadequate starting material is used resulting in inefficient protein solubilisation. Nonetheless the use of amphypols seems a useful approach and further studies may substantially improve its performance.

1.4 Protein Stabilised Phospholipids Bilayer Nanodiscs

1.4.1 Introduction

As described in the previous section, membrane proteins can be reconstituted using several supports, which have their advantages and disadvantages. Nanodiscs are model membranes that seem to solve some of the problems encountered with previous supports. Liposomes, for instance have been used in many occasions to incorporate membrane proteins but they are difficult to prepare with a precise and controlled stoichiometry. An alternative approach is offered by the nanodisc technology, which allows to precisely control the microenvironment around a protein. Indeed, for instance, it was possible to investigate the influence of local changes in phospholipids bilayers composition on the enzyme that triggers blood clotting [62]. Another powerful feature of nanodiscs is that they can be used to isolate proteins in a precise monomeric or oligomeric state, which is something very difficult to achieve with the use of liposomes or other supports [63].

1.4.2 The Origin of Nanodiscs

Nanodiscs are self-assembled discoidal structures, with a diameter ranging from 8 nm to 16 nm and thickness of about 5 nm. They are constituted of a bilayer of phospholipids surrounded by a belt of genetically engineered high-density lipoproteins (HDLs). Lipoproteins are complexes of lipids and proteins, which exist in different sizes and attend to different roles. Lipoprotein complexes are classified according to the amount of lipid in the structure [67]: very low-density lipoproteins (VLDLs), low-density lipoproteins (LDLs), intermediate density lipoproteins (IDLs) and finally high-density lipoproteins (HDLs). High density lipoproteins are involved in reverse cholesterol transport [68], a process by which accumulated cholesterol all over the body is collected and transported to the liver for excretion. The particular proteins involved in the

formation of these complexes are known as apolipoproteins. The genetically engineered MSPs originate from naturally occurring human apolipoproteins [65, 66]. Interactions between proteins and lipids are one of the most important mechanisms in the human body, involved in numerous important processes such as cell movement, replication and signalling.

HDLs are also called membrane scaffold proteins (MSPs) after their ability to self-assemble into more complicated structures incorporating phospholipids or molecules of cholesterol. Reconstitution of membrane proteins in phospholipid bilayer nanodiscs was reported for the first time in 1998 by Sligar, Bayburt et al. [64], the cytochrome P450 reductase was incorporated and analysed by means of scanning force microscopy.

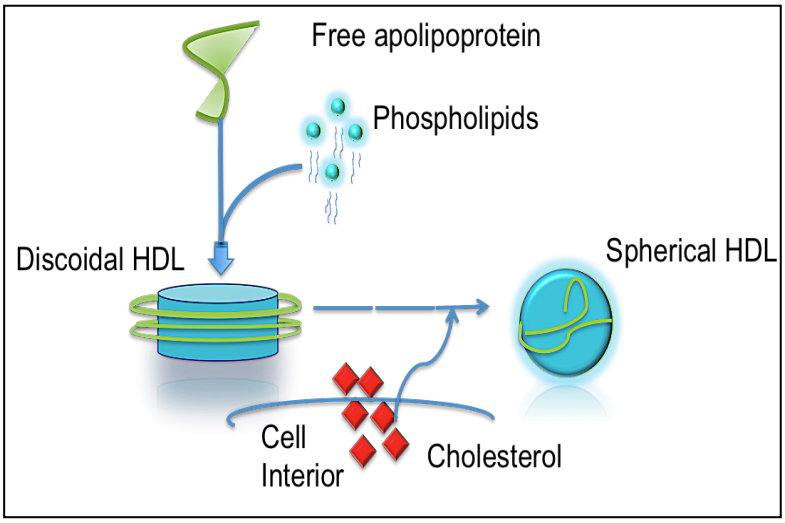

Figure 1.7. Mechanism of Reverse Cholesterol Transport, with the intermediate creation of discoidal phospholipid structures.

In 1990, when Sligar et al. were investigating suitable candidates as supports for structural studies of membrane proteins their attention was captured by studies of the process of reverse cholesterol transport (in Figure 1.7 a schematic representation of the process is reported), where HDLs were involved. These lipid-protein structures were, at the end of their formation process, balls of various sizes but of particularly interest were the transient forms, roughly discoidal in shape, stabilised by the apolipoproteins Attention was captured by the possibility to artificially reproduce these structures stabilised by the apolipoproteins [69]. Indeed, one of the most abundant apolipoprotein

components of plasma HDL, the apolipoprotein A-1 (apoA-1), was showed to be able once incubated with phospholipid vesicles to induce the spontaneous formation of HDL. To distinguish it from the natural HDL, the *in vitro* reconstituted version was named rHDL. The rHDL were structurally analysed by means of scanning force microscopy [70] and infrared spectroscopy [71]

In order to investigate the role of the protein in the discs assembly process, Sligar et al. used the *Escherichia coli* bacteria, as a host to express the ApoA-I protein [72] and to successively work on the protein sequence.

As a result of this work, they created a set of genetically modified apoliproteins, capable of self-assemble in discoidal structures when in the presence of phospholipids. These proteins have been named membrane scaffold proteins (MSPs) after their ability to self-assemble into discoidal structures when in the presence of phospholipids.

These new structures composed of phospholipids and MSP were termed nanodiscs in order to distinguish them from the rHDL formed with the full length natural ApoA-1. Figure 1.8 is a cartoon illustrating the nanodiscs self-assembly process of encapsulating different membrane proteins [69,73]. The different length of membrane scaffold proteins generated were able to create nanodiscs with different sizes but also homogeneous and monodisperse nanodiscs populations. These structures have now been extensively structurally analysed by means of scanning probe microscopy [74] size exclusion chromatography [74,75] thin-layer chromatography [76] atomic force microscopy [70], nuclear magnetic resonance [74], X-ray and neutron scattering [77]. The importance of nanodiscs in membrane protein studies was successively confirmed by further experiments and led to the development of a general method for the assembly of membrane proteins into nanodiscs [64].

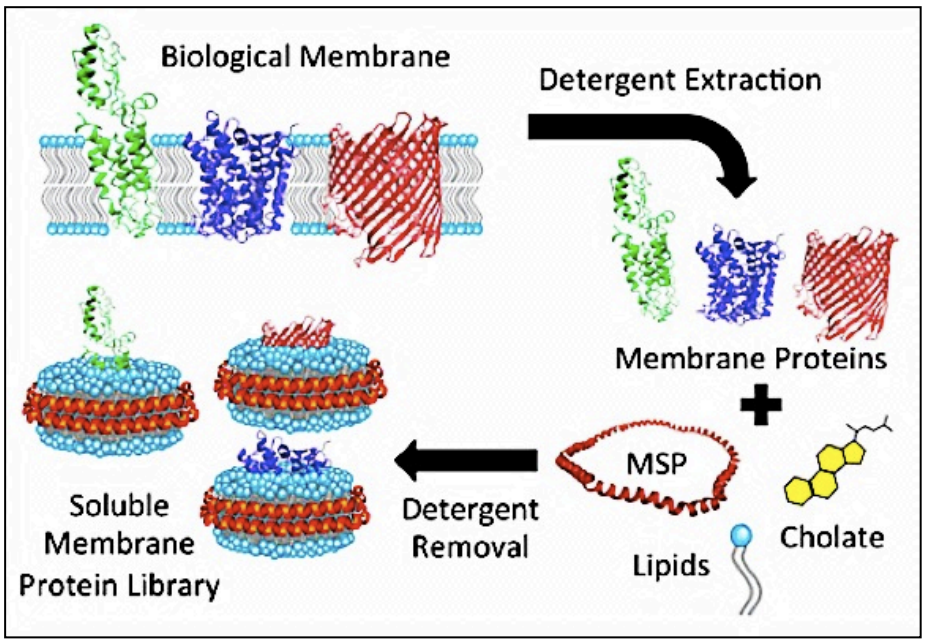

Figure 1.8. Cartoon representation of the nanodiscs encapsulation process of different membrane proteins. Picture has been reprinted with permission from [78].

1.4.3 Optimization and Further Analysis

Further investigations of the role of ApoA-I protein, the exact lipid-protein proportion and the nanodisc structural conformation were subsequently optimised. ApoA-I is formed of 234 amino acids, and it seems that the structural key leading to HDL formation is the alpha helix structure of the MSP. The first artificially produced MSP, called MSP1 and MSP2 were presented in a paper published in 2002 by Sligar and Bayburt [79] based on the ApoA-I sequence, but without a globular domain on the N-terminus, which was shown to be unnecessary for nanodisc formation. For stoichiometric reasons the self-assembly of one nanodisc required two MSP1 molecules. Therefore to avoid a bimolecular self-assembly step, a new molecule called MSP2 was created from the artificial fusion of two MSP1 molecules.

Several studies were successively done changing the protein structure. Different MSPs mutations were genetically engineered which provided nanodiscs of

different dimensions. This gave the important ability to control the dimension of the nanodiscs simply by changing the MSP amino acids sequence [80].

Studying the self-assembly process of nanodiscs with the use of different MSPs and different lipids, Sligar et al. have also conducted empirical experiments in order to understand the optimal ratio of MSPs to phospholipids and to optimise the protocol for the nanodiscs formation. In March 2008, a protocol for the preparation of nanodiscs was published [81]. The following table reports as an example the optimised ratio for MSP1D1 and MSP1E3D1 with different lipids reproduced from the guidelines.

Optimal ratio for:	*MSP1D1*	*MSP1E3D1*	*Incubation Temperature*
DPPC	90:1	170:1	37 °C
DMPC	80:1	150:1	25 °C
POPC	65:1	130:1	4 °C

Table 1.2. Optimised ratio for nanodiscs self-assembly [82]

Moreover, based on the experimental results achieved and assuming a similar overall discoidal structure for the different discs obtained with the use of different MSPs, they formulate an equation connecting the length of the MSP to the number of lipids in the discs [80] as reported in Equation 1.4.

$$\mathrm{M} = \frac{2(\pi r + \sqrt{\pi NS})}{L}$$

Equation 1.4

Where: *M* is the number of residues in the helical protein belt, which indicates the protein length; *r* is the average radius of the MSP helix; *N* is the number of lipids for each protein experimentally determined; *S* is the average surface area per one lipid and finally *L* is the helical pitch per residues taken to be 1.5 Å.

1.4.4 Self-Assembly Process and Structural Organisation

As described in Section 1.4.2 nanodiscs derive from a self-assembly process. This process involves the hydrophobic interaction between the acyl tails of the phospholipids and the MSPs that, encircling the fatty acid chains, expose the hydrophilic residues toward the aqueous exterior, minimising the total hydrophobic surface area in contact with water molecules. Further studies have provided more information about nanodiscs properties and structures.
Denisov et al. prepared an entire library of MSPs of different lengths, used to create nanodiscs of different diameters [80].

The orientation of both lipids and MSPs, in particular the orientation of MSPs around the lipid bilayer in the rHDL in the nanodiscs has been extensively studied in the past thirty years [83-85]. Three main models have been proposed. The “picket fence model” [86] suggests that the two MSP monomers occupy opposite sides of the discs and are arranged orthogonally to the bilayer plane. The second "Hairpin” [87] model sees the protein monomers organised on opposite sides of the discs parallel to the bilayer plane. The last model, the “molecular belt” [88] proposes that the protein is organised in a similar way to the hairpin model, but in this model the monomers are organised head to tail, wrapped all around the disc. As a result of many experimental investigations; infrared spectroscopy [89], mass spectrometry [90], mutagenesis [91], fluorescence spectroscopy [92] and solid-state NMR [74] in addition to computer simulations, the “molecular belt” model has been more and more accepted. Sligar et al investigated the orientation of lipids in the nanodiscs using fluorescence–detected linear dichroism (LD). The experiment was performed by incorporating two different fluorescent probes into the nanodiscs both of which exhibit a specific orientation in natural membranes, which was also observed with the same tilt angle in the nanodisc structures. This experiment gives important evidence of the similarity of the support to the natural membrane protein environment [75].

1.5 Nanodiscs Applications

1.5.1 Nanodiscs as Support for Membrane Proteins Studies

Membrane proteins are strictly connected to their lipid environment, which affects the stability but also the functionality of the protein itself [93, 94]. Therefore in order to be properly characterised a precise control of the lipid environment surrounding the protein is needed. This is one of the most attractive characteristics of the nanodisc supports. The specific ratio between lipids and MSPs required for the nanodiscs self-assembly process gives a precise control over the bilayer composition. Moreover, the wide variety of lipids available and the possibility to incorporate other molecules such as cholesterol, allows these supports to satisfy the specific environment requirements of a number of different membrane proteins.

Control of the nanodiscs size is another important feature. Currently, nanodisc size can be tuned from ~9.5 nm to ~17 nm in diameter by simply changing the length of the MSPs which allows choice of the most appropriate dimension, according to the size of the protein and the number of proteins the disc should accommodate [95]. Another particular powerful aspect of the nanodisc technology is the possibility to study the protein of interest in a known monomeric or oligomeric state [96].

Structures of many membrane proteins have been studied with the aid of the nanodiscs support and an increasing number of techniques. Many proteins belonging to the superfamily of G-proteins coupled receptors [97], which comprises the largest class of molecules involved in the signal transduction cellular process in addition to the structures of other receptors [98], cytochrome P450 [99-101], *Bacteriorhodopsin* [102,103] toxins [104] and blood coagulation protein tissue factor [105] have been investigated. Not only has the nanodisc technology been proved to be extremely useful for biochemical and biophysical studies of membrane proteins but it has also facilitated better understanding of

protein-protein and lipid-protein interactions [106,107], and interaction between nanodiscs encapsulated membrane protein and soluble proteins [108].

1.5.2 Nanodiscs Applications

1.5.2.1 Nanodiscs as Vehicle for Drug Delivery

In addition to the study of membrane proteins, nanodiscs have been proved to be useful as a vehicle for drug delivery [109]. So far, a variety of bioactive molecules have been successfully incorporated into the nanodiscs. The nanodiscs platform appears to be optimal in terms of delivery efficiency and activity retention of the encapsulated compounds [110].

One of the first molecules employed in studies of the nanodisc technology, as a drug carrier was an antibiotic called amphotericin B (AMB) [111]. This molecule, which has been used as antifungal for nearly half a century, is an amphoteric molecule that interacts with cell membranes forming pores that facilitate leakage of cell contents resulting in the death of the cell. The selectivity towards fungal cells is based on the high affinity of the AMB for the ergosterol-containing membranes of fungi rather than the cholesterol-containing membrane of mammalian cells. *In vitro* studies illustrated lower toxicity from this drug when transported using nanodiscs compared to liposomes. In vivo experiments showed that the AMB-nanodiscs formulation overcame the poor water solubility problem presented by the AMB in vesicles with efficient fungicidal activity reached even at low concentration, moreover the AMB-nanodiscs formulation displayed decreased toxicity in an *in vitro* experiment compared to the vesicles formulation.

Another good example in terms of soluble small molecules successfully encapsulated in nanodiscs is Curcumin. This molecule, also known as diferuloylmethane, is a hydrophobic polyphenol derived from an East Indian plant which has been shown to act as an anti-inflammatory, anti-oxidant and

chemo preventive compound [112]. Moreover, Curcumin has been shown to be non-toxic even at high dose [113]. Unfortunately use of this compound has been limited by poor water-solubility. Ghosh et al. [114] studied the nanodisc-encapsulated Curcumin with encouraging results [115]. Cell culture studies revealed that ND-Curcumin formulation was more effective than the free compound in inducing apoptosis in the mantle cell lymphoma.

These only represent a few examples of the potential of the nanodisc formulations. They have proved to possess important advantages that can lead to further implementations. For instance the possibility to artificially modify the MSPs is a great opportunity to implement the system with additional components, to target specific cell receptors and be able to deliver drug to the specific site of interest [110].

1.5.2.2 Nanodiscs for Medical Imaging Applications

HDL, the natural source and inspiration for nanodiscs structures, has been central to studies of contrast agent encapsulation for medical imaging. So far inorganic nanocrystals such as gold nanoparticles, iron oxides or quantum dots have been used as contrast agent for medical imaging. However, recently studies of natural nanosized particles such as viruses or lipoproteins have suggested the idea of overlapping the two areas to create a mixture of organic and inorganic compounds for nanomedicine purposes [116]. An interesting example is the use of the well-known contrast agent, the ion, gadolinium (Gd^{3+}). Chelates (compounds containing a ligand, typically organic, bonded to a central metal atom) of this element are broadly used. Gd-DTPA-DMPE chelates are popular paramagnetic ions used in MRI with the important characteristic of being a non-toxic compound. This Gd chelate has been successfully loaded into nanodisc supports, and a modified version of this molecule has been created in order to use it also with fluorescence imaging techniques.

1.6 Improving the Nanodiscs Platform: Polymer Stabilised Nanodiscs

The work done so far on the protein stabilised nanodisc structures is undoubtedly extremely valuable, nevertheless the procedure used to solubilise, reconstitute and encapsulate membrane proteins into the nanodisc bilayer is not straightforward and it is source of inevitable problems. The first necessary step is the purification and solubilisation of the membrane protein of interest from its native bilayer it is the use of a detergent. After that the protein can be added to the nanodiscs assembly mixture constituting the MSPs in use and the chosen phospholipid(s). The third step is the removal of the detergent by dialysis during which, proteins can aggregate or oligomerise mainly because of protein-protein interactions.

In addition, the MSPs are expensive to make, inherently reactive and labile and can interfere with the signal from the membrane protein, acquired via scattering experiments or any other kind of analysis such as circular dichroism.

1.6.1 Styrene Maleic Acid Lipid Particles (SMALPs)

In 2001, Tonge et al. published a work on the structure and behaviour of hyper coiling polymers and their associated potential pharmaceutical applications, in which they demonstrated [59] that the Poly Styrene-alt Maleic Acid copolymer (SMA) self-assembles when in solution with phospholipids leading to the formation of nanometer-sized discs useful for drug delivery. The system was successively patented and termed Lipodisq® from the Malvern Cosmeceutics Company.

In 2009, the Dafforn and Overduin group at Birmingham University showed the possibility to use these structures for membrane protein encapsulation and analysis. SMA copolymer, in combination with lipids forms monodisperse

discoidal structures, which were thermostable and able to preserve the membrane protein functionality [117]. These were named Styrene Maleic Acid Lipid Particles (SMALPs) after their constituents.

The first important characteristic of SMALP is their assembly process. It has been shown [118] that SMA auto-assembles into discoidal structures when in the presence of lipid membranes at basic pH [119]. In this way the membrane protein already embedded in the lipid bilayer is automatically encapsulated into the structure and polymer-stabilised nanodiscs with a central core containing a phospholipid bilayer, surrounded and controlled by SMA polymer belt are formed. The discs have a diameter between ~9 nm and ~11 nm and a thickness around ≈5 nm, with a homogeneous size distribution. These supports are very similar to the protein-stabilized nanodiscs described in the previous Section 1.4, in terms of structure but in addition the particular formulation mechanism offers some important advantages over the previous supports.

Experiments confirmed the possibility to encapsulate a membrane protein in these structures by simply adding the SMA to the solution containing proteins of interest already embedded into the cell membrane, as well as in bilayers or micelles (a schematic representation of the assembly process is depicted in Figure 1.9). In this way the use of detergents and all the purification steps causing protein denaturation or instability are no longer necessary.

Successful encapsulation of the membrane proteins *bacteriorhodopsin* and PagP demonstrated the formation of stable and monodisperse particles with the capability of retaining the protein integrity [117, 118]. Further analysis showed other important advantages of these structures over the protein-stabilised nanodiscs. For instance, experiments performed using circular dichroism (CD) showed optimal results since absorbance from the discs is negligible, being free from the MSP [118].

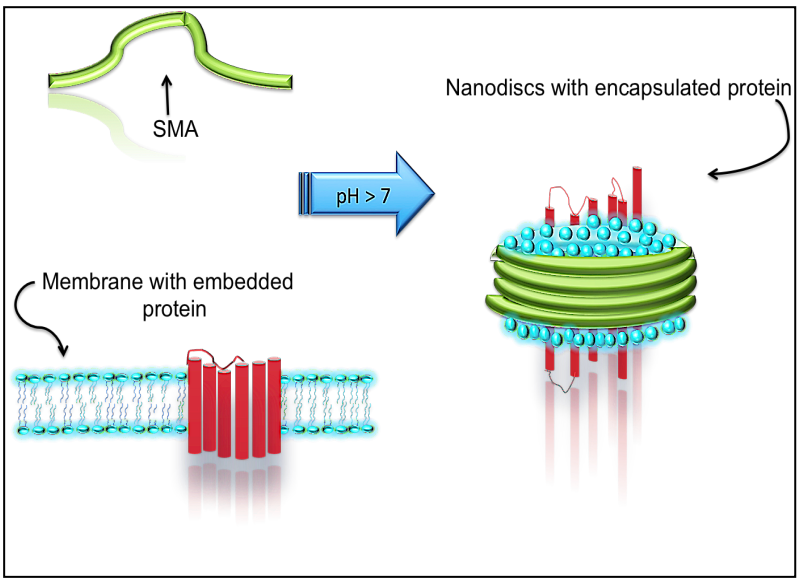

Figure 1.9. Diagrammatic representation of self-assembly process leading to lipid and membrane protein encapsulation by the SMA copolymer. Picture after [119].

The promising work done so far with the use of SMALPs leads to the necessity of a more extensive study aimed to deeply understand the system.

The aim of this project was to investigate and analyse SMALPs under different environmental conditions and to understand the role of the SMA in the SMALPs formation, stability and structure control. The final goal is to reproduce supports useful for the analysis of a broad variety of proteins and non-protein molecules with minimal production cost and maximal efficiency.

The structural characterisation of SMALPs was addressed with a systematic approach designed to understand the contribute to the stability and assembly process arising from each components.

The initial investigations were all performed on the formulation reported by our collaborations from the University of Birmingham constituted by Dimyristoyl phosphatidylcholine (DMPC) and the copolymer SMA-2000P (detailed description of all the copolymers in use and their provenience can be found in Chapter 3 Section 3.5). All SMALPs were analysed with no protein encapsulated as investigation were focused on the understanding of the structure and self-assembly process of the supports.

SMALPs such composed were then analysed via gel filtration chromatography to investigate the eventual presence of extra polymer in solution, then via

Dynamic light scattering for an initial size distribution and sample polydispersity analysis and finally via small angle X-ray and neutrons scattering for an in depth structural analysis and investigation of the interaction of the main components. Data and results can be found in Chapter 4.

An important part of the work here presented is constituted by the work performed to understand the role of the copolymer into the assembly process.
Different SMA copolymers were taken into consideration and analyses were performed on the copolymers on their own (Chapter 3) to complement the work on the corresponded SMALPs assembled with the different SMAs (Chapter 4). A list of the copolymers in use is here reported along with their provenience:

- SMA- 2000P, provided by Sartomer (7 kDa);
- XZ-09-008 provided by Polyscope (11 kDa);
- SZ-33-030 provided by Polyscope (33 kDa);
- SZ-28-065 provided by Polyscope (63 kDa);
- SZ-28-110 provided by Polyscope (110 kDa);
- RAFT polymer in deuterated or non-deuterated form, synthesised in Bath or Warwick laboratories.

Copolymers were characterised via nuclear magnetic resonance (NMR), gel permeation chromatography (GPC), dynamic light scattering and small angle
X-ray and neutron scattering to investigate their chain architectures, properties and the different structures assembled in solution (Chapter 3). Moreover analyses were conducted at different temperatures, pH and salt concentration to pair the corresponded work performed on the SMALPs (Chapter 5) assembled with the different polymers and understand the impact of the copolymer belt into the SMALPs stability and response to external stimuli.
These analyses allowed detection of some of the crucial characteristics that enable the SMA to assemble into SMALPs when in presence of phospholipids. Moreover it enabled to discriminate between successful and unsuccessful formulations.

Attention then moves to the analyses performed on the lipids part of the SMALPs with the use of different phospholipids (Chapter 5) with the final goal of creating a platform tuned according to the particular composition requirements of the encapsulated membrane protein. Work was conducted with the use of SMA-2000P copolymer a list of all the phospholipids used is here reported:

- DMPC (in his deuterated and non deuterated form);
- DMPC combined in different proportions with 1,2-dimyristoyl-sn-glycero-3-phosphoglycerol (DMPG), both used in their deuterated and non-deuterated form;
- DMPC combined in different proportions with 1,2-dipalmitoyl-sn-glycero-3-phosphocholine (DPPC), both used in their deuterated and non-deuterated form;

1.7 Summary

In the present chapter, the importance of solving membrane proteins structures and the difficulty encountered in their study has been described. An overview of the different supports in use has been given, introducing the so-called nanodisc structures and following their development from the first experiments through all their applications.

Finally, the new nanodisc formulation called SMALP, which is the subject of this thesis, has been introduced. From the initial information given so far, it is already possible to highlight some of the important advantages that this new formulation brings to membrane support studies. Before approaching the core of this work the following chapter, will introduce all the techniques used to analyse and characterise the SMALP, with first a brief theoretical introduction followed by the specificity of each instrument used in this work.

1.8 References

1. Fursule, R.A., *Biochemistry Basics And Applied.* 2008: Nirali Prakashan.
2. Brändén, C.I. and J. Tooze, *Introduction to Protein Structure*. Introduction to Protein Structure Series, 1999: Garland Pub.
3. Luckey, M., *Membrane Structural Biology: With Biochemical and Biophysical Foundations.* 2008: Cambridge University Press.
4. Arinaminpathy, Y., et al., *Computational analysis of membrane proteins: the largest class of drug targets.* Drug Discovery Today, 2009. **14**(23–24): p. 1130-1135.
5. Singer, S.J. and G.L. Nicolson, *The fluid mosaic model of the structure of cell membranes.* Science, 1972. **175**(4023): p. 720-31.
6. Morange, M., *What history tells us XXX. The emergence of the fluid mosaic model of membranes.* J Biosci, 2013. **38**(1): p. 3-7.
7. James, Zachary M., et al., *Protein-Protein Interactions in Calcium Transport Regulation Probed by Saturation Transfer Electron Paramagnetic Resonance.* Biophys J, 2012. **103**(6): p. 1370-1378.
8. Mokdad, A., et al., *Ligand-Induced Structural Changes in the Escherichia coli Ferric Citrate Transporter Reveal Modes for Regulating Protein–Protein Interactions.* J. Mol. Biol., 2012. **423**(5): p. 818-830.
9. Laganowsky, A., et al., - *Membrane proteins bind lipids selectively to modulate their structure and function.* 2014. **- 510**(- 7503): p. - 175.
10. Long, S., et al., - *Atomic structure of a voltage-dependent K+ channel in a lipid membrane-like environment.* 2007. **- 450**(- 7168): p. - 382.
11. Dahlquist, F.W., et al., *Deuterium magnetic resonance studies of the interaction of lipids with membrane proteins.* Proc. Natl. Acad. Sci, 1977. **74**(12): p. 5435-5439.
12. Yeagle, P.L., *Non-covalent binding of membrane lipids to membrane proteins.* Biochimica et Biophysica Acta (BBA) - Biomembranes, 2014. **1838**(6): p. 1548-1559.

13. Smith, A.W., *Lipid-protein interactions in biological membranes: A dynamic perspective.* Biochim. Biophys. Acta, Biomembr., 2012. **1818**(2): p. 172-177.
14. Mahendra Kumar Jain and R.C. Wagner, *Introduction to biological membranes*1980, New York ; Chichester : Wiley
15. Hao, M., et al., *Cholesterol depletion induces large scale domain segregation in living cell membranes.* Proc. Natl. Acad. Sci, 2001. **98**(23): p. 13072-13077.
16. Pike, L.J., *Lipid rafts: bringing order to chaos.* The Journal of Lipid Research, 2003. **44**(4): p. 655-667.
17. Simons, K. and D. Toomre, *Lipid rafts and signal transduction.* Nat Rev Mol Cell Biol, 2001. **2**(3): p. 216.
18. Bloom, M., et al., *Physical properties of the fluid lipid-bilayer component of cell membranes: a perspective.* Q Rev Biophys, 1991. **24**(3): p. 293-397.
19. Hung, W.C., et al., *The condensing effect of cholesterol in lipid bilayers.* Biophys J, 2007. **92**(11): p. 3960-7.
20. Stidder, B., et al., *Effect of Low Amounts of Cholesterol on the Swelling Behavior of Floating Bilayers.* Langmuir, 2005. **21**(20): p. 9187-9193.
21. Stidder, B., et al., *Cholesterol Induced Suppression of Large Swelling of Water Layer in Phosphocholine Floating Bilayers.* Langmuir, 2005. **21**(19): p. 8703-8710.
22. Ohvo-Rekila, H., et al., *Cholesterol interactions with phospholipids in membranes.* Progress in lipid research, 2002. **41**(1): p. 66-97.
23. Boggs, J.M., *Lipid intermolecular hydrogen bonding: influence on structural organization and membrane function.* Biochim. Biophys. Acta, Rev. Biomembr, 1987. **906**(3): p. 353-404.
24. Magee, A. and I. Parmryd, *Detergent-resistant membranes and the protein composition of lipid rafts.* Genome Biol, 2003. **4**(11): p. 234.
25. Janes, P., et al., *Aggregation of lipid rafts accompanies signaling via the T cell antigen receptor.* J Cell Biol, 1999. **147**: p. 447 - 461.
26. UBC. http://wiki.ubc.ca/Biological_membranes. 2014 20/07/2014].

27. Uzman, A., *Molecular biology of the cell (4th ed.): Alberts, B., Johnson, A., Lewis, J., Raff, M., Roberts, K., and Walter, P.* Biochem. Mol. Biol. Educ., 2003. **31**(4): p. 212-214.
28. Luzzati, V., Biol. Membr., Ed. Chapman D, Academic Press, New York,1968: p. 71-123.
29. Marsh, D., *General features of phospholipid phase transitions*. Chemistry and Physics of Lipids. Vol. 57. 1991. 109-120.
30. McMahon, H.T. and J.L. Gallop, *Membrane curvature and mechanisms of dynamic cell membrane remodelling.* Nature, 2005. **438**(7068): p. 590-596.
31. Zimmerberg, J. and M. Kozlov, *How proteins produce cellular membrane curvature.* Nature reviews. Molecular cell biology, 2006. **7**(1): p. 9-19.
32. Maniti, O., et al., *Basic cell penetrating peptides induce plasma membrane positive curvature, lipid domain separation and protein redistribution.* The International Journal of Biochemistry & Cell Biology, 2014. **50**(0): p. 73-81.
33. Wu, Q.-Y. and Q. Liang, *Interplay between Curvature and Lateral Organization of Lipids and Peptides/Proteins in Model Membranes.* Langmuir, 2014. **30**(4): p. 1116-1122.
34. Shearman, G.C., et al., *Inverse lyotropic phases of lipids and membrane curvature.* Journal of Physics: Condensed Matter, 2006. **18**(28): p. S1105.
35. Israelachvili, J.N., *Intermolecular and Surface Forces.*Academic Press 3rd ed. 2011.
36. Kirk, G.L., et al., *A thermodynamic model of the lamellar to inverse hexagonal phase transition of lipid membrane-water systems.* Biochem, 1984. **23**(6): p. 1093-1102.
37. Epand, R.M., *Membrane Lipid Polymorphism*, in *Methods in Membrane Lipids*2007. p. 15-26.
38. Drew, D., et al., *Assembly and overexpression of membrane proteins in Escherichia coli.* Biochimica et Biophysica Acta (BBA) - Biomembranes, 2003. **1610**(1): p. 3-10.

39. Seddon, A.M., et al., *Membrane proteins, lipids and detergents: not just a soap opera.* Biochimica et Biophysica Acta (BBA) - Biomembranes, 2004. **1666**(1–2): p. 105-117.
40. Helenius, A., et al., *Properties of detergents.* Methods in Enzymology, 1979. **56**: p. 734-749.
41. Garavito, R.M., *Detergents as Tools in Membrane Biochemistry.* J. Biol. Chem, 2001. **276**(35): p. 32403-32406.
42. Bhairi, S.M. and C. Mohan, *Detergents: A guide to the properties and uses of detergents in biological systems*, 2007. p. 1-50.
43. *An Introduction to Detergents and Their Use in Membrane Protein Studies*, in *Structural Biology of Membrane Proteins*, R. Grisshamer and S.K. Buchanan, Editors. 2006, The Royal Society of Chemistry. p. 72-96.
44. Konigsberg, W.H. and L. Henderson, *[20] Removal of sodium dodecyl sulfate from proteins by ion-pair extraction*, in *Methods in Enzymology*, S.N.T. C.H.W. Hirs, Editor 1983, Academic Press. p. 254-259.
45. Urbani, A. and T. Warne, *A colorimetric determination for glycosidic and bile salt-based detergents: applications in membrane protein research.* Anal. Biochem., 2005. **336**(1): p. 117-124.
46. Whiles, J.A., et al., *Bicelles in structure–function studies of membrane-associated proteins.* Bioorg. Chem., 2002. **30**(6): p. 431-442.
47. Reeves, P.J., et al., *Structure and function in rhodopsin: Kinetic studies of retinal binding to purified opsin mutants in defined phospholipid–detergent mixtures serve as probes of the retinal binding pocket.* Proc. Natl. Acad. Sci, 1999. **96**(5): p. 1927-1931.
48. Kalmbach, R., et al., *Functional Cell-free Synthesis of a Seven Helix Membrane Protein: In situ Insertion of Bacteriorhodopsin into Liposomes.* J. Mol. Biol., 2007. **371**(3): p. 639-648.
49. Beschiaschvili, G. and J. Seelig, *Peptide binding to lipid bilayers. Nonclassical hydrophobic effect and membrane-induced pK shifts.* Biochem, 1992. **31**(41): p. 10044-10053.
50. Costello, M.J., et al., *Morphology of proteoliposomes reconstituted with purified lac carrier protein from Escherichia coli.* J. Biol. Chem, 1984. **259**(24): p. 15579-86.

51. Dezi, M., et al., *Detergent-mediated incorporation of transmembrane proteins in giant unilamellar vesicles with controlled physiological contents.* Proc. Natl. Acad. Sci, 2013. **110**(18): p. 7276-7281.
52. Brockman, H., *Lipid monolayers: why use half a membrane to characterize protein-membrane interactions?* Curr. Opin. Struct. Biol., 1999. **9**(4): p. 438-443.
53. Brezesinski, G. and H. Möhwald, *Langmuir monolayers to study interactions at model membrane surfaces.* Adv. Colloid Interface Sci., 2003. **100–102**(0): p. 563-584.
54. Maget-Dana, R., *The monolayer technique: a potent tool for studying the interfacial properties of antimicrobial and membrane-lytic peptides and their interactions with lipid membranes.* Biochimica et Biophysica Acta (BBA) - Biomembranes, 1999. **1462**(1–2): p. 109-140.
55. Nakahara, H., et al., *Langmuir Monolayer of Artificial Pulmonary Surfactant Mixtures with an Amphiphilic Peptide at the Air/Water Interface: Comparison of New Preparations with Surfacten (Surfactant TA).* Langmuir, 2008. **24**(7): p. 3370-3379.
56. Boucher, J., et al., *Organization, structure and activity of proteins in monolayers.* Colloids Surf., B, 2007. **58**(2): p. 73-90.
57. Schneider, M.F., et al., *Rheology of glycocalix model at air/water interface.* Phys. Chem. Chem. Phys., 2002. **4**(10): p. 1949-1952.
58. Popot, J.-L., *Amphipols, Nanodiscs, and Fluorinated Surfactants: Three Nonconventional Approaches to Studying Membrane Proteins in Aqueous Solutions.* Annual Review of Biochemistry, 2010. **79**(1): p. 737-775.
59. Tonge, S.R. and B.J. Tighe, *Responsive hydrophobically associating polymers: a review of structure and properties.* Adv. Drug Delivery Rev., 2001. **53**(1): p. 109-122.
60. Pocanschi, C.L., et al., *Amphipathic Polymers: Tools To Fold Integral Membrane Proteins to Their Active Form†.* Biochem, 2006. **45**(47): p. 13954-13961.
61. Tribet, C., et al., *Amphipols: Polymers that keep membrane proteins soluble in aqueous solutions.* Proc. Natl. Acad. Sci, 1996. **93**(26): p. 15047-15050.

62. Shaw, A.W., et al., *The local phospholipid environment modulates the activation of blood clotting.* J Biol Chem, 2007. **282**(9): p. 6556-63.

63. Boldog, T., et al., *Using Nanodiscs to Create Water‐Soluble Transmembrane Chemoreceptors Inserted in Lipid Bilayers*, in *Methods in Enzymology*, B.R.C. Melvin I. Simon and C. Alexandrine, Editors. 2007, Academic Press. p. 317-335.

64. Bayburt, T.H., et al., *Reconstitution and Imaging of a Membrane Protein in a Nanometer-Size Phospholipid Bilayer.* Jurnal od Structural Biology 1998. **123**: p. 37-44.

65. Schumaker, V.N. *Advances in protein chemistry. Volume 45, Volume 45*. 1994; Available from: http://site.ebrary.com/id/10240112.

66. Atkinson, D., et al., *X-ray and neutron scattering studies of plasma lipoproteins.* Ann. N.Y. Acad. Sci, 1980. **348**(1 Lipoprotein S): p. 284-298.

67. Forte, T., et al., *Plasma lipoproteins in familial lecithin: cholesterol acyltransferase deficiency: structure of low and high density lipoproteins as revealed by electron microscopy.* J.clinic. investig., 1971. **50**(5): p. 1141-1148.

68. Rothblat, G.H. and M.C. Phillips, *High-density lipoprotein heterogeneity and function in reverse cholesterol transport.* Curr Opin Lipidol, 2010. **21**(3): p. 229-38.

69. Jonas, A., *Reconstitution of high-density lipoproteins*, in *Methods in Enzymology*, J.J.A. Jere P. Segrest, Editor 1986, Academic Press. p. 553-582.

70. Carlson, J.W., et al., *Imaging and manipulation of high-density lipoproteins.* Biophys J, 1997. **73**(3): p. 1184-1189.

71. Wald, J.H., et al., *Investigation of the lipid domains and apolipoprotein orientation in reconstituted high density lipoproteins by fluorescence and IR methods.* J Biol Chem, 1990. **265**(32): p. 20044-50.

72. Schuler, M., et al., *Nanodiscs as a New Tool to Examine Lipid-Protein Interactions.* Methods in molecular biology (Clifton, N.J.), 2013. **974**: p. 415-433.

73. Jonas, A., et al., *Defined apolipoprotein A-I conformations in reconstituted high density lipoprotein discs.* J. Biol. Chem, 1989. **264**(9): p. 4818-24.
74. Li, Y., et al., *Structural Analysis of Nanoscale Self-Assembled Discoidal Lipid Bilayers by Solid-State NMR Spectroscopy.* Biophys J, 2008. **91**(10): p. 3819-3828.
75. Bayburt, T.H. and S.G. Sligar, *Self-assembly of single integral membrane proteins into soluble nanoscale phospholipid bilayers.* Protein Science, 2003. **12**(11): p. 2476-2481.
76. Civjan, N., et al., *Direct solubilization of heterologously expressed membrane proteins by incorporation into nanoscale lipid bilayers.* BioTechniques, 2003. **35**(3): p. 556-60, 562.
77. Wu, Z., et al., *The Low Resolution Structure of ApoA1 in Spherical High Density Lipoprotein Revealed by Small Angle Neutron Scattering.* J. Biol. Chem, 2011. **286**(14): p. 12495-12508.
78. Marty, M., et al., *Nanodisc-solubilized membrane protein library reflects the membrane proteome.* Anal. Bioanal.Chem., 2013. **405**(12): p. 4009-4016.
79. Bayburt, T.H., et al., *Self-Assembly of Discoidal Phospholipid Bilayer Nanoparticles with Membrane Scaffold Proteins.* Nano Lett., 2002. **2**(8): p. 853-856.
80. Denisov, I., et al., *Directed self-assembly of monodisperse phospholipid bilayer nanodiscs with controlled size.* J Am Chem Soc, 2004. **126**(11): p. 3477-3487.
81. Sligar, S.G. *Nanodiscs Technology:Protocols for Preparation of Nanodiscs* http://sligarlab.life.uiuc.edu/nanodisc/protocols.html. 2008 [cited 2014.
82. Sligarlab. http://sligarlab.life.uiuc.edu/nanodisc/protocols.html. [cited 2014 Mon 3 Feb 2014].
83. Shih, A., et al., *Molecular dynamics simulations of discoidal bilayers assembled from truncated human lipoproteins.* Biophys J, 2005. **88**: p. 548-556.

84. Tricerri, M.A., et al., *Interaction of apolipoprotein A-I in three different conformations with palmitoyl oleoyl phosphatidylcholine vesicles.* J.Lipids Res., 2002. **43**: p. 1-11.

85. Klon, A.E., et al., *Molecular Belt Models for the Apolipoprotein A-I Paris and Milano Mutations.* Biophys J, 2000. **79**(3): p. 1679-1685.

86. Tall, A.R., et al., *Structure and Thermodynamic Properties of High-Density Lipoprotein Recombinants.* J. Biol. Chem, 1977. **252**(13): p. 4701-4711.

87. Borhani, D.W., et al., *Crystal structure of truncated human apolipoprotein A-I suggests a lipid-bound conformation.* Proc. Natl. Acad. Sci, 1997. **94**(23): p. 12291-12296.

88. Segrest, J.P., *Amphipathic helixes and plasma lipoproteins: Thermodynamic and geometric considerations.* Chem. Phys. Lipids, 1977. **18**(1): p. 7-22.

89. Koppaka, V., et al., *The structure of human lipoprotein A-I. Evidence for the "belt" model.* J Biol Chem, 1999. **274**(21): p. 14541-4.

90. Davidson, W.S. and G.M. Hilliard, *The Spatial Organization of Apolipoprotein A-I on the Edge of Discoidal High Density Lipoprotein Particles: a mass spectrometry study.* J. Biol. Chem, 2003. **278**(29): p. 27199-27207.

91. Gorshkova, I.N., et al., *Structure and Stability of Apolipoprotein A-I in Solution and in Discoidal High-Density Lipoprotein Probed by Double Charge Ablation and Deletion Mutation†.* Biochem, 2006. **45**(4): p. 1242-1254.

92. Panagotopulos, S.E., et al., *Apolipoprotein A-I Adopts a Belt-like Orientation in Reconstituted High Density Lipoproteins.* J. Biol. Chem, 2001. **276**(46): p. 42965-42970.

93. Jiménez-Monreal, A.M., et al., *Influence of the Physical State of the Membrane on the Enzymatic Activity and Energy of Activation of Protein Kinase C α†.* Biochem, 1999. **38**(24): p. 7747-7754.

94. Lee, A.G., *How lipids affect the activities of integral membrane proteins.* Biochim. Biophys. Acta, Biomembr.ù, 2004. **1666**(1-2): p. 62-87.

95. Inagaki, S., et al., *Biophysical characterization of membrane proteins in nanodiscs.* Elsevier, 2012. **59**(3): p. 287-300.
96. Alami, M., et al., *Nanodiscs unravel the interaction between the SecYEG channel and its cytosolic partner SecA.* The EMBO journal, 2007. **26**: p. 1995-2004.
97. Leitz, A.J., et al., *Functional reconstitution of Beta2-adrenergic receptors utilizing self-assembling Nanodisc technology.* BioTechniques, 2006. **40**(5): p. 601-2, 604, 606, passim.
98. Boldog, T., et al., *Nanodiscs separate chemoreceptor oligomeric states and reveal their signaling properties.* Proc. Natl. Acad. Sci, 2006. **103**(31): p. 11509-11514.
99. Nath, A., et al., *Ligand binding to cytochrome P450 3A4 in phospholipid bilayer nanodiscs: the effect of model membranes.* J Biol Chem, 2007. **282**(39): p. 28309-20.
100. Duan, H., et al., *Co-incorporation of heterologously expressed Arabidopsis cytochrome P450 and P450 reductase into soluble nanoscale lipid bilayers.* Arch. Biochem. Biophys., 2004. **424**(2): p. 141-153.
101. Zhao, J., et al., *Resonance Surface Plasmon Spectroscopy: Low Molecular Weight Substrate Binding to Cytochrome P450.* J. Am. Chem. Soc., 2006. **128**(34): p. 11004-11005.
102. Tsukamoto, H., et al., *Rhodopsin in Nanodiscs Has Native Membrane-like Photointermediates.* Biochem, 2011. **50**(22): p. 5086-5091.
103. Bayburt, T., et al., *Assembly of single bacteriorhodopsin trimers in bilayer nanodiscs.* Arch. Biochem. Biophys., 2006. **450**(2): p. 215.
104. Borch, J., et al., *Nanodiscs for immobilization of lipid bilayers and membrane receptors: kinetic analysis of cholera toxin binding to a glycolipid receptor.* Anal. Chem., 2008.
105. Morrissey, J.H., et al., *Blood clotting reactions on nanoscale phospholipid bilayers.* 2008: p. 1-4.
106. Bayburt, T.H., et al., *Monomeric Rhodopsin Is Sufficient for Normal Rhodopsin Kinase (GRK1) Phosphorylation and Arrestin-1 Binding.* J. Biol. Chem, 2011. **286**(2): p. 1420-1428.

107. Shenkarev, Z.O., et al., *Lipid-protein nanodiscs: Possible application in high-resolution NMR investigations of membrane proteins and membrane-active peptides.* Biochem., 2009. **74**(7): p. 756-765.
108. Morrissey, J.H., et al., *Protein–membrane interactions: blood clotting on nanoscale bilayers.* Journal of Thrombosis and Haemostasis, 2009. **7**: p. 169-172.
109. Oda, M.N., et al., *Reconstituted high density lipoprotein enriched with the polyene antibiotic amphotericin B.* J Lipid Res, 2006. **47**(2): p. 260-7.
110. Ryan, R.O., *Nanodisks: hydrophobic drug delivery vehicles.* Expert Opinion on Drug Delivery, 2008. **5**(3): p. 343-351.
111. Hartsel, S. and J. Bolard, *Amphotericin B: new life for an old drug.* Trends Pharmacol Sci, 1996. **17**(12): p. 445-449.
112. Jurenka, J.S., *Anti-inflammatory Properties of Curcumin, a Major Constituent of Curcuma longa: A Review of Preclinical and Clinical Research.* Alternative Medicine Review, 2009. **14**(2): p. 1-13.
113. Alvarez, F.J.D., et al., *Functional Reconstitution of an ABC Transporter in Nanodiscs for Use in Electron Paramagnetic Resonance Spectroscopy.* J. Am. Chem. Soc., 2010. **132**(28): p. 9513-9515.
114. Ghosh, M., et al., *Curcumin nanodisks: formulation and characterization.* Nanomed. Nanotechnol. Biol. Med., 2011. **7**(2): p. 162-167.
115. Khumsupan, P., et al., *Apolipoprotein E LDL receptor-binding domain-containing high-density lipoprotein: A nanovehicle to transport curcumin, an antioxidant and anti-amyloid bioflavonoid.* BBA - Biomembranes, 2010. **1808**(1): p. 352-359.
116. Cormode, D.P., et al., *Nanocrystal Core High-Density Lipoproteins: A Multimodality Contrast Agent Platform.* Nano Lett., 2008. **8**(11): p. 3715-3723.
117. Knowles, B.T.J., et al., *Supplementary material Membrane proteins solubilized intact in bilayer nanoparticles bounded by styrene maleic acid copolymer.* 2009. **131**: p. 7484-7485.

118. Knowles, T.J., et al., *Membrane Proteins Solubilized Intact in Lipid Containing Nanoparticles Bounded by Styrene Maleic Acid Copolymer.* JACS communications, 2009. **131**(22): p. 7484-7485.

119. Jamshad, M., et al., *Surfactant-free purification of membrane proteins with intact native membrane environment.* Biochem. Soc. Trans., 2011. **39**(3): p. 813.

120 Hjelmeland, L.M., *A nondenaturing zwitterionic detergent for membrane biochemistry: design and synthesis.* Proceedings of the National Academy of Sciences, 1980. **77**(11): p. 6368-6370.

2

2 Characterisation Techniques and Models Used for Data Analysis

2.1 Introduction

In this following chapter a brief overview of the theory of the main techniques used in this project is provided. Introduction to small angle X-ray and neutron scattering is covered in the first section followed by a description of dynamic light scattering instruments. Then, the other techniques used in this work to analyse and characterise either the copolymers or SMALP structures are summarised.

Samples preparation and experimental set-up applied are also described for each experiments performed, together with a generic description of the instruments used. The last Section 2.8 is dedicated to data analysis with a detailed description of the models used to fit SANS and SAXS data, a description of the protocol applied to analyse TEM and Cryo-TEM micrographs and the analysis performed using NMR. Software used for data analyses are also presented.

2.2 Radiation-Matter Interaction

The study of a scattering process arising from the interaction between a probing beam and the sample is nowadays one of the most used analysis structural techniques. The first to use it was Lord Rutherford in 1911 who studied the scattering angle distribution of an alpha particle beam from a gold lamina [1]. To analyse the structure of a sample, two different types of radiation are most widely used namely neutron and X-ray.

X-rays are electro-magnetic waves with a wavelength around ~ 0.1 nm which, are sometimes described as particles called photons possessing no charge and no mass. Therefore the radiation-matter interaction can be described by two models: the oscillator mode, when considered as waves, or the impulse transfer mode, if considered as particles. This is also valid for neutrons where the interaction with matter is described using quantum-mechanical theory. However as explained later, the nature of the interaction between the probing beam and the sample is completely different.
When impinging on matter, X-rays can undergo two types of interactions: they can be scattered or absorbed [2]. However, since absorption is not a phenomenon of interest for the purpose of this work it will not be discussed here. The scattering process can be divided into two main categories, inelastic (also known as incoherent or Compton scattering [3]) and elastic (also known as Rayleigh [3] or coherent scattering).

Inelastic scattering happens when a photon hits an electron. When the photon is bounced away it loses a fraction of its energy, which is taken by the electron. As the inelastic scattering is generally not used to investigate the atomic structure of materials, this process will not be further developed in this chapter.

From a structural point of view, attention is drawn to the *Elastic scattering*, where no energy is lost during the collision between the radiation and the matter. Therefore, in the output signal, there is a phase correlation that produces interference patterns into the detector carrying structural information. The

electrons start oscillating at the same frequency as the incoming radiation. Thus due to this oscillation, the electrons emit radiation with the same frequency. Because the emitted waves of neighboring atoms oscillate strictly synchronously to each other, they produce what are defined to be "coherent waves" which have the capability to interfere at the detector. These interference patterns contain the information about the particle structure. The interference can be constructive (*in phase*) thus the radiation causes a bright spot on the detector. Or it can be destructive (*out of phase*) when the incoming waves have opposite phase thus a dark spot at the detector is observed. At the end of an experiment a 2D diffraction pattern is seen, which carries the structural information of the sample in terms of orientation and interatomic distance [4].

Elastic coherent scattering is the form of scattering in use for the purpose of this work. Therefore from now onwards this form of scattering will be further discussed, however it has to be noted that incoherent scattering can still happen during the experiment. Indeed it is seen as “background” in the scattering pattern.

Different types of scattering experiments could be performed; each of them gives specific information.
Static scattering, which measures the dependence on angle of the average scattered intensity, yields structural information. *Dynamic scattering,* where the time dependence of fluctuations in the scattered intensity is analysed to give information about the Brownian motion and how the particle shapes or configuration fluctuate in time. In addition the absolute scattered intensity (averaged over time or frequency) provides information about mass or molecular weight of the scattering objects.
In this chapter attention will be focused on static scattering experiments, in particular small angle scattering technique. Indeed, main interest of the project was to understand and analyse the structure of objects of nanometer sizes.
Small angle scattering was discovered in the late 1930s by Guinier [5] and the very first monograph, written in 1950 by Guinier and Fournet [6], contains the general equations still in use nowadays. The scattering process can be described with the same theoretical approach for both neutron and X-ray radiation.

Theincoming beam, which is a wave packet associated with a "quantum" of energy E is expressed as $E = h\upsilon$ (where h represents the Planck constant having a value of $6.626069 \times 10^{-34}\ J\ s$ and υ is the frequency associated to the traveling wave packet). The scattering of an X-ray photon, or neutron by a sample is characterized by the change in momentum P and in energy E. Since also the momentum and energy are quantities that must be conserved it is possible to express energy and momentum through respectively Equation 2.1 and Equation 2.2.

$$E = \hbar\omega_i - \hbar\omega_f \qquad \textit{Equation 2.1}$$

And

$$P = \hbar\,(k_I - k_f) = \hbar q \qquad \textit{Equation 2.2}$$

Where k_i and k_f are the wave vectors of the incident and scattered particles, ω_i and ω_f are respectively the angular frequency of the incident and scattered particles, q is the scattering vector expressed as a difference between k_i and k_f is and $\hbar$ is the Planck constant divided by 2π. Both incoming and scattered radiation possess a magnitude defined as expressed in Equation 2.3, where λ is the wavelength.

$$|k| = \frac{2\pi}{\lambda} \qquad \textit{Equation 2.3}$$

Representing the scattering event using geometry the quantity q, known as the *Scattering vector or Momentum transfer,* can be obtained from the formula $q = k_f - k_i$, which can then be used to derive Equation 2.4 from Equation 2.3.

$$q = \frac{4\pi\sin\theta}{\lambda} \qquad \textit{Equation 2.4}$$

The dimension of q is 1 over a length (nm^{-1}), which is why the scattering pattern is usually called "the structure in reciprocal space", while particles in a sample have a structure in real space (nm). If it is assumed that the scattering object is a point and that there is no energy loss during the scattering process, then the elastic scattering event can be represented by the diagram depicted in Figure 2.1.

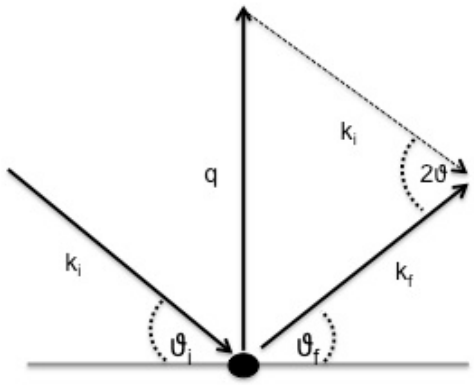

Figure 2.1. Schematic representation of a scattering event.

The scattering of one particle, which is made of many atoms, can be explained as the interference pattern produced by all the waves that are sent to the detector from every electron/atom inside the particle. This pattern oscillates in a fashion that is characteristic of the shape (or the form) of the particle. It is therefore called the *form factor* and it is defined as defined as *F(q)*.

When an ensemble of densely packed particles (i.e. in concentrated samples) is considered, the distances relative to each other particles come into the same order of magnitude as the distances inside the particles. The interference pattern will therefore contain contributions from neighboring particles as well. This additional interference pattern multiplies the form factor of the single particles. It is called the *structure* factor and it is defined as *P(q)*. When a number (N) of particles with an electron density of ρ_1 are embedded into a matrix of electron density ρ_2 then the scattered intensity of the system is defined by Equation 2.5.

$$I_1(q) = I_0 \times (\Delta\rho)^2 \times V_1^{\,2} \times F(q) \times P(q) \qquad \textit{Equation 2.5}$$

Where $\Delta\rho = \rho_2 - \rho_2$, V is the volume and I_0 is the intensity which also takes into account the transmission and the sample detector distance.

Particles are rarely identical among each other. Indeed, it is known that particles possess a range of sizes, which characteristics is called polydispersity or have different shapes, in which case the sample is called "polymorphous".

As it will be discussed later in the chapter, while the X-ray beam interacts with the electron cloud of the system the neutron beam interacts with the nuclei of the system. This is important since the way the scattered intensity varies for different materials depends on the kind of interaction. Considering the sample to be a single atom, the scattering length of that atom, for X-ray, is defined as Zr_e (where Z is the atomic number and r_e is the electron scattering cross-section). Therefore in the case of X-ray being the probing beam interacting with the electron clouds the intensity will increase linearly with increasing atomic number.

It is possible to define a similar scattering length parameter in the case of neutrons, normally denoted *b.* It describes the interaction of the neutron with the nucleus; this parameter shows no linear relationship with the atomic number and is rather random. Scattering lengths for neutrons of different atoms have been measured and available in tables [7] or in dedicated web sites [8].

Another very useful parameter that needs to be introduced at this stage is the so called Scattering Length Density (SLD) which for a generic molecule is defined as expressed in Equation 2.6. Where b_i is the coherent scattering length for the i^{th} atom in a molecule with n atoms and V_m is the molecular volume; this equation can also be modified for a SAXS experiment by inserting instead of b_i the scattering length for X-ray, previously defined as Zr_e.

$$N = \frac{\Sigma_{i=1}^{n} b_i}{v_m} \qquad \textit{Equation 2.6}$$

In the next section, it is discussed how this parameter is of vital importance in designing an experiment in particular for neutron scattering experiments.

2.2.1 Importance of Contrast Variation

Contrast is an essential parameter in any scattering experiment. Indeed, if there is no difference in the scattering arising from the sample and from the solvent it is not possible to distinguish between the two signals. The technique of deliberate varying the contrast arising from one or the other part of the sample examined in order to highlight or hide a part of the system is known as "contrast variation method".

The physical origin of the contrast varies depending on the nature of the probing beam and its interaction with the sample. The contrast variation is therefore achieved in different ways.

In a *SAXS experiment* the contrast variation is achieved by changing the electron density. That could be done for instance by incorporating heavy-metal ions. In many cases contrast variation is rarely achievable without destroying the sample structure. Indeed changing the solvent composition or staining with heavy-metal ions is an invasive process. In such situations SAXS will not be of great use.

Instead, in the context of a *SANS experiment*, contrast can be changed using the difference in scattering length density between hydrogen (-3.74×10^{-13} cm^{-2}) and deuterium (6.67×10^{-13} cm^{-2}) which arises from the different interactions of neutrons with these two isotopic nuclei. Deuteration of a part of the sample is a really useful method used to highlight a part of a sample in the scattering process. Contrast variation using neutrons has had a major impact on the understanding of copolymer conformations, morphologies, rheology and thermodynamics. This method has become a routine analytic characterization method in combination with SAXS.

As for a Dynamic light Scattering *(DLS)* experiment, where light is the radiation scattered, the contrast variation arises from the difference of the refractive indices, related to the polarizability of the considered material.

2.2.2 Small Angle X-ray Scattering (SAXS)

The set-up for all small angle scattering experiments is constituted by a source, a collimation system, a beam stop and a detection system, a schematic representation is reported in Figure 2.2. In SAXS experiments, very small scattering angles are used, typically between 0.1° and 10°. The X-ray beam that comes directly from the source is polychromatic, that is to say it is a mixture of photons of different wavelengths. A sample that scatters the photon of one wavelength in a specific direction will scatter different wavelengths in another direction and this causes wavelength smearing. In order to prevent this broadening, the collimation system selects X-ray only at a particular wavelength.

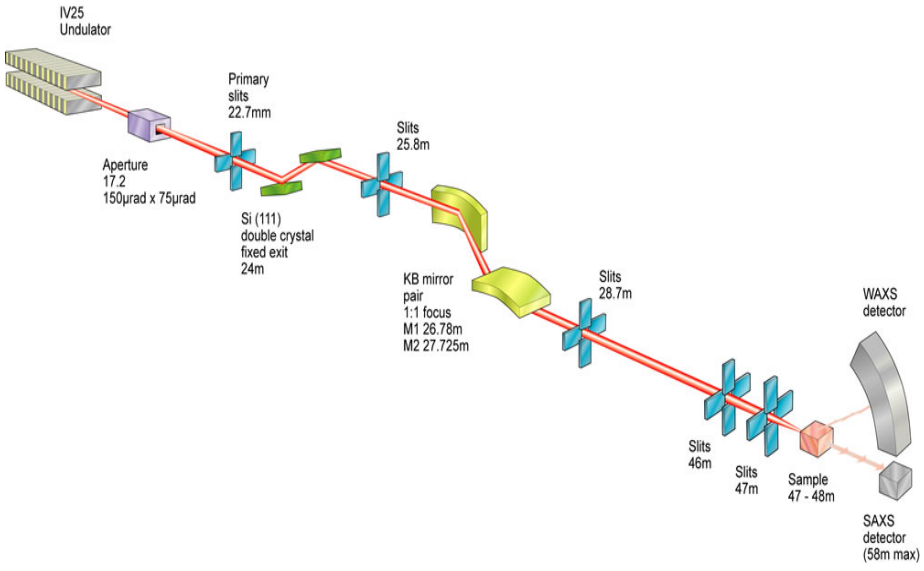

Figure 2.2. Schematic representation of the I22 SAXS instrument located at Diamond institute (Oxfordshire, UK). Picture reproduced from official beamline web site [9].

There are two different types of collimation systems: *Point collimation*: these have pinholes that shape the beam to a small circular spot. The scattering

pattern has then only a little instrumental broadening. However since the volume of sample illuminated is really small the scattered intensity is weak. Therefore, the measurement is very long. *Line collimation*: this system confines the beam in one dimension. The beam profile is a long but narrow line. The illuminated sample volume is much bigger but of course there is more broadening. The recorded pattern from a line collimation system is an integrated superimposition of many adjacent pinhole patterns. In order to take into account this "broadening effect", the beam profile must be measured and incorporated into the data evaluation. This process is called *desmearing.*

Another component of a SAXS instrument is the beamstop. The function of the beamstop is to prevent the direct beam, which is very intense, from hitting the detector. Although some detectors are not necessarily destroyed, such a strong intensity will cover the signal of the sample, which is clearly weaker than the direct beam. At the end of the instrument is located a detector [10]. There are four different types of detectors:
Wire detectors have thin wires inside an absorbing gas atmosphere. Each photon that enters this atmosphere expels an electron from the gas molecules. The electron is accelerated towards the wire by the applied high voltage. When the electron hits the wire an electrical pulse wave is induced inside the wire. This wave propagates towards the end points of the wire where their arrival is recorded. The time difference between the two arrivals is used to determine the position where the electron hit the wire. One wire is capable of delivering a 1D scattering profile and many wires that run parallel can be used to produce a 2D picture. CCD cameras detect the X-ray photons directly by counting the secondary electrons that are produced inside a semiconductor material or they can detect visible light that is produced by a fluorescent screen attached to the semiconductor chip. Imaging plates are made of a material that stores the X-ray energy by exciting the electrons of the material. Imaging plates are flexible sheets that are exposed like photographic films and are scanned by a separate device in a second step. The new generation of detectors is represented by the silicon pixel detectors (e.g. PILATUS [11] detectors used on the I22 beam line in Diamond). The pixels in the detectors are made in silicon, a relatively robust material with a high resistivity. The main concept behind the way they work is

based on the interaction between the electronic beam with the pixels surface creating electrons-holes pairs, the charge collected by each pixel is proportional to the number of photons that hit it and it is eventually read out by a specific device coupled with the detector.

- *X-Ray Sources*

It is known that every object when heated up emits electromagnetic waves. The wavelength of the radiation emitted depends inversely on the temperature *T* through the first Wien law expressed in Equation 2.7.

$$\lambda_{max} = \frac{2.90\ 10^{-3}\mathrm{m}}{\mathrm{T}} \qquad \textit{Equation 2.7}$$

Where *T* is the temperature in Kelvin. Equation 2.7 shows that the wavelength becomes shorter as the temperature increases. Another way to produce photons is to use electrons emitted by a heated filament through the thermionic effect, accelerate them by applying a positive voltage and make them hit a metal target. To optimize the process, the entire experimental tool is under vacuum. When an electron hits a target (usually called the anode) four different processes may take place:

- Excitation of an outer orbital electron;
- Ionization of an outer orbital electron;
- Ionization followed by the emission of a characteristic X-ray;
- Bremsstrahlung ("braking radiation") production.

The first two of these processes lead to the production of heat. In an X-ray tube 95% to 99% of the energy from decelerating electrons goes to heat via excitation and ionisation of outer orbital electrons. The third and fourth of these processes lead to the production of X-ray photons. The most interesting process is the X-ray indirect production via ionisation, since Bremsstrahlung yields a continuum spectrum. In the indirect process, an electron hits one electron of the

inner shell of an atom making it jump to a higher energy level. Since this is not a stable state the electron tends to come back to the initial level and this process is accompanied by the emission of a photon. As a consequence of the quantized nature of the energy level, the photons are produced at discrete set of wavelengths, as expressed by Equation 2.8 in which two energy levels are indicated with E_j and E_i and the wavelength corresponding to the emitted photon is λ_{ij} that is characteristic of the anode material.

$$\lambda_{ij} = \frac{hc}{E_j - E_i} \qquad \textit{Equation 2.8}$$

Indeed, this is the way in which X-rays have been produced for over a century and is still in use in small laboratories. A huge step forward has come with the use of synchrotron facilities. A synchrotron is a particular type of cyclic particle accelerator in which the magnetic field and the electric field are synchronised with the travelling particle beam. The charged particles (electrons or protons) are forced to move along a circular path with high speed. It is known that an accelerated particle produces energy. The photons produced by the Bremsstrahlung effect are subsequently extracted and used for different purposes. For example, each scientific application can be optimized by selecting the best possible X-ray wavelength according to the specific purpose. Therefore, it is convenient to change the source wavelength as desired. This is difficult for conventional X-ray sources, but is easier with synchrotron light.

2.2.3 Small Angle Neutron Scattering (SANS)

The main difference between neutron and X-ray scattering is in the way the radiation interacts with the sample. X-rays are scattered by the electrons in the atomic shells, which means that the probability of scattering is proportional to the Z of the material. Neutrons interact with matter via nuclear rather than electrical forces, and nuclear forces are very short range, of the order of a few Fermi (1 Fermi is equal to 10^{-15} m). If there are unpaired electrons in the material, neutrons may also interact by a second mechanism: a dipole-dipole interaction between the magnetic moment of the neutron and the magnetic moment of the unpaired electrons. The general instrumental layout is the same as for X-rays however neutron detectors differ from photon detectors.

- *Neutron Sources*

Neutron scattering facilities around the world generate neutrons either with nuclear reactors or with high-energy particle accelerators. Reactors operate in a continuous neutron generation mode whereas spallation sources function in a pulsed mode. Inside a reactor, neutrons are produced via a process called fission, in which a heavy nucleus splits into two lighter ones and generates neutrons but also gamma rays and other subatomic particles. The principal material is uranium U^{235}. The neutrons produced have energies up to tens or even hundreds of mega-electron volts (MeV), and the corresponding neutron wavelengths are far too short for investigating condensed matter. Furthermore, neutrons whose energies are very high tend to damage the sample. For this reason, neutrons must be "cooled down" before being used for scattering experiments. To do this a moderating material with a large scattering cross section is used, such as water or D_2O (heavy water). Inside the moderator neutrons scatter many times, losing energy in each collision until they have an average thermal energy that is characteristic of the moderator temperature. After that, thermal neutrons are emitted from the moderator surface with a spectrum of energies around an average value determined by the moderator temperature.

Another way to produce neutrons is the so-called spallation source (for instance the research center ISIS (Oxfordshire, UK). These sources are combined with a synchrotron particle accelerator. To generate neutrons, a beam of high-energy protons (around 1 GeV) hits a target made of a heavy element, such as tungsten. This causes the emission of neutrons and protons and other subatomic byproducts, which have been knocked out of the nuclei in a process called spallation. Unlike in the nuclear reactors, neutrons in a spallation source are not produced in continuous mode since they are produced by "packet" of protons that are made to hit the target periodically. After being produced, the neutron beam is attenuated by a moderator. Moderators under-moderate the neutrons to produce a high flux of epithermal neutrons, the moderator material produces different pulse shapes as a function of its dimensions and it is possible to control the energy range of the produced neutrons by changing the moderator temperature. The spallation source at ISIS [12] is combined with the Time of Flight technique namely the energy of neutrons produced is then selected as a function of their velocity, as these two parameters are strictly correlated.
From the different neutrons production arise relative advantages and disadvantages

Pulsed sources produce less neutrons than the continuous ones but they produce higher energy than do reactors. The debate whether pulsed sources are better than continuous ones depends on many circumstances. It is possible to affirm that pulsed sources are better if high energy neutrons are required however on the other side, continuous sources allow more flexibility in the spectrometer design and location (for instance on the spallation source very long guides are required in order to achieve high resolution). Time of flight instruments also have the advantages of measuring a wide Q range at once.

Neutron detectors are designed in a way that the incoming neutron particles are absorbed by a suitable nucleus and the charged particle produced is successively detected. A very common material in neutron detectors is ^{3}He as described in Scheme 2.1. A neutron is absorbed by the helium and a nucleus of tritium together with a proton is produced. Other light nuclei in use are also ^{1}Li and ^{10}B.

$$^{3}He + n \longrightarrow {}^{3}H + {}^{1}H + 0.77\ MeV$$

Scheme 2.1

Fast ions are produced and used for the actual detection process. The geometrical set up of these gas detectors is usually cylindrical of diameter of few centimeters and length up to ten centimeters. The anode collecting and accelerating the ionized particles is placed along the central axis. An electron cloud is created and detected according to the so-called coincidence method where two cathodes are placed along the X and Y axis and only events that arrive at the same time are counted. The two main suppliers of neutron area detectors are CERCA (Grenoble, France) and ORDELA (Oak Ridge, Tennessee, USA).

2.3 Dynamic Light Scattering (DLS)

Dynamic Light Scattering [13] (DLS), also known as Photon Correlation Spectroscopy (PCS) or quasi Elastic Light Scattering (qELS), is one of the most popular methods used to determine the size of sub-micron particles in liquid suspensions [14]. The great advantage of this technique consists of the possibility to analyse a broad variety of particles in a non-invasive and non-destructive way. Furthermore, it does not require a large volume or highly concentrated samples. DLS is a fast and relatively cheap way of analysing samples so it is often used to check samples before more expensive or time-consuming analysis such as SANS or SAXS experiments.

This technique is based on the principle that when light interacts with matter, the electric field of the beam induces an oscillating polarization of electrons in the molecules in the sample, hence providing a secondary source of light and subsequently producing scattered light. The frequency shifts, the angular distribution, the polarization, and the intensity of the scattered light are determined by the size, shape and molecular interactions in the scattering material. It is therefore possible to extract information about the structure and

dimension of the scattering objects through the light scattering characteristics of the system. The typical experimental setup is constituted of a monochromatic laser source providing light that interacts with the sample in a plastic or quartz cuvette. Signal is detected from the photon-counting device and then acquired by the correlator device, which will give a correlation function represented by an exponential decay, which will vary depending on the size of particles analysed. Finally the appropriate algorithm is applied. A schematic representation is reported in Figure 2.3.

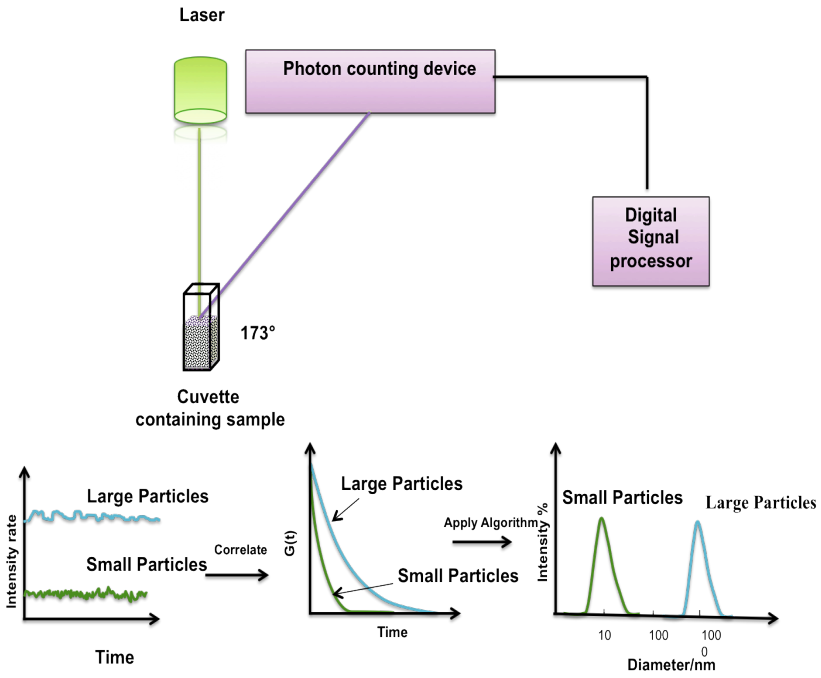

Figure 2.3. Schematic representation of the DLS instrument setup and of data elaboration process.

DLS experiments are essentially based on two assumptions. Firstly the principle of Brownian motion (also called random walk) is applied: particles are assumed to move in a random walk at a speed, which is related to their size, the viscosity of the surrounding medium and temperature. Secondly particles are assumed to be hard spheres. Hard spheres are defined simply as impenetrable spheres that

cannot overlap in space. In the case of non-spherical objects DLS measurements will give the diameter of a sphere that has the same average translational diffusion coefficient. During the measurement, the instrument initially measures the intensity of the scattering at a time t, which is *I(t)*. At the time $t + \tau$, in which τ indicates a small variation in time, the diffusing particles will have new positions and the intensity at the detector will have a value $I(t + \tau)$. The detector saves the values for $I(t + \tau)$ at numerous times, and initially $I(t + \tau)$ is correlated with *I(t)*. As time passes, there is less and less similarity between the starting state and the current state, so the measured intensities no longer correlate to the initial intensity. This process will happen faster if the particles are smaller since smaller particles move faster. Data obtained are used to quantify how fast the correlation takes to break down between the starting measurement and one recorded at a short time later.

The function used to calculate this correlation is the autocorrelation function. It describes how a given measurement relates to itself in a time dependent manner. The autocorrelation function normalized by the average intensity $\langle I(q,\tau)\rangle$ is given in Equation 2.9 , in which the average symbol refers to an averaging over time.

$$g^2(q,\tau) = \frac{\langle I(q,t)I(q,t+\tau)\rangle}{\langle I(q,t)\rangle^2} \qquad \textit{Equation 2.9}$$

$g^2(q,\tau)$ is referred to the fact that it is a second order correlation function i.e. involving intensities which are the squares of the electric fields.
Therefore Equation 2.9 can also be expressed as Equation 2.10 where the $g^1(q,\tau)$ is the electric field autocorrelation function. This equation is also known as Siegert equation.

$$g^2(q,\tau) = 1 + |g^1(q,\tau)|^2 \qquad \textit{Equation 2.10}$$

The decay of the autocorrelation function is described by an exponential decay function $\Gamma(t)$ as expressed in Equation 2.11 which in case of monodisperse samples relates the electric field autocorrelation function to the diffusion coefficient *D* and the wave vector *q* as expressed in Equation 2.12.

$$g^1(q,t) = e^{(-\Gamma t)} \qquad \textit{Equation 2.11}$$

$$g^1(q,t) = e^{-2Dq^2} \qquad \textit{Equation 2.12}$$

From the Stokes-Einstein equation [15] (reported in Equation 2.13), it is possible to calculate the hydrodynamic radius [16] of the particle.

$$D = \frac{k_B T}{6r\pi\eta} \qquad \textit{Equation 2.13}$$

Where: D is the diffusion coefficient; r is the hydrodynamic radius of the scattering objects; k_B is the Boltzmann constant; T is the temperature (in Kelvin) and η is the viscosity of the solvent.

However, it is important to point out that the radius obtained is an approximation. Indeed the hydrodynamic radius could include for instance counterions and molecules of solvent or others that move at the same speed surrounding the particle. The hydrodynamic radius not only depends on the size of the particle "core" but also on the electric double layer related to the type and concentration of any ion present in solution; as schematically represented in Figure 2.4 A. A low concentration of ions in the medium will have the effect of extending the double layer of ions around the particle, reducing the diffusion coefficient which will result in a increased diameter. On the other hand a high concentration medium (higher than 10 mM) will have the effect of reducing the double layer resulting in a decreased apparent diameter. In addition the nature of the surface can affect the size of the analysed object. For instance it can be composed of structures projecting out of the core, which could for instance be sensitive to the ion concentration and consequently change the apparent size of the object as depicted in Figure 2.4 B.

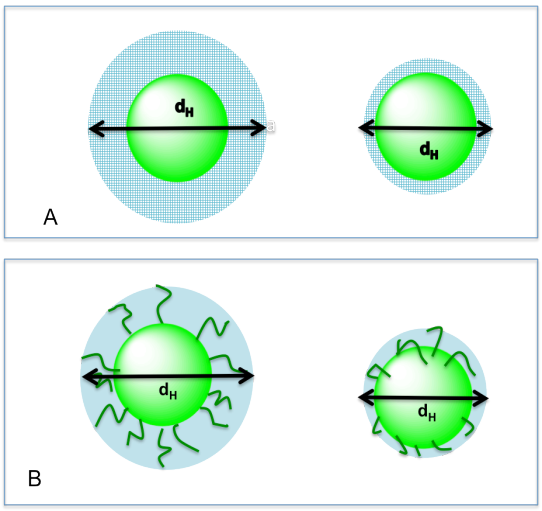

Figure 2.4. Schematic example of how the electronic double layer (A) or the nature of the sample surface(B) can affect the apparent size of objects in a DLS experiment.

The diffusion coefficient information is contained in the decay constant of the correlation function, which is obtained by fitting the function to a suitable algorithm. There are two methods of analysis that can be used, the cumulant analysis and the distribution analysis. The choice of one or another depends on the polydispersity of the sample analysed, a value which ranges from 0 to 1. Values greater than 1 indicate that the sample is so polydisperse that it might not be suitable for DLS measurements. For monomodal distributions (in the case of samples with low polydispersity values), with the assumpion that the particles distribution is centred on a mean with a Gaussian-like distribution, the cumulant analysis can be applied. Cumulant analysis gives the particle mean size (called the z average) and an estimate of the width of the distribution, which corresponds to the polydispersity index. The cumulant analysis is the fit of the correlation function to a polynomial expressed in Equation 2.14

$$\mathrm{LnG} = a + bt + ct^2 + dt^3 + et^4 + \cdots \qquad \textit{Equation 2.14}$$

The value of *b* is known as the second order cumulant and it is the z-average diffusion coefficient, which is then converted to a size using Equation 2.13.

When the sample is polydisperse, the distribution analysis is used, which is calculated through a non-negative least square analysis (NNLS) using either a general purpose algorithm, suitable for most of samples where no knowledge of the distribution is available, or using a model with multiple narrow modes which is useful where the presence of a discrete population is suspected or else using the protein analysis, for protein samples.

Once the most suitable analysis method is chosen, the primary size distribution obtained from a DLS measurement is the intensity-weighted distribution. The size distribution is displayed as a plot of the relative intensity by particle size on the Y-axis versus various size classes on the X-axis. The general-purpose analysis applied in this work uses 70 size classes. However, it is important to point out that the intensity distribution analysis is very sensitive to the presence of large particles. Indeed, according to the Rayleigh approximation the intensity of a particle is proportional to the 6^{th} power of the radius. This is why in the case of samples with multiple peaks, very common in "multimodal" samples, it is more appropriate to represent the results in a volume distribution plot, which is linked to the spherical approximation, and depends on the 3^{rd} power of the radius. Data from DLS experiments were then fitted to a lognormal distribution using IGORpro^{TM} (Wavemetrics Inc.) version 6.32A.

2.4 Chromatographic and Spectroscopic Techniques

2.4.1 Size Exclusion Chromatography

This technique allows the separation of molecules according to their size as they pass through a gel filtration medium packed in a column [17]. It was invented by Grant Henry Lathe and Colin R Ruthven, working at Queen Charlotte's Hospital, London [18] but was only when J.C. Moore published his work [19] that it became very popular in the copolymer field. It is a very versatile technique where parameters such as the type of buffer, pH and temperature can be varied to suit the sample characteristics [20]. Typically,

when an aqueous solution is used as the mobile phase this technique is known as gel filtration chromatography in comparison with the gel permeation chromatography, which uses an organic solvent as the mobile phase.
Gel permeation chromatography is mainly used to determine the molecular weight distribution of non water-soluble macromolecules. Gel filtration chromatography is mainly used to separate proteins or other water-soluble macromolecules.

Gel Filtration is often used to separate multiple components in a sample on the basis of differences in their size, but can also be used as a tool for protein purification or as a fast method for buffer exchange [21]. The medium is a porous matrix usually in the form of spherical particles that have been chosen for their chemical and physical stability and inertness. The column is equilibrated with a buffer, which fills the pores of the matrix and the space between the particles. When a sample containing large and small molecules elutes through the column, small molecules penetrate the pores where they are retained and elute later than larger molecules, which are flushed quickly in the mobile phase. Those molecules which do not enter the matrix are eluted in the so-called void volume V° as they pass directly through the column at the same speed as the flow of buffer. Molecules with a partial access to the pores of the matrix elute from the column in order of decreasing size. Small molecules that have full access to the pores move down to the column but do not separate from each other. A schematic representation of the gel filtration process is reported in Figure 2.5.

Results are usually expressed as an elution profile that shows the variation in concentration in terms of absorbance detected by a UV-Vis detector. The wavelength is chosen according to the chromophore group present in the sample.
Many factors can influence the final resolution, namely the ratio of sample volume to column volume, column dimensions, particle size distribution, packing density pore size of the particles flow rate and viscosity of the sample and buffer.

The molecular weight range over which a gel filtration medium can separate molecules is referred to as the selectivity of the medium. Resolution is a function of the selectivity of the medium and the efficiency of that medium to produce narrow peaks. After selecting a gel filtration medium with the correct selectivity, sample volume and column volume become two of the most critical parameters that will affect the resolution of the separation. Today's gel filtration media cover a molecular weight range from peptides to very large proteins and protein complexes.

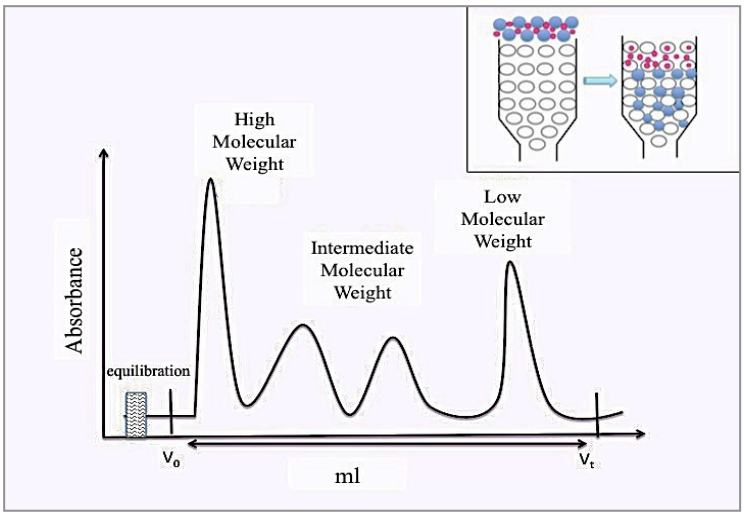

Figure 2.5. Illustration of a gel-filtration chromatogram. Graph is plotted in Absorbance versus column elution volume.

2.4.2 Spectroscopy

Spectroscopy is the study of absorption and emission processes occurring when a probing electromagnetic beam interact with matter.

Molecules are characterised by different energy levels, electronic energy levels that are split in vibrational energy levels, which in turn are split into rotational energy levels. When incoming electromagnetic waves interact with molecules they cause transitions between the energy levels. Transitions involving

electronic energy levels occur in the UV-visible (UV-Vis) spectroscopy region, while transitions between vibrational levels are in the Infrared Spectroscopy (IR) region while, in the case of rotational levels transitions occur in the microwave region.

2.4.2.1 Ultra Violet -Visible Spectroscopy (UV-Vis)

The spectroscopic region of the electromagnetic spectrum that goes from 100 nm up to 800 nm is known as the ultraviolet (UV) or visible region. This broad region is then divided into Far UV (from 100 nm to 200 nm), UV (from 200 nm to 350 nm) and visible (from 350 nm to 800 nm). The part of the molecule containing the electrons involved in the electronic transition is called the chromophore. A large number of chromophores analysed have transitions in the region of 200 nm-800 nm, which makes the analysis process easier and does not require special equipment.

The wavelength of light absorbed is the energy required to move an electron from a lower to a higher energy level [22]. When the radiation passes through a sample, the amount of radiation absorbed is the difference between I_0 the incident radiation and I the transmitted radiation. The amount of radiation absorbed is expressed either in Transmittance (Equation 2.15), or as the Absorbance (Equation 2.16).

$$T = {}^{I}/_{I_0} \qquad \textit{Equation 2.15}$$

$$A = -\log T \qquad \textit{Equation 2.16}$$

Absorbance is also related to the compound concentration and this dependence can be expressed through the Beer-Lambert law [23] (Equation 2.17).

$$A = cl\varepsilon \qquad \textit{Equation 2.17}$$

Where c is the molar concentration of solute, l is the cuvette path length and ε is the extinction coefficient also known as molar absorptivity, a property that is characteristic of each absorbing molecule and is usually expressed in the unit L mol^{-1} cm^{-1}.

2.4.2.2 Fourier Transform Infrared Spectroscopy

The infrared (IR) is a portion of the electromagnetic spectrum that is usually divided into three regions; the Far –IR (300 - 10 cm^{-1}), Mid-IR (4000 - 200 cm^{1}) and Near-IR (12.000 - 4000 cm^{-1}). For organic chemical analysis the most interesting region is the Mid-IR where all the most commonly studied vibrational transitions in molecules happen. Infrared spectroscopy uses the molecular vibrations to identify specific functional group characteristic of the molecule. Tables are available for the main chemical groups.

IR transitions arise from the interaction of the incoming wave with the oscillating dipole moment of the molecule and it involves the vibrational states of the molecule. A molecule can vibrate in many ways that are called vibrational modes. The vibrational degrees of freedom are 3N-5 for linear molecules and 3N-6 for non-linear molecules, where N is the number of atoms.

In order for a vibrational mode to be “IR active” a net dipole moment must exist and display a change during the transition. A typical IR experiment consists of a beam of infrared light passing through the sample [24]. When the frequency of the light is the same as the vibrational frequency of one bond, absorption occurs and examining the transmitted light the energy absorbed at each frequency is found. IR experiments were originally performed with the use of a monochromator, an instrument able to mechanically select a narrow range of wavelengths. The detector measures the amount of energy at each frequency

passing through the sample giving a spectrum of the intensity versus the frequency. The weakness of these experiments was the fact that they were quite time consuming due to the slow scanning process. At the present time this technique has been almost completely substituted by the Fourier Transform Infrared (FTIR) technique [24, 25], the spectrum is in this case obtained with a single illumination by light and all the frequencies are excited at once. The resulting data are Fourier transformed to give the conventional looking spectrum. This technique presents the important advantage that allows several scans within seconds that can then be added together, resulting in a decreased signal-to-noise ratio.

2.5 Nuclear Magnetic Resonance (NMR)

Nuclear Magnetic Resonance is a spectroscopic technique involving the use of a particular property of nuclei, called spin, to investigate physical, chemical and biological properties of matter [26]. NMR has been successfully applied in many scientific areas such as chemistry, physics and biology [27]. From quantum mechanics it is known that each nucleus can be associated with an angular Momentum, defined by Equation 2.18.

$$L = \sqrt{\hbar I(I+1)} \qquad \textit{Equation 2.18}$$

Where $\hbar$ represents the Plank constant h divided by 2π. The term I is known as nuclear angular momentum more often called nuclear spin. The nuclear spin can assume different values that can be calculated according to Table 2.1, where the atomic mass is defined as the number of protons plus the number of neutrons in the nucleus and the atomic number indicates the number of protons in the nucleus.

I	*Atomic Mass*	*Atomic Number*	*Example*
Fraction	Odd	Odd or Even	^{1}H=1/2 ;^{13} C=1/2
Integer	Even	Odd	^{1}D=1; ^{14}N=1
Zero	Even	Even	^{12}C=0; ^{18}O=0

Table 2.1. Nuclear spin values based on the atomic mass and atomic number general rule with examples for each possible combination.

Moving charges are associated with a magnetic moment therefore the nuclear spin magnetic moment can be expressed through Equation 2.19.

$$\vec{\mu} = \gamma \vec{L} \qquad \textit{Equation 2.19}$$

Where γ indicates the gyromagnetic ratio. Equation 2.19 implicitly states that nuclei with a spin value equal to zero do not possess a magnetic moment therefore cannot be detected in an NMR experiment.

In the absence of an external magnetic field B_0, the magnetic moments of the single nuclei are randomly orientated. If an external magnetic field is applied ($B_0 \neq 0$) then the angular moment of spin *L* aligns in such a way that the component along the axis *Z* where the field is applied is expressed as in Equation 2.20.

$$L_z = m\hbar \qquad \textit{Equation 2.20}$$

Where *m* represents the associated directional quantum number and can assume values that go from *+I* to *–I* depending on the value of *I* magnetic moment of spin. For instance, for nuclei with a spin quantum number = 1/2, such as ^{1}H, there are going to be two possible orientations *m= +1/2* and *m= -1/2* as illustrated in Figure 2.6. The frequency of precession, defined as ν around the *Z*

axis, is called the Larmor frequency and is related to the intensity of the applied magnetic field as shown in Equation 2.21.

$$\nu = {}^{\gamma}/_{2\pi}\, B_0 \qquad \textit{Equation 2.21}$$

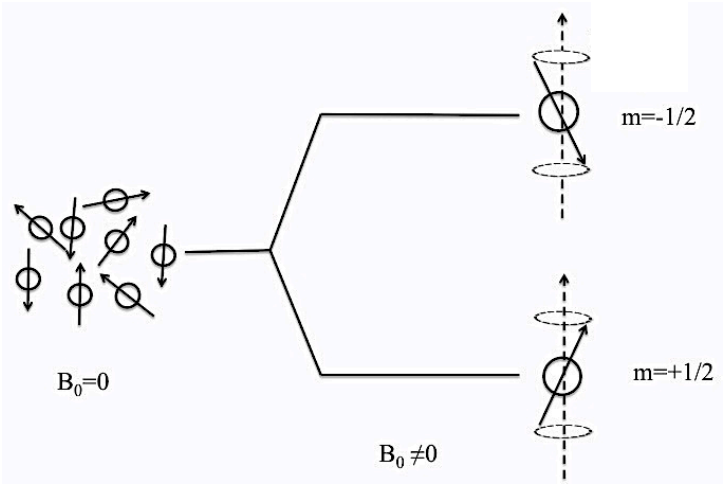

Figure 2.6. Schematic representation of the different energy levels associated with the presence of an external magnetic field B_0.

The population of nuclei is distributed according to the Boltzmann statistic as expressed in Equation 2.22 where k_B is the Boltzmann constant, T is the temperature in Kelvin and N_+ and N_- are the populations in the energy levels corresponding to $m = +1/2$ and $m = -1/2$ and ΔE is the difference in Energy between the two levels involved.

$$\frac{N_+}{N_-} = e^{-\Delta E/k_B T} \qquad \textit{Equation 2.22}$$

Since the energy difference between the two levels is very small the population is almost equally distributed, except for a small prevalence in the lowest energy level aligned with the applied B_0. Even if in a very small number, these nuclei are those that generate the signal in a NMR experiment. The sum of all nuclear

magnetic moments is M_0, which, due to the small excess of nuclei aligned with B_0, is going to be a small vector aligned with B_0.

In modern NMR instruments, the signal is generated with the so-called impulse technique in which the desired sample is immersed in a static magnetic field B_0. In this equilibrium condition, only M_0 possesses a Z component whereas there is no transverse magnetization (M_X, M_Y). A radiofrequency (RF) pulse is then applied along the XY plane, containing also the Larmor frequency corresponding to the energy difference between the energy levels. This will cause a change of the spin in an orientation opposite to that of the B_0 with a resulting increase in population of the excited energy level. From the macroscopic point of view, the vector M_0 will start a precession movement approaching the XY plane. Once the RF pulse is interrupted the nuclei in the sample will gradually come back to the equilibrium status emitting a signal that is called Free Induction Decay (FID), which can be recorded and transformed through a Fourier Transform into a graph as a function of Frequency known as an NMR spectrum. The time constant, which describes how M_z returns to the equilibrium value, is called the spin lattice relaxation time. It is due to the interaction of the energy emitted by the nucleus coming back to the equilibrium energy level and the dipoles of the surrounding lattice molecules. M_z can be defined as expressed in the Equation 2.23.

$$M_Z = M_0 \ (1 - e^{-t/T1}) \qquad \textit{Equation 2.23}$$

The most common NMR experiments use ^{1}H and ^{13}C NMR. Hydrogen NMR is used since it is a very common element in nature whereas ^{13}C is used in substitution of the more common ^{12}C isotope since ^{12}C possess a nuclear spin= 0. Both ^{1}H and ^{13}C possess a momentum of spin= 1/2 which make them good candidates for NMR experiments.

2.5.1 Chemical Shift

Unlike infrared and UV-vis spectroscopy where absorption peaks are identified by a frequency or a wavelength, the NMR signal coming from a particular nucleus is heavily influenced by the chemical surroundings. This is due to the electron cloud surrounding the nucleus which, being made of charged particles, generates a small induced magnetic field opposite to the much stronger applied B_0. As a result, the induced magnetic field shields the nucleus. For instance, in the case of ^1H if it is connected to atoms with a low electronegativity value, the bonding electrons are closer to the hydrogen atom, creating a higher shielding effect. Therefore this hydrogen nucleus will experience an energy transition at higher frequencies then the same hydrogen nucleus bonded to an atom with high electronegativity values. Historically, it was of general agreement to use the NMR peak arising from tetramethylsilane (TMS) as an internal reference in which hydrogens and carbons experience the highest shielding comparing to most of other organic molecules. Nowadays, modern spectrometers are able to reference spectra based on the residual protons in the solvent in use.

Since the chemical shift is also related to the magnitude of the applied frequency, in order to be able to compare experiments performed on different instruments, it has been decided to define the relative chemical shift δ. This makes the scale independent from the spectrometer frequency and more manageable, expressing it in part per million (ppm).

$$\delta \text{ (in ppm)} = \frac{\text{Frequency of Signal} - \text{Frequency of TMS in Hz}}{\text{Frequency of NMR spectrometer in MHz}}$$

For ^1H NMR the scale is usually from 0 to 12 ppm whereas for ^{13}C NMR it is generally larger, from 0 up to 200 ppm.

2.5.2 ^{1}H NMR

Proton NMR is the application of the NMR technique using the hydrogen present in the sample molecules to investigate their structure and properties using the phenomenon of the chemical shift explained in Section 2.5.1. Most common NMR samples are prepared in a deuterated solvent, in order not to cover the signal from the sample with signal coming from the solvent. Another characteristic of the proton NMR is the proportion between the number of hydrogen and the intensity of a particular NMR peak, which allows calculation of the number of protons contributing to a particular peak therefore experiencing the same chemical environment.

Another important phenomenon used in ^{1}H NMR as a source of information of the sample analysed is the so-called Spin-Spin splitting. This is due to the fact that during a ^{1}H NMR experiment the proton experiences two different magnetic fields, one arising from the shielded external magnetic field B_0 and the other coming from all the nuclei of the protons around. Spin-Spin splitting can only occur between non-equivalent protons, that is, between protons with different chemical shift. For instance, if a CH_3 group has only one non-equivalent hydrogen close by, which can have a parallel or non-parallel orientation compared to the external magnetic field and therefore the signal from the CH_3 portion of a molecule will be split into a doublet with virtually equal peak areas. In general, a proton signal will split in $n + 1$ peaks when n, is the number of non-equivalent hydrogens that are present.

2.5.3 ^{13}C NMR

Performing a carbon NMR [28] is not as straightforward as a simple ^{1}H NMR, as already anticipated in Section 2.5. Due to the zero spin possessed by the ^{12}C, the only way to examine the NMR signal from the carbon in a sample is to look at the signal of the ^{13}C isotope which unfortunately is not very abundant (only

1.1% abundance in nature) therefore very concentrated samples are required. Moreover the signal from carbon is almost 50 times lower in a ^{13}C NMR experiment than that from a proton. As in ^{1}H NMR the particular chemical shift may suggest the type of carbon giving rise to the particular peak, however in the ^{13}C case the intensity of the signal will not be proportional to the number of carbons contributing to the peak.

2.6 Other Techniques

2.6.1 Electron Microscopy Images: TEM and Cryo-TEM

The first light microscopes were developed in the early 1600's. Very interesting discoveries were made by the Dutch scientist Anton van Leeuwenhoek [29], who observed bacteria, blood cells and different structures within the animal cells using early microscopes.

Nowadays there are many microscopy techniques that have been classified into three main categories: optical, charged particles (electrons and ions) and scanning probe microscopes. The conventional optical microscopy, still very important for biological research, uses a light source and a system of one or more lenses that produce an enlarged picture of an object placed in the focal plane of the lenses. This technique has a limited resolution, around the size of a few μm because of the wavelength of radiation in use, which is between 400 nm and 780 nm. The angular resolution can be calculated from the *Rayleigh criterion* [30], express by Equation 2.24.

$$\vartheta = 1.22\frac{\lambda}{D} \qquad \textit{Equation 2.24}$$

Where: ϑ is the angular resolution expressed in radians, D is the diameter of the lens through which the objects are observed and 1.22 is a constant derived from the Bessel function.

Attention here will be focused on electron microscopy, which has been used in this project. In this type of microscopy a beam of charged particles is used instead of light and a system of electromagnetic lenses instead of the classical glass lenses.

The electron column consists of an electron gun and set of 5 or more electromagnetic lenses operating in vacuum. The TEM instrument could be divided into three components: the illumination system, the objective lens, and the imaging system. The illumination system comprises the gun and the condenser lenses and its role is to take the electrons from the source and to transfer them to the specimen.

The electron beam is accelerated to energy in the range 100-200 KeV in the electron gun for the standard TEM or, to get a better resolution, in the range of 500 KeV-3MeV in the high voltage electron microscopy (HVEM). The electron beam then passes through a set of condenser lenses in order to produce a beam of electrons with a desired diameter. The imaging system uses several lenses to magnify the image produced by the objective lens and to focus these on the viewing screen or computer display via a detector, CCD, or TV camera. Due to the fact that the instrument operates in a vacuum, any trace of water present in the sample evaporates; therefore it is usually removed during the sample preparation. Furthermore, most of the biological samples do not offer a good enough natural contrast so a stain is usually applied. Commonly a heavy metal salt such as uranyl acetate is used.

The inevitable disadvantage of this technique is the fact that samples can be damaged during their preparation giving therefore unreliable results. Alternatively, Cryo-TEM is used for analysis of biological samples. Samples for Cryo-TEM experiment are shock frozen allowing the sample to keep the same shape and dimension of which in the suspension. The fact that the sample has

not been manipulated permits observation of the true shape of the hydrated molecule that has not been distorted by attaching itself and flattening against the supporting film. Absence of the stain is also an advantage since the stain does not always spread evenly, which can generate artifacts and altered contrasts when reconstructing the structure of a sample.

2.6.2 Surface Tension

The cohesive forces between molecules in a liquid are responsible for a phenomenon known as surface tension. Molecules situated at the liquid surface are not surrounded by other molecules and as a consequence they interact more strongly with the molecules situated at their sides creating a "surface film". Typically the surface tension is measured in mN m^{-1} corresponding to the force necessary to break a film of 1 cm length equivalently it can also be expressed as energy for surface area (cm^2). Changes in the physical chemistry properties of the medium such as in the specific case studied here of a copolymer in solution cause changes in the surface tension. For instance the aggregation of the copolymer itself can be detected by studying the changes in the surface tension values. The Du Noüy method [31, 32] is one of the techniques by which it is possible to measure the surface tension. The method consists of slowly lifting a metal ring (usually platinum) from the surface of the liquid. The force necessary to lift the ring above the surface is measured and related to the surface tension γ, of the liquid through the relation expressed in Equation 2.25, where r_i represents the inner radius of the ring and $r_a$the outer radius.

$$F = 2\pi (r_i + r_a) \gamma \qquad \textit{Equation 2.25}$$

2.7 Instrument Specifications and Experimental Setups

2.7.1 SAXS Instruments

The SAXSess instrument, purchased from the Anton Paar Company, is located at the University of Bath, Chemistry Department Building 1 South. The X-ray source is a PANalytical PW3830 X-ray generator using a copper tube (40 kV/50 mA, λ= 0.1542 nm). The accessible q range is between q_{min} = 0.07 nm^{-1} and a q_{max}= 27 nm^{-1}. The scattering signal is detected with a two-dimensional imaging-plate detection system. There are 2 different reusable imaging plates small (SAXS) or large (SAXS/WAXS). The angles at which the scattered X-ray are detected can be selected between the small-angle X-ray scattering (SAXS) range (of about 2θ = 0.05° to 10°) and the small-and-wide-angle X-ray scattering (SWAXS) range (of about 2θ = 0.05° to 41°). The exposed imaging plates are then read out and converted into electronic pictures. The standard imaging-plate detection system is a Cyclone™, Storage Phosphor System from Perkin Elmer. The geometry of the irradiating beam can be switched between line and point collimations. The slit collimation has been selected over the point collimation setup. The advantage of this collimation system is the possibility to analyse isotropic samples using higher flux in shorter experiments. However due to the geometry of the collimation a de-smearing process of the data is required. The SAXSess instrument uses a semi-transparent beam stop to attenuate the direct beam intensity so that the zero angle can be found while preventing damage to the plate. A multilayer mirror that focuses the X-ray beam that comes divergently out from an X-ray tube makes the collimation system of this SAXSess. The X-ray path to the sample is kept below the 5 mbar pressure with the use of a vacuum pump. After calculating the 1D profile from the experimental 2D pictures with the use of the software SAXSquant 2D data were further processed using background and dark current subtraction and normalization steps.

The I22 SAXS instrument is located at Diamond Light Source (Didcot, Oxfordshire, UK). The Diamond Light Source is a synchrotron source, which

accelerates electrons to 3GeV. This instrument has an energy range between 3.7-20 KeV. The sample is located about 48 m from the source and 9 m from the detector in use, which is a Pilatus 2M. Temperature was controlled with the use of a water bath circulating through a copper capillary holder. Samples were held in 1.5 mm diameter borosilicate glass capillaries. Data collected were then reduced in situ with the use of the software Data Analysis WorkbeNch (DAWN) free reduction package [33].

2.7.2 SANS Instruments

LOQ [12] is one of the Small Angle Neutron Scattering instruments present at the ISIS Spallation Neutron Source run by the Science and Technology Facilities Council at the Rutherford Appleton Laboratory located in Harwell, Didcot (Oxfordshire, UK). LOQ is a time of flight instrument in which the beam passes through a 3 m evacuated guide where wavelengths less than 2 Å and higher than 12 Å are being removed. At the end of this first block of collimation, a second aperture is placed in order to define the sample beam size. The sample position is around 11 m from the moderator. Temperature was controlled with the use of two interchangeable water baths, which circulate fluid through a 20 positions sample changer. Samples were held in 1mm thick, 1cm wide single stopper quartz Hellma cells. Normally this instrument operates at 25 Hz with a wavelength between 2.2 and 10 Å. with a q range between 0.006 and 0.26 $Å^{-1}$. The detector in use is a ^{3}He-CF_4 filled Ordela, "area" detector 15.15 m from the moderator. The active area is 64 cm x 64 cm with 5 mm resolution. Data reduction software on this beam line used the Mantid open source software [34]. The data was normalised to absolute intensities using a standard TK49, which is a calibrated copolymer sample. Data were background subtracted prior to analysis.

The D11 [35] instrument is located at the Institute Laue Langevin (Grenoble, France). It receives neutrons from the cold source of the ILL high flux reactor,

which is situated about 100 m from the first part of the instrument (the selector) and about 140 m from the sample position. The polychromatic beam from the cold source is monochromated using a helical slot (ASTRIUM) velocity selector that selects neutrons of ±9% about a mean wavelength determined by the rotation speed of the drum. Neutrons are then collimated and directed toward the sample, which is situated 40 m far from the velocity selector. Temperature was controlled with a water bath, which circulated fluid through a 20 positions sample changer. Samples were held in 1mm thick, 1cm wide single stopper quartz Hellma cells. Water was used as a standard to calibrate data to an absolute intensity. Empty cells and all buffers were analysed in order to successively reduce the data. All samples and buffer were analysed using three detector-sample distances respectively of 1.204 m, 6.994 m and 13.495 m. Data collected from the three different setups were then combined to obtain a single pattern after correction for sample holder and background noise.

2.7.3 TEM and Cryo-TEM

- TEM on SMALPs

The standard sample preparation procedure was followed for the production of empty nanodiscs using the 6 kDa RAFT copolymer with DMPC in 50 mM phosphate buffer solution containing 200 mM NaCl at pH 8. Results were compared with the images taken of empty nanodiscs formed using the 7 kDa commercial copolymer (SMA 2000P) and DMPC also in phosphate buffer solution. For the 6 kDa SMALPs TEM imaging the following procedure was applied for the sample preparation: 20 µL of sample solution was deposited on a carbon-formvar coated grid (purchased from Agar Scientific) and left for 2 min. The excess was removed with filter paper, and the grid washed twice with 20 µl of distilled water to remove the phosphate buffer. Finally, in order to enhance the contrast of the nanodiscs, the background was negatively stained [36] by applying 20 µL of uranyl acetate (UA) solution in water, with the excess

removed with filter paper. Micrographs were taken at the Microscopy Analysis Suite of the University of Bath by Ursula Potter. The instrument in use was a TEM-JEOL, JEMI200EXII operating at 120 KV. The scale reported in the pictures was automatically inserted by the software.

❖ Cryo-TEM on SMALPs

The sample analysed was composed of empty nanodiscs made with the 6 kDa RAFT copolymer and 100% DMPC, in phosphate buffer at pH 8. The images were taken in Paris at the “Institut de Mineralogie et de Physique des Milieux Condensés” (IMPMC) Université Pierre et Marie Curie, by Dr. Jean Michel Guigner and Dr. Amani El Fagui. A drop of solution (0.1 wt% solid content) was deposited on a "quantifoil"® grid (Micro Tools GmbH, Germany) with a carbon membrane. The excess of solution was then blotted off with a filter paper and, before evaporation; the grid was quench-frozen in liquid ethane to form a thin vitreous ice film in which the nanodiscs were entrapped. The grid was then maintained all the time at 90K to prevent evaporation and crystallization of the ice film. A LaB6 JEOL JEM 2100 (JEOL, Japan) Cryo-TEM equipped with a cryo-pole piece and operating at 200 kV was used. The images were taken on an ultra-scan 2k CCD camera (GATAN, USA) and with a JEOL low dose system (Minimum Dose System, MDS) to protect the thin ice film from any irradiation before imaging and reduce the irradiation during the image capture.

2.7.4 Other Instruments

Dynamic Light Scattering (DLS) measurements were carried out in a commercially available instrument purchased from Malvern. The apparatus in use was a Zetasizer Nano ZS fitted with a 4 mW, 633 nm red laser source. Instrument & software specifications are described in Table 2.2.

Size Range (Diameter)	*Temperature Range*	*Analysis Algorithm*	*Minimum Volume*
0.6 nm to 6 μm	0 °C to 90 °C ± 0.1 °C	NNL, Proteins, Multiple narrow modes	12 μL

Table 2.2. Technical specification of the DLS instrument in use. Information taken from the Zetasizer user manual [37].

Gel filtration experiments were performed at 6 °C using a Superdex 200 10/300 GL column, with height of 30 cm, diameter of 1cm column volume of 23.562 mL, attached to an AKTA^{TM} purifier FPLC purification system (GE healthcare). A 500 μL loop was used, however 600 μL were injected to avoid air bubbles in the system. The flow rate was kept at 0.5 mL/min with a pressure value around 1.05 MPa, Sample fractions were collected in tubes of 16 mm diameter and 15 mL volume capacity.

A Copolymer Laboratories PL-GPC 50 integrated system was used to perform the GPC analyses. The column oven was maintained at 35 °C, using a PLgel 5μM MIXED-D 30 x 7.5 mm column, with THF as the eluent, at a flow rate of 1.00 mL/min. The system was calibrated against 12 narrow molecular weight polystyrene standards with the range of Mw from 1050 Da to 2650 kDa.

FTIR measurements were carried out on a PerkinElmer Spectrum 100 Series FT-IR spectrometer. A scan was performed on samples in powder form, using a pattern taken from air as background. Spectra were recorded from 4000 to 600 cm^{-1}.

Analysis performed via pH titrations were done using a Metrohom/Brinkmann 655 Dosimat, with a 50 mL burette cylinder, pH was recorded with a Mettler Toledo SevenMulti pH meter.

Surface Tension experiments were done on an Attension Force Tensiometer, Sigma 700/701, with use of a Du Noüy Ring that was flamed after dipping in ethanol before the experiment; surface tension of ultrapure water (72 m Nm^{-1}) was also recorded as instrumental calibration test. All measurements were conducted at room temperature.

All the NMR spectra were obtained using a Bruker 250.13 MHz, 300.22 MHz, 400.13 MHz or 500.13 MHz Avance NMR spectrometer (where specified). NMR samples were prepared either by dissolving PSMA in Acetone-d6 at concentrations of approximately 30 mg/mL, or by dissolving PSMAnh in d-THF as specified. All spectra acquired were internally referenced to the signal of the solvent in use, coupling constants are given in Hertz and chemical shifts are given in ppm. Peak integrals were calculated with the use of ACDLab software [38].

2.8 Models, Software and Data Analysis

Data collected in SANS and SAXS experiments have been analyzed with the use of the NIST SANS Analysis package [39] available within the IGORpro™ (Wavemetrics Inc.) version 6.32A. This software is designed for visualization, analysis, interpretation and presentation of experimental data.

2.8.1 Use of Standard Plots

One of the first tools that can be used to analyse SANS or SAXS data consists of a set of standard plots that allow some preliminary information to be obtained [40]. Looking at a scattering diagram in function of q can be compared to the use of a lens in the microscopy technique, being the power of the order of q^{-1}. Working at low q can be compared to using a low power magnifier glass and objects are seen as points. It is not possible to determine information about their structures but one can measure the molar mass. If one increase q in order to get q^{-1} of the order of the radius of gyration then one does not see the details of the shape or the structures but one can measure their dimensions. This is called the Guinier domain and allows to determine the radius of gyration of the analysed particles. The Guinier plot is obtained plotting *Ln(I)* versus q^2; the slope of the graph obtained gives the radius of gyration (R_g) of the scattering objects which represents the effective size of the scattering particles.
Another commonly used plot is the so-called Porod Plot [76], which involves plotting *Log(I)* versus *Log(q)*. The Porod plot gives information about the so-called fractal dimension of the scattering objects. The Porod region corresponds to a probed range smaller than the scattering objects. Fitting the plotted experimental data with a straight line, gives a slope, which will be related to the characteristics of the particular object investigated. At high q in the case of two-dimensional objects the scattering intensity follows the exponential behaviour expressed with the Equation 2.26 in which the exponent corresponds to the

slope of the graph. Whereas for surface fractals, the exponent (and the slope value) is considered equal to 6-α.

$$I(q) = q^{-\alpha} \qquad \textit{Equation 2.26}$$

A list of values and corresponding objects is given in Table 2.3. In the table values indicated refer to mass fractals, which is a polymer structure containing branching and crosslinking to form a 3D network. Values referring to the surface fractals are related to particles that do not possess a smooth surface but instead a so-called fractal (i.e. rough) surface.

Curve slope value for Mass Fractals	*Related Scattering Object Characteristics*
1	Rigid rod
5/3	Fully swollen coil
2	Linear gaussian chain
2.25	Branched copolymer
Curve slope Value for Surface Fractals	*Related Scattering Object Characteristics*
2	Disc
3 to 4	Rough interfaces
4	Smooth surfaces

Table 2.3. Table illustrating different possible values for slope calculated from a Porod plot and corresponding possible scattering objects.

Another important standard plot that has been used in this project to analyse in particular the copolymer solution data is the so-called Kratky plot. This type of plot involves graphing $q^2 I(q)$ versus q. To better clarify this concept three different cases are reported in Figure 2.7.

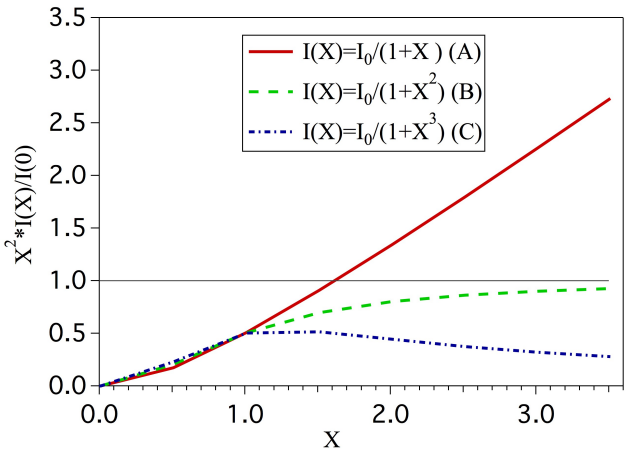

Figure 2.7. Representation of plot for: A) a rigid rod B) a Gaussian chain and C) a mass fractal. X is a dimensionless variable defined as X= q ×ξ, where ξ is a characteristic length of the system such as the radius of gyration.

Figure 2.7 shows how the Gaussian chain curve tends to 1 whereas in the case of branched systems it reaches a maximum and then it decreases. Stiff rods tend instead to show a linear increasing behaviour.

2.8.2 Copolymers Data

For the analysis of the copolymers in solution, data were plotted using Porod and Kratky plots to extrapolate preliminary information about their shape in solution. For copolymer data collected in the SANS experiments performed on the LOQ instrument, these preliminary analyses showed the copolymers in deuterated buffer solution to be in a swollen coil conformation with Porod slope values between 1.66 and 2. Data were fitted with a variety of different models. Indeed due the solvent characteristics, the copolymers were not expected to be in a completely stretched conformation. The best results were obtained with the use of a form factor expressed by the Debye function [41] expressed in Equation 2.28. This model has a scattering factor given in Equation 2.27.

$$\frac{d\Sigma}{d\Omega} = \text{scale} \times D(x) + \text{Background} \qquad \textit{Equation 2.27}$$

Where:

$$D(x) = \frac{2(e^{-x} + x - 1)}{x^2} \qquad \textit{Equation 2.28}$$

D(x) in Equation 2.28 represents the form factor of a linear copolymer in dilute solution in a theta solvent, in which $x = (q \times R_g)^2$ the scale factor (Equation 2.29) is composed of the copolymer volume fraction ϕ; scattering contrast between the copolymer and the solvent $\Delta\rho$; the concentration of monomers Z and the volume of one monomer V_m.

$$\text{scale} = \phi \times (\Delta\rho)^2 \, Z V_m \qquad \textit{Equation 2.29}$$

For copolymer data collected on SAXS instrument I22 best fitting results were obtained with the use of a straight cylinder model with polydisperse radius. This model calculates the form factor of a straight cylinder averaged over all the possible orientations. Since the solutions were dilute no structure factor was used. The form factor is expressed in the Equation 2.30.

$$P(Q) = \frac{\text{scale}}{V_{poly}} \int_0^x f(r)dr \int_0^{\pi/2} F^2(Q, \alpha) \sin\alpha \, d\alpha \qquad \textit{Equation 2.30}$$

Where the scale is a multiplicative factor. The straight cylinder is expressed in the second integral where the function F(q, α) is defined in Equation 2.31. In order to average among all possible cylinder orientations the angle between the cylinder main axis and the scattering vector q is defined as α; the radius of the cylinder is defined as r and the length of the cylinder is defined as $2H$; the contrast is defined as the difference between the SLD of the cylinder ρ_{cyl} and the SLD of the solvent ρ_{solv}. The term J indicates the zero and first order of the Bessel function, being $J_0 = Sin(x)/x$.

$$F(q, \alpha) = 2V_{cyl}(\rho_{cyl} - \rho_{sov}) J_0(qH\cos\alpha) \frac{J_1(qr\sin\alpha)}{qr\sin\alpha} \qquad \textit{Equation 2.31}$$

The volume of the object V_{poly} is calculated from the radius of the object and is also influenced by the polydispersity on the radius. The formula for the polydispersity term is reported in Equation 2.32.

$$V_{poly} = \pi r^2 L \left(\frac{z+2}{z+1}\right) \qquad \textit{Equation 2.32}$$

The term within parentheses comes from the Shultz distribution function applied for the polydispersity on the radius.

The 6 kDa RAFT copolymer in phosphate buffer solution showed a different behaviour when measured on the SAXSess instrument in the Chemistry Department of Bath University. The sample was also analysed with standard plot, which showed aggregates not in rod-like shapes as found for the previous copolymers but in more spherical shapes. Optimal fitting of the data was obtained using a model combining a polydisperse core-shell sphere with aHayter Penfold [42] charged sphere approximation to take into account the interparticle interaction effect due to the screened Coulomb repulsion between them. The model was combined to a larger solid sphere model with Shultz polydispersity on the radius. This model calculates the form factor for a polydisperse population of spherical particles in which the polydispersity of the radii is calculated using a Shultz distribution function.

The intensity for a solid sphere is calculated as expressed in the Equation 2.33; in which *f(R)* express the Shultz distribution related to the radius polydispersity, N_0 is the total number of particles for unit volume having size between *R* and *R+dR* being *R* the particle radius; $\Delta\rho$ expresses the contrast given by the difference between the scattering length density (SLD) of the copolymer and the SLD of the solvent.

$$I(q) = \left(\frac{4\pi}{3}\right)^2 N_0 \Delta\rho^2 \int_0^\infty f(R)\, R^6\, F^2(q,R)\, dR \qquad \textit{Equation 2.33}$$

F(q;R) indicates the scattering amplitude for a solid sphere expressed in Equation 2.34.

$$F(X) = \frac{\sin(x) - x\cos(x)}{x^3} \qquad \textit{Equation 2.34}$$

Core-shell sphere calculates the form factor of the core plus the shell. The function is expressed in Equation 2.35.

$$P(Q) = \frac{scale}{V_s}\left[\frac{3V_c(\rho_c - \rho_s)J_1 qr_c}{qr_c} + \frac{3V_c(\rho_s - \rho_{solvent})J_1 qr_s}{qr_s}\right]^2 + Bkg \qquad \textit{Equation 2.35}$$

Where: $J_1(x) = sinx - xcosx/x^2$;r_s=r_c+t; *Vs* is the volume of the sphere calculate with the $V_{i=(4\pi/3)}r_i{}^3$ which defines the volume of the i-sphere; ρ indicates the scattering length density of respectively the sphere shell (ρ_s), the sphere core (ρ_c) and the solvent ($\rho_{solvent}$).

A schematic representation of the core-shell sphere model is given in Figure 2.8.

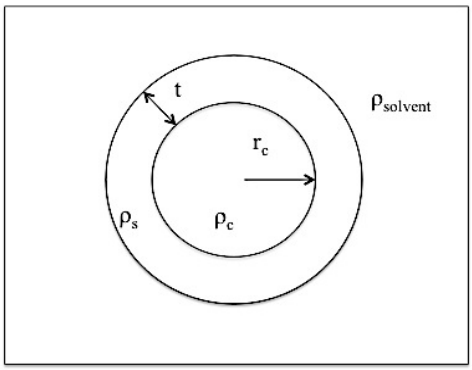

Figure 2.8. Schematic representation of the core-shell model. Where ρ indicates the scattering length densities of respectively the core, the shell and the solvent and t indicates the thickness of the shell.

2.8.3 SMALPs Data

Protein-stabilized nanodiscs closely resemble the HDLs [35] since the scaffold protein that controls their diameter derives from the Apo-AI.

HDLs have been extensively studied [43-48] in order to understand their structural and dynamic characteristics. As explained in detail in Chapter one, among the past thirty years of studies, a number of different models for the discoidal HDLs have been proposed [49-52]. Following these studies, nanodisc structures have been analysed with a wide range of techniques, SAXS and SANS [53-56], NMR [35, 57-59], molecular dynamic simulations [56, 60-62] and Atomic Force Microscopy [63], which generated the generally accepted theory of a circular disk-like structure of the nanodisc. However, the way the protein belt is wrapped around the phospholipid core is still under debate [64, 65]. Also, it is yet to be fully decided whether the nanodisc is a discoidal structure with circular cross-section, a discoidal structure with ellipsoid section or a prolate lipid core surrounded by a double super helical Apo A-I. A schematic representation of the proposed structures is reported in Figure 2.9.

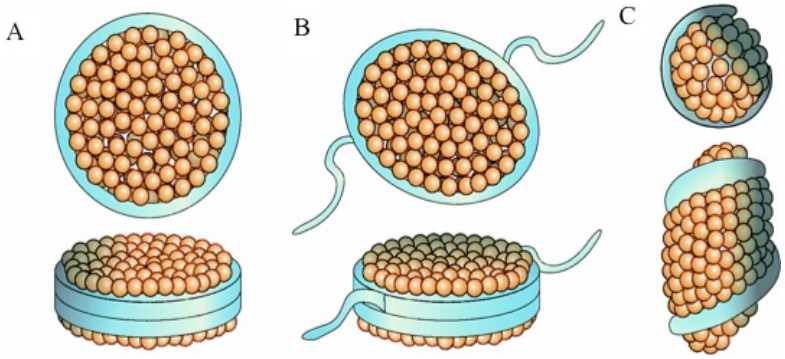

*Figure 2.9. Different suggested models for HDLs and protein-stabilised nanodiscs. Structures are showed from two different directions (top and side) A) Discoidal nanodiscs with circular cross section [53, 54, 66]. B) Discoidal nanodiscs with elliptical cross section and protruding His-tags [67] *; C) Double super helical Apo A1 with prolate core [68]. * A His-tag is an amino acid motif in proteins consisting of at least 6 histidine (a human amino acid) residue often located at the end of the protein. Reprinted with permission from (Skar-Gislinge, N.; Simonsen, J.; Mortensen, K.; Feidenhans'l, R.; Sligar, S.; Lindberg Møller, B.; Bjørnholm, T.;*

Arleth, L., Elliptical structure of phospholipid bilayer nanodiscs encapsulated by scaffold proteins: casting the roles of the lipids and the protein. In J Am Chem Soc, 2010; Vol. 132, pp 13713-13722). Copyright (2014) American Chemical Society [67].

In 2010, Skar-Gisliege and colleagues [67] optimised a new model for the fitting and interpretation of SANS and SAXS data which confirmed the theory already anticipated through the twisted-belt model [65] of an elliptical cross section disc. Contrary to the models previously used, this new approach (based on a previously proposed model [57]) was based on the separation of the singular nanodiscs components (phospholipids heads, protein belts and so on). Analysis and results obtained for the protein-stabilised nanodiscs were taken as a reference point for the analysis and experiments performed on the SMALP structures.

In this study, SMALPs data from SANS and SAXS experiments were fitted to a model of a core-shell cylinder, the core radius was convoluted by a Shultz (see Section 2.8.1) distribution to add polydispersity; model also includes a "face" layer on top and bottom to take into account the phospholipid headgroups. The fitting calculates the water content of head groups (constituting the faces of the cylinder) and in the copolymer (constituting the rim of the structure) based on the respective scattering length densities of head groups, copolymer and solvent in use. Calculations were done using the following expression:
$SLD_{fitting} = X \times (SLD_{solvent}) + (1-X) \times (SLD_{calculated})$ in which the $SLD_{calculated}$ is the calculated scattering length density for the copolymer belt or the head groups region with the assumption of no solvent penetration, $SLD_{fitting}$ is the scatting length density resulting from fitting of experimental data and finally X represents the mol% of solvent within the considered SMALP region.
A list of the main parameters in use in the model routine is here presented:

- Mean core radius: gives the radius of the phospholipids core constituting the core of the cylinder. This parameter was fitted.
- Radial polydispersity: is referred to the polydispersity of the cylinder radius. This parameter was fitted.

- Core length: indicates the length of the phospholipids acyl chains not including the thickness of the heads. This parameter was fitted.
- Radial shell thickness: indicates the thickness of the copolymer belt wrapped around the phospholipids core. This parameter was fitted.
- Face shell thickness: is constituted of phospholipids heads on the top and bottom of the cylinder. This parameter was fitted.
- SLD rim: represents the scattering length density of the copolymer belt. This parameter is inserted into the code routine and kept constant during fitting.
- SLD core: represents the scattering length density of the phospholipid chains. This parameter was fitted to take into account polymer penetration within the core, which was calculated with the following formula: $SLD_{fitting} = X \times (SLD_{poly}) + (1 - X) \times (SLD_{calculated})$ in which the $SLD_{calculated}$ is the calculated, or reported from the literature, scattering length density for the phospholipids tails with the assumption of no polymer penetration, $SLD_{fitting}$ is the scatting length density resulting from fitting of experimental data and finally X represents the mol% of styrene within the considered SMALP region.
- SLD face: is the scattering length density of the head groups of the phospholipids chains. This parameter is inserted into the code routine and held during fitting when specified.
- Mol% solvent in rim: represents the amount of solvent penetrated into the copolymer belt. It is calculated by the model with the use of the formula $SLD_{fitting} = X \times (SLD_{solvent}) + (1 - X) \times (SLD_{calculated})$ in which the $SLD_{calculated}$ is the calculated scattering length density for the copolymer belt with the assumption of no solvent penetration, $SLD_{fitting}$ is the scatting length density resulting from fitting of experimental data and finally X represents the mol% of solvent within the considered SMALP region.

- SLD solvent: it represents the scattering length density of the phosphate buffer solution in which SMALPs were assembled. This parameter is fixed and only sometimes fitted to take into account a not perfect deuteration.

- Charge: this parameter represents the charge possessed by SMALPs also caused by the use of heads-charged phospholipids. This parameter was fitted.
- Salt concentration: is constituted by the concentration of phosphate buffer and NaCl in use in the buffer.
- Temperature: is the temperature at which the samples were analysed. This parameter was held during fitting.
- Dielectric constant: is the dielectric constant of the solvent in use, the value of water was here used being the solvent constituted by 99% of water. This parameter was held during fitting.

Model parameters also include volume fraction and incoherent background.
The interactions between discs were fitted using a Hayter Penfold [42] charged sphere approximation. A schematic representation of the model is reproduced in Figure 2.10. The Hayter Penfold routine allows calculation of the structure factor for a system composed of charged particles in a dielectric medium. In this way it is possible to take into account the interparticle interaction effect due to the screened Coulomb repulsion between them. It uses the salt concentration parameter to calculate the ionic strength of the solution. All the scattering length densities parameters were calculated and held when specified; a summary of the values held during fitting is reported in Appendix A4.

When otherwise fitted the values calculated or reported from the literature were taken into consideration for structural analysis such for instance the copolymer penetration in the core, as earlier specified.

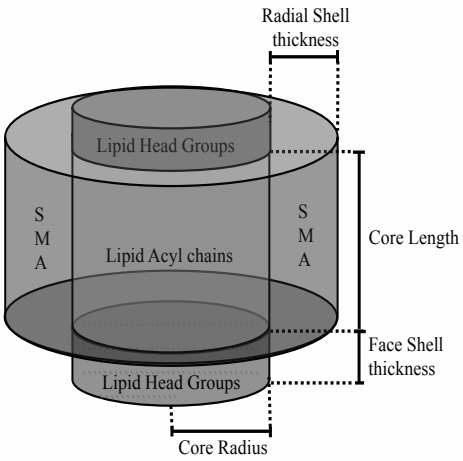

Figure 2.10. Schematic representation of the model used to fit SMALPs experimental data, highlighting all the different parts of the structures that were analysed. Picture reproduced with author's permission from reference [69].

In order to investigate whether the SMALP structure had an elliptical section a model of a core shell cylinder with elliptical cross section was also tested to fit the data. The model included faces to take into account the phospholipids heads and a Hayter Penfold charged sphere approximation for the structure factor that acted as previously reported. Although it was possible to fit the data using this model, results showed the maximum and the minimum radius to be around the same value proving the circular shape of the structures. Therefore the circular cylindrical model was used in preference since it contained fewer variables and could fit the data equally well.

In 2010 [70] and 2009 [71], Myazaki et al. showed how the protein-stabilised nanodiscs assembled with 1-palmitoyl-2-oleyl-sn-glycero-3-phopshocholine (POPC) and Apo A-1 no longer forms planar bilayer but instead possessed negative curvature.

Curvature can be altered either by changing the overall repulsive force among charged head groups or by modifying the chain region (as described in Chapter 1 Section 1.2.3). In order to probe the presence of curvature in SMALPs samples prepared with the use of a mixture of negatively charged phospholipids (DMPG) and DMPC (samples preparation, composition and data collection are

described in Chapter 5 Section 5.3.2) scattering data from these samples were analysed with an *ad hoc* model which description is reported in Appendix A1. However results suggested that SMALPs did not possess any curvature and the model was therefore abandoned in favour of the core-shell cylinder model previously describe.

2.8.4 TEM and Cryo-TEM Pictures Analysis

Analysis of the pictures obtained from the TEM and CryoTEM experiments was done with the aid of several pieces of software. Pictures were first manipulated with the use of the software GIMP, which is a GNU [72] (a Unix-like operating system) image manipulation program freely distributed [63]. An average of 85 particles for TEM and 255 particles for Cryo-TEM were highlighted with the use of an ellipsoidal selector. The selected shapes were transformed to a 2-colour image (black particles on a white background) in order to facilitate the analysis in the next step, by enabling the software to take into consideration only the desired particles.

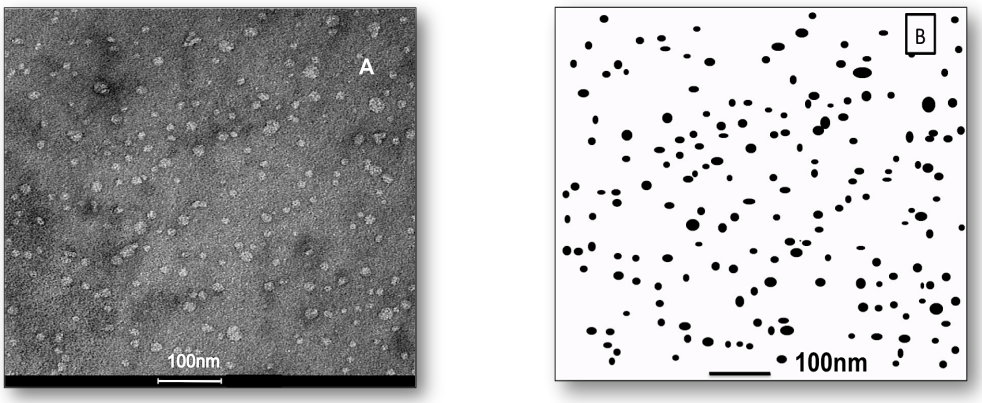

Figure 2.11. Example of first step of the protocol followed to analyse TEM and CryoTEM images. The left hand picture is a TEM image of nanodiscs made with 7 kDa commercial copolymer and DMPC. The original picture (A) Only the particles of interest are selected with the aid of the software GIMP to convert the image into black discs on a white background picture (B).

Considering the non-spherical shape of particles, the concept of *Feret's* diameter was applied [73]. The Feret diameter is defined as the maximum distance between two parallel lines on the opposite side of a randomly orientated particle, at a specific angle. The black-and-white pictures were analysed using the software ImageJ in order to obtain the Feret's diameter values for each object measured.
ImageJ is an image-processing program, which is also freeware [74, 75].

To provide a more realistic representation, the minimum Feret diameter was also calculated giving a range of particle sizes, which reflects the condition of the sample. Finally, values obtained for the maximum and minimum Feret diameter were converted into a distribution of number of particles for a particular diameter with the use of OriginLab, a data analysis and graphing software, which can be purchased online [53]. An example of table data obtained is reported in Table 2.4. These distributions were plotted as a function of the maximum Feret's diameter as a histogram, and then fitted using the IGORpro™ (Wavemetrics Inc.) software to a Gaussian distribution. An example is reported in Figure 2.12.

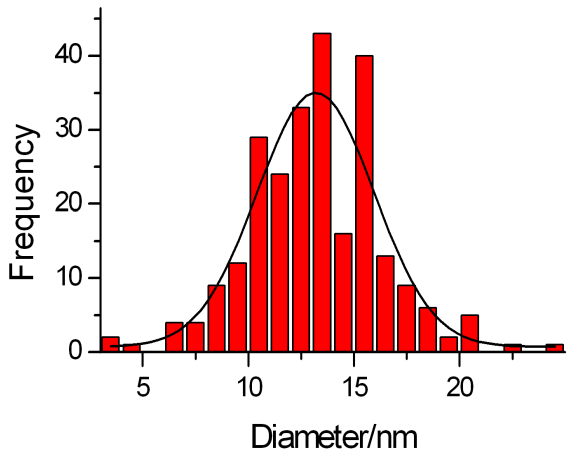

Figure 2.12. Histogram of experimental data from a Cryo-TEM analysis performed on a sample of SMALPs assembled with 6 kDa copolymer and h-DMPC. Data are fitted to a Gaussian distribution (continuous black line).

Diameter (nm)	*Frequency*
2	3.5
1	4.5
0	5.5
4	6.5
4	7.5
9	8.5
12	9.5
29	10.5
24	11.5
33	12.5
43	13.5
16	14.5
40	15.5
13	16.5
9	17.5
6	18.5
2	19.5
5	20.5
0	21.5
1	22.5

Table 2.4. Values obtained from a statistical analysis of the Cryo-TEM image reported in Figure 2.11. In column one are listed the maximum Feret Diameters and in column two the corresponding frequencies.

2.9 Summary

The present chapter concludes the theoretical introduction to the work presented in this thesis. All the techniques here described are quite versatile and their application is very broad, however for the purpose of this work it has been chosen to apply the surface tension, GPC, FTIR and NMR analyses exclusively to the analysis of the copolymer whereas DLS, SANS, SAXS, EM and gel filtration experiments were predominantly used to characterise SMALP samples.

The following chapters present the core of the experimental work performed on both copolymer solutions and SMALPs. The reader should approach the following chapters considering that Chapter 3 and Chapter 4 are strictly connected and partially overlap each other on the work performed on the copolymer belt surrounding the SMALPs core. Whereas Chapter 5 focuses on the assemble of SMALPs with use of different lipids, although this chapter is quite independent the work performed is still strictly connected to the work presented on Chapter 4.

2.10 References

1. Rutherford, E., *The scattering of α and β particles by matter and the structure of the atom.* Philos. Mag., 2012. **92**(4): p. 379-398.
2. Hippert, F., *Neutron and X-ray Spectroscopy.* 2006: Springer.
3. Christillin, P., *Nuclear Compton scattering.* J. Phys.G: Nucl. Phys, 1986. **12**(9): p. 837.
4. Zemb, T. and P. Lindner, *Neutrons, X-rays and light: scattering methods applied to soft condensed matter* 2002: Elsevier.
5. Guinier, A., *La diffraction des rayons X aux très pétits angles: applications à l'etude de phénomènes ultramicroscopiques*, Thèse Univ. Paris ,1939.
6. Guinier, A. and G. Fournet, *Small-angle scattering of X-rays*. Structure of matter series, 1955, New York: Wiley. 268
7. Sears, V.F., *Neutron scattering lengths and cross sections.* Neutron News, 1992. **3**(3): p. 26-37.
8. Debye, P., *Molecular-weight Determination by Light Scattering.* J. Phys. Colloid Chem., 1947. **51**(1): p. 18-32.
9. Mishra, V.K.R., *Living Radical Polymerisation: a Review,* 2012: p. 1-36.
10. Gabriella Carini, P.D., Sol Gruner, *Neutrons and X-ray detectors*, in *Report of the Basic Energy Sciences Workshop on Neutron and X-ray Detectors,* 2012, U.S. department of Energy office of science.
11. Kraft, P., *PILATUS 2M A Detector for Small Angle X-ray Scattering*, 2010, ETH Zurich.
12. Heenan, R.K., et al., *SANS at Pulsed Neutron Sources: Present and Future Prospects.* J. Appl. Crtstallogr., 1997. **30**(6): p. 1140-1147.
13. Schärtl, W., *Light Scattering from Polymer Solutions and Nanoparticle Dispersions: With 16 Tables*. Springer Laboratory, 2007: Springer.
14. Pecora, R., *Dynamic light scattering : applications of photon correlation spectroscopy,* 1985, New York: Plenum Press.
15. Lindsay, S., *Introduction to Nanoscience,* 2009: OUP Oxford.

16. Whittaker, G., et al., *Instant Notes in Physical Chemistry*. Instant Notes, 2004: Taylor & Francis.
17. Mori, S.B.H.G., *Size exclusion chromatography.* 1999, Berlin; New York: Springer.
18. Ruthven, G.H.L.a.C.R.J., *The separation of substances and estimation of their relative molecular sizes by the use of columns of starch in water.* Biochem. J., 1956. **62**(4): p. 665-674.
19. Lathe, G. and C. Ruthven, *The separation of substances and estimation of their relative molecular sizes by the use of columns of starch in water.* Biochem. J., 1956. **62**(4): p. 665-674.
20. Hagel, L., *Gel Filtration*. in *eLS,* 2001, John Wiley & Sons, Ltd.
21. Phillips, M., *André M. Striegel, Wallace W. Yau, Joseph J. Kirkland, and Donald D. Bly (Eds.): Modern size-exclusion liquid chromatography. Practice of gel permeation and gel filtration chromatography, 2nd ed.* Anal Bioanal Chem, 2011. **399**(4): p. 1571-1572.
22. Hollas, J.M., *Basic atomic and molecular spectroscopy*. Tutorial Chemistry Text, ed. C. Royal Society of Chemistry, 2002.
23. Skoog, D.A.S.D.A., *Analytical chemistry : an introduction,* 2000, Fort Worth: Saunders College Pub.
24. Larkin and P. Larkin, *Infrared and Raman Spectroscopy,* 2011.
25. Berthomieu, C. and R. Hienerwadel, *Fourier transform infrared (FTIR) spectroscopy.* Photosynth Res, 2009. **101**(2-3): p. 157-170.
26. Friebolin, H., *Basic one-and two-dimensional NMR spectroscopy* 1998, Weinheim; New York: WILEY-VCH.
27. Carbajo, R.J.N.J.L., *NMR for chemists and biologists,* 2013, Dordrecht; New York: Springer.
28. Wehrli, F.W.M.A.P.W.S., *Interpretation of carbon-13 NMR spectra,* 1988, Chichester; New York: Wiley.
29. Dobell, C., *Antony Van Leeuwenhoek And His 'Little Animals',* 1960, New York, NY: Dover Publications.
30. Born, M., et al., *Principles of Optics: Electromagnetic Theory of Propagation, Interference and Diffraction of Light.* 2002, Cambridge University Press.

31. du Nouy, P.L., *A New Apparatus for Measuring Surface Tension.* J. Gen. Physiol. 1919. **1**(5): p. 521-4.
32. du Nouy, P.L., *An Interfacial Tensiometer for Universal Use.* J. Gen. Physiol. 1925. **7**(5): p. 625-31.
33. Carothers, W.H., J.Am.Chem.Soc., 1928. **51**(2548).
34. Project, M., *Mantid (2013): Manipulation and Analysis Toolkit for Instrument Data*, 2013.
35. Li, Y., et al., *Structural Analysis of Nanoscale Self-Assembled Discoidal Lipid Bilayers by Solid-State NMR Spectroscopy.* Biophys. J., 2008. **91**(10): p. 3819-3828.
36. Zhang, L., et al., *Optimized negative-staining electron microscopy for lipoprotein studies.* Biochim Biophys Acta, 2013. **1830**(1): p. 2150-9.
37. *Zetasizer nano series manual*, 2004: England.
38. *ACD/NMR Processor Academic Edition*, in *Advanced Chemestry Development,INC*, I. Advanced Chemistry Development, Editor 2013: Toronto,Ontario, Canada. p. http://www.acdlabs.com.
39. Kline, S.R., *Reduction and analysis of SANS and USANS data using IGOR Pro.* Journal of Applied Crystallography, 2006. **39**(6): p. 895-900.
40. Hammouda, B., *Probing Nanoscale Structures: The SANS Toolbox* http://www.ncnr.nist.gov/staff/hammouda/the_SANS_toolbox.pdf, 2008: National Instutute of Standards and Technology, Centre for Neutron Research Gaithersburg.
41. Pedersen, J.S., *Form factors of block copolymer micelles with spherical, ellipsoidal and cylindrical cores.* Journal of Applied Crystallography, 2000. **33**(3-1): p. 637-640.
42. Hansen, J.-P. and J.B. Hayter, *A rescaled MSA structure factor for dilute charged colloidal dispersions.* Mol. Phys, 1982. **46**(3): p. 651-656.
43. Segrest, J.P., et al., *A detailed molecular belt model for apolipoprotein A-I in discoidal high density lipoprotein.* J. Biol. Chem., 1999. **274**(45): p. 31755-8.
44. Segrest, J.P., et al., *Detailed molecular model of apolipoprotein A-I on the surface of high-density lipoproteins and its functional implications.* Trends Cardiovasc Med, 2000. **10**(6): p. 246-52.

45. Jones, M.K., et al., *Assessment of the Validity of the Double Superhelix Model for Reconstituted High Density Lipoproteins: a combined computational-experimental approach.* J. Biol. Chem., 2010. **285**(52): p. 41161-41171.
46. Catte, A., et al., *Structure of Spheroidal HDL Particles Revealed by Combined Atomistic and Coarse-Grained Simulations.* Biophys. J., 2008. **94**(6): p. 2306-2319.
47. Sevugan Chetty, P., et al., *Apolipoprotein A-I helical structure and stability in discoidal high-density lipoprotein (HDL) particles by hydrogen exchange and mass spectrometry.* Proceedings of the National Academy of Sciences, 2012. **109**(29): p. 11687-11692.
48. Segrest, J.P., et al., *Validation of previous computer models and MD simulations of discoidal HDL by a recent crystal structure of apoA-I.* J. Lipid Res., 2012. **53**(9): p. 1851-1863.
49. Brouillette, C.G. and G.M. Anantharamaiah, *Structural models of human apolipoprotein A-I.* Biochim. Biophys. Acta, Lipids Lipid Metab., 1995. **1256**(2): p. 103-129.
50. Koppaka, V., et al., *The structure of human lipoprotein A-I. Evidence for the "belt" model.* J Biol Chem, 1999. **274**(21): p. 14541-4.
51. Segrest, J.P., *Amphipathic helixes and plasma lipoproteins: thermodynamic and geometric considerations.* Chem Phys Lipids, 1977. **18**(1): p. 7-22.
52. Klon, A.E., et al., *Molecular belt models for the apolipoprotein A-I Paris and Milano mutations.* Biophys J, 2000. **79**(3): p. 1679-85.
53. Denisov, I., et al., *Directed self-assembly of monodisperse phospholipid bilayer nanodiscs with controlled size.* J Am Chem Soc, 2004. **126**(11): p. 3477-3487.
54. Nakano, M., et al., *Static and Dynamic Properties of Phospholipid Bilayer Nanodiscs.* Journal Of The American Chemical Society, 2009. **131**(23): p. 8308-8312.
55. Denisov, I., et al., *Thermotropic phase transition in soluble nanoscale lipid bilayers.* J. Phys. Chem. B, 2005. **109**(32): p. 15580-15588.
56. Shih, A., et al., *Assembly of lipids and proteins into lipoprotein particles.* J. Phys. Chem. B, 2007. **111**(38): p. 11095-11104.

57. Gluck, J.M., et al., *Integral membrane proteins in nanodiscs can be studied by solution NMR spectroscopy.* J Am Chem Soc, 2009. **131**(34): p. 12060-1.
58. Shenkarev, Z.O., et al., *Lipid−Protein Nanodiscs as Reference Medium in Detergent Screening for High-Resolution NMR Studies of Integral Membrane Proteins.* J. Am. Chem. Soc., 2010. **132**(16): p. 5628-5629.
59. Kijac, A., et al., *Lipid−Protein Correlations in Nanoscale Phospholipid Bilayers Determined by Solid-State Nuclear Magnetic Resonance.* Biochemistry, 2010. **49**(43): p. 9190-9198.
60. Shih, A.Y., et al., *Molecular Dynamics Simulations of Discoidal Bilayers Assembled from Truncated Human Lipoproteins.* Biophys. J., 2005. **88**(1): p. 548-556.
61. Jones, M.K., et al., *Thermal Stability of Apolipoprotein A-I in High-Density Lipoproteins by Molecular Dynamics.* Biophys. J., 2009. **96**(2): p. 354-371.
62. Catte, A., et al., *Novel Changes in Discoidal High Density Lipoprotein Morphology: A Molecular Dynamics Study.* Biophys. J., 2006. **90**(12): p. 4345-4360.
63. Blanchette, C.D., et al., *Atomic force microscopy differentiates discrete size distributions between membrane protein containing and empty nanolipoprotein particles.* Biochim. Biophys. Acta, 2009. **1788**(3): p. 724-31.
64. Wu, Z., et al., *The low resolution structure of ApoA1 in spherical high density lipoprotein revealed by small angle neutron scattering.* J. Biol. Chem., 2011. **286**(14): p. 12495-508.
65. Thomas, M.J., et al., *three dimensional models of high density lipoprotein apoa-i: implications for its assembly and function.* J. Lipid Res., 2008: p. 1-24.
66. Shih, A.Y., et al., *Disassembly of nanodiscs with cholate.* Nano Lett, 2007. **7**(6): p. 1692-6.
67. Skar-Gislinge, N., et al., *Elliptical structure of phospholipid bilayer nanodiscs encapsulated by scaffold proteins: casting the roles of the lipids and the protein.* J. Am. Chem. Soc., 2010. **132**(39): p. 13713-22.

68. Wu, Z., et al., *Double Superhelix Model of High Density Lipoprotein.* J. Biol. Chem., 2009. **284**(52): p. 36605-36619.
69. Jamshad, M., Grimard V.*, Idini, I. *, Knowles,T.J:, Dowle; M., et al., *Structural analysis of a nanoparticle containing a lipid bilayer used for detergent-free extraction of membrane proteins.*, 2014, Nano Research.
70. Miyazaki, M., et al., *Static and dynamic characterization of nanodiscs with apolipoprotein A-I and its model peptide.* J Phys Chem B, 2010. **114**(38): p. 12376-82.
71. Miyazaki, M., et al., *Smaller Discoidal High-Density Lipoprotein Particles Form Saddle Surfaces, but Not Planar Bilayers.* Biochemistry, 2009. **48**(32): p. 7756-7763.
72. Amant, K.S. and B. Still, *Handbook of Research on Open Source Software: Technological, Economic, and Social Perspectives*. IGI Global research collection, 2007: Information Science Reference.
73. Merkus, H., *Microscopy and Image Analysis*, in *Particle Size Measurements,* 2009, Springer Netherlands. p. 195-217.
74. Schneider, C.A., et al., *NIH Image to ImageJ: 25 years of image analysis.* Nature methods, 2012. **9**(7): p. 671-5.
75. Wadsater, M., et al., *Aligning nanodiscs at the air-water interface, a neutron reflectivity study.* Langmuir, 2011. **27**(24): p. 15065-15073.
76 Hammouda, B., *Small-Angle Scattering From Branched Polymers.* Macromolecular Theory and Simulations, 2012. **21**(6): p. 372-381.

3

3 Characterisation of Poly (Styrene-Alt-Maleic Acid) Copolymers Used in SMALP Formulation

3.1 Introduction

The previous chapter described the first studies performed on the new nanodiscs formulation called SMALPs (Styrene-alt-Maleic Acid Lipid Particles), giving in the last few paragraphs particular relevance to the role of the polymer in the nanodiscs self-assembly process and in the structure control.

In this chapter, attention is focused on the study of the polymeric part of SMALPs. Indeed the understanding of the physical and chemical properties of the polymer is strictly related to the comprehension of the formation of the SMALP structure and its stability. After an introduction dedicated to the most common polymerisation techniques, the core of this chapter draws the attention specifically on the styrene-alt-maleic acid (SMA) copolymer synthesis.
The second part of the chapter reports the analyses performed on the SMAs in order to elucidate their structural characteristics and properties that allow the SMALPs assembly process.
The work is then completed by a systematic study on the SMAs behaviour under different environmental conditions such as temperature, pH or salt concentration. In particular this last part is strictly related to the analyses performed on the SMALP structures with the attempt to link the properties of the copolymer itself to the SMALPs behaviour under the same environmental conditions.

3.2 General Introduction to Polymers

3.2.1 Terminology

The name *polymer* comes from the Greek *poly* (many) and *mer* (part). It refers to a class of large molecules made up of simply repeating units called *monomers* [1] covalently linked together. Polymers can be classified in two sub-categories: synthetic and natural polymers. Naturally occurring polymers include proteins, nucleic acids or carbohydrates whereas synthetic polymers [2] are, for example, polystyrene, nylon, and low or high-density polyethylene. When only few repeating units are joined together the structure is called an *oligomer*. A polymer prepared from a single type of monomer is defined *homopolymer* whereas if two or more monomers are employed it is called *copolymer* [3] in addition copolymers can have the monomeric units distributed in various ways. If M_1 and M_2 are two different monomers an *alternating copolymer* has M_1 and M_2 equally distributed in the chain in a perfectly alternating way; whereas *random copolymers* are constituted of a statistical distribution of M_1 and M_2 in the chain. Another category is constituted by *block copolymers*, formed of a sequence of monomers M_1 attached to another sequence or block of monomers M_2. Finally, *graft copolymers* are composed of a backbone formed of only one monomer specie with one or more chains made of repeating units of a different monomer branching from it [3]. A schematic representation of the different copolymer structures is reported in Figure 3.1.

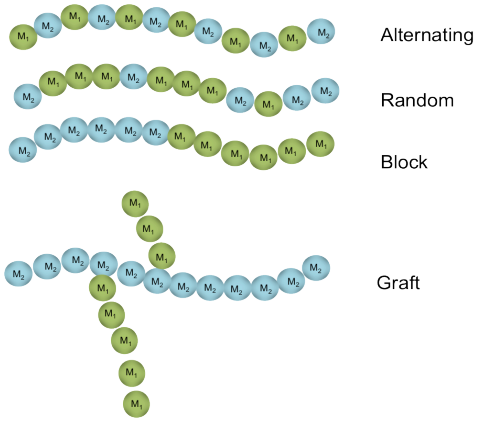

Figure 3.1 Schematic representation of copolymer structures. M_1 and M_2 represent two different monomers.

Moreover polymers can have different chain architectures [4], which can be divided into *linear* (when the repeating units are connected through the carbons atoms) or *branched* (where a polymer can have a segment protruding from the main backbone for example the low density polyethylene). When these branches further react with another polymer chain, they form what is called a *network* polymer, in the case of a simple structure ladder-like is it called cross-linked. Those listed here are only some of the most common architectures in addition to some less usual structures.

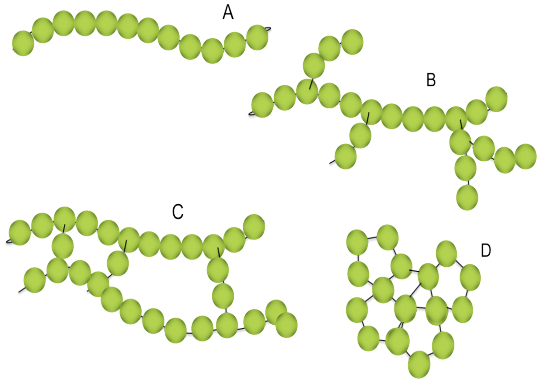

Figure 3.2. Schematic representation of polymer types. A) linear, B) Branched, C) cross-linked and D) networked polymers.

In a polymer, the smallest possible repeating unit is called *base unit,* whereas the unit that terminates the polymer chain is referred to as the *end group.* An

important role in the polymerisation process is played by the so called *functional groups,* which are defined to be specific chemical groups or bonds within a molecule that are responsible for the characteristic chemical reactions. When an organic compound contains only one reactive group, that can give rise to only one linkage into the occurring reaction it is called mono-functional, otherwise it can be called bi-tri- or oligo-functional according to how many functional groups are present in the molecule. Monomers that form a polymer are at least bi-functional molecules, and for branched or cross-linked type of polymers the molecules involved are tri-or oligo-functional.

Some of the important characteristics of a polymer are the *degree of polymerisation* and the *molecular weight*, since a number of important properties depend on them [5], for instance viscosity, toughness, stiffness or the transition temperature from liquid to waxes [5-7].

The degree of polymerisation (DP) is generally defined as the number of monomeric units in a macromolecule or a polymer chain [8].
Polymers can have molecular weight as high as millions and as low as thousands depending on the chemical structure but also on the polymer application. Unlike small molecules, a polymer's molecular weight is not a unique value but it is instead represented by a distribution of molecular weights [9]. That is the reason why an average molecular weight is considered instead.

There are many techniques that can be used to experimentally determine the average molecular weight, such as NMR [10], gel permeation chromatography [11, 12] or light scattering [13], based on the choice of one or another different numeric results are obtained. As the different methods employed to estimate the molecular weights use different averaging procedures the calculated molecular weight is defined accordingly [14]:

Number Average Molecular Weight ($\overline{M_n}$), this value is obtained when properties that only depend on the number of molecules present in solution are being studied, such as boiling point or osmotic pressure. It is defined as the total weight divided by the number of polymer molecules N_i. The number average

molecular weight indicates a value calculated according to the number of molecules with each molecular weight within the sample:

$$\overline{M_n} = \frac{\sum_1^\infty M_i N_i}{\sum_1^\infty N_i} \qquad \textit{Equation 3.1}$$

Where M_i indicates the molecular weight of the i chain and N_i represents the number of chains.

Weight Average Molecular Weight ($\overline{M_w}$) is used when we the property studied is related not only to the number of polymers in solution but also to the size or weight of each polymer, for instance in case of analysis performed via light scattering experiments. It can be defined as expressed in Equation 3.2.

$$\overline{M_w} = \frac{\sum_1^\infty M_i^2 N_i}{\sum_1^\infty M_i N_i} \qquad \textit{Equation 3.2}$$

Where M_i indicates the molecular weight of the i chain and N_i the number of chains.

In the calculation of the weight average molecular weight $\overline{M_w}$ the contribution of chains with high molecular weight dominates the final result. In measurements of colligative properties each molecule within the sample will give an equal contribution whereas in the case of light scattering larger molecules will scatter more giving a higher contribution. For this reason: $\overline{M_w}$ has a greater value than $\overline{M_n}$ except in the case when all molecules have the same weight. Macromolecules are not usually composed of structures with same sizes and molecular weights; instead they consist of a mixture of molecules with different molecular weights and degree of polymerisation therefore they are called *polydisperse*. The ratio $\overline{M_w}\ /\overline{M_n}$ is a measure of the range of molecular sizes, this ratio is known as the *polydispersity index* (PDI).

3.3 Overview of Polymerisation Techniques

Polymers are synthesised through a chemical reaction called polymerisation. There are different methods of polymerisation and the very first classification has been made back in 1930 by Wallace Hume Carothers [15] who proposed the distinction between two classes of polymers: *addition polymers,* which have a composition of monomeric units that is identical with that of monomer molecules and *condensation polymers,* which possess different monomeric units from the monomers due to the formation of by-products also called leaving molecules (for example formation of H_2O). The corresponding polymerisation reactions were then called *addition polymerisation* and *condensation polymerisation.* However new classes of reaction processes were discovered after that classification was made and since some of them did not fall into one or other category in order to avoid ambiguity, polymerisation reactions are now classified according to the particular process occurring during the reaction in two categories: *Step-growth polymerisation*. The random union of monomer molecules builds up the polymer chain. *Chain-growth polymerisation*. The polymer increases by the successive linking of monomer molecules to the end of a growing chain.

3.3.1 Step-Growth Polymerisation

Two different cases can occur when two monomers react together: both reactive functional groups can be present in the same molecule or two di-functional monomers are reacting together.

The molecule will build up upon random union of monomers that will form dimers, trimers and higher species. In order to start the reaction an initiator is not required and once the process ends the functional end stays active and can cause further polymerisation when more monomers are added. Molecular weight increases slowly even at high levels of conversion. This is explained by the Carothers equation [8] relating the average degree of polymerisation ($\overline{DP}$) to

the reactions conversion (p), this equation is derived by considering N_0, the initial number of molecules and N the total number of molecules after a given reaction period, the reaction conversion is expressed in Equation 3.3.

$$p = \frac{N_0 - N}{N_0} \qquad \textit{Equation 3.3}$$

Since the average number of repeating units of all molecules present $\overline{DP}$ is equal to the ratio N_0/N, the previous equation can be written as expressed in Equation 3.4.

$$\overline{DP} = \frac{1}{1-p} \qquad \textit{Equation 3.4}$$

Linear polymers with high molecular weight are difficult to obtain with this technique since an exact stoichiometry balance and highly purified monomers are necessary and eventually side reactions would compromise the reaction.

3.3.2 Chain Growth Polymerisation

Chain Growth polymerisation (also called *addition polymerisation*) is a process that involves three main steps:

Initiation. In order to start the reaction the presence of a particular molecule called *initiator* is required, this molecule reacts with the monomer forming an intermediate compound, which can be a free radical (R*), a anion or cation capable of linking with other monomers, thus the radical species reacts with the monomer (M) to form a new radical centre involving the radical unit and the monomer (RM*), as illustrated in the Scheme 3.1.

$$R^* + M \rightarrow RM^*$$

Scheme 3.1 Scheme of the reaction between a general initiator molecule, the radical R and the monomer M.*

Propagation. In this process consecutive monomers are added at the end of a chain. Once the reaction starts, each time that a monomer is added at the end of a chain a new active centre is created which again is able to add another monomer. (Scheme 3.2)

$$\mathrm{RM^*}_{\mathrm{n}} + \mathrm{M} \rightarrow \ \mathrm{RM^*}_{\mathrm{n+1}}$$

Scheme 3.2 Scheme of the propagation process where the active centre n *reacts with another monomer creating another active centre n+1.*

Termination. The reaction can continue until monomers are completely consumed or a termination reaction occurs making the end of the chain unreactive. This reaction can be for example a combination of radicals. Monomers appropriate for chain growth polymerisation either contain a double or triple bond or are cyclic.

The polymerisation rate increases initially and then it stays relatively constant until the end of the process. The disadvantage of radical polymerisations is that they tend to produce materials with a quite broad molecular weight distribution.

3.3.3 Living/Controlled Radical Polymerisation

The development of a polymerisation technique able to control composition, structure and molecular weight distribution in particular has attracted more and more attention during the past decades due to the increasing application of polymers in industry [16]. *Controlled (or living) Radical Polymerisation* (CRP)

enables synthesis of polymers with narrow polydispersity. The first formal definition of controlled polymerisation: “a chain growth process without chain breaking reactions (transfer or termination)” is due to Szwarc in 1954 [17, 18].

A living polymer chain does not undergo a specific termination step and being a “living chain” means that it is reactive even after the synthesis process and it is possible to work successively on the same chain and create block polymers or other architecture. Radicals can react among themselves and give rise to a “dead chain”. Unfortunately these reactions are not reversible and it is not possible to completely eliminate them. The main goal of a living controlled radical polymerisation is therefore to reduce and control them. This is achieved by introducing into the system a “*capping*” species (X) that reacts with the growing radical chains creating *dormant* radical chains, which are not able to grow more but which do not terminate either. In this way the radical can undergo under three different reactions: it can react with another radical and cause a termination; create a *dormant* chain or react with a monomer and propagate the chain;

To control this process and to obtain a higher number of dormant chains compared to the dead chains an appropriate concentration of X is introduced chosen with the right reactivity in order to increase the number of reactions with the radicals R*. However anionic polymerisation is very sensitive to the presence of water or other impurities and this focused studies on CRP to develop three main, more versatile, ways to perform it:

- Nitroxide Mediated Polymerisation (NMP)

Nitroxide Mediated Polymerisation technique was first reported by Rizzardo et al. in 1982 [19]. This polymerisation process is based on the reversible combination of the living chain with the “capping species” X (the nitroxide radical) forming a dormant chain [20]. It has been successfully used in the homopolymerisation of styrene and copolymerisation of Styrene-alt Maleic Anhydride [9, 21] using one of the first discovered nitroxide radicals: 2,2,6,6-

tetramethylpiperidinyloxy (TEMPO), which however failed in controlling other systems. A schematic representation of a generic NMP polymerization reaction is given in Scheme 3.3.

$$R_n^* + X^* \rightleftarrows R_nX$$

Scheme 3.3. Schematic repprsentation of a NMP reaction. R_n reppresents a generic polymer chain reaction with a nitroxide radical X.

- Atom Transfer Radical Polymerisation (ATRP)

Atom Transfer Radical Polymerisation is a catalysed process where the catalyst is typically a transition metal (such as copper) attached to an amine based ligand and an initiator called haloalkane, also known as halogenoalkane or alkyl halides. They are a group of chemical compounds derived from alkanes and possessing one or more halogens. This technique possesses numerous advantages, it can be applied to a many monomers and it can be carried out at a wide range of temperatures. The drawback is the presence of the catalytic metal, which must be removed at the end of the reaction. This kind of polymerisation technique has been proved to be unsuitable for PSMAnh polymerisation. Indeed the different attempts to the copolymerisation of Styrene with Maleic Anhydride using ATRP showed to be unsuccessful with no polymerisation taking place, which might be due to the reaction of the Maleic anhydride with one of the catalyst [22, 23].

- Reverse Addition-Fragmentation Chain Transfer (RAFT)

This process is one of the most popular among the living polymerisation processes. Some of the great advantages of the RAFT polymerisation technique are its compatibility with a wide range of monomers, providing the possibility to synthetize a number of polymers with narrow polydispersity and the possibility to carry out the reaction at relatively low temperatures [19]. Being

the technique chosen in this project a detailed description is reported in Section 3.3.4.

3.3.4 Reverse Addition-Fragmentation Chain Transfer Polymerisation (RAFT)

Reverse Addition Fragmentation Chain Transfer was first discovered by Chiefari et al. and published in 1998 [24]. The main characteristic of this reaction is the use of the so-called, RAFT agent, which possesses the general structure represented in Figure 3.3.

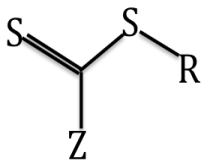

Figure 3.3. Representation of the structure of a generic RAFT agent, where "Z "and "R" indicates the two reactive groups.

The RAFT agents also known as Chain Transfer Agents (CTA) are thiocarbonylthio species which belongs to a variety of chemical families [25],[26-28]. The choice of an appropriate CTA is of vital importance for the reaction; indeed a non appropriate choice can lead to retardation, inhibition and/or poor control of the reaction. Attention must also be paid to the presence of oxygen in the system, which can cause delays in the polymerisation processes and also inhibition. Two groups govern the activity of the CTA, the Z-group that controls the activation or deactivation of the thiocarbonyl double bond to promote radical addition, and the R-group that interacts with monomers to activate the formation of other growing chains [25].

3.3.4.1 RAFT Mechanism

RAFT polymerisation occurs in five steps and the main characteristic of this mechanism is the addition fragmentation process. Schematic representation of the RAFT mechanism is reported in Scheme 3.4:

Initiation

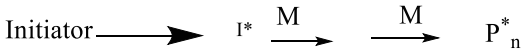

Scheme 3.4. Schematic representation of a RAFT polymerisation mechanism where I represents the Initiator; M is the monomer unit and P is the polymer chain constituted of n units.

In the first step, the propagating polymer chain P_n* is formed upon addition of an initiator. The initiator used in this project is the azobisisobutyronitrile (AIBN) an organic compound which undergoes a process of thermal decomposition forming two 2-cyano prop-2-yl radicals liberating a nitrogen molecule as schematised in Figure 3.4.

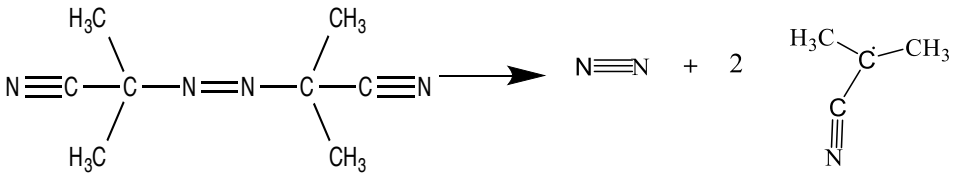

Figure 3.4. Thermal Decomposition of AIBN

Addition / Fragmentation

In the second step, the RAFT agent reacts via an addition/fragmentation process with the propagating polymer chains creating a dormant chain and a new radical species R* as in:

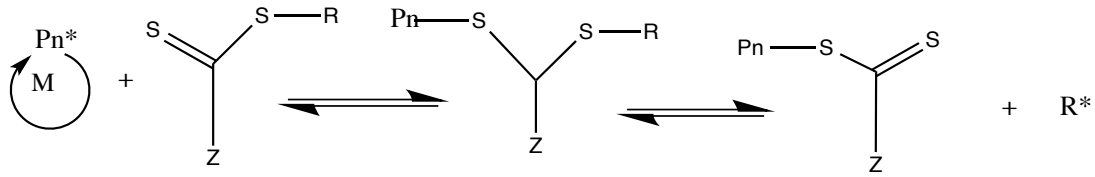

The third step is known as *Re-initiation*. This new radical reacts with the monomers creating another propagating chain Pm*

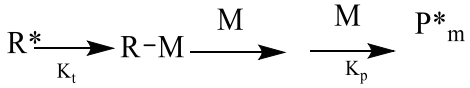

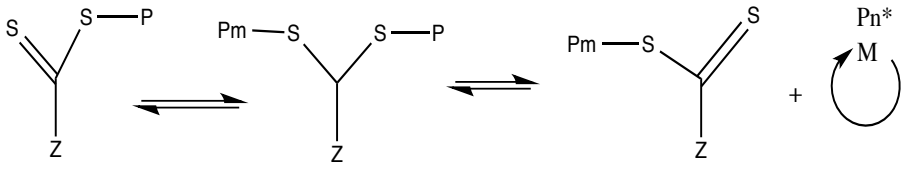

Equilibrium between the two propagating chains is then reached and the dormant polymeric RAFT compound gives equal probability for all chains to grow allowing a low polydispersity of the synthetised polymer.

The last step is the *Termination.* The thiocarbonyl thio group is kept as end group in the majority of polymer chains when polymerisation is either complete or stopped. The end group might be visible to ^{1}H NMR or FTIR analysis.

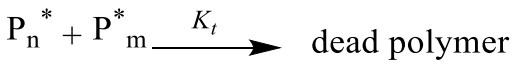

3.3.4.2 End Group Removal

Once the RAFT polymerisation process is finished, the thiocarbonylthio group is retained in the final product. Polymers before removal of the RAFT agent are called “living polymers” since upon addition of more monomers and an initiator, the polymerisation process can start once again. Although this is a useful characteristic, since it allows creation of more complex structures, it can have some disadvantages. Polymers keeping the thiocarbonylthio group are coloured, with a range of colours varying form violet to yellow depending on the chromophore group present [29]. The C-S bond is labile and the polymer product may sometimes release odour when the thiocarbonyl group decomposes [25]. However if the removal of the end group is desired there are a number of methods to cleave the thiocarbonylthio groups such for instance the thermal elimination [30].

3.3.4.3 Factors Contributing to the RAFT Polymerisation

The RAFT polymerisation method possesses many advantages that make it very attractive. It can be performed with a large choice of solvents, including water, and within a wide temperature range, it is also suitable for use with many different functional groups (e.g. –OH, -COOH, -$CONR_2$, NR_2, -SO_3Na) and finally it does not require highly rigorous removal of oxygen and other impurities, although attention must be paid to operate in an oxygen-free atmosphere. The down side is that a particular RAFT agent can be suitable only for a limited number of monomers, moreover it can be unstable over a long period of time and the presence of sulphur and colours can be undesired for some applications. For example, if the resulting sample needs to be analysed via spectroscopic techniques, then the presence of colours in the sample might interfere with the analysis.

3.4 Poly (Styrene-alt-Maleic acid) Copolymers

SMA copolymers have received in the past few decades' considerable attention due to their many different applications [31-33]. SMA is part of a class of polymers known as *smart polymers* the generic structure of SMA is reported in Figure 3.5. This class of polymers possess characteristic features like being membrane destabilising, but also pH and temperature responsive. SMA has been successfully used in medical and pharmaceutical applications, such as in cancer research as drug delivery carriers [34]. Polymer-protein conjugates were some of the first polymer therapeutics used as an anticancer vehicle in 1985. Styrene-maleic anhydride neocarzinostatin (SMANS), polymer-protein conjugates designed by Maeda et al., were the first to be introduced in clinical tumour treatments [32,35], and are now a well-known polymer-protein conjugate for treatment of liver cancer. In this project SMA was used as a substitute [36-38] for the membrane scaffold protein (MSP), which has been used so far in the nanodisc formulations. The capability of SMA to self assembles when in presence of phospholipids in discoidal structures was first introduced in 2001 by the work of Tonge and colleagues on the properties of hypercoiling polymers [66].

.

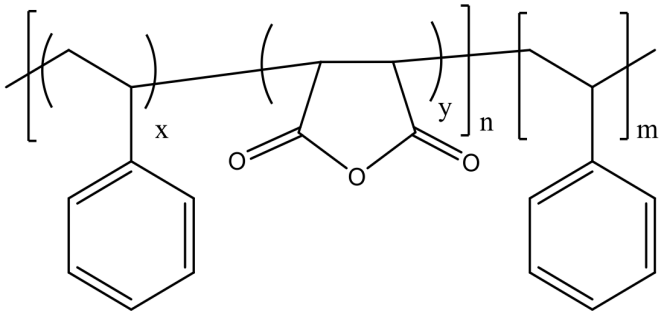

Figure 3.5. Structure of a poly(styrene-alt-maleic acid)–block-polystyrene copolymer constituted of n blocks of alternating units made up of a number X of Styrene and a number Y of Maleic Anhydride and followed by a block of m number of units of Styrene.

These polymers when in presence of film forming lipids they associate to for lipids-polymer nanostructures analogous to the HDL behaviour. In the particular

case of the SMA the amphipathic segment surrounds the lipids core creating a nanodiscs like structure. Tonge et colleagues were interested in the applications of these structures as drug delivery and together with Malvern Cosmeceutics the SMA-lipid assemble structure was patented with the name of Lipodisq® [67].
In 2009 as previously introduced our collaborators from the University of Birmingham demonstrated the possibility to use these supports to encapsulate and analyse membrane scaffold proteins, naming them SMALP from their components. In particular this original formulation used the SMA copolymer provided from Malvern Cosmeceutics SMA-2000P with a 2:1 Styrene to Maleic Acid total proportion and a copolymer M_w of 7 kDa. Lately in 2012 also the Lipodisq® technology involving this time the use of SMA-3000P a copolymer from Malvern Cosmeceutics with a 3:1 Styrene to Maleic Acid proportion and a M_w of 9 kDa [68].

- *Choice of the Polymerisation Technique for SMA*

Different polymerisation techniques have been applied in attempts to synthetize the SMA polymer. However, not all proved to be suitable for the synthesis of this particular polymer. Indeed Li et al. and Hawker et al. tried the polymerisation via ATPR technique but it showed to be unsuccessful. The reason was attributed to the maleic anhydride interaction with the ATRP catalyst [39]. One of the interesting features of the polymerisation of styrene with maleic anhydride is the strong alternating character of the two monomers, which has been attributed to the nature of electron rich of the styrene monomer while the maleic anhydride is an electron poor monomer. Moreover maleic anhydride hardly homopolymerises, which means that MA-MA diads are rarely present in the copolymer chains [40]. However the alternating character of the styrene-maleic acid copolymerisation is also a function of the temperature at which the polymerisation has been carried out. In particular, it has been shown that to achieve the best alternating character a relatively low temperature is beneficial [21].
NMP of styrene with maleic anhydride was successfully reported in few studies [21, 22, 41] in particular, Lessard at al. [22] attempted to characterise the

styrene-maleic acid NMP polymerisation as a function of different parameters such as reaction temperature or monomer concentration in order to find the optimal conditions to polymerise a poly(styrene-alt-maleic acid)–b-polystyrene polymer with a perfect alternation of styrene and maleic acid units. However, so far the most commonly used technique for polymerisation of SMA is the RAFT polymerisation, which allows the use of relatively low temperatures (between 60 °C and 80 °C). There have been many reported cases of successful RAFT polymerisation of SMA with a good control of molecular weight and low polydispersity [42].

3.5 Materials Used in the Synthesis and Hydrolysis Process

SMA copolymers were synthesised at the University of Bath and University of Warwick laboratories, and analysed along with the copolymers received from our collaborators at the University of Birmingham, which were supplied by Polyscope and Sartomer. A detailed list of polymer codes and suppliers is displayed in Table 3.1. SMAs from the companies were provided as poly (styrene-alt-maleic anhydride) copolymers and required hydrolysis to the acid form before use.

Product Code	*RAFT*	*SMA 2000P*	*XZ 09-008*	*SZ 33030*	*SZ 28065*	*SZ 28110*
Supplier	Bath; Warwick	Sartomer	Polyscope	Polyscope	Polyscope	Polyscope
Mw (kDa)	6	7	11	33	63	110
STY: MA total ratio	1.7:1 2:1 3:1	2:1	2:1	1.95: 1	2.43:1	2.45:1

Table 3.1. List of copolymers studied in the present work.

The RAFT polymerisation required the following materials: Maleic Anhydride (purity ≥ 99%) used as received. Styrene (purity ≥ 99%) purified of inhibitor by passage through an "Inhibitor Remover" column; the disposable column for the removal of tert-butylcatechol, together with the styrene and maleic acid was purchased from Sigma-Aldrich. Two RAFT agents were used in this project: 2 Cyano-2propyl dodecyl trithiocarbonate 97% HPLC grade and the 2-(Dodecylthiocarbonothioylthio)-2-methylpropionic acid (DDMAT) 98% HPLC grade. Toluene (HPLC grade 99.8%), sodium hydroxide (NaOH, General Purpose Grade), hydrochloric acid (HCl, Laboratory Reagent Grade 95%) 2M concentration, azobisisobutyronitrile (AIBN, 98% purity) were all purchased from Sigma-Aldrich and used as received with the exception of AIBN which, was stored in a cold room at 2 °C and was re-crystallized before use. 10ml of methanol were added drop-wise under gentle agitation with a magnetic stirrer to 0.5 g of AIBN, temperature was kept at 40 °C. Solution was cooled down to room temperature (20 °C) and then placed in the freezer at -8 °C, and finally vacuum filtrated to collect the AIBN powder. Sodium di-hydrogen phosphate (NaH_2PO_4, purity ≥ 99%) and sodium chloride (NaCl purity ≥ 99%) from Sigma Aldrich were used as received. Sodium phosphate dibasic (Na_2HPO_4, purity ≥ 99%), tetra-hydrofuran (THF, HPLC 99.8% grade) and diethyl ether (laboratory reagent grade) were purchased from Fisher and were used as received. Phosphate Buffer solutions used in SANS, SAXS and DLS experiments were

made using ultrapure water with a resistivity of 18 MΩ cm, or for SANS measurements in D_2O (from Sigma Aldrich, purity ≥ 99%) or mixtures of ultrapure water with D_2O.

3.6 Synthesis of Poly (Styrene-Alt-Maleic Anhydride)

The procedure from the literature [43] reported below was followed in order to synthesise the poly (styrene-alt-maleic anhydride) also referred as PSMAnh. A detailed description of quantities used is displayed in Table 3.2. Purified styrene, maleic anhydride, RAFT agent, AIBN and dioxane were added to a single neck bottom flask containing a magnetic stirrer. The content within the flask was de-gassed and the flask filled with nitrogen via a three freeze-pump-thaw cycles. The solution was then heated at 60 °C for 21 hours. Once cooled to room temperature (approximately 20 °C) the polymer was precipitated from solution in ice-cold diethyl ether. The precipitate was finally collected via filtration using a Buchner filtration apparatus with nylon filter and then dried overnight at the temperature of 40 °C.

STY: MA Total Ratio	*1.7:1*	*2:1*	*3:1*
Styrene (mg)	500	500	500
Maleic Anhydride (mg)	273	202	154
RAFT (mg)	3.6	A) 3.6 B) 3.8	3.6
AIBN (mg)	3.43	3.43	3.43
Dioxane (mL)	0.7	0.7	0.7

Table 3.2. Reagent quantities used for RAFT copolymerisation of PSMAnh. RAFT agent used for synthesis of 3:1 and 1:1 SMA was A) the 2-cyano-2-propyl dodecyl trithiocarbonate (CPDT) whereas for the 2:1 polymer two different types of RAFT agent was also used B) 2-(dodecylthicarbonolthiolylthiol)-2-methylpropionic acid (DDMAT).

As one can see from the values reported in Table 3.3 the copolymerisation was conducted in the presence of excess of styrene in order to promote an alternating copolymerisation initially. Then, once the maleic acid was entirely consumed, the homopolymerisation of the styrene with formation of a pure styrene tail took place. Conversion was estimated by gravimetric analysis.

STY:MA	*STY: MA: RAFT: AIBN*	*Conversion*	*% MA[(a)]*	*Composition[(b)]*
1.7:1	38: 22: 1: 0.2	90%	30%	$(STY\text{-}alt\text{-}MA)_{44}\text{-}STY_{14}$
2:1	44: 20:1: 02	90%	28%	$(STY\text{-}alt\text{-}MA)_{40}\text{-}STY_{22}$
3:1	46: 15:1: 02	90%	25%	$(STY\text{-}alt\text{-}MA)_{30}\text{-}STY_{28}$

Table 3.3. Table reporting the details of composition of different 6kDa copolymers synthetised via RAFT polymerisation. [(a)] MA acid percentage was calculated from final composition. [(b)] Styrene was calculated from: (STYeq-MAeq)×conversion whereas STY-alt-MA was calculated from [STYeq-(STYeq-MAeq)]×2.

A schematic representation of the reaction is displayed in the Figure 3.6.

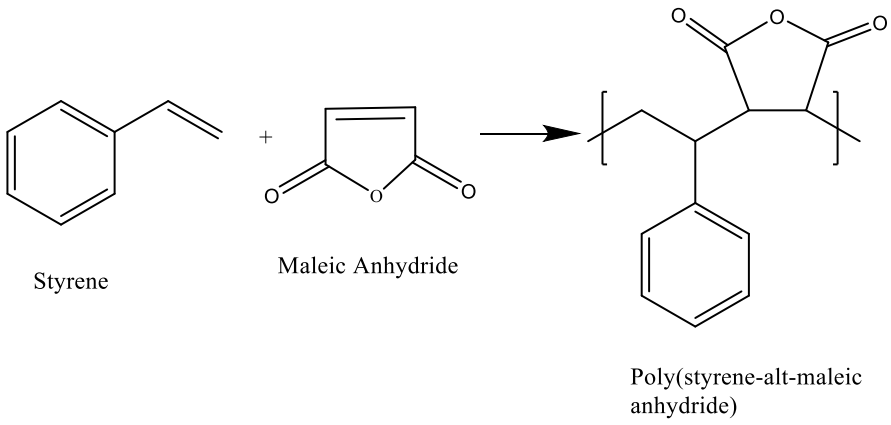

Figure 3.6. Schematic representation of the synthesis route for RAFT polymerisation of SMA.

3.7 Hydrolysis of Poly (Styrene-Alt-Maleic Anhydride)

The fractions of PSMAnh were converted into maleic acid (PSMAcid) via reflux in basic conditions. Approximately 0.3 g of polymer was refluxed in 30 mL of 2 M NaOH for 3 hrs in a 50 mL round bottom flask fitted with a condenser also containing a magnetic stirrer (the process is depicted in Figure 3.7). The solution was left to cool down at room temperature and then added drop wise to 300 mL of 2 M HCl solution. The resulting mixture was then centrifuged at 5000 rpm for 10 min. A polymer pellet was collected and washed three times with ultrapure water via centrifugation at 5000 rpm for 10 min. This polymer, presenting a gel texture, was then collected and dissolved in the minimum amount of 1M NaOH in order to reach a final solution pH close to 8. Finally the polymer solution was freeze dried overnight. The powder was finally collected and re-suspended in a 50 mM phosphate buffer solution at pH 8.

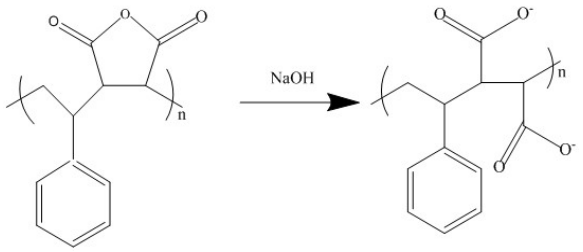

Figure 3.7. Schematic representation of the PSMAnh hydrolysis process to PSMAcid.

3.8 Copolymers Characterisation

In order to check the full conversion from SMAnh to SMAcid, FTIR analysis was performed on the copolymers synthesised in Bath via RAFT polymerisation. A GPC analysis was also implemented in order to check polydispersity and M_w obtained. GPC experiments were also performed on the commercial copolymers in order to confirm the values for PDIs and M_{ws} reported by the Polyscope data sheets. Finally ^{1}H NMR experiments were

performed in order to confirm the alternating structure of the copolymers and the styrene to maleic acid total ratio. Moreover to further characterise the SMA polymer architectures, a pH titration was implemented in order to obtain pKa values, and a surface tension measurement was also carried out in conjunction with the pH titration to monitor the effect on surface tension upon decreasing the pH.

3.8.1 FTIR and GPC Analysis

Conversion from anhydride to acid was checked by means of FTIR. Figure 3.8 shows two typical FTIR spectra from a 6 kDa 2:1 styrene to maleic acid molar ratio sample. The principal peaks, characteristic of the anhydride C=O group, are the peaks labelled "1" and "2" corresponding to 1856 cm^{-1} and 1775 cm^{-1} respectively. The peak labelled as "3" (1500 cm^{-1}) is a styrene band whereas the peak labelled as "4" (1450 cm^{-1}) is due to the aromatic stretching of the styrene. The other characteristic anhydride signal, arising from the cyclic ring ether C-O-C, is related to the peak around 1220 cm^{-1} labelled as "5".

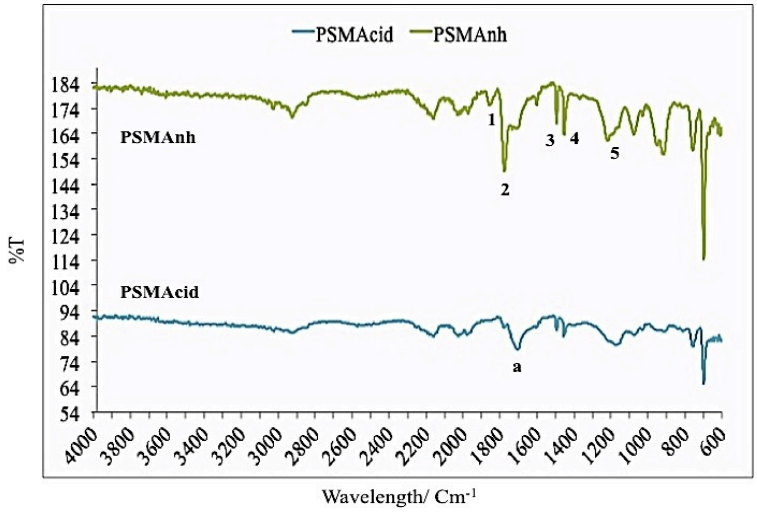

Figure 3.8. FTIR of poly (styrene-alt-maleic anhydride) spectrum (green, top) compared to the poly (styrene-alt-maleic acid) spectrum (blue, bottom) of a 6 kDa polymer with a 2:1 styrene to maleic acid total molar ratio [44].

Upon conversion to PSMAcid the anhydride peaks are no longer present. In particular the strong peak around 1775 cm^{-1} disappears and the band around 1705 cm^{-1} indicated as "a", characteristic of the carboxylic group is now observed [45,46] thus confirming conversion from PSMAnh to PSMAcid polymer.

Results of analyses performed for all the different copolymers are listed in Table 3.4.

Copolymer	*Mn*	*Mw*	*PDI*
6 kDa 1.7:1 STY to MA	5300	6000	1.1
6 kDa 2:1 STY to MA	5600	6300	1.1
6 kDa 3:1 STY to MA	5300	5800	1.1
SMA 2000P	3900	6400	1.6
XZ -09008	6800	10900	1.6
SZ-33030	20000	33200	1.7
SZ-28065	36500	63200	1.7
SZ-28110	54600	11000	2.0

Table 3.4. Summary of the results obtained from GPC analysis.

GPC results showed a higher polydispersity for the commercial copolymers compared to the copolymers synthesised via RAFT polymerisation. The GPC analysis also confirmed the desired average molecular weight and narrow polydispersity as expected from a polymer synthetized via RAFT copolymerisation. Example of a typical GPC plot is reported in Figure 3.9.

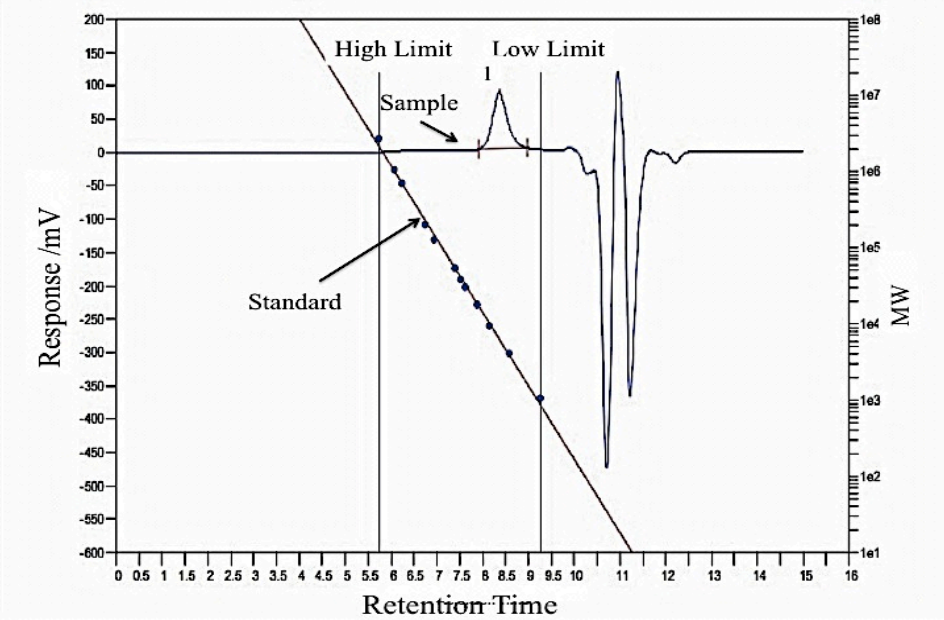

Figure 3.9. Graph showing the retention time of a PSMAnh sample, compared to a standard of polystyrene of known molecular weight represented with dots and a red line being the calibration curve as indicated in the graph. The number "1" refers to the number of peaks identified and analysed by the software.

3.8.2 ^{1}H NMR and ^{13}C NMR Analysis

^{1}H NMR was performed in order to estimate the styrene to maleic acid mole fractions in the copolymers. Figure 3.10 displays a typical ^{1}H NMR spectrum comparable to those found in literature [33]. As shown in the inset picture, the PSMAnh structure has been marked "a", "b" and "c" according to the main peaks presents in the ^{1}H NMR polymer spectrum: "a" represent the broad peak at 7.29 ppm assigned to the aromatic region in the styrene monomers, "b" around 2.33 ppm belongs to the proton in the aliphatic region of the maleic anhydride and finally "c" is attributed to the protons in the aliphatic region of the styrene (CH and CH_2).

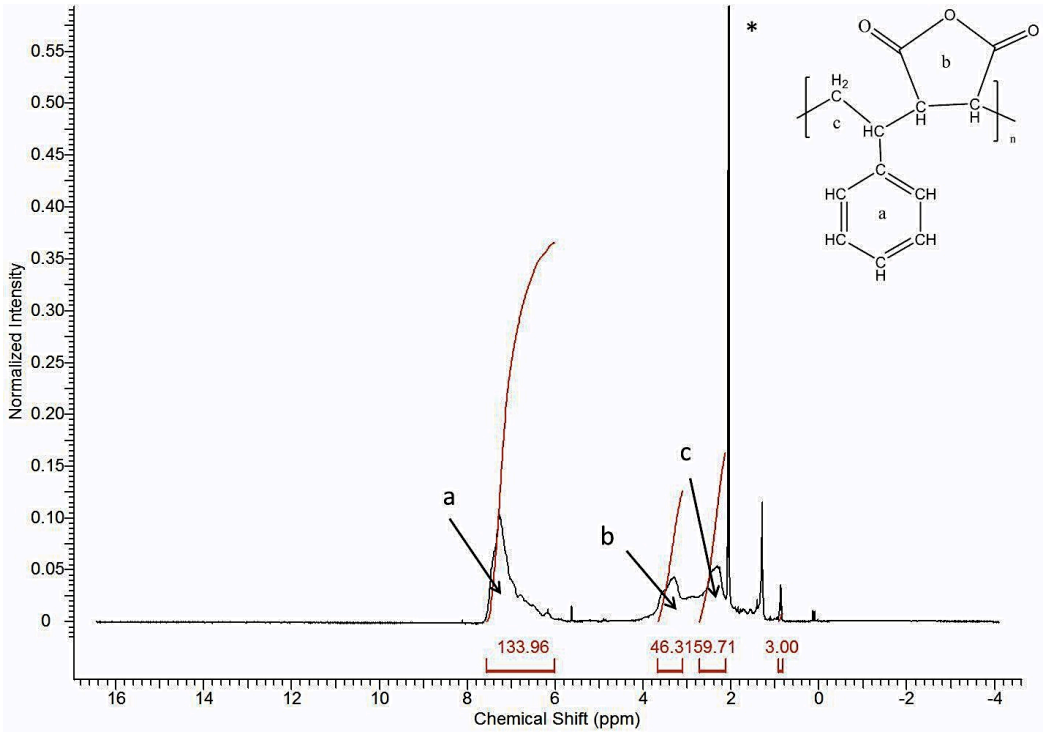

*Figure 3.10. [1]H NMR Spectrum in d-Acetone, of the 6 kDa RAFT polymer synthesized in Bath with a 2:1 styrene to maleic Acid ratio. * Indicates peaks from the solvent.*

Unfortunately for most of the commercial polymer in the ^{1}H NMR spectra the signals from the CH and CH_2 groups were not clear enough to be properly integrated. Therefore the peak data were integrated using a different approach. The peak corresponding to the aromatic region was integrated and divided by the number of protons present in the styrene group contributing to that signal using the formula reported in Equation 3.5

$$\int 1\text{H St} = \frac{\int \text{Aromatic region}}{5} \qquad \textit{Equation 3.5}$$

Through the above formula the value of 1 single proton from the styrene was calculated.

Since the peak in the region from 0 to 4 ppm was due to the contributes of 2 protons from the maleic acid but also 3 hydrogens from the styrene, the

calculation expressed in the Equation 3.6 was used in order to get an approximate value corresponding to the 1 proton from the maleic acid part.

$$\int 1\text{H MA} = \frac{\int \text{Hydrocarbon Region} - 3 \int 1\text{HSt}}{2} \qquad \textit{Equation 3.6}$$

From the ratio of these two values the ratio between styrene and maleic acid was calculated. Results are summarised in Table 3.5.

Copolymer	*STY: MA total ratio*
6 kDa 1.7:1 RAFT	1.7:1
6 kDa 2:1 RAFT	2.1
6 kDa 3:1 RAFT	3:1
7 kDa	2:1
11 kDa	1.85:1
33 kDa	1.95:1
63 kDa	2.43:1
110 kDa	2:1

Table 3.5. Table reporting styrene to maleic acid total ratio of the different copolymers in use, results are from NMR spectra analyses.

Since all the commercial copolymers were synthesized via free radical polymerization in an industrial process, the structure is not expected to be a strictly alternating block of styrene and maleic acid followed by the tail of styrene but rather a more complicated architecture. Indeed it is known that since the maleic anhydride is a strong electron acceptor it does not in general homopolymerise [47]. Instead it forms copolymers composed of blocks of alternating styrene and maleic acid (SMS) plus the presence of semi-alternating block (SSM/MSS) and non-alternating sequences (SSS). Based on the maleic acid content provided by the company Polyscope, it was possible to estimate the triad sequence distribution referring to the previous work done on the poly (styrene alt maleic) acid polymer by Klumperman et al [48, 49]. In an earlier

study [50] they analysed the SMA copolymerisation plotting the triad distribution versus the polymer composition (Figure 3.11). Although there is some scatter in the experimental data, the data for copolymers prepared in different solvents appear to be described by a set of curves that have been used to calculate the percentage of the different sequences. Results obtained are summarised in Table 3.6.

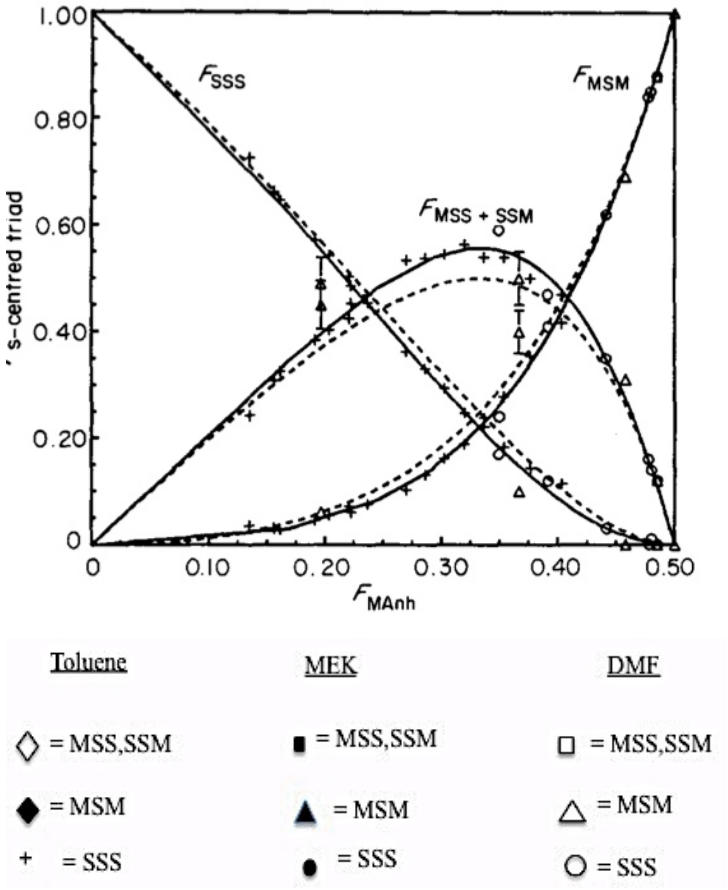

Figure 3.11. Mole fraction of STY centered triads versus *polymer composition (F_{STY}) of SMA copolymerization in three different solvents, Toluene, Methyl Ethyl Ketone (MEK) and Dimethylformamide (DMF). Picture from [48] was reproduced with the permission of the author*

Copolymer	*Maleic Anhydride Content*	*Styrene Content*	*SMS*	*SSM/ MSS*	*SSS*
*7 kDa *(SMA-2000P)*	28%*	72%	11%	54%	35%
11 kDa (XZ-09-008)	25%	75%	10%	52%	38%
33 kDa (SZ-33030)	33%	67%	20%	55%	25%
63 kDa (SZ-28065)	28%	72%	11%	54%	35%
110 kDa (SZ-28110)	28%	72%	11%	54%	35%

*Table 3.6. Summary of the percentage distribution of the different blocks that make up the polymer architectures. * Maleic acid percentage was calculated from pH titration results.*

Since no information was available from the company Malvern Cosmeceutics regarding the 7 kDa SMA-2000P polymer, the sample was analysed via ^{13}C NMR in the attempt to evaluate the architecture from the analysis of the different peaks that reveal the presence of semi-alternating and non-alternating blocks within the copolymers. Analysis of the spectrum was performed according to the work done by Lessard et al. [21] and Ha et al. [51]. Spectrum is reported in Figure 3.12 where for clarity, the inset on the top right hand side shows the structure of the polymer, the different carbons contributing to the peaks were marked "C1" to "C10".

Two predominant markers need to be considered. The first is the resonance representing the aromatic carbon "next to polymer chain" indicated as "C7", as reported in the work of Chernikova et al. [52] and Nguyen and Ha [51] a perfectly alternating sequence (SMS) will have a "C7" resonance between δ= 136-141 ppm If a pure styrene block (SSS) is present then it will be shown as a shift of "C7" to δ=145-148 ppm. Finally the presence of semi-alternating blocks (SSM/MSS) is revealed by an upshift around δ=142-145 ppm. The second is the methylene (-CH_2-) "polymer chain" carbon was reported to be sensitive to the styrene centred triad distribution observed via ^{13}C NMR [53]. When in presence of a perfectly alternating sequence (SMS) "C1" will show a resonance at δ= 33-37 ppm whereas as reported by Lessard et al [21] the presence of SSS is shown by a upshift of "C1" at δ= 42-47 ppm and between the SSS and SMS peaks is the area which represents the semi-alternating block SSM or MSS with δ= 37-

42 ppm. However the characteristic peaks of "C2" and "C8" will also be present between δ= 40-46 ppm therefore the presence of SSS and SSM/MSS blocks needs to be confirmed by the shifts in the "C7" area.

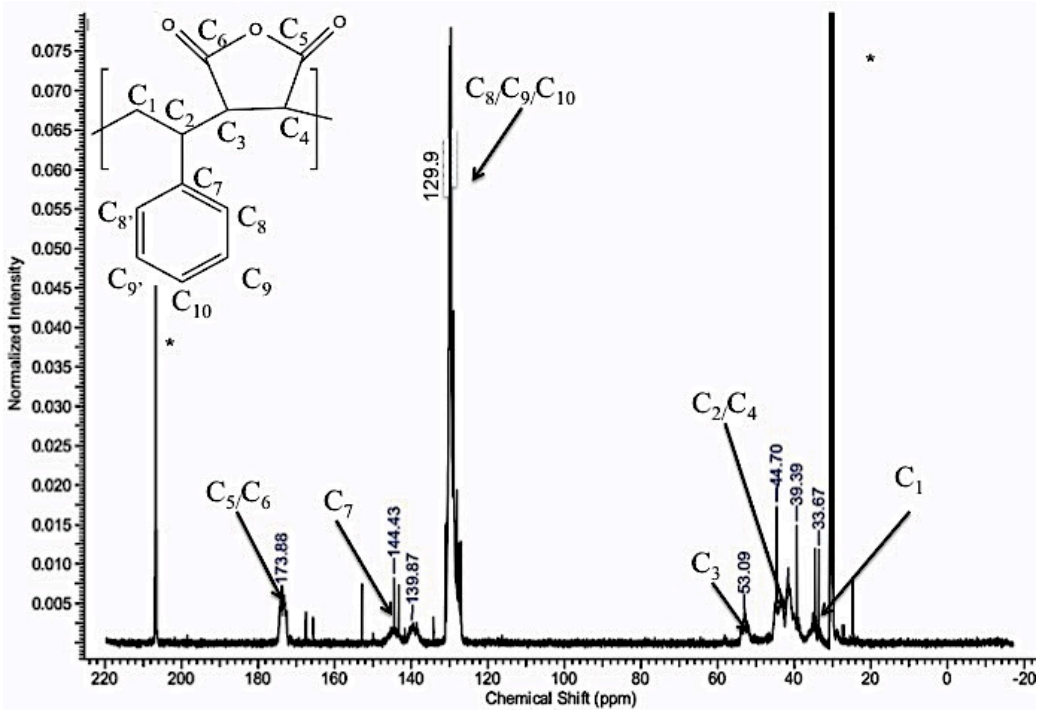

*Figure 3.12. ^{13}C NMR Spectrum (Acetone-d_6) of 7 kDa SMA-2000P anhydride taken on a 500.13 MHz Bruker spectrometer. * Indicates solvent peaks.*

The analysis of the ^{13}C NMR spectrum of the 7 kDa SMA-2000P commercial polymer, revealed the classical alternating structure with a "C7" shift in the region δ = 136-141 ppm and "C1" shift in the δ = 32-37 ppm, already reported in literature [51]. Also in the area of the "C7" peaks a peak is expected revealing the non-alternating (SSS) around δ = 145-148 ppm, and the semi-alternating (SSM/MSS) shift, predicted at δ = 142-145 ppm. However in the specific case of the spectrum analysed here only a broad peak between δ = 141-148 ppm is clear, which shows the presence of both SSS and SSM/MSSS blocks but makes it difficult to precisely identify and integrate the two separate peaks. Also the spectrum showed the presence of SSS blocks with a "C1" signal present in the region δ = 42-47 ppm. The presence of semi-alternating blocks

(SSM/MSS) was confirmed by the presence of a small second peak related to "C1" in the region δ = 37-42 ppm.

The same analysis was also performed on the 6 kDa polymer synthetised in Bath via RAFT polymerisation. For copolymers synthetised with this technique the expected architecture consists of alternating blocks (SMS) followed, when all the maleic acid has reacted, by a tail of only styrene (SSS). This was confirmed by the shift of the "C7" carbon, showing two peaks one in the region δ = 136-141ppm for the SMS structure and the other in the region δ = 145-148 ppm for the styrene tail (SSS). Also in the aliphatic carbon region, the three small peaks also related to the alternating triad are observed between δ = 30-60 ppm as reported by Chernikova et al. [52] who also reported ^{13}C NMR analysis of poly(styrene alt maleic) acid polymerised via RAFT polymerisation at 60 °C. The graph is reported in Figure 3.13.

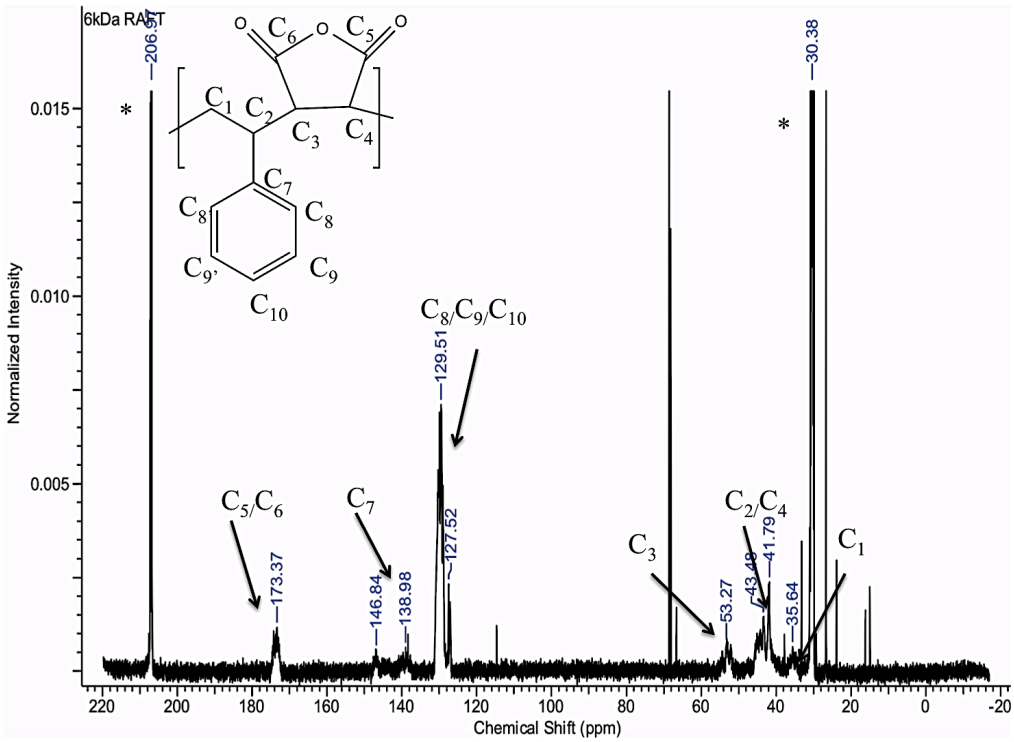

*Figure 3.13. ^{13}C NMR spectrum (THF-d8) of 6 kDa anhydride 2:1 total ration taken on a 500 MHz Bruker spectrometer. * Indicates solvent peaks.*

The Software ChemBioDraw [54] was used to estimate the approximate length of each monomer units present in the three different blocks constituting the

commercial copolymers has been measured, with the final purpose to calculate the average length occupied by the hydrophobic and hydrophilic parts of the polymer. The values calculated are an approximation and do not take into consideration the changes in length expected when the polymer is in different solutions due to solvent effects, or the copolymer coiling due to entropic effects. Results for triad lengths are reported in Table 3.7 and the Figure 3.14 shows which distance has been taken into consideration on the triad molecular structures.

	SSS	*SMS*	*SSM/MSS*
Unit length	0.25 nm	0.49 nm	0.59 nm

Table 3.7 Length of triad repetitive units found in SMA copolymers.

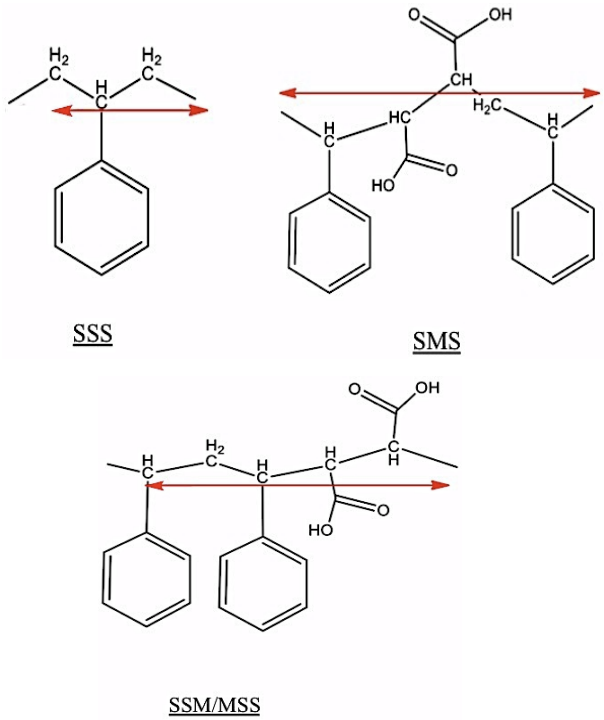

Figure 3.14. Structures of the different units taken into account for the calculation of the length of each triad block constituting the polymer architecture.

Based on the different percentage of SSS, SMS; SSM/MSS blocks previously calculated and the values found, assuming the polymer to be completely stretched it was calculated the maximum length occupied by each part. Moreover the total polymer length was also calculated even if only indicative of

the maximum possible length occupied by the polymer in a complete stretched condition such as in presence of a good solvent. Values are reported in Table 3.8.

Block/ Copolymer	*SSS Length (nm)*	*SMS Length (nm)*	*SSM/MSS Length (nm)*
**6 kDa 1.7:1*	3.60	21.80	___
**6 kDa 2:1*	5.20	19.80	___
**6 kDa 3:1*	6.90	14.80	___
7 kDa	5.46	1.60	10.83
11 kDa	9.97	2.45	10.32
33 kDa	19.95	14.92	33.25
63 kDa	53.15	15.63	62.13
110 kDa	92.5	27.19	107.97

*Table 3.8. The length of the different blocks constituting copolymer architectures. *Values for the length of SSS and SMS polymer blocks have been calculated based on the conversion value calculated via gravimetric analysis.*

3.9 Investigation of SMA Copolymers Aggregation State in Solution

Some interesting work has been previously done on the structures that SMAs form in solution [55]. According to this work the self-assembly process can be divided into primary, secondary and tertiary self-assembly properties, which are schematised in Figure 3.15, 3.16 and 3.17. The primary structure (Figure 3.15) corresponds to the polymer conformation, which determines the formation of higher order of structural organisations. The SMA primary organisation was investigated by Malardier- Jugroot et al [56, 57] in three different conditions: when the polymer was completely deprotonated, semi-protonated and fully protonated. It was found that the linear conformation of the polymer chain, allows the assembly into a secondary conformation of the polymer constituted

of cylindrically shaped nanotubes (Figure 3.16). This linear conformation is only present at pH 7 when the polymer is half protonated and strong hydrogen bonds are formed (see Figure 3.31). At higher (pH 12) and lower (pH 3) pHs values SMA showed not to associate into nanotubes [58]. Moreover nanotubes can further assemble into bundles constituting the tertiary SMA organisation structure (Figure 3.17).

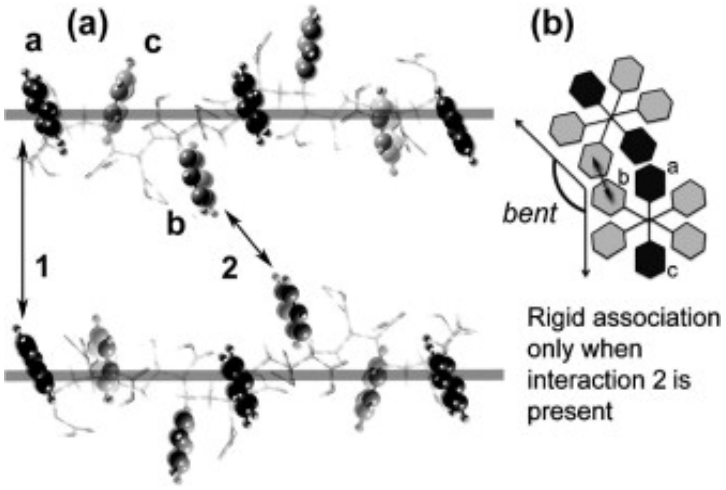

Figure 3.15. a) Association between two SMA polymer chains, association is always sideways because of the alternating sequence of the polymer. 1 represents the styrene-styrene association which is always present, 2 represents the association between two maleic acid groups. When this association is present the polymer is in a more rigid configuration as schematised in b) Figure reprinted with permission from [55].

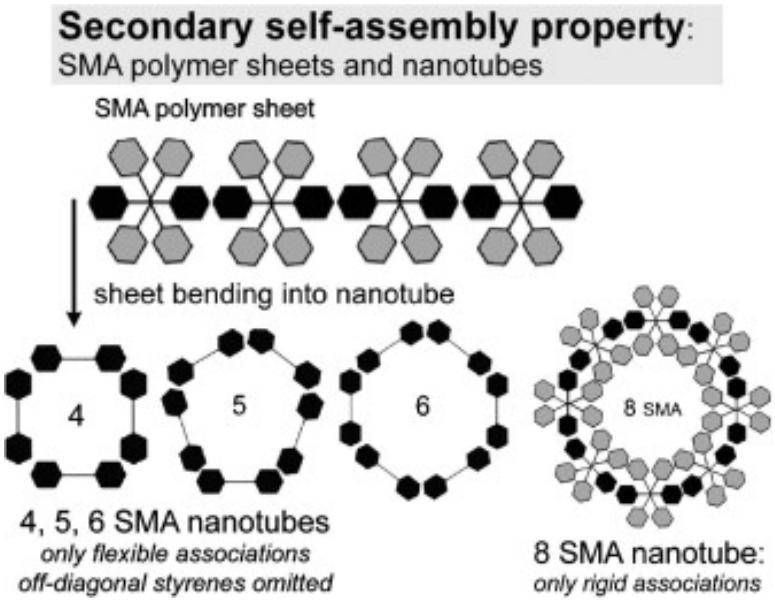

Figure 3.16. SMA polymer sheets can associate in groups of 4, 5, 6 or 8. The octagonal nanotubes is composed of only rigid associations and is energetically more stable, whereas 4,5 and 6 are shown with flexible association only. Figure reprinted with permission from [55].

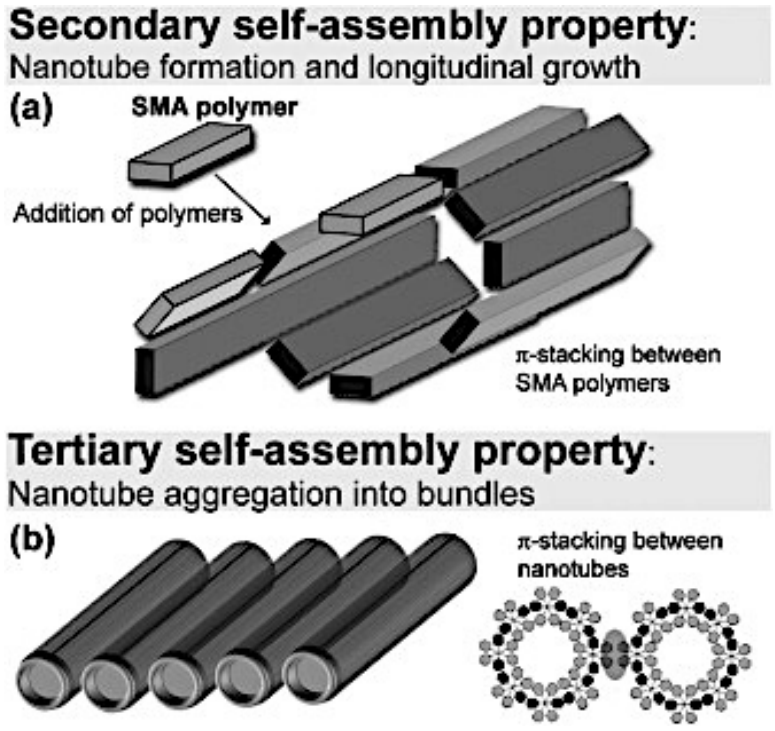

Figure 3.17. a) Formation of secondary structures represented by nanotubes. The nanotubes grow longitudinally via π stacking between SMA chains. b) Nanotubes then aggregates to form the tertiary structure of SMA. Reprinted with permission from [55].

In order to investigate the dimension of the structures formed in solution by the SMAs DLS analyses were performed on all the copolymer solutions.
A solution concentration of 1.5 wt% was chosen, in order to be equal to the polymer concentration in the nanodisc solution. Detailed description of the DLS experiment, sample preparation and model used for data analysis is reported in Chapter 2 Sections 2.7 and 2.8. The work done on the DLS showed two different behaviours of the different SMA copolymers studies in solution. The copolymers either formed only small structures (between 3 nm and 20 nm in diameter) or else the presence of two separate peaks, indicating aggregation of the polymer into larger structures (up to 600 nm) that might be due to the formation of polymer clusters. On a first analysis one can assume a correlation between the polymer Mw and the dimension of structures formed in solution. Indeed above all 33 kDa, the copolymers do seem to form larger structures, however in this analysis a major correlation can also be made between the size of the hydrophobic part compared to the hydrophilic component of the polymer architecture (values are reported in Table 3.8) since the hydrophobic interaction plays a crucial role in polymer assembly in solution [59].

Data from DLS analysis were plotted in volume% versus the hydrodynamic diameter and successively fitted to a lognormal distribution (Figure 3.18) to obtain an average diameter.

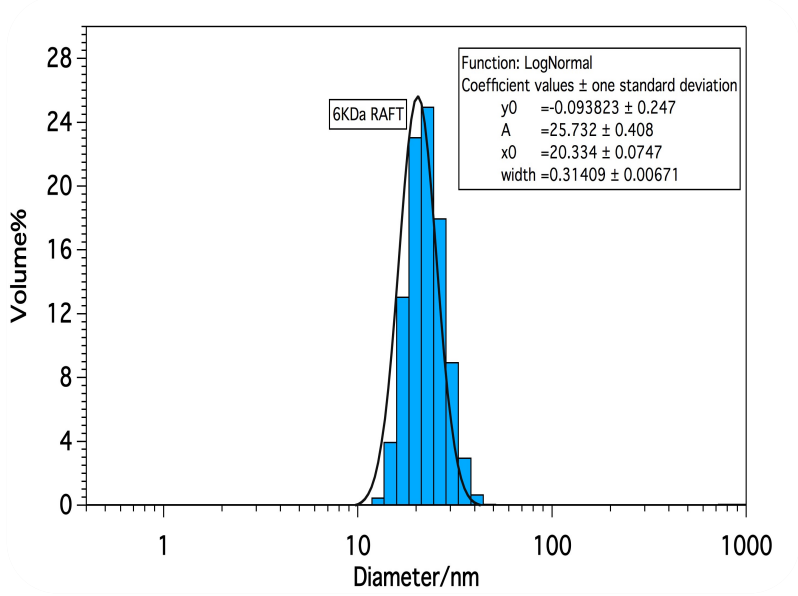

Figure 3.18. Plot of Volume% versus Diameter obtained from a DLS measurement of 6 kDa RAFT polymer synthesized in Bath with a total Styrene to Maleic Acid ratio of 2:1 (Bar chart) The data was fitted to a Log normal distribution (black continuous line).

To allow a more in depth structural characterisation of the copolymers in solution all the samples were also analysed via SANS on the LOQ instrument (ISIS). Data were treated according to the general procedure described in Chapter 2 Section 2.7.

In order to get a better signal, polymer solutions were analysed at a concentration of 6.5 wt% for all the polymer solutions, except the 110 kDa, which was analysed at a concentration of 6.1 wt%. These concentrations correspond to the stock solution values at which the copolymers were dissolved after hydrolysis. Although the concentrations of the DLS experiments are much lower, the data obtained from the two analyses can still be compared; assuming that the size of the structures formed by the copolymers in aqueous solution is not hugely affected by the concentration. Han et al. [59] showed a constant particle size distribution of SMA in aqueous media at pH 6.5 over a range of concentrations between 0.025 mg/mL to 1 mg/mL, so the concentrations measured in our case should be comparable.

In order to support this hypothesis, a sample of 11 kDa polymer in 50 mM phosphate buffer solution at pH 8 was analysed at three different concentrations using DLS (Figure 3.19). Although very concentrated samples are not ideal for DLS measurements results showed to be in a range from 1.7 ± 0.1 nm to of 1.9 ± 0.1 nm. One must point out that these values are from fitting of experimental data to a log normal distribution function and errors here reported correspond to ± one standard deviation also from the fitting analysis. This is not indicative of the precision of the technique that does not give an error of only ± 0.1 nm since measurements are affected by many parameters and results are expressed as a distribution of values.

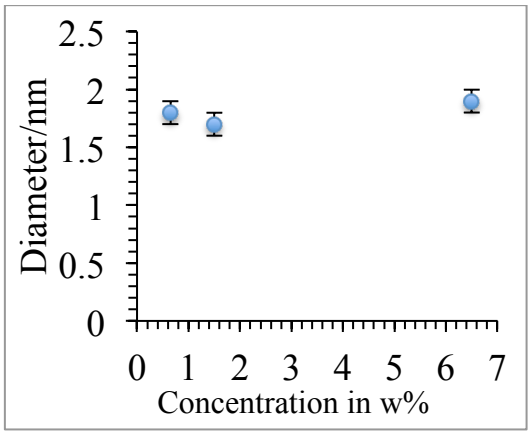

Figure 3.19. Diameter of 11 kDa polymer structures formed in 50 mM phosphate buffer solution at 25 °C, kept at pH 8 or higher, analysed using DLS at different wt% concentration. Values are from fitting of experimental results to a lognormal distribution function and error bars are ± one standard deviation.

After the preliminary analysis performed on DLS experiment all the copolymers were analysed via small angle neutron and X-ray scattering in order to be able to investigate in depth the aggregation behaviour in each solution. In the SANS and SAXS analysis, due to the q range selected, the big aggregates shown in the DLS analysis were not detected. Therefore, results for the 63 kDa and 110 kDa copolymers, listed in the Table 3.13 only refer to the smallest structures present in solution.

For the SANS experiments, all the copolymers were analysed in a 50 mM deuterated phosphate buffer solution to maximise the contrast between the polymer and the solvent. Considering the amphiphilic nature of the SMA the polymer conformation is not expected to be in a completely stretched conformation which is characteristic of a polymer in a selective solvent. Instead since the deuterated phosphate buffer solution is a good solvent only for the hydrophilic part of the SMA it is more likely that the styrene groups will tend to assemble together, minimizing the contact with the water.

A preliminary analysis of the data was done using the standard *Porod* and *Kratky* plots in order to have indications about the aggregation of the structures in solution. Representative examples of typical plots obtained for the SANS results are reported in Figure 3.20 A and B.

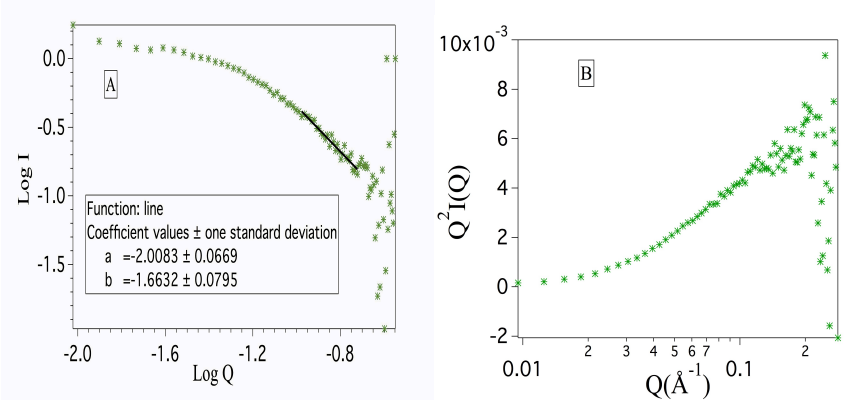

Figure 3.20. A) Porod plot and B) Kratky plot of 63 kDa polymer 6.5 wt% in completely deuterated phosphate buffer solution.

The Porod slope for all the copolymers analysed via SANS showed a value around 1.7, which is characteristic of a swollen polymer coil. SANS data from the 7 kDa, 11 kDa, 33 kDa, 63 kDa and 110 kDa (Figure 3.21) were therefore fitted to a Debye model for Gaussian polymer chains using the NIST SANS Analysis package in "Igor Pro". Detailed descriptions of software and of the models used are reported in Chapter 2 Section 2.8. Results of the fitting are summarised in Table 3.11.

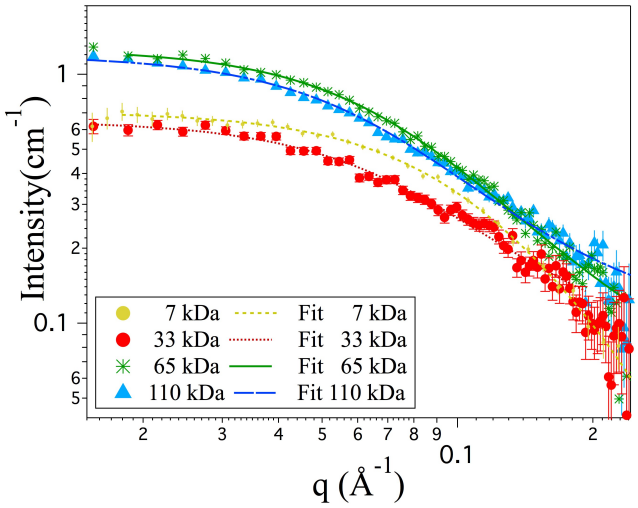

Figure 3.21. SANS experiment performed on LOQ (ISIS, UK), fitted to a Debye model (continuous lines) of three different polymer Mws in 50 mM phosphate buffer solution prepared with 100% D_2O, 200 mM NaCl at pH 8 and 25 °C.

SAXS data for all the copolymers were also collected on the I22 instrument located at the Diamond Light source (Figure 3.21) and at the SAXSess instrument located at the University of Bath for the 6 kDa RAFT SMA (Figure 3.25) and the 7 kDa SMA 2000P copolymers. Polymer solutions were prepared at the same polymer concentration (6.5 wt%) in 100% H_2O phosphate buffer at pH 8. As suggested by comparison in the plot for the different polymer data (Figure 3.22), similar structures were formed by the 33 kDa, 63 kDa and 110 kDa whereas the 11 kDa showed more compact aggregates. Prior to fitting with an appropriate model, Porod and Kratky plots were analysed revealing the presence of more compact shapes with respect to the same copolymers in deuterated solutions, including structures with a rod-like shape a representative example is reported in Figure 3.23. However it was not possible to fit the data from the 11 kDa polymer to any of the models attempted.

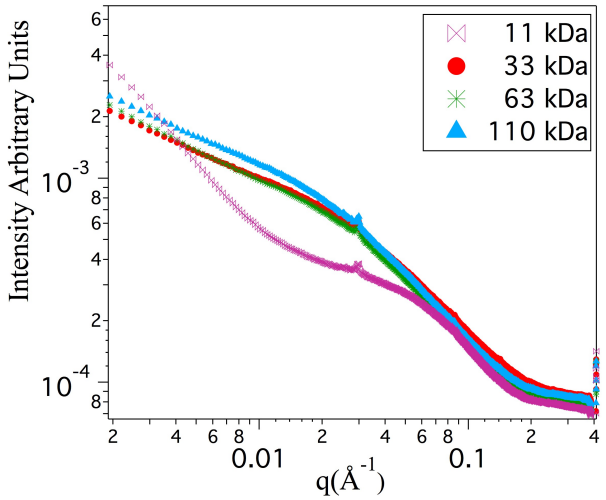

Figure 3.22. Data from 11 kDa, 33 kDa, 63 kDa and 110 kDa copolymers collected on the I22 instrument at Diamond Light Source, temperature was kept at 25 °C, all the copolymers are at 6.5 wt% concentration in a 50 mM phosphate buffer solution at pH8. The small peak at q ≈ 0.03Å^{-1} is a detector artefact.

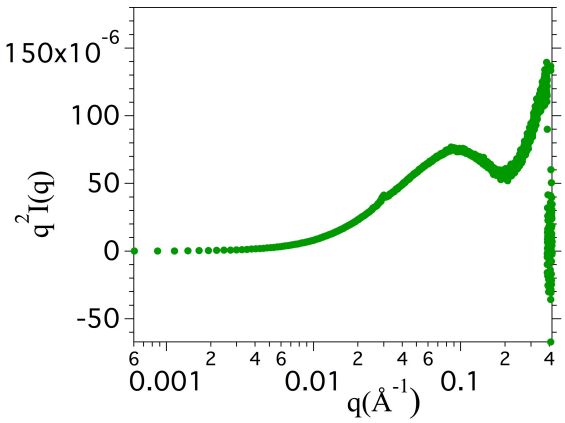

Figure 3.23. Kratky plot of 63kDa Polymer 6.5 wt% in 100 %H_2O analysed on the I22 instrument located in Diamond (Oxford UK).

Data from the 33 kDa, 63 kDa and 110 kDa were fitted to a straight cylinder model with polydispersity on the radius (a detailed description of the model is reported in Chapter 2 Section 2.8). In Figure 3.24 is reported a representative example of the I22 SAXS fitting results for the 33 kDa. Fitting of 63 kDa and 110 kDa are not reported on the same graph for clarity as they partially overlap

each other. In Table 3.9 are reported results from the fitting of the three data sets.

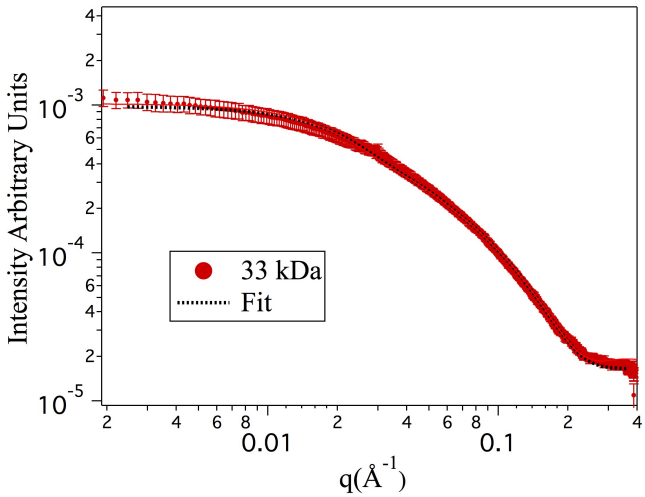

Figure 3.24. SAXS data of 33 kDa polymer in 50 mM phosphate buffer solution (filled red circles) fitted to a cylinder model (black dotted line).

The SLD of the solvent was calculated (9.40×10^{10} cm^{-2}) and held during the fitting, all the others parameters were fitted including the SLD of the cylinder. It is likely that the hydrophobic part of the polymer tends to concentrate toward the interior part of the cylinder protected by the hydrophilic part of the polymer in contact with the buffer solution; however copolymers are not organised into a well-defined core-shell structures therefore the straight cylinder showed to be the most appropriate model for fitting of these data sets.

Model Parameters	*33 kDa*	*63 kDa*	*110 kDa*
Scale	0.04 ± 0.01	0.01 ± 0.01	0.06 ± 0.01
Radius (nm)	1.28 ± 0.05	1.31 ± 0.05	1.48 ± 0.5
Length (nm)	207 ± 10	273 ±10	264 ± 10
Polydispersity of Radius	0.14 ± 0.01	0.18 ± 0.01	0.13 ± 0.01
SLD cylinder (cm^{-2})	$9.45\times10^{10} \pm 0.5\times10^{10}$	$9.47\times10^{10} \pm 0.5\times10^{10}$	$9.43\times10^{10} \pm 0.5\times10^{10}$
Background (cm^{-1})	$1.61\times10^{11} \pm 0.5\times10^{11}$	$9.66\times10^{10} \pm 0.5\times10^{10}$	$1.52\times10^{11} \pm 0.5\times10^{11}$

Table 3.9. Fitting values from data of 33 kDa, 63 kDa and 110 kDa fitted to a Straight Cylinder Model.

Scattering from the 6 kDa RAFT and 7 kDa SMA-2000P copolymers were both analysed on the in house SAXSess instrument. Also for these data a preliminary analysis was conducted using the Porod and Kratky plot, revealing also for the 7 kDa a slope around 1, which is indicative of rigid rod-like structures in solution, however data were too noisy to be properly analysed.

Since the 6 kDa RAFT polymer sample was measured at high pH (pH = 8.5) the formation of nanotubes was not expected. However the dimensions found in the DLS analyses indicated a tendency of the polymer to form larger aggregates. Therefore the structure was hypothesised to consist of spherical aggregates with a core of hydrophobic styrene molecules surrounded by a shell of maleic anhydride molecules. A single core-shell sphere model was not able to fit the data, particularly due to the presence of larger structures giving rise to scattering at low q. Therefore the data was fitted to a core-shell sphere model in combination with a larger sphere model with Schultz polydispersity on the radius, generally used for a population of polydisperse spherical particles (a

more detailed description of the model, detailed descriptions of the models in use is reported in Chapter 2 Section 2.8). Experimental results are summarised in Table 3.10.

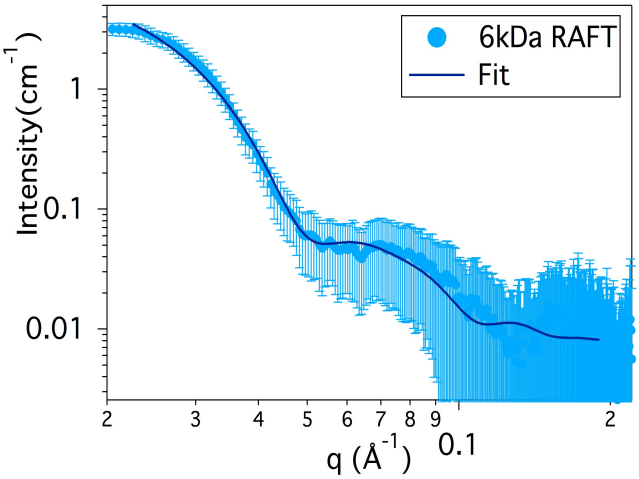

Figure 3.25. SAXS profile of a 6 kDa RAFT polymer analysed in Bath (filled blue circles) fitted to a combined model of large spheres with a Shultz polydispersity and smaller core shell spheres (continuous black line).

In the fitting the SLD of the sphere for the Shultz sphere model was calculated as the SLD of the SMA whereas for the core shell model the SLD of the core was initially calculated to be equal to the SLD of styrene and the SLD of the shell equal to that of the maleic acid component. Both were then fitted in order to take into account solvent penetration and the presence of styrene into the shell and maleic acid in the core of the structures. SLD for the solvent was calculated and held during the fitting (9.40×10^{10} cm^{-2}), also charge (0.31), salt concentration (0.25 M), dielectric constant (78) and temperature were calculated or set from literature and held during the fitting; all the other parameter were fitted and results of the fitting are reported in Table 3.10.

Parameters	*Values From Fitting*
Volume Fraction (scale)	0.0018 ± 0.0001
Mean radius (nm)	8.9 ± 0.1
Polydispersity	0.12 ± 0.02
SLD sphere (cm^{-2})	$1.08\times10^{11} \pm 0.5\times10^{11}$
Volume fraction	0.001 ± 0.001
Average core radius (nm)	4.5 ± 0.1
Core polydispersity	0.07 ± 0.04
Shell thickness (nm)	1.8 ± 0.1
SLD core (cm^{-2})	$9.85\times10^{10} \pm 0.5\times10^{10}$
SLD shell (cm^{-2})	$1.25\times10^{11} \pm 0.5\times10^{11}$
Background (cm^{-1})	$9.44\times10^{-7} \pm$ 1e-10^{-7}

Table 3.10. Results from fitting of SAXS data of 6 kDa RAFT to a core shell model combined with a Shultz sphere.

In these results the polymer appears to form smaller spheres around 4.5 nm in core radius and larger ones, which are roughly double in size. Given that the fully extended hydrophobic portion of the polymer was calculated to have a length of roughly 5.3 nm and the hydrophilic part to be 20 nm the core size of the smaller aggregates is similar to the length of the hydrophobic chain of the polymer. However the much larger hydrophilic alternating SMS part must also be mainly incorporated in the core of the core-shell structures, since the shell is much thinner.

Comparing the results obtained with data reported in literature [58] it can be concluded that the copolymers were not organised into nanotubes due to the pH used (pH was always between 8 and 8.5) which is confirmed by the absence of peaks around 0.7 nm^{-1}, indicative of the presence of ordered systems [57]. In solution instead they probably were single monomers in a more extended conformation but with still the hydrophobic part of the polymer arranged in a way that minimises the contact with the solvent.

The different behaviour in water compared to the deuterated solvent might be due to the higher hydrogen bonding strength of D_2O with the hydrophilic part of

the polymer resulting in water being a poorer solvent for the polymer compared to D_2O.

An isolated case is represented by the 6 kDa RAFT polymer, which had a higher level of organisation into spherical structures. This is probably related to the different architectures of the polymer which is characterised by a tail of only styrene monomers that are occupying the core of the sphere as also suggested by the SLD found in the fitting which value (9.85×10^{10} cm^{-2}) is very close to the value of only styrene in solution (9.6×10^{10} cm^{-2}) one can attribute the difference in values to the presence of solvent and maleic acid into the core. The structure formed seems to be rather than composed of a well-defined core of styrene and shell of maleic acid more like aggregate of polymer chains which being constituted of a more ordered architecture with a SSS tail a low polydispersity assemble into similar structures of roughly the same dimension.

Diameter values reported for SAXS experiments refer to the smaller diameter found in the fitting. Disagreement between DLS and small angle scattering data for the size of structures formed by the 63 kDa and 110 kDa are due to the q range selected during scattering experiments.

	DLS Diameter [(a)] *(nm)*	*SANS Diameter* [(b)] *(nm)*	*SAXS Diameter* [(b)] *(nm)*
6 kDa RAFT	20 ± 0.2	8.9 ± 0.1	12.8 ± 0.2
7 kDa	3.21 ± 0.04	1.6 ± 0.1	1.1 ± 0.2
33 kDa	2.5 ± 0.03	4 ± 0.1	2.6 ± 0.2
63 kDa	497 ± 6	4.4 ± 0.1	2.6 ± 0.2
110 kDa	9.6 ± 0.07/509 ± 6	5.1 ± 0.1	3.0 ± 0.2

Table 3.11. Table summarising results of analysis performed at 1.5 wt% (a) and 6.5 wt% (b) via DLS and small angle scattering, for different polymer molecular weights.

3.10 Study of SMA Copolymers Under Different Conditions

Further investigations of the polymer structures were made under different salt concentration, temperatures and pHs in order to complete the analysis of the SMALPs structures under the same conditions. This should enable a better understanding of the role of the polymeric belt in the self-assembly process of nanodiscs and to identify the eventual contribution of the polymer to the stability of the nanodiscs when these important parameters are changed.

3.10.1 Investigation of SMA Copolymers at Different Salt Concentrations

The ionic strength impact on the self-assembled systems has been already investigated proving to be an important factor in the stability of the structure [60, 61]. For example, it has been found that an increase in salt concentration leads to swelling effects on micelles formed in solution by 2-(diethyl amino) ethyl methacrylate (DEAEMA) [61].

An analysis of the effect of different ionic strengths on polymer structures in aqueous solution was done using the SANS instrument LOQ. The effect of the ionic strength on SMA conformation was studied using two different salt concentrations of 50 mM and 200 mM NaCl.

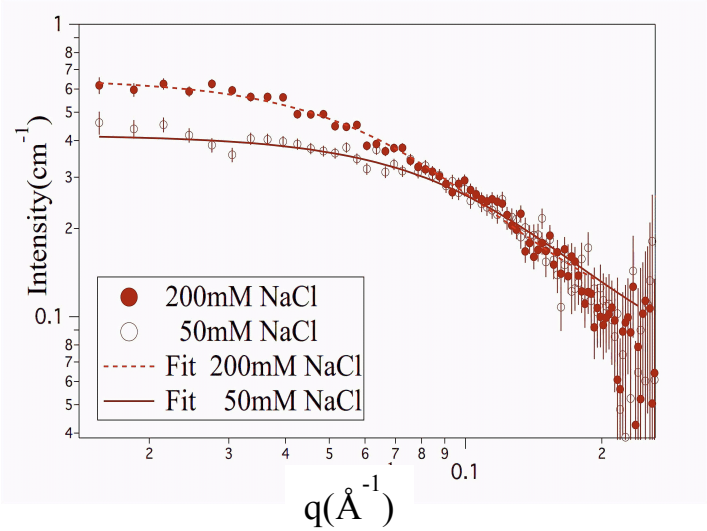

Figure 3.26. SANS patterns from 33 kDa copolymer in phosphate buffer solution with 200 mM NaCl (top curve, filled circles) and 50 mM NaCl (bottom curve empty circles). Both sets of experimental data have been fitted to a Debye model (continuous and dashed lines in the graph).

	33 kDa	*63 kDa*	*110 kDa*
50 mM NaCl	2.6 ± 0.2 nm	3.7 ± 0.2 nm	3.3 ± 0.2 nm
200 mM NaCl	4.3 ± 0.2 nm	4.4 ± 0.2 nm	5.1 ± 0.2 nm

Table 3.12. Diameters in nm, found from fitting to a Debye model of SANS data collected on LOQ of copolymers in different salt concentrations in Phosphate buffer 50 mM solution pH 8.

From the results of analysis performed on different copolymer molecular weight (values are reported in Table 3.12) it was observed a small increase in the diameter of the structures analysed when the salt concentration is increased. This effect might be due to the interaction of the ions in solution with the charged part of the copolymer represented by the maleic acid part of the copolymer. The salt screens the negative charge and therefore the repulsion effect and at the same time increasing the aggregation number resulting in a global increase in the total diameter.

Investigation of SMA Copolymers at Different Temperatures

The stability of SMALP structures was investigated at different temperatures in order to enable the use of these structures for many different potential applications. For instance many proteins need to be stored at low temperature therefore the support in which they are encapsulated has to be stable not only at room temperature but also between temperatures as low as typical refrigerated storage temperatures around 5/8 °C but also at all the intermediate temperatures up to 25 °C considered the average room temperature. Moreover the SMALPs technology might be employed in the drug delivery field, as already successfully done with the protein stabilised version [62] then stability at the average body temperature of 37 °C is required.

Analyses conducted on the SMALPs structures (see Chapter 5 Section 5.2) were replicated on the copolymers in solution in order to fully understand their impact on the stability of the SMALP structures. However the analysis performed via DLS was particularly difficult due to the high polydispersity of the copolymers and the presence of large aggregates, to which this particular analysis is very sensitive. Particularly in the case of commercial copolymers the distribution of particles sizes around the mean values are very broad.

As a general behaviour polymer structures proved to be stable over the range of temperatures analysed, which is particularly evident from the analysis of the 6 kDa RAFT polymer, and 33 kDa on DLS experiments resulting in a stability in size and in the polydispersity of the sample that was not maintained by other copolymers such as the 11 kDa. However, no obvious relationship was found between the increase in temperature and increasing or decreasing of the structure diameters. Two representative samples are reported in Figures 3.27. The DLS results for all the copolymers studied are summarised in Table 3.13.

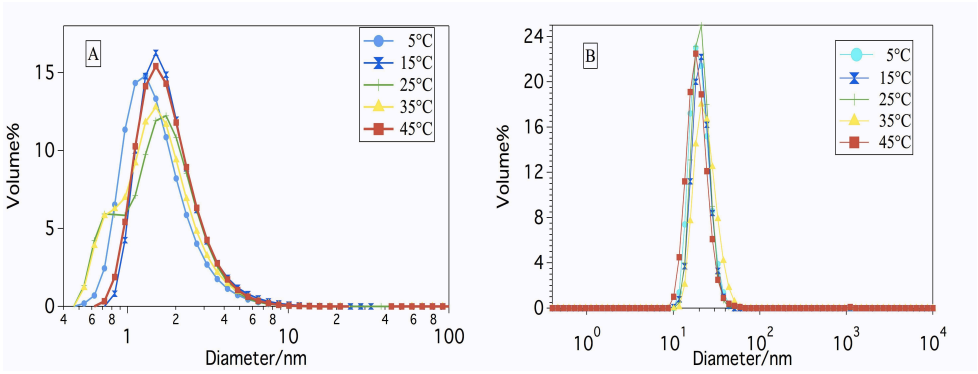

Figure 3.27. Plot of DLS diameter results of A) 11 kDa commercial polymer B) 6 kDa RAFT polymer both analysed in a range from 5°C to 45°C.

	5 °C		*15 °C*		*25 °C*		*35 °C*		*45 °C*	
	Small	*Large*	*Small*	*Large*	*Small*	*Large*	*Small*	*Large*	*Small*	*Large*
6 kDa RAFT	19.50 ± 0.06	—	20.5 ± 0.08	—	20.3 ± 0.03	—	22.5 ± 0.2	—	18.3 ± 0.03	—
7 kDa	3.07 ± 0.03	—	3.07 ± 0.03	—	3.21 ± 0.04	—	0.7 ± 0.01	2.98 ± 0.02	3.54 ± 0.04	—
11 kDa	1.3 ± 0.02	—	1.6 ± 0.03	—	1.8 ± 0.04	—	1.4 ± 0.03	—	1.6 ± 0.02	—
33 kDa	2.5 ± 0.03	—	2.5 ± 0.03	—	2.5 ±0.03	—	2.5 ± 0.03	—	2.4 ± 0.02	—
63 kDa	—	516± 8	—	492 ± 5	—	497 ± 6	—	429 ± 2.2	—	430 ± 3.9
110 kDa	1.9 ± 0.02	7.4 ± 0.1	10.7 ±0.3	510 ± 6	9.6 ± 0.07	509 ± 6	12.2 ±0.02	453 ±2.6	12.4 ±0.04	452 ± 1.6

Table 3.13. Diameters (nm) from DLS measurements after experimental data have been fitted to a log normal distribution. Data have been collected increasing temperature from 5 °C up to 45 °C for solutions at 1.5 wt% concentration in 50 mM phosphate buffer in water with 200 mM NaCl at pH 8.

The general tendency observed among all the copolymers is the stability around an average diameter. However the data reported in Table 3.13 show some fluctuations in the values that are likely to be related to the kind of analysis performed. During the evaluation of the results the statistical population

analysed should be taken into account. For the experimental data here reported, 7 runs were performed for 11 repeats on the same sample for each temperature, which can be increased to obtain better statistics.

The 6 kDa RAFT polymer appeared to be the most stable in size over the range of temperature analysed. This stable temperature behaviour was seen for all copolymers at this molecular weight, even comparing those synthesised in different batches of RAFT polymerisation. This feature is probably related to the high purity and low polydispersity of this polymer when compared to that of the commercial polymer samples.

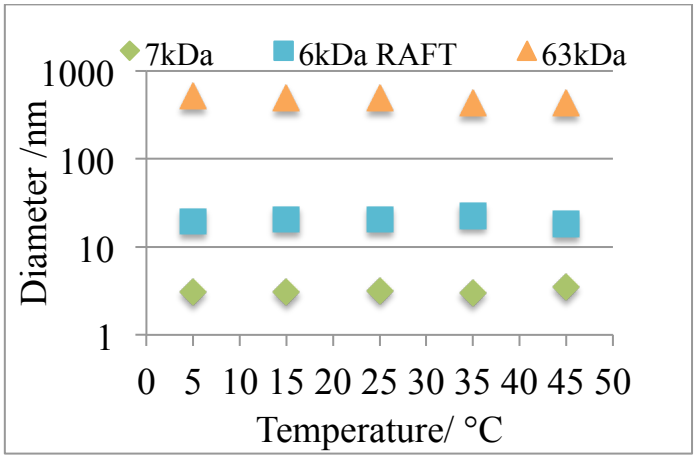

Figure 3.28. DLS data from experiments performed on: 6 kDa RAFT polymer (blue squares), 7 kDa SMA-2000P (green rhombus) and 63 kDa (orange triangles) in phosphate buffer solution. Diameters of the structures are plotted as a function of the temperature.

The general trend was confirmed by the same analysis performed using small angle scattering on 6.5 wt% polymer solutions, either on the I22 instrument at Diamond light source (Figure 3.29) and the SAXSess instrument (Figure 3.30) in Bath. Considering the preliminary analysis performed on the 25 °C data to probe the shape of the structures in solution and choose the most appropriate model all the data sets at different temperature were fitted accordingly. Therefore data from the temperature scan performed on the 33 kDa, 65 kDa and 110 kDa were all fitted to a cylinder model whereas the 6 kDa RAFT data were

fitted to combined models of a core-shell sphere with a polydisperse core combined with a larger solid sphere spheres with a Schulz polydispersity.

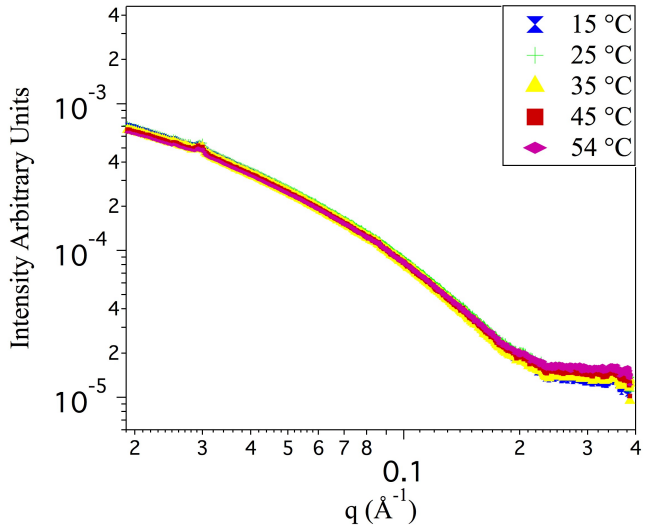

Figure 3.29. Data set of temperature scan performed on 110 kDa polymer 6.5 % in a phosphate buffer solution kept at pH 8. Data were collected on the I22 instrument (Diamond). The small peak at $q \approx 0.03 Å^{-1}$ is a detector artefact.

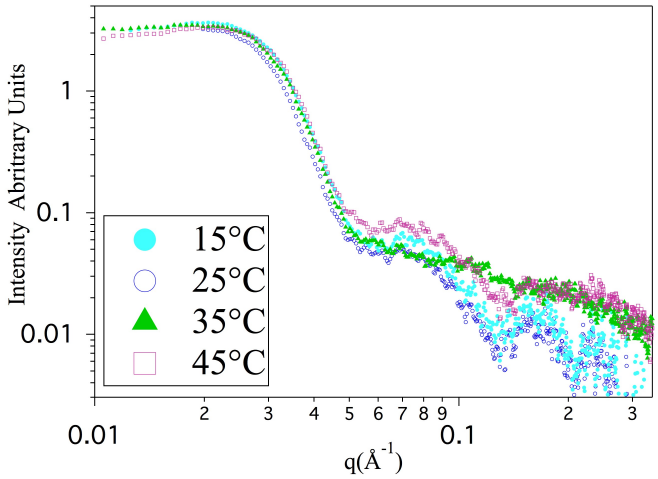

Figure 3.30. Data set of temperature scan performed on 6Da RAFT polymer 6.5wt% in a phosphate buffer solution kept at pH 8. Data were collected on the SAXSess instrument (University of Bath).

Moreover sample of 6 kDa RAFT polymer and 7 kDa SMA-2000P were also analysed via SANS experiments performed at the LOQ instrument located in

ISIS. Structures behaviour was probed over a range of temperature from 15 °C raising up to 45°C. Copolymers were prepared in the standard 50 mM phosphate buffer solution and analysed at a 6.5 wt% concentration. 6kDa RAFT data were fitted to a sphere with core shell structure and polydispersity on the radius and hard sphere structure factor. Whereas 7 kDa data were fitted to Debye model as discussed in Section 3.9.Temperature scan of both polymer solutions are reported in Figure A3AppendixA2.

Data from the experiment performed using SAXS, SANS and DLS are summarised in the Table 3.14. Errors reported are for the DLS measurements referred to the values of ± one standard deviation obtained from fitting of DLS data to a lognormal distribution function whereas for SAXS and SANS indicates the variation possible in this parameter while the χ^2 parameter (the goodness of fit) remains minimized.

Polymer/ Temperature	*Diameter /nm*		
*6 kDa RAFT**	*SAXS (core +shell)*	*SANS Debye diameter*	*DLS*
5 °C	—	—	19.5 ± 0.06
15 °C	16.2 ± 0.2	—	20.5 ± 008
25 °C	16.2 ± 0.2	—	20.3 ± 0.03
35 °C	16.2 ± 0.2	—	22.5 ± 0.2
45 °C	16.2 ± 0.2	—	18.3 ± 0.03
54 °C	16.2 ± 0.2	—	—
7 kDa			
5 °C	—	—	3.1 ± 0.03
15 °C	—	2.1 ± 0.1	3.1 ± 0.03
25 °C	1.1±0.2	1.6 ± 0.1	3.2 ± 0.04
35 °C	—	1.6 ± 0.1	3.0 ±0.02
45 °C	—	1.5 ± 0.1	3.5 ± 0.02
54 °C	—	—	—
11 kDa			
5 °C	—	—	1.3 ± 0.02
15 °C	—	—	1.6 ± 0.03
25 °C	—	—	1.8 ± 0.04
35 °C	—	—	1.4 ± 0.03

45 °C	—	—	1.6 ± 0.02
54 °C	—	—	—
33 kDa			
5 °C	—	—	2.5 ± 0.03
15 °C	2.9 ± 0.1	—	2.5 ± 0.03
25 °C	3 ± 0.1	4±0.1	2.5 ± 0.03
35 °C	2.9 ± 0.1	—	2.5 ± 0.03
45 °C	2.9 ± 0.1	—	2.4 ± 0.02
54 °C	2.4 ± 0.1	—	—
63 kDa			
5 °C	—	—	516 ± 7.6
15 °C	2.6 ± 0.1	—	492 ± 5
25 °C	2.8 ± 0.1	4.4 ± 0.2	497 ± 6
35 °C	2.8 ± 0.1	—	429 ± 2.2
45 °C	2.9 ± 0.1	—	430 ± 3.9
54 °C	2.8 ± 0.1	—	—
110 kDa			
5 °C	—	—	1.9 ± 0.02/ 7.4 ± 0.1
15 °C	10.2 ± 0.03	—	10.7±0.3/ 512 ± 6
25 °C	10.6 ± 0.03	5.1 ± 0.2	9.6 ± 0.07/ 509 ± 6
35 °C	10.4 ± 0.03	—	12.23 ± 0.02/ 453 ± 3
45 °C	10.8 ± 0.03	—	12.4 ± 0.04/ 4518 ± 2
54 °C	10.4 ± 0.03	—	-

Table 3.14. Diameter values (nm) for different copolymers collected increasing temperature from 5 °C up to 45 °C. SAXS (column 2) *data collected on I22 fitted to a cylinder model with polydispersity on the radius. * Data collected on SAXSess in Bath and fitted to a combined model of core shell sphere model in combination with a larger sphere model with Shultz polydispersity on the radius, generally used for a population of polydisperse spherical particles, values reported here are the mean radius. Data collected at LOQ* (column 3*) fitted to a Debye model. (*Column 4) *Results of DLS measurements after experimental data have been fitted to a log normal distribution. Details of models in use are reported in Chapter 2 Section 2.8 and a detailed description of sample preparation and experimental setup is reported in Chapter 2 Section 2.7.*

From Figure 3.27 A the typical behaviours of commercial copolymers can be compared to that of the 6 kDa RAFT polymer shown on Figure 3.27 B. Dimensions of the structures formed in solution by the commercial copolymers proved to depend on the batch of hydrolysed polymer used. This is probably due to the high polydispersity and potentially also variation in the degree of hydrolysis, however since copolymers were provided already hydrolysed it was not possible to validate this hypothesis. However, the 6 kDa SMA synthesised via RAFT polymerisation gives rise to structures all in the range of 20 nm, and these are stable over a wide range of temperatures, as observed in the data reported in Table 3.16.

3.10.2 Investigation of SMA Copolymers at Different pHs

All the SMA copolymers are composed of a hydrophilic and a hydrophobic part and the charge on the hydrophilic part of the polymer is pH dependent. A pH titration was carried out using 20 mL of 1wt% polymer solution titrated against 0.01 M HCl to determine the pKa of these copolymers. In order to start the titration with the polymer completely deprotonated, the original pH=8 was raised to pH=12 by addition of 2.16 mL of a 2 M NaOH solution. A diagrammatic representation of the titration process is depicted in Figure 3.31.

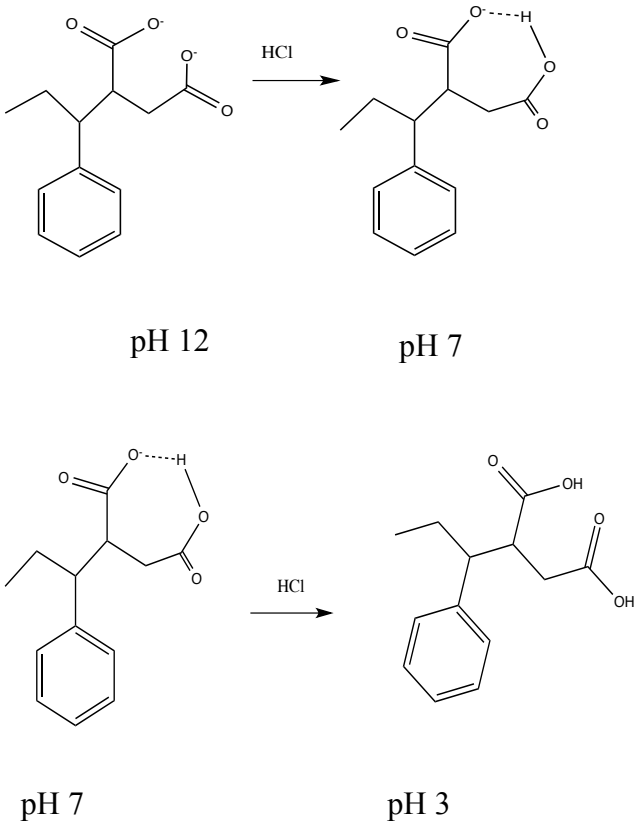

Figure 3.31. Scheme of protonation of SMA copolymer showing the hydrogen bond formed at pH 7.

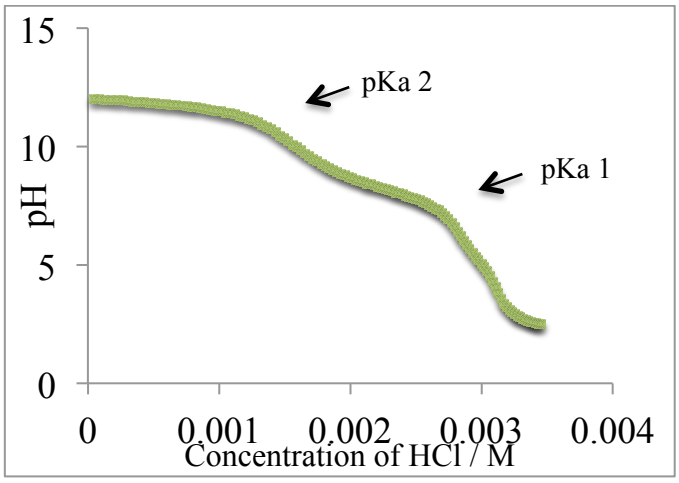

Figure 3.32. pH titration of 7 kDa SMA-2000P commercial copolymer, titrated against 0.01 M HCl. Error bars were too small to be visible in the graph therefore have not been included.

From the analysis of the results the polymer was shown to possess two pKa values. The first pKa was found to be at pH= 5 and the other at pH = 9.7. These results are supported by the previous work of Cao [63, 64] and Kitano [64] which suggests that the two pKa values are due to the formation of strong hydrogen bonds due to the presence of two carboxylic acid groups. Once the first carboxylic acid group is ionised a strong intra hydrogen bond forms with the other, preventing the ionisation of the second group.

Surface tension analysis of the 7 kDa SMA-2000P commercial copolymer was performed in parallel with a pH titration experiment in order to monitor how the surface tension of the copolymer in solution was affected with varying pH, due to the degree of ionization of the maleic acid group present in the copolymer; analysis was done between pH 5 and pH 12. Details of the experimental setup and the instrument in use are reported in Chapter 2 Section 2.7.4.

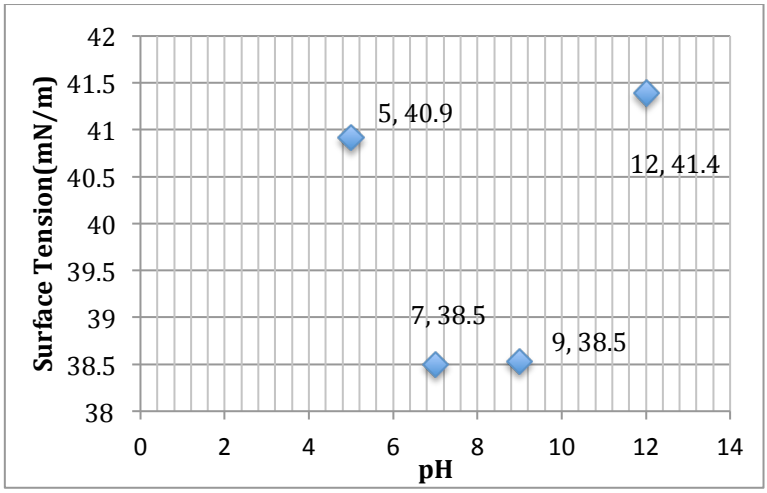

Figure 3.33. Plot of surface tension versus pH values for the 7 kDa SMA-2000P commercial copolymer.

As can be observed from the graph showed in Figure 3.33, starting with the polymer in a phosphate buffer solution at pH 12 there is a decrease in surface tension values as the solution become more acidic. This could be explained as the polymer becoming partially protonated, and thus less soluble in the solution, causing it to favour adsorption at the hydrophobic air interface. It can also be

observed that surface tension values reach a plateau between pH 7 and 9, which correspond to the second pKa of the polymer observed at pH 9.7 (Figure 3.32). Further decrease in the pH caused the polymer to be no longer soluble in solution showing the formation of aggregates (at pH<5). Precipitation of insoluble polymer removes material from the interface, causing the increase in surface tension values registered at pH 5.

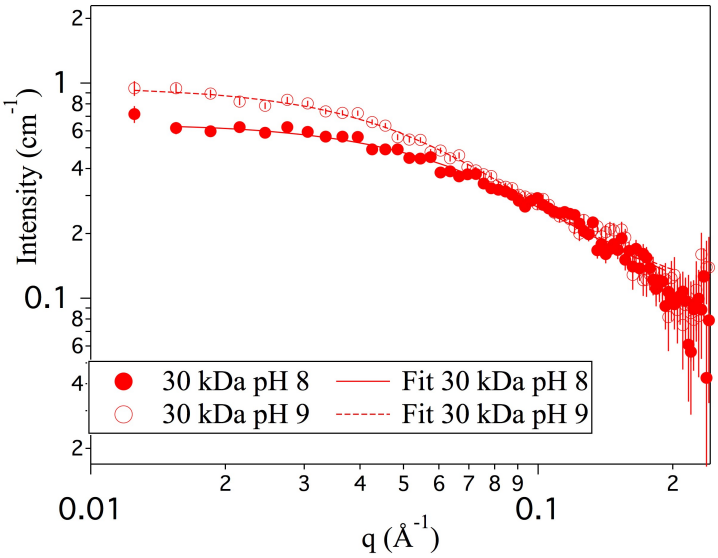

Figure 3.34. SANS data of a 33 kDa SMA copolymer analysed at pH 8 (filled red circle) and pH 9 (empty red circle).

Polymer Mw	*33 kDa*	*63 kDa*	*110 kDa*
pH 8	4.3 ± 0.2 nm	4.4 ± 0.2 nm	5.1 ± 0.2 nm
pH 9	5.7 ± 0.2 nm	4.7 ± 0.2 nm	7.2 ± 0.2 nm

Table 3.15. Diameters in nm of polymer aggregates formed in 50 mM phosphate buffer solution with 200 mM NaCl concentration, and two different pHs. Results reported are from fitting of SANS data to a Debye model for copolymers of different pH and molecular weights values.

As can be seen from the results reported in the Table 3.15 the dimensions of the SMA aggregates showed only a very small change between pH 8 and pH 9. This is as expected considering changes in the primary structure of the polymer at this level of protonation as discussed in the Section 3.9. These results are coherent with the behaviour observed from the surface tension analysis and also with the fact that the copolymers are observed to swell in higher salt concentration.

3.11 Discussion and Conclusions

Analyses performed on the various copolymers were found to be very challenging particularly because of the high polydispersity of all the commercial copolymers and the fact that the copolymers were synthesised and hydrolysed in different laboratories, so the initial conditions during these processes were not possible to be monitored. This might be part of the reason why results showed the 6 kDa RAFT polymer to be the most stable and reliable in term of size distribution analysis among all of the copolymers analysed.

Nonetheless the information collected with the experiments reported here (see Table 3.16 for a summary) supported by the work found in literature allows some conclusions to be drawn on which factors affect the assembly of the SMALPs structures. From the analysis on the styrene to maleic acid total proportion one can conclude that copolymers with a styrene to maleic acid total molar ratio higher that 2:1 were not able to form nanodiscs In addition, from the copolymers synthesised in Bath, also the 1.7:1 styrene to maleic acid total molar ratio was found not suitable for formation, giving an indicative lower limit for the hydrophobic to hydrophilic proportion in the SMA polymer structure. As later explained in Chapter 4 Section 4.5.1.

Copolymer	*STY : MA proportion*	*SSS Dimension (nm)*	*SMS Dimension (nm)*	*SSM/MSS Dimension (nm)*	*Structures in Solution* (nm)*	*Forms SMALP*
6 kDa RAFT	2:1	5.25	19.8	____	20.33 ± 0.03	Yes
7 kDa SMA-2000P	2:1	5.47	1.61	10.83	2.9 ± 0.07	Yes
11 kDa	1.85:1	9.97	2.47	10.34	1.9 ± 0.02	Yes
33 kDa	1.95:1	19.95	15.07	33.30	2.55 ± 0.03	Yes
63 kDa	2.43:1	53.15	15.78	62.23	497 ± 6	No
110 kDa	2:1	92.5	27.47	108.15	9.62 ± 0.07/ 509 ± 6	No

*Table 3.16. Table summarising the principal findings of the investigation performed on the polymer structural characteristics. * Indicate dimensions of copolymers in phosphate buffer solutions measured via DLS experiment at 25 °C with a 1.5 wt% polymer concentration.*

Moreover since the hydrophobic interaction between the phospholipids tails and the non-polar part of the polymers the driving force of the self-assembly process, it is likely that the one of the key structural elements consists of the proportion between the different groups (SSS, SMS, SSM, MSS) composing the polymer architecture. Indeed the copolymers that were not able to assemble into nanodiscs both possess a consistent portion of hydrophobic region. Another characteristic of the polymer not forming SMALPs is that they form large structures in solution, so that the molecular weight may be too high to allow nanodiscs to form.

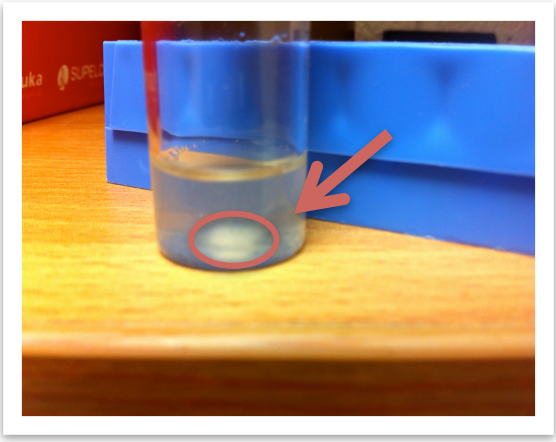

Figure 3.35. Large aggregates in a 6.5 wt% solution of 7 kDa SMA-2000P commercial copolymer, in 50 mM phosphate buffer solution pH 8, kept at 4 °C for 6 months.

Moreover, SAXS, SANS and DLS analysis were performed on copolymers hydrolysed and prepared at different times. Also some of them were kept in the fridge after hydrolysis and after some time these solutions sometimes formed visibly large aggregates. Figure 3.35 shows a sample of a 7 kDa SMA-2000P commercial polymer kept in the fridge for the period of 6 months where aggregates are clearly visible at the bottom of the vial. Even though this is an extreme example, since care was made to guarantee the quality of samples prepared for measurements using fresh solutions, it still shows that copolymers can aggregate as time passes and thus change considerably the aggregate dimensions. This could be one factor, which can justify the imperfect accordance of DLS, SANS, and SAXS experimental results.

In addition when comparing the different results it should be noted that the DLS technique measures (as explained more in detail in Chapter 2 Section 2.3) not the "bare" polymer radius but what is called "hydrodynamic radius" which takes into consideration not only the core particle size but also the electric double layer around the particles, which is affected by the ionic concentration of the medium increasing the apparent total diameter.
Also samples analysed via DLS and SAXS were all in H_2O whereas samples analysed in SANS experiments were all in D_2O buffer, which may affect the way the copolymers assemble [65] as also suggested by the different results obtained with SAXS and SANS.

In summary, based on the results here discussed it can be concluded that the optimal polymer for assemble of SMALP structures seems to be the 6 kDa polymer synthesised in Bath via RAFT polymerisation. This polymer showed to be particularly stable over time allowing high reproducibility in the experimental results. Polydispersity of the sample was also much lower compared to the commercial copolymers analysed. As will be discussed in Chapter 4, many of these features reflect on the SMALPs structures themselves showing the importance of the polymeric belt around the discs not only in the SMALPs self-assembly process but also in their behaviour under different conditions.

3.12 References

1. Cowie, J.M.G., *Polymers: chemistry and physics of modern materials.* 1991, Glasgow; New York: Blackie ; Chapman and Hall.
2. Campbell, I.M., *Introduction to synthetic polymers,* 2000, Oxford; New York: Oxford University Press.
3. Stevens, M.P., *Polymer Chemistry an Introduction*. 3rd Edition, 1999, New York: Oxford University Press.
4. Gowariker, V.R., et al., *Polymer Science,* 1986: New Age International Pub. (P) Limited.
5. Fetters, L.J., et al., *Connection between Polymer Molecular Weight, Density, Chain Dimensions, and Melt Viscoelastic Properties.* Macromolecules, 1994. **27**(17): p. 4639-4647.
6. Harland, W.G., *Relation between Intrinsic Viscosity and Degree of Polymerization.* Nature, 1952. **170**(4329): p. 667-667.
7. Percec, V. and A. Keller, *A thermodynamic interpretation of polymer molecular weight effect on the phase transitions of main-chain and side-chain liquid-crystal polymers.* Macromolecules, 1990. **23**(20): p. 4347-4350.
8. Cowie, J.M.G., *Polymers: chemistry and physics of modern materials,* 1973, Aylesbury: Intertext.
9. Klumperman, B., *Polymer Chemistry.* 2010. **1**: p. 558-562.
10. Izunobi, J.U. and C.L. Higginbotham, *Polymer Molecular Weight Analysis by 1H NMR Spectroscopy.* J. Chem. Educ., 2011. **88**(8): p. 1098-1104.
11. Benoît, H., *Perspective: Comments on "Gel permeation chromatography. I. A new method for molecular weight distribution of high polymers," by J. C. Moore, J. Polym. Sci. A, 2, 835 (1964).* J. Polym. Sci., Part A: Polym. Chem., 1996. **34**(10): p. 1831-1832.
12. Penn, L.S. and T.F. Hunter, *A method for evaluation of molecular weight distribution of polydisperse grafted layers.* J. Polym. Sci., Part A: Polym. Chem., 1999. **37**(3): p. 261-266.

13. Debye, P., *Molecular-weight Determination by Light Scattering.* J. Phys. Colloid Chem., 1947. **51**(1): p. 18-32.
14. Cowie, J.M.G., *Polymers: Chemistry and Physics of Modern Materials, 2nd Edition,* 1991: Taylor & Francis.
15. Carothers, W.H., J.Amer.Chem.Soc., 1928. **51**(2548).
16. Mishra, V.K.R., *Living Radical Polymerisation: a Review,* 2012: p. 1-36.
17. Szware, M., Nature, 1956(178): p. 1168-1170.
18. Moad, G. and H. Solomon, *The Chemistry of Radical Polymerisation,* 2006.
19. Rizzardo, E. and D.H. Solomon, *On the Origins of Nitroxide Mediated Polymerization (NMP) and Reversible Addition–Fragmentation Chain Transfer (RAFT)*.* Aust. J. Chem., 2012. **65**(8): p. 945-969.
20. Solomon, E.R.a.D.H., *On the Origins of Nitroxide Mediated Polymerization (NMP) and Reversible Addition-Fragmentation Chain Transfer (RAFT)**, 2012. p. 1-25.
21. Lessard, B.t. and M. Marić, *One-Step Poly(styrene- alt-maleic anhydride)- block-poly(styrene) Copolymers with Highly Alternating Styrene/Maleic Anhydride Sequences Are Possible by Nitroxide-Mediated Polymerization.* Macromolecules, 2010. **43**(2): p. 879-885.
22. Benoit, D., et al., *One-Step Formation of Functionalized Block Copolymers.* Macromolecules, 2000. **33**(5): p. 1505-1507.
23. Chen, G.-Q., et al., *Synthesis of Alternating Copolymers of N-Substituted Maleimides with Styrene via Atom Transfer Radical Polymerization.* Macromolecules, 1999. **33**(2): p. 232-234.
24. Chiefari, J., et al., *Living free-radical polymerization by reversible addition-fragmentation chain transfer: the RAFT process.* Macromolecules, 1998. **31**(16): p. 5559-5562.
25. Graeme Moad, E.R., San H.Thang, *Living Radical Polymerisation by the RAFT Process.* 2005: p. 1-32.
26. Wang, R. and A.B. Lowe, *RAFT polymerization of styrenic-based phosphonium monomers and a new family of well-defined statistical and block polyampholytes.* J. Polym. Sci., Part A: Polym. Chem., 2007. **45**(12): p. 2468-2483.

27. Stenzel, M.H., et al., *Xanthate Mediated Living Polymerization of Vinyl Acetate: A Systematic Variation in MADIX/RAFT Agent Structure.* Macromol. Chem. Phys., 2003. **204**(9): p. 1160-1168.
28. Mori, H., et al., *Xanthate-Mediated Controlled Radical Polymerization of N-Vinylcarbazole.* Macromol. Chem. Phys., 2006. **207**(12): p. 1005-1017.
29. Willcock, H. and R. O'Reilly, *End group removal and modification of RAFT polymers.* Polym. Chem., 2010. **1**(2): p. 149-157.
30. Willcock, H. and R.K. O'Reilly, *End group removal and modification of RAFT polymers.* Polym. Chem., 2010. **1**(2): p. 149-157.
31. Xi, H.P., et al., *Synthesis and Characterization of pH- and Temperature-sensitive Hydrogels of Poly (Styrene-alt-Maleic Anhydride)-co-Pluronic for Drug Release.* J Macromol Sci B, 2013. **52**(9): p. 1198-1211.
32. Greish, K., et al., *Copoly (styrene-maleic acid)-Pirarubicin Micelles: High Tumor-Targeting Efficiency with Little Toxicity.* Bioconj. Chem., 2005. **16**(1): p. 230-236.
33. Henry, S.M., et al., *pH-Responsive Poly(styrene-alt-maleic anhydride) Alkylamide Copolymers for Intracellular Drug Delivery.* Biomacromolecules, 2006. **7**(8): p. 2407-2414.
34. Mu, Y., et al., *Bioconjugation of Laminin Peptide YIGSR with Poly(Styrene Co-maleic Acid) Increases Its Antimetastatic Effect on Lung Metastasis of B16-BL6 Melanoma Cells.* Biochem. Biophys. Res. Commun., 1999. **255**(1): p. 75-79.
35. Tong, R. and J. Cheng, *Anticancer Polymeric Nanomedicines.* Polymer Revs., 2007. **47**(3): p. 345-381.
36. Orwick-Rydmark, M., et al., *Detergent-Free Incorporation of a Seven-Transmembrane Receptor Protein into Nanosized Bilayer Lipodisq Particles for Functional and Biophysical Studies.* Nano Lett., 2012. **12**(9): p. 4687-4692.
37. Knowles, T.J., et al., *Membrane Proteins Solubilized Intact in Lipid Containing Nanoparticles Bounded by Styrene Maleic Acid Copolymer.* JACS communications, 2009. **131**(22): p. 7484-7485.
38. Rajesh, S., et al., *Production of membrane proteins without cells or detergents.* New Biotechnol., 2011. **28**(3): p. 250-254.

39. Chen Xiaoping, Q.K., *Study of Living and Controlled Radical Polymerization.* Prog. Chem., 2001. **13**(03): p. 224-.
40. Hill, D.J.T., et al., *Analysis of the mechanism of copolymerization of styrene and maleic anhydride.* Macromolecules, 1985. **18**(1): p. 9-17.
41. Chen, F., et al., *Synthesis and characterization of copolymer grafted magnetic nanoparticles via surface-initiated nitroxide-mediated radical polymerization.* Poly.Eng. Scienc., 2013. **53**(5): p. 956-962.
42. Klumperman, B., *Mechanistic considerations on styrene–maleic anhydride copolymerization reactions.* Polym. Chem., 2010. **1**(5): p. 558.
43. Harrisson, S. and K.L. Wooley, *Shell-crosslinked nanostructures from amphiphilic AB and ABA block copolymers of styrene-alt-(maleic anhydride) and styrene: polymerization, assembly and stabilization in one pot.* Chem. Commun., 2005(26): p. 3259-3261.
44. Ryan, R.O., *Nanodisks: hydrophobic drug delivery vehicles.* Expert Opinion on Drug Delivery, 2008. **5**(3): p. 343-351.
45. Khotso, M., *Synthesis and characterization of styrene–maleic anhydride copolymer derivatives*, in *Department of Chemistry and Polymer Science,* 2009, University of Stellenbosch.
46. Qiu, G.-M., et al., *Synthesis of ultrahigh molecular weight poly (styrene-alt-maleic anhydride) in supercritical carbon dioxide.* Macromolecules, 2006. **39**(9): p. 3231-3237.
47. *Maleic anhydride, B. C. Trivedi and B. M. Culbertson, Plenum, New York, 1982, 871 pp.* . Journal of Polymer Science: Polymer Letters Edition. Vol. 21. 1983: John Wiley & Sons, Inc. 958-958.
48. Kluperman, B., *Free Radical Copolymerisation of Styrene and Maleic Anhydride Kinetic studies at low and intermediate conversion* 1994: Eindhoven.
49. Klumperman, B., *Mechanistic considerations on styrene-maleic anhydride copolymerization reactions.* Polym. Chem., 2010. **1**(5): p. 558-562.
50. Klumperman, B. and P.G. Brown, *Interpretation of Solvent Effects on Styrene/Maleic Anhydride Copolymer Sequence Distribution and*

Microstructure in Terms of the Bootstrap Effect. Macromolecules, 1994. **27**(21): p. 6100-6101.

51. Ha, N., *Determination of triad sequence distribution of copolymers of maleic anhydride and its derivates with donor monomers by< sup> 13</sup> C nmr spectroscopy.* Polymer, 1999. **40**(4): p. 1081-1086.
52. Chernikova, E., et al., *Effect of comonomer composition on the controlled free-radical copolymerization of styrene and maleic anhydride by reversible addition–fragmentation chain transfer (RAFT).* Polymer, 2003. **44**(15): p. 4101-4107.
53. Barron, P.F., et al., *Applications of DEPT experiments to the carbon-13 NMR of copolymers: poly(styrene-co-maleic anhydride) and poly(styrene-co-acrylonitrile).* Macromolecules, 1984. **17**(10): p. 1967-1972.
54. Milne, G.W.A., *ChemBioDraw 12.0.* J. Chem. Inf. Model., 2010. **50**(11): p. 2053-2053.
55. Lazzara, T.D., et al., *Linear nano-templates of styrene and maleic anhydride alternating copolymers.* Eur. Polym. J., 2009. **45**(7): p. 1883-1890.
56. Malardier-Jugroot, C., et al., *Linear Conformation of Poly(styrene-alt-maleic anhydride) Capable of Self-Assembly: A Result of Chain Stiffening by Internal Hydrogen Bonds.* J. Phys. Chem. B, 2005. **109**(15): p. 7022-7032.
57. Malardier-Jugroot, C., et al., *Novel Self-Assembly of Amphiphilic Copolymers into Nanotubes: Characterization by Small-Angle Neutron Scattering†.* Langmuir, 2005. **21**(22): p. 10179-10187.
58. Malardier-Jugroot, C., et al., *Characterization of a novel self-association of an alternating copolymer into nanotubes in solution.* Mol. Simul., 2005. **31**(2-3): p. 173-178.
59. Han, J., et al., *Preparation and characterization of poly(styrene-alt-maleic acid)-b-polystyrene block copolymer self-assembled nanoparticles.* Colloid Polym Sci, 2008. **286**(14-15): p. 1605-1612.
60. Rodríguez-Hernández, J., et al., *Toward 'smart' nano-objects by self-assembly of block copolymers in solution.* Prog. Polym. Sci., 2005. **30**(7): p. 691-724.

61. Lee, A.S., et al., *Structure of pH-Dependent Block Copolymer Micelles: Charge and Ionic Strength Dependence.* Macromolecules, 2002. **35**(22): p. 8540-8551.

62. Murakami, T., *Phospholipid nanodisc engineering for drug delivery systems.* Biotechnol. J., 2012. **7**(6): p. 762-767.

63. Cao, S., et al., *Synthesis of pH-responsive crosslinked poly[styrene-co-(maleic sodium anhydride)] and cellulose composite hydrogel nanofibers by electrospinning.* Polym. Int., 2009. **58**(5): p. 545-551.

64. Kitano, T., et al., *Dissociation behavior of poly(fumaric acid) and poly(maleic acid). 1. Potentiometric titration and intrinsic viscosity.* Macromolecules, 1987. **20**(7): p. 1598-1606.

65. Berr, S.S., *Solvent isotope effects on alkytrimethylammonium bromide micelles as a function of alkyl chain length.* J. Phys. Chem., 1987. **91**(18): p. 4760-4765.

66. Tonge, S.R. and B.J. Tighe, *Responsive hydrophobically associating polymers: a review of structure and properties.* Adv. Drug Delivery Rev., 2001. **53**(1): p. 109-122.

67 Tonge, S.R., *Patent GB2426703*, WO2006/1291272006.

68 Orwick, M.C., et al., *Detergent-Free Formation and Physicochemical Characterization of Nanosized Lipid–Polymer Complexes: Lipodisq.* Angewandte Chemie International Edition, 2012. **51**(19): p. 4653-4657.

4

4 Styrene Maleic Acid Lipid Particles (SMALPs)

4.1 Introduction

The aim of the present Chapter is to provide a description of the general self-assembly process of the Styrene alt Maleic Acid Lipid Particles (SMALPs), also called *copolymer stabilised nanodiscs*, in contrast to the protein stabilised nanodiscs discussed in the introductory Chapter 1.

Here attention will be focused on the initial studies performed on SMALPs assembled with the SMA-2000P commercial copolymer [1, 2]. Followed by an introduction to the work done with the copolymer synthesised at the University of Bath laboratories. This particular copolymer appears to be so far the only one to entirely contribute to the SMALPs formation with no free copolymer left in solution. Detailed description of the characterisation analyses performed on both SMALP versions via small angle X-ray and neutron scattering, together with dynamic light scattering and transmission electron microscopy experiments is provided in order to highlight the main differences between the two systems. Thus, the work done on understanding the role of the SMA in the SMALP self-assembly process, with the study of the styrene to maleic acid ratio and the impact of the copolymer molecular weight on formation and the physical chemical properties of the nanodiscs is herein described.

4.2 Preparation of SMALPs: Protocol

SMALP samples were all prepared following the same procedure, with the only exception for SMALPs prepared with the use of 6 kDa RAFT copolymer. Indeed this copolymer showed the unique characteristic of being completely incorporated into the nanodisc structure thus further purification via gel filtration chromatography was no longer needed. Materials in use for samples considered in this Chapter were as follows:

For Buffer Preparation: NaH_2PO_4 (sodium phosphate monobasic, purity ≥ 99%), Na_2HPO_4 (sodium phosphate dibasic, purity ≥ 99%) and *NaCl* (purity ≥ 99%) were purchased from Sigma Aldrich. Solutions were prepared using *ultrapure water* with a resistivity of 18 MΩ × cm, or for SANS measurements in D_2O (Sigma Aldrich, purity ≥ 99%) or mixtures of ultrapure water with D_2O. All chemicals were used without any further purification. Lipids: The following lipids (Figure 4.1 and 4.2) were purchased either from Sigma Aldrich in case of the hydrogenated form (purity ≥ 99%) or from Avanti Polar Lipids, for the deuterated version (purity ≥ 99%), all were used as received.

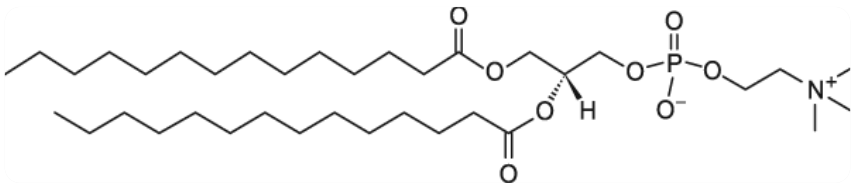

Figure 4.1. Structure of 1 2-dimyristoyl-sn-glycero-3-phosphocholine (DMPC), M_w 677.93 g/mol.

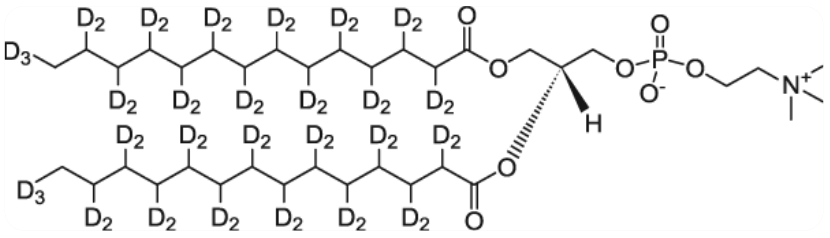

Figure 4.2. Structure of 1 2-dimyristoyl (d54)-sn-glycero-3-phosphocholine (deuterated DMPC), M_w 737.27 g/mol.

Copolymers: The copolymer selected was a Poly(styrene-alt-maleic acid) (SMA), in use with a number of different molecular weights. Copolymers were mainly provided by the company Polyscope and Sartomer as specified, with the only exception of those synthesised in Bath and Warwick laboratories. A detailed description of the analysis performed on the SMA can be found in Chapter 3 Section 3.5.

Buffer Preparation Protocol:

Phosphate buffer 50 mM solution was prepared either in 100% H_2O or 100% D_2O, with 200 mM NaCl at pH 8 using the following protocol (Quantities indicated are for preparation of 1L of solution):
A first solution (A) was prepared adding 1.3 g of NaH_2PO_4 to 50 mL of H_2O. The solution was mixed with the use of a magnetic stirrer for five minutes in order to let the sodium phosphate monobasic completely dissolve in the solution; A second solution (B) was made adding 7.075 g of Na_2HPO_4 to 250 mL of H_2O, which was also stirred for five minutes. Successively 13.25 mL of the first solution (A) was combined with 236.75 mL of the second solution (B) and a further 750 mL of H_2O (or D_2O) were added to reach the final concentration of 50 mM phosphate buffer solution at pH 8. Finally in order to obtain a 200 mM NaCl concentration, 11.688 g of NaCl powder was added and stirred until completely dissolved. Buffer solutions containing 60% D_2O/40% H_2O were obtained by adding 40 mL of buffer already prepared in 100% H_2O to 60 mL of buffer prepared in 100% D_2O. For 32% D_2O/68% H_2O buffers 32 mL of buffer already prepared in 100% D_2O were added to 68ml of buffer already prepared in 100% H_2O. Buffer solution in 100% H_2O was used to prepare SMALP samples and also for the gel filtration chromatography process.

Samples Preparation Protocol:

In 2001, Tighe and Tonge showed the capability of SMA to produce nanoparticles containing a lipid bilayer [3]. In 2009, our collaborators in Birmingham University showed that this new technology could be used to solubilise membrane proteins without the use of detergent. The procedure was optimised using SMA containing a 2:1 molar ratio of styrene to maleic acid [4]. The SMALP preparation process described in previous published literature [2, 4] involves the addition of the SMA copolymer to a solution containing the membrane protein of interest already embedded in phospholipids and the further purification of the final solution from empty discs via affinity chromatography.

The main purpose of this work was to characterise the SMALP structures and analyse the self-assembly process along with the individual contribution of copolymer and lipids. Therefore the sample preparation followed in this work differs slightly from the reported preparation of protein encapsulating nanodiscs. Quantities here reported are for the preparation of 5 mL of sample solution.

Two separate solutions were initially prepared: 0.5 wt% of the lipid chosen, corresponding to 0.025 g of powder was suspended in 3.92 mL of 50 mM phosphate buffer solution with 200 mM NaCl. This solution was sonicated for about five minutes to let the lipids fully dispersed. Finally 1.08 mL of a 6.5 wt% copolymer in 50 mM phosphate buffer solution was added to the initial lipids solution, to give a final copolymer concentration of 1.5 wt%. The final solution was shaken by hand for approximately one minute in order to accelerate the spontaneous assembly process. At the end the solution was completely clear, as shown in Figure 4.3.

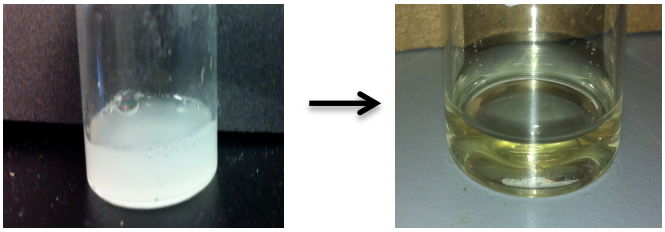

Figure 4.3. SMALPs self-assembly process: (left) a suspension of DMPC in 50 mM phosphate buffer. (Right) the same solution after addition of 6 kDa RAFT copolymer.

All the samples produced using commercial copolymers were purified from the extra copolymer that did not contribute to the SMALPs formation via gel filtration chromatography. However, the samples prepared using the 6 kDa RAFT copolymer di not required any further purification, as the entire amount of copolymer in solution was shown to be part of the SMALP structures (a more detailed explanation is reported in Section 4.3).

Samples Prepared in Deuterated Buffers

The protocol for preparation of samples in 100% D_2O or a mixture of D_2O/ H_2O starts with the standard preparation of samples in 100% H_2O and after the gel filtration step, the resulting purified solutions were dialysed against the specific buffer required. Dialysis was carried out using a dialysis membrane with a 10.000 Mw cut-off, held in the top of an Eppendorf tube into the lid of which a hole had been previously made. The buffer in use was changed after one hour twice, left overnight and then changed one more time and stirred for another hour in an attempt to obtain the desired level of solvent deuteration.

4.2.1 Purification via Gel Filtration Chromatography

Work presented in this Chapter is dedicated to the description of the analysis performed on SMALPs prepared with the use of DMPC phospholipid in its

deuterated and non-deuterated form. The first part of this project focused on the commercial copolymer characterised by a Mw of 7 kDa (SMA-2000P). The samples were prepared using the procedure reported in Section 4.2. A preliminary analysis was performed via the gel filtration chromatography process. The instrument was equipped with an UVvis detector which enables detection of structures containing a chromophore group, such as the styrene ring present in the copolymer which adsorbs at a wavelength around 254 nm [5].

Spectra of the samples analysed revealed the presence of two peaks. The first one showed structures of the dimension of the nanodiscs whereas the second peak showed the presence of smaller structures presumably constituted of single copolymer chains, which eluted more slowly. An example of a typical gel filtration spectrum is reported in Figure 4.4. The presence of free DMPC or clusters of only DMPC was not possible to detect with this technique since no chromophore group is present into the DMPC molecule. Once separated, the solution corresponding to the nanodisc peak was collected and analysed by means of DLS, which confirmed the expected size for the nanodiscs, around 100 Å (10 nm) in diameter. These solutions were then successively analysed via SAXS and SANS experiments.

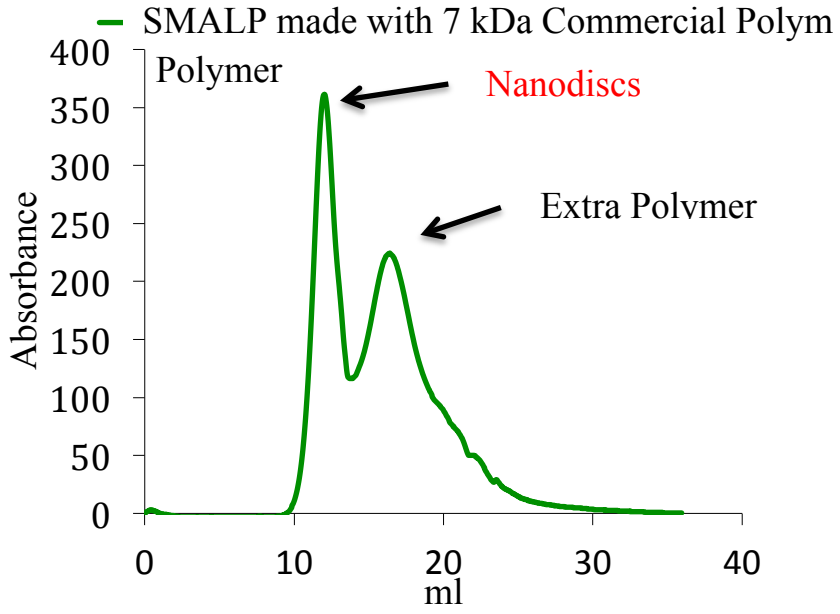

Figure 4.4. Typical gel filtration chromatography trace of a sample made from 100% DMPC and commercial copolymer SMA-2000P.

Once gel filtered, the resulting purified sample was very diluted compared to the original concentration. In order to obtain a concentration suitable for SANS and SAXS experiments, samples were then concentrated using a spin concentrator centrifuge tube with a filter membrane of 5K Mw cut off, and centrifuged at 5000 rpm for about 1hr. Finally, the re-concentrated sample was analysed via UVvis and the adsorption intensity compared to the calibration curve (graph is reported in the Appendix A3) to ensure that a suitable concentration for SANS and SAXS experiments was reached.

4.2.2 Impact of the Use of Deuterated Lipids on the SMALPs Size

The use of deuterium in neutron scattering represents a huge advantage in the structures investigation [6]. However it is necessary to take into account the impact of the replacement of H_2O molecules with D_2O. The effect of D_2O on the physical properties of biological molecules has been previously reported [7, 8].

In order to enhance the contrast of different parts of the SMALP structures and to better understand their structural architecture, either hydrogenated lipids in D_2O solvent and deuterated lipids in H_2O were used during experiments performed using neutron scattering. To take into consideration the potential impact of the use of deuterium the hydrodynamic diameters of SMALPs formed with non-deuterated lipids and with tail-deuterated lipids were initially investigated via DLS experiments. As showed in Figure 4.5, deuteration of the phospholipids tails had little impact on the SMALPs size, within the measurement resolution of this technique, revealing a decrease in the total diameter between the hydrogenated DMPC (h-DMPC) and the tails deuterated DMPC (d-DMPC) of a about 1nm. Considering the precision of the instrument and the reproducibility of the size (which was slightly different from sample to sample even though always in the same range of hydrodynamic diameter) the

change in dimension within 1 nm was considered negligible. The SANS analyses of samples prepared with deuterated and non-deuterated solvents also showed a non-significant impact of the presence of deuterium on the SMALPs structures.

Analysis of the impact of deuterated solvent was also carried out via SANS, confirming also in this case a non-significant impact on the SMALP dimensions.

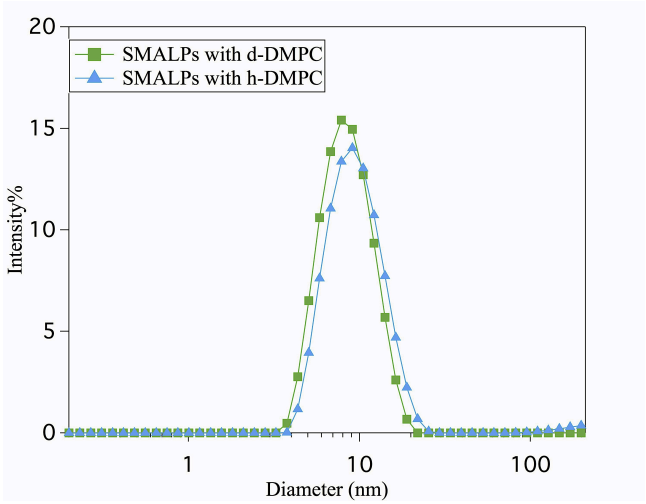

Figure 4.5. DLS plot of the intensity percentage versus diameter in nm of a SMALP sample prepared with 7 kDa commercial copolymer (SMA-2000P) and non deuterated DMPC.

4.3 Characterisation of SMALPs Assembled with 7 kDa SMA-2000P

The first objective of this project was to investigate the spatial organization and structural dimension of SMALPs arising from the organisation of the lipids and copolymer components within the structure. A preliminary gel filtration purification experiment allowed the detection of the presence of small aggregates, showing that not all the copolymer in solution was contributing to the SMALPs formation. A typical gel filtration path is reported in Figure 4.6. The graph shows the integration of the area below the first peak, which corresponds to the SMALP structures. Integration of the area below the second

peak corresponding to the excess of copolymer and of the total area was also performed. Values are reported in Table 4.1. Details of the instrument in use and experimental set up are reported in Chapter 2 Section 2.4. Data collected were analysed with the aid of the software Igor Pro (Wavemetrics); from the integration of the area below the two peaks, it was possible to calculate the amount of copolymer within the single SMALP structure. An example of the integration performed is showed in the Figure 4.6, results of the integration are reported in Table 4.1.

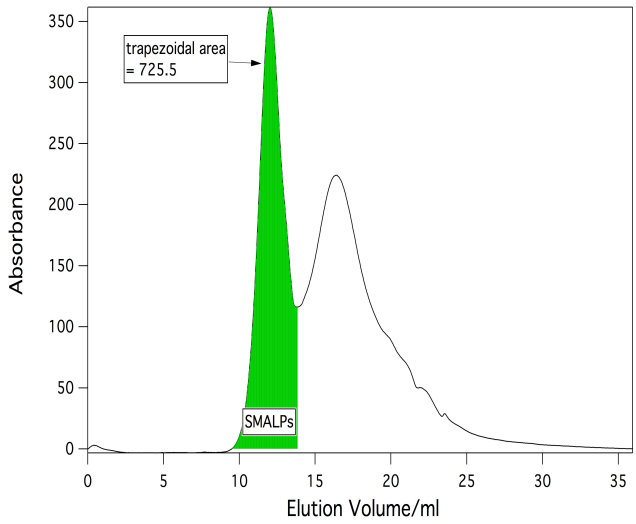

Figure 4.6. Gel filtration path of SMALPs prepared with SMA-2000P and 100% h-DMPC.

Value of Integration of Area below SMALPs Peak	*Value of Integration of Area below Copolymer Excess Peak*	*Value of the Integration of Total Area*
725 ± 10	1229 ± 10	1954 ± 10

Table 4.1. Table reporting values of integration of the two peaks performed using Igor Pro software. Peak start and end points were manually selected.

From the analysis of the gel filtration data the amount of copolymer contributing to the SMALPs formation was found to be approximately 40% of the total copolymer in solution. This corresponds to 0.1 g of copolymer, taking

into consideration that the sample was initially prepared using 0.25 g of copolymer.
Therefore it seems that a consistent portion of the copolymer in solution is not involved in the SMALPs formation but it aggregates in smaller structures.

4.3.1 Dynamic Light Scattering Analysis

SMALPs were analysed via Dynamic Light Scattering (DLS) experiments for a preliminary investigation of the size. A graph of the DLS analysis is shown in Figure 4.7. The experiment was conducted using a Malvern Zetasizer instrument (characteristics of the instrument in use and experimental setup details can be found in Chapter 2 Section 2.7.3). Solutions were filtered with a filter membrane of 0.45 μm pore size to avoid the presence of dust particles and then analysed at the temperature of 25 °C. Prior to analysis the sample was left to equilibrate for 5 minutes, after which 11 experimental runs were performed in order to gain better statistics, these results were then averaged. Experimental data were imported into Igor Pro software and fitted to a lognormal distribution model. Sample showed a distribution of particles with a main diameter of 8 ± 0.04 nm (error reported are plus or minus one standard deviation). The dimensions found were in agreement with the size of the average protein stabilised nanodiscs (around 10 nm). The work reported by Orwick and colleagues on the so-called Lipodisq® technology revealed an average diameter around 9 nm [9].
The Lipodisq® technology follows the initial work of Tighe and Tonge which involved the use of a SMA copolymer with molecular weight 9.5 kDa and a 3:1 styrene to maleic acid molar ratio [9, 10].

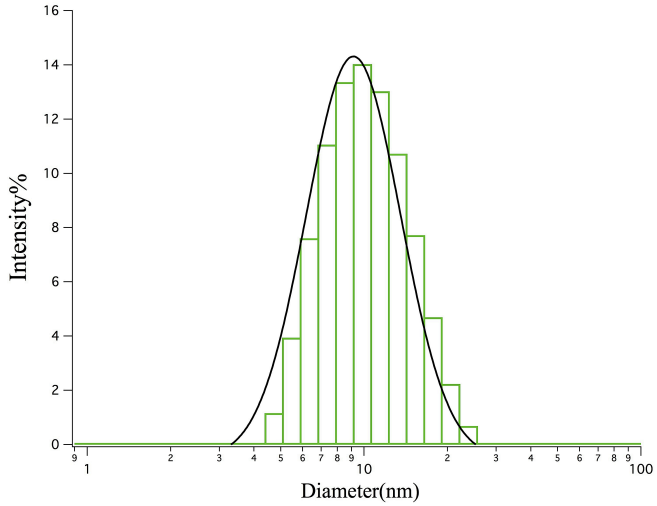

Figure 4.7. DLS experimental data (green bars) of a SMALP sample prepared with 7 kDa commercial SMA-2000P copolymer and DMPC phospholipid, after gel filtration purification. Data were fitted to a lognormal distribution (black continuous line).

Although DLS is a useful instrument for particle size distribution analysis the intrinsic limitation of this technique must be taken into account [11] (a detailed explanation of Dynamic Light Scattering theory is reported in Chapter 2 Section 2.3). A very important factor that needs to be considered is that diameter values measured via DLS are usually larger than the real particle diameter since this analysis takes also into account the hydration shell and counterions around the particles. Moreover analyses performed with this instrument do not give any particular indication of the shape of the object and, when calculating the diameter, particles are assumed to be spherical [12].

4.3.2 Small Angle X-ray and Neutron Scattering Analysis

As results of these considerations, a more in depth analysis was needed. In order to be able to investigate the shape and molecular architecture of SMALPs neutron and X-ray scattering experiments were performed.

Both SAXS and SANS techniques have already been successfully used to investigate the detailed structure of protein stabilized nanodiscs [13-15]. Nanodiscs have also been successfully investigated via neutrons and X-ray

reflectivity studies at the air-water interface [16-18] showing the large versatility of the system.

Samples analysed via SAXS were prepared following the protocol presented in Section 4.2 and successively analysed at the temperature of 25 °C using a 12 hour exposure in the in-house SAXSess instrument located at the University of Bath (for instrumental setup see Chapter 2 Section 2.7.1). Data were reduced from the initially recorded image following the protocol reported in Chapter 2 Section 2.8.1, and analysed using the SANS Analysis package [19] from NIST written in Igor Pro to a model of a core-shell cylinder. The core radius was convoluted by a Schultz distribution to add polydispersity; the model also includes a "face" layer on top and bottom to take into account the phospholipid headgroups. The interactions between discs were fitted using a Hayter Penfold charged sphere approximation. A schematic representation of the model and its parameters is given in Figure 4.8. Description of the model and equations in use is also reported in Chapter 2 Section 2.8.2.1.

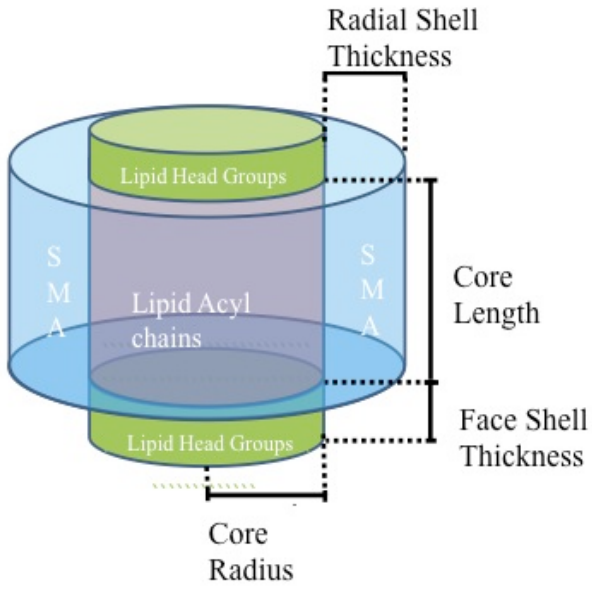

Figure 4.8. Schematic representation of the model used to fit SANS and SAXS data of SMALPs.

During fitting, the X-ray scattering length density of the lipid head groups was calculated and set to be equal to 11.5×10^{10} cm^{-2}, according also to the value reported in literature [20]. The water content within the faces of the SMALPs was fitted based on this value and the value of the SLD of the solvent in use.

The SLD of the SMA based on the reported styrene: maleic acid molar ratio in the copolymer was calculated to be 10.8×10^{10} cm^{-2} and the water content in the rim was then fitted based on this value and the value of the solvent. The scattering length density of the phosphate buffer solvent was calculated to be 9.4×10^{10} cm^{-2} and held during the fitting, the temperature (25 °C), the dielectric constant of the solution [21] (78), the monovalent salt concentration (0.25 M) were also held during the fitting. The SLD of the cylinder core composed of phospholipid tails was calculated to be 9.4×10^{10} cm^{-2} and then fitted to take into account copolymer penetration within the core. The remaining parameters were fitted and results are reported in Table 4.2.

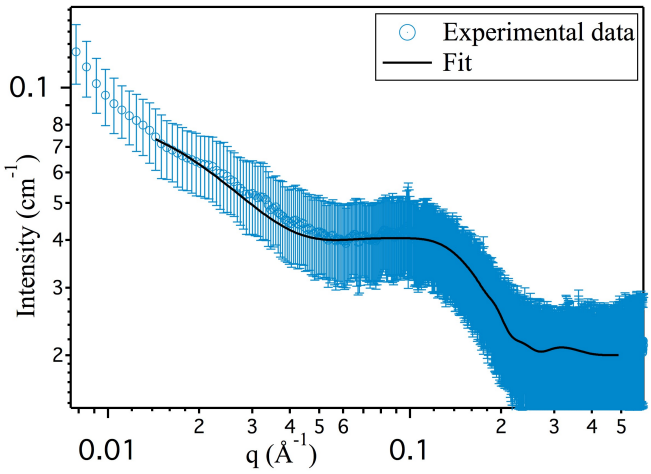

Figure 4.9. SAXS experimental data (blue empty circles) of a SMALP sample prepared with 7 kDa SMA-2000P copolymer and DMPC in phosphate buffer recorded on the SAXSess instrument located at the University of Bath. Data was fitted to the core-shell cylinder model (black continuous line). Error bars are also reported, calculated based on the measurement statistics

Fitting of experimental data revealed discs with a total diameter of approximately 8.6 nm and a thickness of about 4.2 nm. Using the calculated value for the copolymer and the SLD value found from the fitting it was calculated the presence of approximately 29 mol% of copolymer into the core composed of only the acyl chain of the phospholipids.

Solvent penetration within the phospholipid heads constituting the faces of the discs was also taken into account showing inclusion of water molecules at a volume fraction of approximately 0.55. Also the hydrophilic part of the copolymer wrapped around the discs and constituting what is defined as a rim in the fitting model includes water molecules with a volume fraction of 0.65. Results were then compared to another set of experimental data from SANS analysis which was performed using four different phosphate buffer contrasts, 0% D_2O, 100% D_2O, 60% D_2O and 32% D_2O to elucidate the spatial organization of the SMALPs (graph reported in Figure 4.10). Samples were prepared following the protocol described in Section 4.2 for deuterated phospholipid and deuterated buffer preparation and analysed at 25 °C on the D11 instrument located at the ILL in Grenoble (France). For instrument details and configuration see Chapter 2 Section 2.7.2.

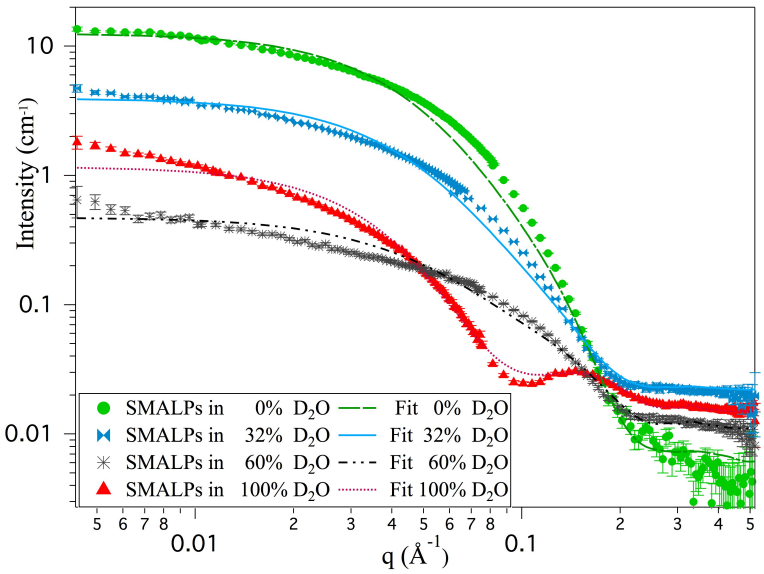

Figure 4.10. Plot of experimental SANS data collected on the D11 instrument, located at the ILL Grenoble. Experimental data for samples analysed with four different solvent contrasts are shown with the respective fitting curves for the core-shell cylinder model.

Data were reduced and corrected following the protocol reported in Chapter 2 Section 2.8.1 and simultaneously fitted to the same charged core-shell cylinder model using the SANS Analysis package in Igor Pro [19]. The neutron scattering length density of the head groups was set to be 1.84×10^{10} cm^{-2} based

on the value reported by Smith et al [23] while the water content was set at a mole fraction of 0.57 based on their results of fitting the headgroups region of a deuterated DMPC bilayer. The SLD of the copolymer was calculated to be 1.8×10^{10} cm^{-2} and the water content in the rim was then fitted based on this value and the SLD values of the solvents. The scattering length density of the 100% D_2O solvent (6.29×10^{10} cm^{-2}) and 100% H_2O (-0.57×10^{10} cm^{-2}) were calculated and held during the fitting. Other model parameters were calculated and held during the fitting such as the temperature (25 °C), the dielectric constant of the solution (78) and the monovalent salt concentration (0.25 M). The remaining parameters were fitted and results are reported in Table 4.2.

Model Coefficients/Contrast	*SAXS*	*100% D_2O*	*60% D_2O*	*32% D_2O*	*0% D_2O*
Volume fraction	0.04 ± 0.01	0.019 ± 0.01			
Mean core radius (nm)	3.8 ± 0.1	3.8 ± 0.1			
Radial polydispersity (σ)	0.4 ± 0.05	0.35 ± 0.05			
Core length (nm)	2.6 ± 0.1	2.6 ± 0.1			
Radial shell thickness (nm)	1.3 ± 0.1	0.9 ± 0.1			
Face shell thickness (nm)	1 ± 0.1	1.0 ± 0.2			
SLD core (cm^{-2})	$8.4\times10^{10}\pm 0.05\times10^{10}$	$6.5\times10^{10}\pm 0.05\times10^{10}$			
Mol% solvent in face	0.58 ± 0.05	0.57*			
Mol% solvent in rim	0.45 ± 0.05	0.42 ± 0.05			
Solvent SLD (cm^{-2})	-0.57×10^{10}	6.29×10^{10}*	$3.86\times10^{10}\pm 0.05\times10^{10}$	$1.87\times10^{10}\pm 0.05\times10^{10}$	-0.57×10^{10}*
Charge	0.31	0.31± 0.05			
Incoherent background (cm^{-1})	0.019±0.01	0.015± 0.05	0.011 ± 0.05	0.022± 0.05	0.006±0.05

*Table 4.2. Fit parameters for fitting SAXS experimental results (2 column) and SANS data of SMALPs made using 7 kDa SMA-2000P copolymer and tail deuterated-DMPC, in different solvent contrasts to a model of a charged core-shell cylinder with polydisperse core and head-group regions at top and bottom of the cylinder. *Calculated or set from literature values and held during fitting.*

These results show a structure consisting of a phospholipid core with a radius of approximately 3.8 ± 0.2 nm encircled by a copolymer belt of 0.9 ± 0.2 nm, suggesting that the annulus is likely to be made up of a single loop of the copolymer. The core was found to be 2.6 ± 0.2 nm thick, a value that agrees well with the previous work on DMPC bilayers reported in the literature [24]. The thickness of the faces, which represents the head-groups of the phospholipids, also agrees well with previous measurements [24].

Based on the analysis of the sample via SAXS and SANS experiments the number of phospholipids within one SMALP structure was also calculated. From the fitting of the SAXS and SANS experimental data, the discs showed a diameter around 7.6 ± 0.2 nm with a copolymer belt of a thickness of approximately 0.8 ± 0.2 nm. Based on these results the total area occupied by the phospholipid core is between 43 nm^2 and 48 nm^2. With the assumption that the area of each phospholipid in the bilayer is around 0.59 nm^2 [24] it was calculated that there are approximately a total of 154 DMPC molecules constituting the core of the SMALPs structures (i.e. ~77 in each leaflet of the bilayer). This value is similar to the value found for the membrane scaffold proteins stabilised nanodiscs [15, 25]. The copolymer penetration into the core was found to be around 16%, very close to the value obtained from SAXS data, and the amount of solvent penetration into the rim also agrees with SAXS results.

4.4 Characterisation of SMALPs Prepared with 6 kDa RAFT Copolymer

In order to have better control over as many parameters as possible involved in the SMALP assembly process and also to further understand the key factors behind their self-assembly process, a new copolymer with 6 kDa Mw was synthesised via RAFT polymerisation (a detailed description can be found in Chapter 4 Section 4.5) and used to form nanodiscs. SMALPs were assembled following the standard procedure reported in Section 4.2. The sample homogeneity was immediately evident by gel filtration chromatography analysis, which revealed a single narrow peak corresponding to a relatively monodisperse SMALP population. Figure 4.11 compares the chromatogram for SMALPs prepared with the 6 kDa RAFT copolymer and h-DMPC phospholipids to the trace of a sample assembled with 7 kDa SMA-2000P commercial copolymer and h-DMPC.

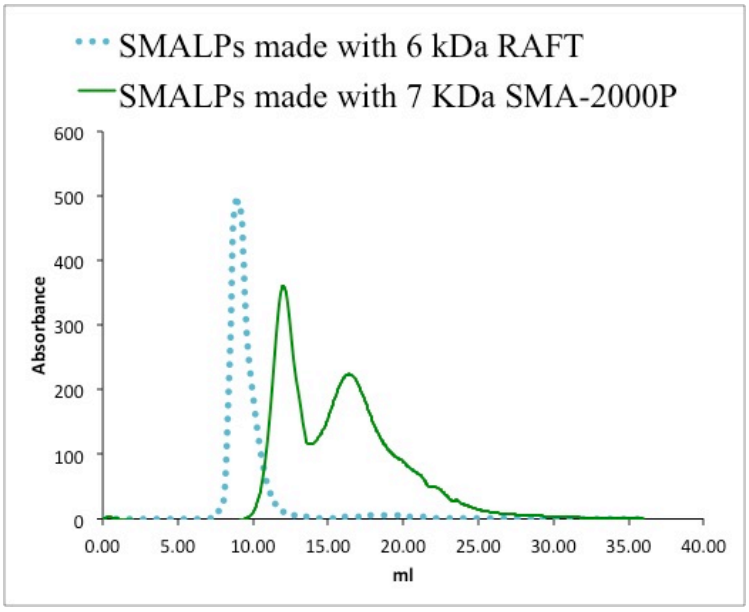

Figure 4.11. Gel filtration chromatograms of SMALPs made with two different copolymers. The absorbance of the SMALPs prepared with 6 kDa RAFT copolymer was divided by 10 in order to report both graphs on the same scale. Analysis was performed at 254 nm wavelength, corresponding to the absorbance of the chromophore group presents.

4.4.1 Dynamic Light Scattering Analysis

Following the same procedure performed for samples prepared using the 7 kDa SMA-2000P copolymer, a DLS measurement was performed after the gel filtration step showing the presence of one single peak indicating larger SMALPs structures with a diameter around 16 ± 0.2 nm.

In order to further characterise the new formulation, a non gel-filtered sample was also analysed via DLS and results were compared to the DLS data from a gel-filtered sample. The gel-filtered sample showed a clear narrow peak corresponding to the nanodisc structures with SMALPs, whereas the non gel-filtered sample revealed the presence of a second peak due presumably to the presence of very large aggregates. This second peak was only visible in the Intensity% analysis since the volume% occupied by this structure actually corresponded to only 0.1 volume%.

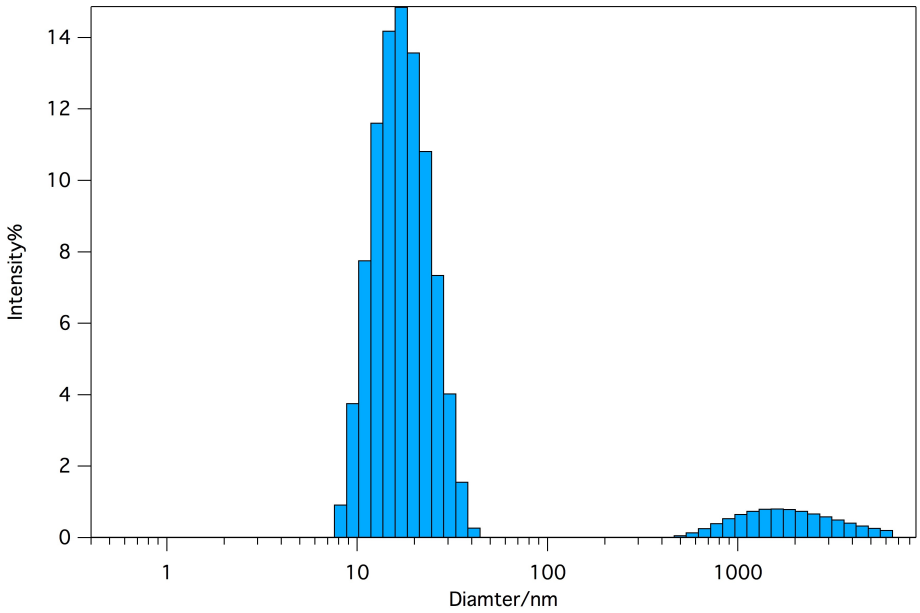

Figure 4.12. DLS plot of a non-purified sample made with use of h-DMPC and 6 kDa RAFT copolymer.

The absence of a second peak in the gel filtration chromatogram, which measures only the chromophore group present in the copolymer, excluded the possibility that the second peak was caused by extra copolymer not taking part in the SMALP assembly as demonstrated for SMALP prepared with the SMA-2000P. Thus the idea that the second peak seen in DLS was caused by excess DMPC was considered. The presence of small quantities of excess DMPC might also be related to the dynamics of the SMALP structures, since DMPC is exchanged between discs over time. Experiments were carried out to alter the added ratio of DMPC to 6 kDa RAFT copolymer but small amounts of excess DMPC were observed at every ratio suggesting that this structure remains in equilibrium with the nanodiscs even at optimum lipid-copolymer proportions. Also from values reported in Table 4.3 the standard DMPC percentage in use was confirmed to be the optimal choice with the lowest sample polydispersity and the highest total volume% occupied by SMALPs.

DMPC content in wt%	SMALP Size	Volume% Occupied by SMALPs	Volume % of the second peak	PDI
0.6%	15.9± 0.2	98.9%	1.1%	0.5
0.5%*	15.1± 0.2	99.9%	0.1%	0.2
0.4%	22.0± 0.3	99%	1%	0.4
0.3%	17.7± 0.3	99.4%	0.6%	0.4

*Table 4.3. Data from DLS experiments on SMALPS made using different DMPC/Copolymer proportions. The SMALPs sizes were calculated from volume % analysis, PDIs reported are from DLS analysis * Standard percentage in use in SMALP preparation.*

In conclusion, the 6 kDa RAFT copolymer was shown to completely contribute to the SMALP self-assembly process. By using this copolymer therefore, samples can be prepared with no need of further purification from excess copolymer, giving this system many important advantages such as the complete control of the copolymer belt, when for instance the nanodiscs structure is used to investigate lipid-lipid interactions. Above all, the use of this copolymer allows a more precise control of the initial nanodiscs concentration. In addition, in the case of neutron experiments when the use of deuterated samples is required, this copolymer gave the possibility of preparing them directly in the deuterated buffers with no need for dialysis, which is a time consuming operation and difficult to control in terms of quality of the results obtained, causing sometimes loss of sample.

4.4.2 SANS Analysis

The architecture of the SMALPs structure formed with the 6 kDa RAFT copolymer was further investigated via SANS experiments. Samples were prepared with hydrogenated copolymer, hydrogenated DMPC in deuterated and non-deuterated phosphate buffer following the sample preparation procedure described in Section 4.1. Data were collected on the LOQ instrument located at ISIS (Oxfordshire, UK) shown in Figure 4.13. Data were reduced and corrected

following the standard protocol and analysed using the SANS Analysis package within Igor Pro [19]. Data taken at different solvent contrasts were simultaneously fitted to a model of a charged core-shell cylinder. The SLD of the core of the discs considered to be formed of only phospholipid tails was calculated to be -0.42 × 10^{9} cm^{-2} value confirmed by published literature [22] and then fitted to take into account the possible presence of copolymer into the core. The scattering length density of the 100% D_2O solvent (6.29 × 10^{10} cm^{-2}) and 100% H_2O (-0.57 × 10^{10} cm^{-2}) were calculated and held during the fitting. Other model parameters were calculated and held during the fitting such as the temperature (25 °C), the dielectric constant of the solution (78), the monovalent salt concentration (0.25 M) and the charge (0.31), the water content within the faces (0.57). The remaining parameters were fitted and results are reported in Table 4.4.

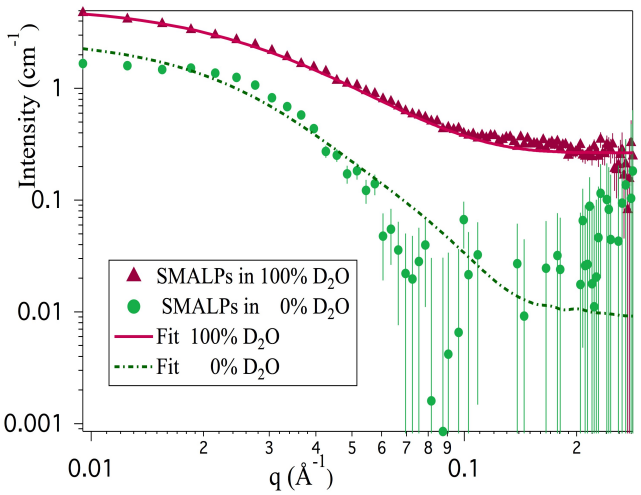

Figure 4.13. SANS data for samples made with 6 kDa RAFT copolymer and non-deuterated DMPC with two different solvent contrasts, fitted with the model described in the text above. Data were collected on LOQ instrument at ISIS.

SANS data, in agreement with DLS results, showed the formation of larger SMALPs structures using the RAFT copolymer, compared to those prepared using the SMA-2000P copolymer, possessing an average diameter of 14 ± 0.2 nm. However this is still within the range of sizes reported for the protein stabilised nanodiscs [26]. The thickness of the core of the discs equals to 2.7 ±

0.2 nm is slightly larger than the core dimension detected for SMALPs formed with SMA-2000P but still agrees well with the value reported in literature for the hydrophobic region of DMPC lipid bilayers of about 2.6 nm [24] and also with the dimensions reported for the protein stabilised nanodiscs [27, 28].

As demonstrated by the results obtained from the gel filtration and DLS analysis, all the 6 kDa RAFT copolymer contributes to the nanodisc formation, forming a thicker copolymer belt wrapped around the core with a thickness of 2.4 ± 0.2 nm compared to 0.7/0.9 nm for the SMA-2000P stabilized discs. This, considered together with the increased solvent molar content within the rim, is also indicative of a different geometrical conformation of the copolymer around the hydrophobic phospholipid core. Such behaviour might be explained by the different molecular architecture of the two copolymers (extensively analysed in Chapter 3). Copolymer penetration into the core was found to be around 12%, a slightly lower value compared to the value found for SMALPs assembled with the 7 kDa SMA-2000P.

In order to better understand the geometrical arrangement of the SMA around the phospholipids core, a SANS experiment was conducted with the use of deuterated SMA. This copolymer was synthesised via RAFT polymerisation with the use of deuterated styrene (purchased from Sigma Aldrich) and hydrogenated maleic acid.
Deuterated copolymer was then combined with hydrogenated DMPC in hydrogenated phosphate buffer (Figure 4.14). The analysis was performed on LOQ. Experimental data were reduced and fitted to the same core-shell cylinder model used for the analysis of the data previously reported, holding values during fitting as for the hydrogenated copolymer, and closely comparing values for this sample with those from the fitted h-RAFT copolymer data to ensure the fitting was consistent and reliable.

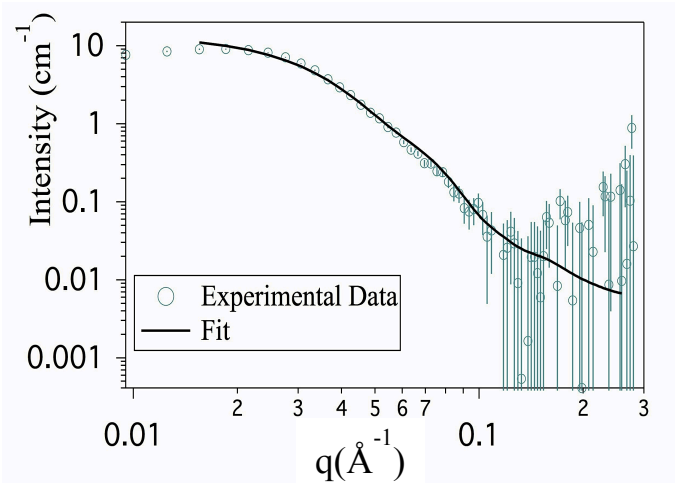

Figure 4.14. Scattering patterns from SMALPs made with 6 kDa RAFT deuterated copolymer and hydrogenated DMPC in hydrogenated phosphate buffer solution (empty green circles) fitted to the model described in the text (continuous black line).

Only the styrene groups of the SMA were deuterated and SLD for the copolymer was calculated and set to be 6.67×10^{10} cm^{-2}, also the SLD for the head groups of DMPC was set to be 1.86×10^{10} cm^{-2}. Based on this value the solvent proportion within the faces corresponding to the lipid headgroup regions was set to the value of 0.57 and held during the fitting. The molar volume of solvent penetrating into the rim was fitted based on the value of the styrene part of the copolymer SLD (6.47×10^{10} cm^{-2}) and solvent SLD (-0.57×10^{10} cm^{-2}). Results of fitting are reported in Table 4.4.

Model Coefficients	*Deuterated SMA in 0% D_2O*	*100% D_2O*	*0% D_2O*
Volume fraction	0.05 ± 0.01	0.012 ± 0.01	
Mean core radius (nm)	4.4 ± 0.2	4.4 ± 0.2	
Radial polydispersity (σ)	0.32 ± 0.05	0.42 ± 0.05	
Core length (nm)	2.9 ± 0.5	2.7 ± 0.2	
Radial shell thickness (nm)	2.8 ± 0.2	2.4 ± 0.2	
Face shell thickness (nm)	1.7± 0.2	0.8 ± 0.2	
SLD core (cm^{-2})	$1.2 \times 10^{10} \pm 0.05 \times 10^{10}$	$0.7 \times 10^{10} \pm 0.05 \times 10^{10}$	
Mol% solvent in rim	0.6 ± 0.05	0.8 ± 0.05	
Incoherent background (cm^{-1})	0.0056 ± 0.05	0.015 ± 0.05	0.006 ± 0.05

Table 4.4. Parameters values from fitting of SANS data from SMALPs made with 6 kDa SMA deuterated copolymer and hydrogenated DMPC in hydrogenated phosphate buffer solution and of simultaneously fit of SANS data from SMALPs made using 6 kDa RAFT copolymer and DMPC at different solution contrasts, to a model of a charged core-shell cylinder with polydisperse core and head-group regions at top and bottom of the cylinder.

Analysis of the data reported in Table 4.4 shows an increased core length and shell thickness. Two plausible explanations could be suggested in this case. It might be related to the model itself that assumes the copolymer belt to be the same height as the core of phospholipids; or there is an extension of the copolymer to the faces of the structure, which causes an increment in the face parameter.

This might be related to the model itself that assumes a copolymer belt with the same height as the core. However it might be the case that the copolymer belt extends to the faces of the phospholipids with an interaction between the hydrophilic part of the copolymer and the heads of the phospholipids.

4.4.3 TEM and Cryo-TEM Analysis

A TEM-JEOL instrument was used to take TEM images (Figure 4.15) in the University of Bath whereas the CryoTEM analysis was performed at Université Pierre et Marie Curie (Paris, France) with a LaB6 JEOL JEM 2100 (details of the sample preparation and instrumentation can be found in Chapter 2 Section 2.7.3). A total of 85 particles for TEM micrograph and 255 for Cryo-TEM micrograph were counted and distribution of sizes was analysed by means of the protocol reported in Chapter 2 Section 2.8.4. An example of a typical histogram obtained, fitted to a Gaussian distribution is reported in Figure 4.16.

Results of analyses performed with both TEM and CryoTEM instruments on a sample of SMALPs prepared using the 6 kDa RAFT copolymer and h-DMPC showed a distribution of diameters between 9 and 12.3 nm. On average a larger diameter was found for samples analysed via Cryo-TEM. With cryo-TEM, the suspension is shock-frozen in liquid ethane, therefore the water is super cooled to form a glass and SMALPs are observed with no dimensional alteration. Conversely the SMALPs analysed by conventional TEM are said to be in "dry state". The sample preparation of TEM might have modified the size.

Nevertheless the range of values obtained for the Feret diameter is in accordance with the analysis performed by DLS, SANS and SAXS. Representative micrographs of both experiments are reported in Figure 4.15 showing the narrow distribution of SMALPs sizes. These pictures provide a direct visualisation of the dimension previously reported by SANS, SAXS and DLS analyses.

	Minimum Feret Diameter (nm)	*Feret Diameter (nm)*
TEM Results	8.1 ± 0.2	11.4 ± 0.4
Cryo-TEM Results	10.2 ± 0.3	13.2 ± 0.3

Table 4.5. Summary of results obtained for analysis of TEM and Cryo-TEM experiments performed on SMALPs assembled with 6 kDa RAFT copolymer and h-DMPC.

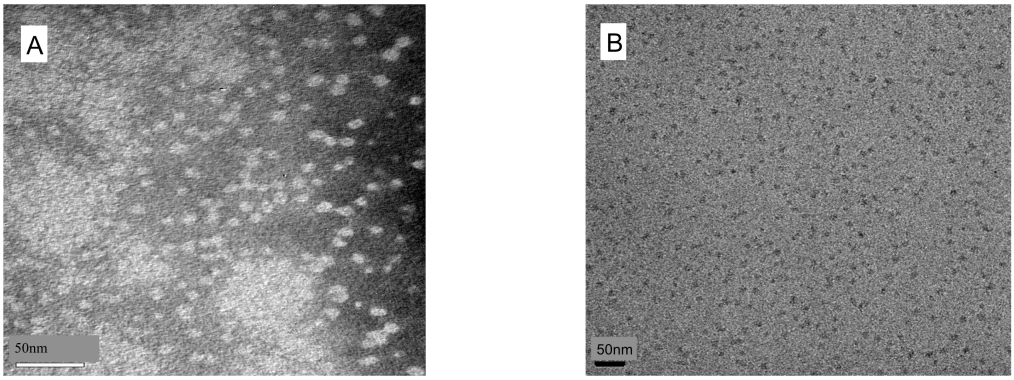

Figure 4.15. TEM (A) and Cryo-TEM (B) micrograph of empty SMALPs prepared using 6 kDa RAFT copolymer and h-DMPC.

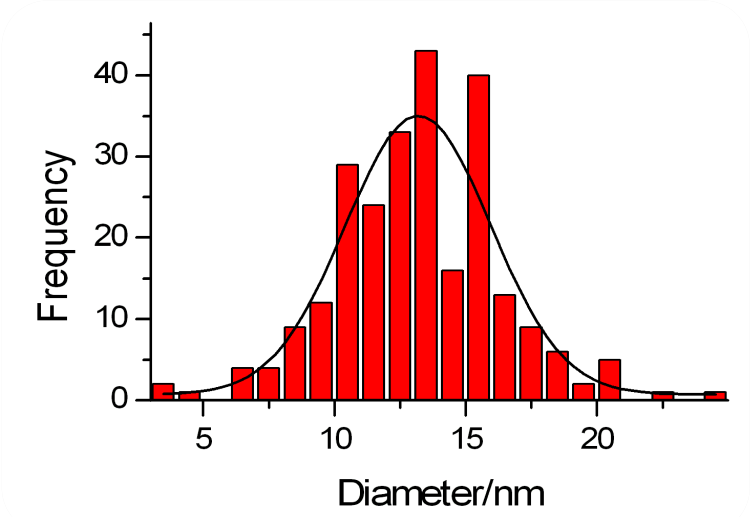

Figure 4.16. Feret diameter distribution from a Cryo-TEM micrograph of SMALPs prepared with 6 kDa RAFT copolymer and h-DMPC. The distribution was fitted to a Gaussian distribution (black continuous line).

These results were compared to the analysis performed on SMALPs assembled with the use of the 7 kDa SMA-2000P commercial copolymer (Figure 4.16). This sample was analysed in Birmingham on a FEI Tecnai 12, 120 kV as reported in our recent paper [29]. A bimodal size distribution was presented. However a new analysis of the micrograph, following the same procedure previously reported, showed a distribution of maximum Feret diameters around the mean value of 15.3 ± 0.3 nm. In our study the minimum Feret diameter value was found to be very close to the maximum Feret diameter value. The

difference in the final results could be attributed to the initially different analysis performed. In the present analysis a total of 180 particles were analysed. Results are in good agreement with the range of values between 5 and 15 nm found by Orwell and colleagues on a TEM analysis of the Lipodisq® structures [30]. Also good agreement in the results was found with the same analysis performed on the protein-stabilised nanodiscs assembled with different lipids and in which different proteins have been analysed [27, 31, 32].

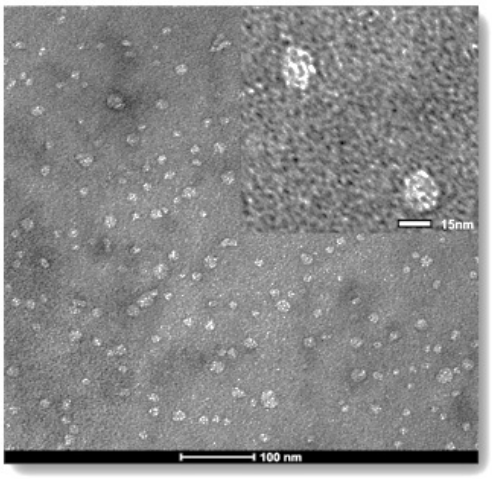

Figure 4.17. TEM micrograph of SMALPs prepared with SMA-2000P (7 kDa commercial copolymer) Inset at the top right corner is the same image zoomed in, to a 15 nm scale. Picture is reproduced with permission from [29].

Sample	*SMALPs with 6 kDa RAFT*	*SMALPs with 7 kDa (SMA-2000P)*
TEM Maximum Feret Diameter (nm)	13.2 ± 0.3	15.3 ± 0.3
TEM Minimum Feret Diameter (nm)	10.2 ± 0.3	15.0 ± 0.3

Table 4.6. Summary of TEM results on SMALPs made with the use of different copolymers. Errors are the standard deviation of the fitted Gaussian distribution.

Values obtained via TEM analysis do not agree with the general tendency observed by DLS, SAXS and SANS analysis in which the 6 kDa RAFT copolymer was shown to form larger structures compared to the SMALPs formed with 7 kDa commercial copolymer. The difference in diameters found between SANS and SAXS analysis and TEM measurements for SMALP prepared with 7 kDa SMA-2000P are likely to be related to the different sample preparation. Indeed as all scattering measurements were performed on samples in buffered solutions whereas TEM images were taken from a dried sample negatively stained with uranyl acetate. The drying step may have caused the apparent size of the SMALPs to change. Uranyl ions are also known to bind to proteins, carboxyl groups (such as those found in the SMA copolymer) and to lipid phosphate groups [33, 34]. This might consequentially lead to the presence of some aggregation in the examined sample [35]. Finally osmotic shock from the high concentration staining solution could also alter the size and shape of unfixed aggregates during staining.

4.5 Probing the Role of the Copolymer in the SMALP Assembly Process

One of the attractive characteristics of the protein-stabilised nanodiscs is the possibility to finely tune the diameter of the structure simply by modifying the membrane scaffold protein length. In this way during the past decades a large database of nanodiscs with different dimensions has been created [27].

Since the SMALP assembly process is governed by the copolymer-phospholipids interaction the attention was focused here on the role of the copolymer, with particular attention to the properties of the polymeric chains that represent the key to the SMALP formation. An investigation of the copolymer properties in solution and a structural characterisation was carried out to analyse SMALPs made with copolymers of different molecular weights.

The driving force for the self-assembly process is assumed to be the amphiphilic nature of the SMA favouring the interaction with the phospholipid tails, with a similar mechanism to that of the amphiphilic protein in protein stabilised nanodiscs [14]. Therefore, investigations were carried out via the synthesis of three different copolymers using the RAFT polymerisation technique. Copolymers were synthesised with a constant molecular weight but different styrene to maleic acid proportions. This allowed the study of the effect of altering the hydrophobic/hydrophilic ratio in the copolymers on the self-assembly of the SMALPs. Results were then compared to a series of commercial copolymers with different molecular weights.

4.5.1 Study of the Impact of the Styrene to Maleic Acid Proportion on the SMALPs Assembly Process

Three different copolymers with constant molecular weight and different styrene to maleic acid total molar ratios, respectively a 3:1, 2:1 and 1.7:1 styrene to maleic acid molar ratios were made. Synthesised samples were prepared using the standard sample preparation procedure, which detailed description is reported in Chapter 3 Section 3.6. DLS experiments were then performed in order to analyse the size and polydispersity of the samples.

SMALP samples prepared with a 1.7:1 styrene to maleic acid proportion in the copolymer showed a very high polydispersity value and multiple peaks in the intensity distribution analysis, indicating the presence of a second larger population in the sample (Figure 4.18).
DLS is very sensitive to the presence of large aggregates therefore in order to have a better representation of the real sample composition results are reported in volume% versus the diameter. The distribution obtained showed the presence of two peaks which dimensions are reported in Table 4.7.

Volume distribution for a sample prepared with the lowest styrene to maleic acid proportion is reported in Figure 4.18 which shows that even a slight

decrease in the ratio can cause a big variation in the way the copolymer associates with the DMPC bilayer in solution.

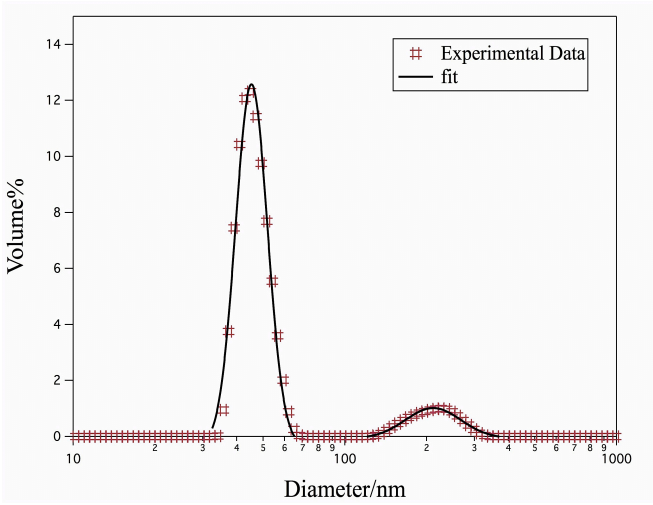

Figure 4.18. Volume distribution derived from a sample prepared with a 6 kDa RAFT copolymer with a 1.7:1 styrene to maleic acid molar ratio. Data are fitted to a lognormal distribution model function using the software Igor Pro 6. Each peach was fitted individually.

Styrene-to Maleic Acid Total Proportion	*1St Peak Diameter*	*2nd Peak Diameter*
1.7:1	45 ± 0.2 nm	211 ± 1.2 nm
3:1	232 ± 1.3 nm	1600 ± 28 nm

Table 4.7. Dimension of structures formed after the addition of SMA with a total molar ratio of respectively 1.7:1 and 3:1 styrene to maleic acid to a solution of DMPC in phosphate buffer (protocol for SMALPs preparation is reported in Section 4.2) Values are derived from fitting of a volume weighted distribution fitted to a log normal distribution function.

Results of the analysis performed revealed the styrene to maleic acid ratio to be a crucial parameter governing the SMALPs formation. Indeed comparing the values reported in Table 4.7 to results obtained with the use of the 2:1 styrene to maleic acid ratio and with the values of the commercial copolymer reported in Table 4.8; it is evident that the 2:1 ratio represents the optimal proportion leading to SMALPs formation. Indeed samples prepared with copolymers

characterised by the same architecture and molecular weight but either lower or higher styrene to maleic acid ratio did not assemble into SMALPs. Instead they tend to form aggregates of much larger structures, probably due to the changed hydrophobic/ hydrophilic balance of forces taking place in the solution.

4.5.2 Study of the Effect of SMA Molecular Weight on SMALP Formation

A systematic study was conducted to investigate the effect of copolymer molecular weights. Copolymers used were provided by the company Polyscope and results of analysis were compared to the analyses performed on the SMALPs prepared with molecular weights of 7 kDa (SMA-2000P from Sartomer) and 6 kDa (copolymer synthesised in our laboratory via RAFT polymerisation). The results of these experiments, performed using SANS, SAXS and DLS on the SMALPs structures obtained, were coupled to the investigation performed on the copolymers when studied separately in the same buffer solution (a detailed description of the analysis conducted on the copolymers is reported in Chapter 3).

Samples were prepared following the same procedure employed for SMALPs obtained with the 6 kDa RAFT and the 7 kDa SMA-2000P copolymers, using DMPC phospholipids in their deuterated form. However from the early stage of the samples preparation a different behaviour was observed for these copolymers. The DMPC solution, after addition of the copolymer, became clear as expected when using the 11 kDa and the 33 kDa copolymers. Conversely the 63 kDa and 110 kDa copolymers left the solution cloudy. This indicated that not all the DMPC present in solution was incorporated into the small copolymer-lipid aggregates and large aggregates of lipids and copolymer were formed.
All the solutions prepared were consequently gel filtered in order to detect the presence of copolymer aggregates and to be able to select the structures of interest.

As observed from the gel filtration paths reported in Figures 4.19 and 4.20 the quality of the samples prepared using these copolymers was poorer in comparison with the samples prepared using 7 kDa SMA-2000P and 6 kDa RAFT copolymers. The gel filtration traces in these cases consisted of one single broad peak, so it was extremely difficult and mostly impossible to individuate different species and therefore completely remove the presence of copolymer aggregates. This might be caused by the presence of copolymer aggregates of the same dimension of the SMALP structures. Nonetheless comparing the gel filtration paths with that of a sample prepared with the 7 kDa SMA-2000P it was possible to limit the selection of the gel-filtered product to the elution volume region equivalent to those samples where nanodisc structures were found.

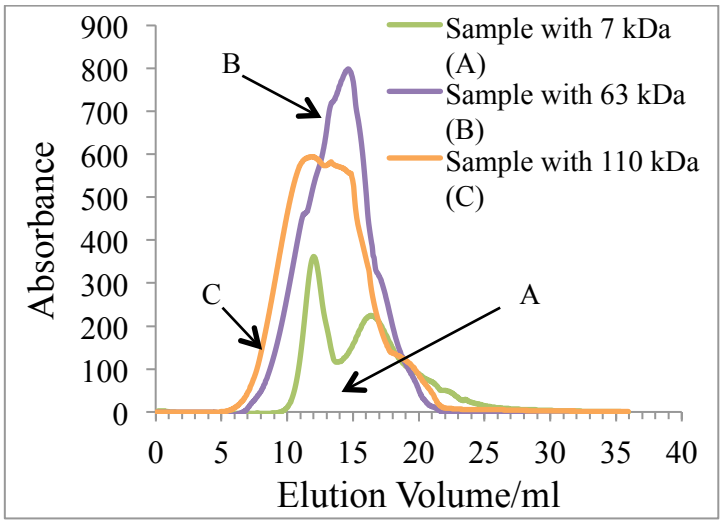

Figure 4.19. Gel filtration path of samples prepared using 63 kDa and 110 kDa copolymer molecular weights compared to the gel filtration path obtained from a sample made with 7 kDa copolymer.

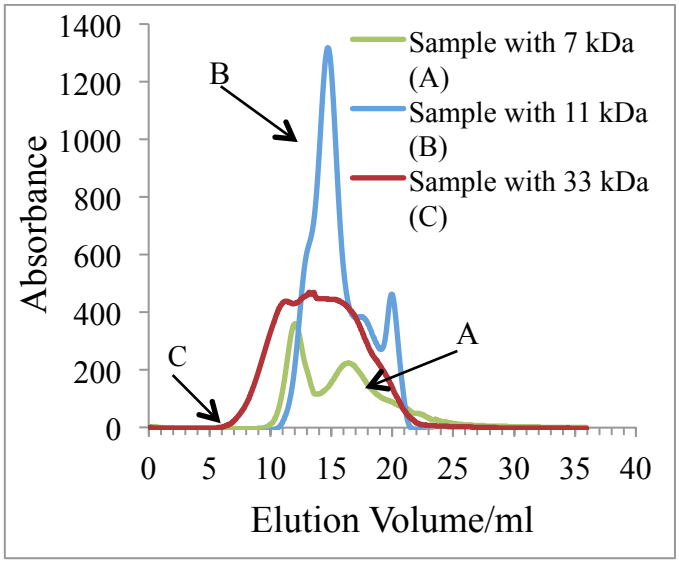

Figure 4.20. Gel filtration path of samples prepared with copolymers of molecular weights 11 kDa and 33 kDa compared to the gel filtration path obtained from a sample made with 7 kDa copolymer.

4.5.2.1 Dynamic Light Scattering Analysis

All the samples were successively analysed via DLS. Figure 4.21 shows size distributions for SMALPs made with 7 kDa, 11 kDa and 33 kDa copolymers. Results of a preliminary analysis revealed, a high value of polydispersity for the 11 kDa and the 33 kDa and the presence of multiple peaks in the intensity% analysis. Due to the very poor sample quality, high polydispersity and presence of large aggregates, the cumulant analysis was not appropriate; therefore results are reported as volume distribution data (a description of the theory of DLS technique and the analysis of the results is reported in Chapter 2 Section 2.3). Data were fitted to a lognormal function in order to obtain the average structure diameters (Table 4.10).

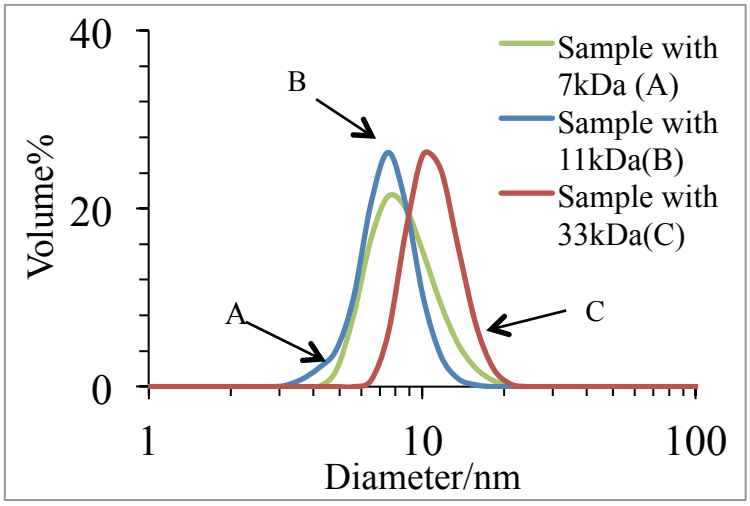

Figure 4.21. DLS data showing the hydrodynamic diameters of SMALPs assembled using copolymer of different molecular weights. All the samples have been analysed at 25 °C in the same buffer composition. Results are from the average of 7 experiments each composed of 11 runs.

Copolymer in use	*Diameter of structures formed with DMPC*
7 kDa	8.3 ± 0.04 nm
6 kDa RAFT	16 ± 0.2 nm
11 kDa	6.8 ± 0.04 nm
33 kDa	10 ± 0.2 nm
63 kDa	6.9 ± 0.06 nm
110 kDa	9.6 ± 0.08/ 509 ± 6.8 nm

Table 4.8. Table summarising the diameter of the structures formed with DMPC obtained from fitting to a lognormal distribution of DLS experimental data after all samples were gel filtered.

From the evaluation of results obtained during DLS experiments it seems that all the solutions contained structures in the expected range of the SMALPs dimension. Therefore, in order to investigate the nature of these structures, further analysis was done via SAXS and SANS. As part of the sample

preparation procedure, explained in Section 4.2, all samples were concentrated via ultracentrifugation in order to get a stronger signal when using these techniques.

4.5.2.2 Small Angle X-ray and Neutron Analysis

SAXS experiments were performed in part in the I22 instrument (Diamond Light Source, Oxford) for samples prepared with 7 kDa, 33 kDa, 63 kDa and 110 kDa copolymers using a q range between 0.007 nm^{-1} and 0.4 nm^{-1} and in part also on the SAXSess located in the University of Bath for sample prepared with 6 kDa RAFT copolymer. As suspected from the preliminary observations made on these samples, 63 kDa and 110 kDa were not able to form SMALPs.
SAXS data revealed the presence of relatively big structures. These data were fitted to a polydisperse core shell cylinder model (results for both set of data are reported in Table 4.11). The SLD of the solvent was calculated and held during the fitting, all the other parameters were fitted. However SLD for all the copolymer where calculated as reference values and are reported in Appendix A4.

From the analysis of the results, the copolymers used still incorporated the DMPC into the core of the structures. The analysis also revealed the presence of styrene in the cores, as the SLD value for the core was found to be between the SLD value of DMPC tails (7.2×10^{10} cm^{-2}) and the SLD value of styrene (9.2×10^{10} cm^{-2}). As shown in the inset of Figure 4.22 the SAXS pattern of pure copolymer compared to the pattern of copolymer in solution with DMPC also confirms the different arrangements of the copolymer when in presence of phospholipids. Cylindrical structures formed by the 110 kDa with DMPC in solution had a diameter of about 5 nm.

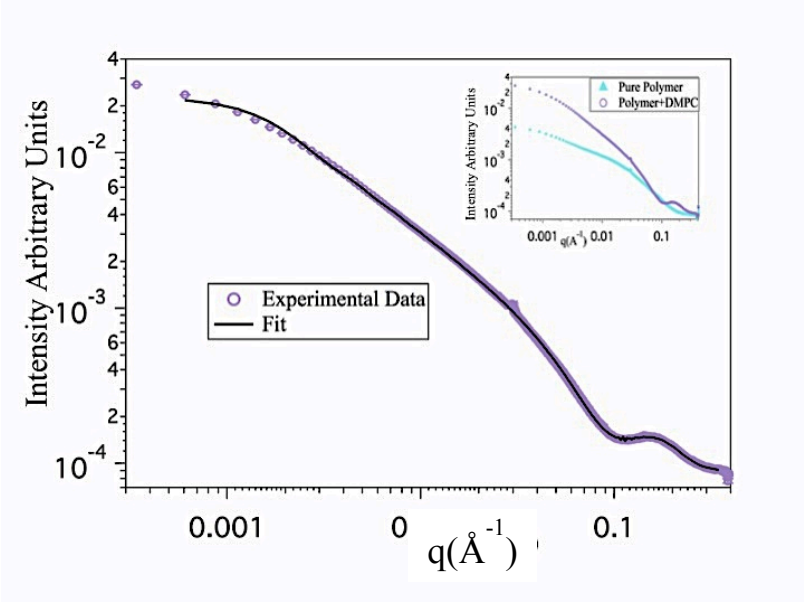

Figure 4.22. SAXS data for structures formed by 110 kDa SMA with DMPC in 50 mM phosphate buffer solution with 200 mM NaCl at pH 8 and 25 °C. Experimental data (filled purple circle) were fitted to a polydisperse-core-shell cylinder model (continuous black line) Error bars are also shown. Top right hand side inset compares experimental results obtained for pure 110 kDa copolymer in phosphate buffer solution at same pH and temperature to the experimental results for the 110 kDa in solution with DMPC. Data were collected using the same instrument with the same experimental conditions (more details for the copolymer data can be found on Chapter 3 Section 3.9). The small peak at $q \approx 0.03$ Å^{-1} is a detector artefact.

Model Coefficients	*110 kDa*	*63 kDa*
Scale	0.0001 ± 0.0001	0.0003 ± 0.0001
Mean core radius (nm)	1.3 ± 2	9.3 ± 2
Radial polydispersity (σ)	0.32 ± 0.05	0.42 ± 0.05
Core length (nm)	132 ± 4	251 ± 4
Radial shell thickness (nm)	1.1 ± 0.2	1.5 ± 0.2
Face shell thickness (nm)	1.2 ± 0.2	1.5 ± 0.2
*SLD core (*cm^{-2}*)*	8.6×10^{10} $\pm 0.05 \times 10^{10}$	8.4×10^{10} $\pm 0.05 \times 10^{10}$
*SLD shell (*cm^{-2}*)*	1.0×10^{10} $\pm 0.05 \times 10^{10}$	9.7×10^{10} $\pm 0.05 \times 10^{10}$
Incoherent background (cm^{-1})	8×10^{-5} $\pm 0.05 \times 10^{-5}$	7×10^{-5} $\pm 0.05 \times 10^{-5}$

Table 4.9. Table reporting values of experimental SAXS data of structures composed of DMPC and either 110 kDa and 63 kDa copolymers in 50 mM phosphate buffer with 200 mM NaCl, fitted to a polydisperse core-shell cylinder.

SMALPs prepared with the 33 kDa copolymer showed a very broad peak on the gel filtration path, (Figure 4.20). This made it very difficult to ensure purification from extra copolymer aggregates in solution which did not contribute to the SMALPs structures. Immediately after the gel filtration step, the sample was analysed via DLS showing presence of structures within the range of nanodiscs but which were on average larger than sample prepared with the use of SMA-2000P.

Once analysed using SAXS (Figure 4.23) experimental data revealed the presence of larger structures, probably composed of copolymer aggregates. Data collected on the I22 instrument were therefore fitted to a combined model of a core-shell cylinder and a charged polydisperse core bicelle, the standard model used for fitting the SMALPs structures.

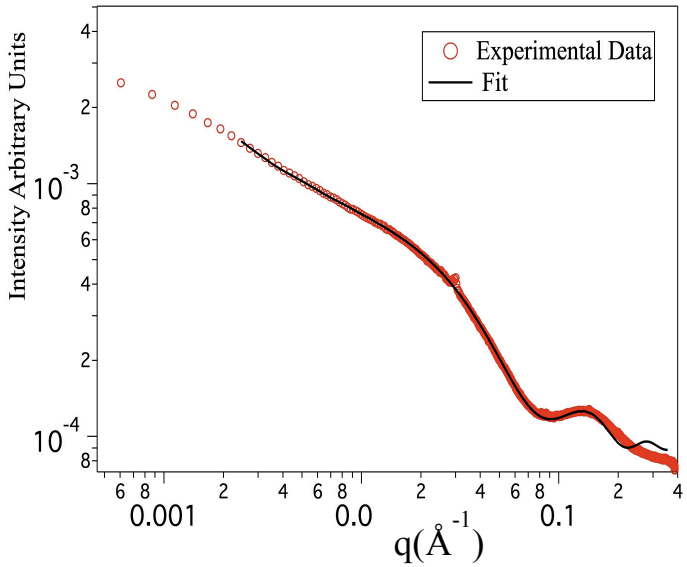

Figure 4.23. Scattering SAXS pattern from SMALPs made with 33 kDa copolymer and DMPC in phosphate buffer (empty red circles) fitted to the model described in the text (continuous black line). The small peak at q ≈0.03 Å^{-1} is a detector artefact.

For fitting the SAXS data, the SLD of the faces of SMALPs was calculated and held during fitting, the water content of head groups within the faces assumed to be 0.57, a value based on the work of Smith et al [23]. Other parameters also calculated and held during the fitting were the SLD of solvent (9.4×10^{10} cm^{-2}), temperature (25 °C) dielectric constant (78) of the solution [36] and monovalent

salt concentration (0.25 M). The remaining parameters were fitted and results are reported in Table 4.10.

Model Parameters	*Fitting results*
Scale	$2\times10^{-5} \pm 0.05\times10^{-5}$
Core radius (nm)	2.3 ± 0.2
Shell Thickness (nm)	0.27 ± 0.2
Core length (nm)	201± 10
SLD core (cm^{-2})	$8.5\times10^{10} \pm 0.05\times10^{10}$
SLD shell (cm^{-2})	$1.5\times10^{11} \pm 0.05\times10^{11}$
Incoherent Background (cm^{-1})	$1\times10^{10} \pm 0.05\times10^{11}$
Volume fraction	$1.6\times10^{-5} \pm 0.05\times10^{-5}$
Mean core radius (nm)	3.6 ± 0.2
Radial polydispersity (σ)	0.4 ± 0.1
Core length (nm)	2.9 ± 0.2
Radial shell thickness (nm)	2.0 ± 0.2
Face shell thickness (nm)	0.7 ± 0.2
SLD core (cm^{-2})	$9\times10^{10} \pm 0.05\times10^{10}$
mol% solvent in rim	0.6 ± 0.01

Table 4.10. Fit parameters for fitting SAXS data of SMALPs made using 33 kDa copolymer and DMPC, to a model of a core-shell cylinder summed to a charged polydisperse core-shell cyilinder model with polydisperse core and head groups regions at the top and the bottom of the cylinder.

SANS experiments were performed on the LOQ instrument (see Chapter 2 Section 2.7.1 for more information about instrument and experimental setup), in 1 cm wide Hellma quartz cuvettes having a 1 mm path length. Temperature was kept at 25 °C and a q range between 0.0095 $Å^{-1}$ and 0.2825 $Å^{-1}$ was recorded. Data were treated according to the general procedure described in Chapter 2 Section 2.7.

SMALP samples were produced using 11 kDa copolymer and hydrogenated DMPC in both deuterated and hydrogenated phosphate buffer and

simultaneously fitted (Figure 4.24). Samples of 33 kDa copolymer and DMPC were also prepared using deuterated DMPC and hydrogenated DMPC in both deuterated and hydrogenated buffer. However due to some technical difficulties during the dialysis only the deuterated DMPC in hydrogenated buffer proved to be suitable for further analysis (Figure 4.24).

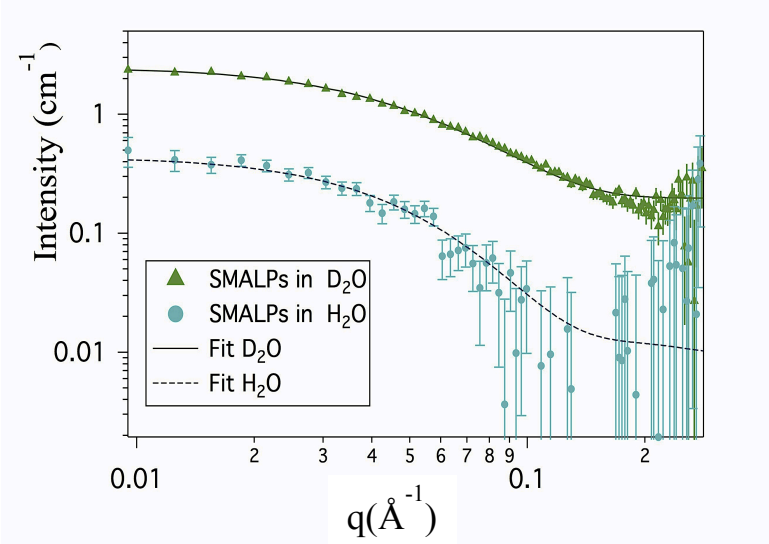

Figure 4.24. SANS data of SMALPs made with 11 kDa copolymer and d-DMPC in either hydrogenated phosphate buffer (filled light blue circles) and deuterated phosphate buffer solution (green filled triangles) fitted to a polydisperse core bicelle model (continuous and dotted lines).

All data were reduced and corrected following the protocol reported in Chapter 2 Section 2.8.1 and fitted (simultaneously in the case of the SMALPs prepared with 11 kDa) to the same charged core-shell cylinder model using the SANS Analysis package in Igor Pro [19]. The neutron scattering length density of the head groups was set to be 1.86×10^{10} cm^{-2} based on the value reported by Smith et al [23] while the water content was set at a mole fraction of 0.57 based on their results of fitting the headgroups region of a deuterated DMPC bilayer. The SLD of the copolymer was calculated to be 1.78×10^{10} cm^{-2} for the 11 kDa copolymer and of 1.58×10^{10} cm^{-2} for the 33 kDa. The water content in the rim was then fitted based on this value and the value of the solvents. The scattering length density of the 100% D_2O solvent (6.29×10^{10} cm^{-2}) and 100% H_2O

(-0.57 × 10^{10} cm^{-2}) were calculated and held during the fitting. Other model parameters were calculated and held during the fitting such as the temperature (25 °C), the dielectric constant of the solution [36] (ε=78) and the monovalent salt concentration (0.25 M). The remaining parameters were fitted and results are reported in Table 4.11.

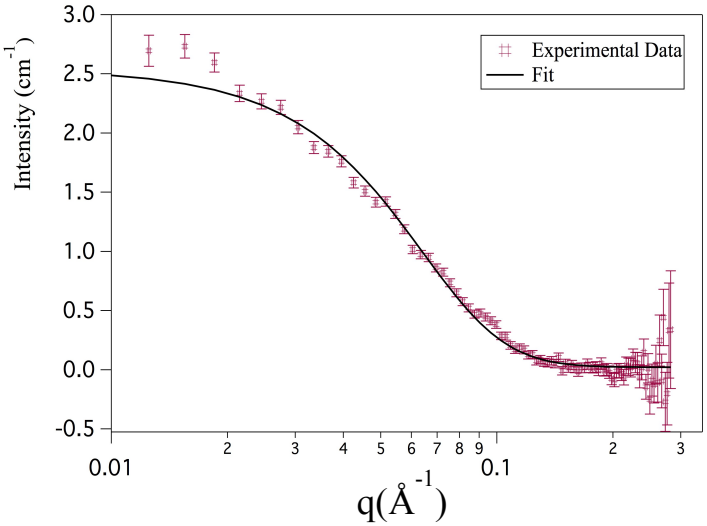

Figure 4.25. SANS data from SMALP made with 33 kDa copolymer and d-DMPC in hydrogenated phosphate buffer fitted to a polydisperse core-shell cylinder model (continuous black line).

Model Coefficients	*33 kDa in 0% D_2O*	*11 kDa in 100% D_2O*	*11 kDa in 0% D_2O*
Volume fraction	0.01 ± 0.01	0.009 ± 0.01	
Mean core radius (nm)	3.1 ± 0.2	2.2 ± 0.2	
Radial polydispersity (σ)	0.21 ± 0.05	0.4 ± 0.05	
Core length (nm)	3.2 ± 0.2	2.6 ± 0.2	
Radial shell thickness (nm)	1.14 ± 0.2	0.4 ± 0.2	
Face shell thickness (nm)	0.8 ± 2	0.8 ± 0.2	
SLD core (cm^{-2})	6.8×10^{10} ± 0.05×10^{10}	1.87×10^{9} ± 0.05×10^{9}	
Mol% solvent in rim	0.8 ± 0.1	0.6 ± 0.1	
Incoherent background (cm^{-1})	0.0177 ± 0.05	0.195 ± 0.05	0.009 ± 0.05

Table 4.11. Fit parameters for fitting SANS data of SMALPs made using 11 kDa and h-DMPC and 33 kDa copolymer and d-DMPC, to a model of a core-shell cylinder with polydisperse core and head-group regions at top and bottom of the cylinder.

From the analysis of the fitting of both samples it was found that SMALPs formed using the 33 kDa copolymer showed a core diameter around 6.2 nm and a much thicker copolymer belt of 1.14 nm. The length of the discs is also larger than the average dimension of 2.9 nm found for SMALPs assembled with the 7 kDa SMA-2000P and 6 kDa RAFT copolymers. These results might be the consequence of the much higher copolymer molecular weight giving a total theoretical length of the copolymer that is almost three times larger. Also a higher percentage of solvent within the rim was found consistent with the hydrophilic percentage in the copolymer calculated which is the highest among all the copolymers forming SMALPs.

4.6 Discussion

Experiments performed with the copolymers synthesised via RAFT polymerisation with different styrene to maleic acid molar ratios have given the source of important information. These copolymers were synthesised via RAFT polymerisation keeping the molecular weight of 6 kDa and the same architecture, consisting of a first block of alternating styrene and maleic acid and a tail of only styrene. The similar architecture highlighted how crucial the proportion between the hydrophobic and hydrophilic part of the copolymer is to SMALPs formation. As observed from the values reported in Table 4.12, the optimal total ratio of styrene to maleic acid was found to be 2:1.

Copolymer in Use	*SSS Dimension (nm)*	*SMS Dimension (nm)*	*Total copolymer length (nm)*	*STY: MA total ratio*	*SMALPs Diameter (nm)*	*SMALPs Circumference (nm)*
6 kDa RAFT 1.7:1	3.6	21.8	25.38	1.7:1	___	___
6 kDa RAFT 2:1	5.25	19.8	25.05	2:1	14 ± 2	43.96
6 kDa RAFT 3:1	6.97	14.85	21.82	3:1	___	___

Table 4.12. Table summarising the findings obtained for different styrene to maleic acid proportions using the 6 kDa copolymer synthesized in Bath via RAFT polymerisation.

Results obtained were then compared to a parallel work performed on the commercial copolymers (Table 4.13), characterised by an architecture which was not well defined, but instead composed of randomly organised blocks of non-alternating (SSS), semi alternating (SSM/MSS) or completely alternation (SMS) styrene and maleic acid units.

It has been found that also the molecular weight might have an impact on the SMALPs formation. The 110 kDa copolymer even if possessing an optimal ratio of 2:1 styrene to maleic acid, did not form SMALPs but incorporated DMPC into larger cylindrical structures.

Among all the commercial copolymers in use, the best results were confirmed to be obtained with the 7 kDa SMA-2000P, the first copolymer used by our collaborators. These samples are stable, showing results with good reproducibility over different experiments performed over time. Decent results were also obtained with the 11 kDa copolymer from Polyscope. However the quality of the samples in term of stability and reproducibility was not as good as the 7 kDa SMA-2000P or 6 kDa RAFT copolymers. Conversely samples assembled with the use of the 33 kDa copolymer (also from Polyscope) were not stable with time, leading to the discrepancy in values obtained from SAXS and SANS experiments. Also, the gel filtration path showed a very broad size distribution.

SMA M_w	*SSS Length (nm)*	*SSM/ MSS Length (nm)*	*SMS Length (nm)*	*Total copolymer length (nm)*	*Hydrophilic length (SSM/MSS+SMS) (nm)*	*STY: MA total ratio*	*SMALP* diameter (nm)*	*SMALP circumference (nm)*
7 kDa	5.46	6.29	1.57	13.32	7.96	2:1	8 ± 0.2	25.1 ± 1.3
11 kDa	9.97	10.32	2.45	22.74	12.77	1.8:1	5 ± 0.2	15.7 ± 1.3
33 kDa	19.95	33.25	14.92	68.11	48.17	1.9:1	11 ± 0.2	34.5 ± 1.3
63 kDa	53.15	62.13	15.63	130.9	77.76	2.4:1	—	—
110 kDa	92.5	107.97	27.19	227.66	135.16	2:1	—	—

*Table 4.13. Table summarising main copolymer properties investigated in Chapter 3 in connection to the work done in the attempt to individuate the key properties allowing the SMALPs formation. * Value of SMALP diameter indicated is result of fitting of SANS and SAXS data.*

From the analysis of the global properties of the copolymer (Table 4.16) linked to the SMALPs structures formed and the analysis performed on the stability, dimension and reproducibility of the samples it is concluded that there is no clear linear trend that connects the copolymer architecture with the SMALPs dimension.

Comparing the commercial copolymers to the 6 kDa RAFT copolymer proved to be the most suitable for SMALPs assembly. It seems that a less predominant presence of semi alternating units (SSM/MSS) within the copolymer architecture allows the formation of more stable structures. Indeed the 7 kDa SMA-2000P, compared to the other commercial copolymers possess the smallest amount of SSM/MSS units and proved to give the most reproducible results.

Another important parameter to be considered is the length of the non-alternating unit (SSS) present in the copolymer chain. The value of this length

found for the copolymer SMA-2000P (21.81 nm) is indeed very close to the 6 kDa RAFT SSS dimension of 21 nm. This value is obviously strictly connected to the volume occupied by the hydrophobic copolymer part, represented by all the styrene in the copolymer. Therefore not only the SSS blocks were included but also the styrene present in the SMS blocks. This volume in the SMA-2000P is again very close to the 6 kDa copolymer (respectively 8.5 nm^3 and 8.4 nm^3). Results are summarised in Table 4.15. However when comparing the volumes of the hydrophobic units to the SMALPs volumes it was not possible to draw any trend or deduct any possible correlations among the two.

Commercial copolymer with molecular weight of 33 kDa showed to be the less suitable for SMALPs assembly. Indeed the sizes of structures formed were not very reproducible. This indicates that there is likely a limitation in the dimension of the hydrophobic copolymer block that allows the SMALPs formation.

When comparing the value found for the length of the polymeric chain to the circumference of the disc, it was found that for SMALPs assembled with 6 kDa RAFT and 7 kDa approximately two copolymer chains are contributing to the structure for each structure. Conversely to the SMALPs formed with the 11 kDa and 33 kDa copolymers only one copolymer chain per SMALP was found to contribute to the formation of each SMALP.

Copolymer	*Volume of Hydrophobic Copolymer Block (nm^3)*	*SMALPs Core Volume [(a)] (nm^3)*	*Copolymer mol % in the core [(b)]*
6 kDa RAFT	8.4	446.4	39%
7 kDa SMA- 2000P	8.5	147.8	20%
11 kDa	15.1	56.9	22%
33 kDa	40.6	159.5	7.9%
63 kDa	84.0	—	—
110 kDa	146	—	—

Table 4.14. Table summarising volumes occupied by the hydrophobic part of the copolymers in comparison with the volume of the core of the SMALP structures. (a) Values calculated from average diameter found in solution. (b) Values resulting from fitting of SANS data.

Analysis of SMALPs assembled with different copolymer molecular weights and also different copolymer architectures possess different diameters. Results of experiments performed using SAXS, SANS and DLS analysis showed that the 6 kDa RAFT copolymer forms SMALPs with the largest diameter (14 nm) accommodating an average of 202 DMPC molecules compared to the smallest diameter obtained with the 11 kDa (5.2 nm) that only accommodates 42 DMPC molecules.

Copolymer	*Overall Bilayer Size (nm^2)*		*Mol% Solvent in the Rim*	*DMPC molecules In the bilayer**
	Min	*Max*		
6 kDa RAFT	55.4	66.4	0.61 ± 0.05	202
7 kDa SMA-2000P	40.7	50.3	0.42 ± 0.0.5	152
11 kDa	12.6	18.1	0.61± 0.05	42
33 kDa	12.6	18.1	0.6 ± 0.05	42

*Table 4.15. SMALPs formed with different copolymers accommodating a different number of DMPC molecules. * Indicates number of DMPC molecules in the bilayer, calculated from the total diameter of the core assuming the area occupied by each DMPC molecule [24] to be 0.596 nm^2.*

4.7 Conclusions

Work conducted on SMALPs assembled with the use of different copolymer molecular weights, in conjunction with the experiments performed on the separate copolymer solutions, enables us to draw conclusions regarding their architectures and physical chemical properties.

Results of analyses presented in this chapter suggest that one of the key factors regulating the lipids-SMA assembly process into SMALPs structure relies on the styrene to maleic acid proportion in strict combination with the copolymer molecular weight.

Optimal conditions are found to be for copolymers with a 2:1 styrene to maleic acid proportion and a molecular weight of 6 kDa or 7 kDa. Indeed, copolymers with an optimal styrene to maleic acid proportion but high molecular weight (110 kDa and 63 kDa) showed to not be able to form SMALPs.
On the contrary the 33 kDa although assembling into SMALPs revealed to be unstable over time and results obtained were difficult to reproduce.

All together these results suggest that there might be an upper limit in the molecular weight of the copolymer used to be able to take part to the formation of SMALPs.

Investigations conducted on the architecture of the SMA copolymers revealed that the copolymers with a more defined architecture constituted of a first block of alternation styrene and maleic acid followed by a completely hydrophobic tail of styrene are the most suitable to form SMALPs.
Very interesting properties were found regarding the 6 kDa RAFT copolymer with a 2:1 styrene to maleic acid proportion. This copolymer seems to completely contribute to the SMALPs formation with no free copolymer in solution. This offers the great advantage of no need of further purification of the sample via gel filtration chromatography giving a better control on the sample composition and concentration with no loss of precious material. Moreover,

SMALPs assembled with this copolymer showed to be extremely stable over time giving the possibility to store and reuse samples for multiple non-destructive experiments.

Dimension of SMALPs showed a very good agreement with the protein-stabilised nanodiscs reported in literature [25]. Moreover interesting results were obtained with the use of copolymers with different molecular weights.

Experimental data showed that the SMA molecular weight controls the diameter of the SMALPs, showing similarity with the role of the MSP in the protein-stabilised version [27]. Indeed, different samples assembled with the 6 kDa RAFT copolymer revealed to possess a larger diameter compared to the SMALPs assembled with the 7 kDa SMA-2000P. This will leave open the opportunity with further investigation to create a library of SMALPs with different sizes.

4.8 References

1. Knowles, T.J., et al., *Membrane proteins solubilized intact in lipid containing nanoparticles bounded by styrene maleic acid copolymer*. J Am Chem Soc, 2009. **131**(22): p. 7484-5.
2. Jamshad, M., et al., *Surfactant-free purification of membrane proteins with intact native membrane environment*. Biochem.Soc.Trans, 2011. **39**(3): p. 813.
3. Tonge, S.R. and B.J. Tighe, *Responsive hydrophobically associating copolymers: a review of structure and properties*. Adv Drug Deliv Rev, 2001. **53**(1): p. 109-122.
4. Knowles, T.J., et al., *Membrane Proteins Solubilized Intact in Lipid Containing Nanoparticles Bounded by Styrene Maleic Acid Copolymer.* J. Am. Chem. Soc., 2009. **131**(22): p. 7484-7485.
5. Li, T., et al., *UV absorption spectra of polystyrene.* Polymer Bulletin, 1991. **25**(2): p. 211-216.
6. Harroun, T.A., et al., *Neutron and X-ray scattering for biophysics and biotechnology: examples of self-assembled lipid systems*. Soft matter, 2009. **5**: p. 2694-2703
7. Chen, C.H., *Interactions of lipid vesicles with solvent in heavy and light water*. J. Phys. Chem., 1982. **86**(18): p. 3559-3562.
8. R.Rennie, A., *Physical Properties of H_2O and D_2O-Comparisons*, 2014.
9. Orwick, M.C., et al., *Detergent-Free Formation and Physicochemical Characterization of Nanosized Lipid–Polymer Complexes: Lipodisq*. Angew Chem Int Ed Engl, 2012. **51**(19): p. 4653-4657.
10. Orwick-Rydmark, M., et al., *Detergent-free incorporation of a seven-transmembrane receptor protein into nanosized bilayer Lipodisq particles for functional and biophysical studies*. Nano Lett., 2012. **12**(9): p. 4687-92.
11. Tomaszewska, E., et al., Detection Limits of DLS and UV-Vis *Spectroscopy in Characterization of Polydisperse Nanoparticles Colloids*. J. Nanomater., 2013. **2013**: p. 10.

12. Schärtl, W., *Light Scattering from Polymer Solutions and Nanoparticle Dispersions.* Sringer Laboratory, 2007: Springer
13. Skar-Gislinge, N. and L. Arleth, *Small-angle scattering from phospholipid nanodiscs: derivation and refinement of a molecular constrained analytical model form factor.* Phys. Chem. Chem. Phys., 2011. **13**(8): p. 3161.
14. Skar-Gislinge, N., et al*., Elliptical structure of phospholipid bilayer nanodiscs encapsulated by scaffold proteins: casting the roles of the lipids and the protein*. J Am Chem Soc, 2010. **132**(39): p. 13713-13722.
15. Denisov, I., et al., *Thermotropic phase transition in soluble nanoscale lipid bilayers.* J. Phys. Chem. B, 2005. **109**(32): p. 15580-15588.
16. Tveten, E.G., *X-ray and neutron reflectivity studies of nanodiscs below the air water interface*, in Faculty of Science, 2011, University of Copenaghen.
17. Wadsäter, M., et al., Effect of Phospholipid Composition and Phase on Nanodisc Films at the Solid–Liquid Interface as Studied by Neutron Reflectivity. Langmuir, 2013. **29**: p. 2871-2880.
18. Wadsater, M., et al*., Aligning nanodiscs at the air–water interface, a neutron reflectivity stu*dy. Langmuir, 2011. **27**: p. 15065-15073.
19. Kline, S.R., *Reduction and analysis of SANS and USANS data using IGOR Pro*. J Appl Crystallogr, 2006. **39**: p. 895-900.
20. Tveten, E.G*., X-ray and neutron reflectivity studies of nanodiscs below the air water interface*, 2011. University of Copenaghen.
21. Anslyn, E.V. and D.A. Dougherty, *Modern Physical Organic Chemistry,* 2006: University Science.
22. Wadsater, M., et al., *Aligning nanodiscs at the air-water interface, a neutron reflectivity study*. Langmuir, 2011. **27**(24): p. 15065-15073.
23. Smith, M.B., et al., *Neutron reflectometry of supported hybrid bilayers with inserted peptide*. Soft matter, 2010. **6**(5): p. 862-865.
24. Nagle, J.F. and S. Tristram-Nagle, *Structure of lipid bilayers.* Biochim. Biophys. Acta, 2000. **1469**(3): p. 159-195.
25. Bayburt, T.H. and S.G. Sligar, *Membrane protein assembly into Nanodiscs.* FEBS letters, 2010. **584**(9): p. 1721-1727.

26. Ritchie, T.K., et al., *Chapter 11 Reconstitution of Membrane Proteins in Phospholipid Bilayer Nanodiscs, in Methods in enzymology*, D. Nejat, Editor, 2009, Academic Press. p. 211-231.
27. Denisov, I., et al., *Directed self-assembly of monodisperse phospholipid bilayer nanodiscs with controlled size*. J Am Chem Soc, 2004. **126**(11): p. 3477-3487.
28. Rasmussen, T.E., *Application of Nanodiscs for Studies of Model Membrane Organization nad Dynamics, in Department of Physics and Chemistry & the Department of Biochemistry and Molecular Biology*, 2010, University of Southern Denmark. p. 1-108.
29. Mohammed Jamshad*, V.G., Ilaria Idini *, Tim J. Knowles, Miriam Dowle, et al., *Structural analysis of a nanoparticle containing a lipid bilayer used for detergent-free extraction of membrane proteins*., 2014, Nano Research.
30. Orwick-Rydmark, M., et al., Detergent-Free Incorporation of a Seven-Transmembrane Receptor Protein into Nanosized Bilayer Lipodisq Particles for Functional and Biophysical Studies. Nano Lett., 2012. **12**(9): p. 4687-4692.
31. Bayburt, T.H., et al., Self-Assembly of Discoidal Phospholipid Bilayer Nanoparticles with Membrane Scaffold Proteins. Nano Lett., 2002. **2**(8): p. 853-856.
32. Hernández-Rocamora, V.M., et al., Reconstitution of the Escherichia coli cell division ZipA–FtsZ complexes in nanodiscs as revealed by electron microscopy. J.Struct. Biol., 2012. **180**(3): p. 531-538.
33. Lin, Y.-W. and L.-F. Liao, *Probing interactions between uranyl ions and lipid membrane by molecular dynamics simulation.* Computational and Theoretical Chemistry, 2011. **976**(1–3): p. 130-134.
34. Ting-Beall, H.P., *Interactions of uranyl ions with lipid bilayer membranes.* J.Microscop., 1980. **118**(2): p. 221-227.
35. Caffrey, M., et al., Uranyl acetate induces gel phase formation in model lipid and biological membranes. Biophys. J., 1987. **52**(3): p. 501-505.
36. Aragones, J.L., et al., *Dielectric Constant of Ices and Water: A Lesson about Water Interactions.* The Journal of Physical Chemistry A, 2010. **115**(23): p. 5745-5758.

5

5 Effect of Solution Conditions and Lipid Mixtures on SMALPs Stability

5.1 Introduction

After primarily investigations performed with the aim to understand the SMALPs assembly process and their structural characterisation, further work was carried out in order to investigate their stability under various environmental conditions.

The present chapter is organised in two main sections: in the first one attention is drawn toward the study of the stability of SMALPs under a range of temperatures, pHs and salt concentrations. Given the results reported in Chapter 4 showing the optimal performance of the 7 kDa SMA-2000P and 6 kDa RAFT copolymers, analyses were performed on SMALPs assembled with the use of these copolymers and deuterated or non-deuterated DMPC. The second section of this chapter is dedicated to the work performed on the lipid component of the SMALP structures in order to understand which lipid compositions are able to assemble with the copolymer to form a SMALP structure and the impact that the use of charged phospholipid heads or different tail lengths might have on the structures.

5.2 Investigation of SMALPs Stability at Different Temperatures

After almost 15 years of studies dedicated to the understanding of the cell lipid bilayer the theory of compartmentalisation in lipid rafts [1-4] is nowadays generally accepted as well as the close interaction between lipids membrane and proteins is subject of attention [4, 5]. Indeed numerous studies have been carried out to investigate the lipid bilayer influence on the function of membrane proteins [6-8].

One of the primary SMALP applications is its use as a support for membrane proteins studies. Therefore it is important to understand the lipid phase transition in this particular system, as it will affect the activity of the inserted protein [9, 10].

Analysis of the SMALP system at different temperatures was carried out not only to assess their stability but also, given the demonstrated interaction between the copolymer and the phospholipids, to investigate whether they still mimic the lipid membrane and whether this interaction affects the lipid transition temperatures. Samples were analysed at different temperatures in order to investigate the region around the DMPC main transition temperature (24 °C) and at temperatures above and below this region of interest for storage applications (for instance, samples may be stored and transported at low temperatures) or for experimental purposes (analysis of membrane proteins at body temperature (≈38 °C) or above).

5.2.1 Analysis of SMALPs Assembled with 7 kDa SMA-2000P Copolymer

SMALP samples were all prepared following the protocol reported in Chapter 4 Section 4.2 in which the materials used for samples analysed here are also reported. The SMALPs dilute solution resulting from the gel filtration process was analysed via DLS.

DLS experiments were performed on the Zetasizer instrument which complete description is reported in Chapter 2 Section 2.3. Samples were analysed at four different temperatures (15 °C, 25 °C, 35 °C and 45 °C) allowing the sample to equilibrate for twenty minutes between each temperature, experimental data are reported in Figure 5.1 A.

From analysis of the DLS experimental results the total diameter of the structures examined was found to increase from a value of 8.6 nm to 11 nm. Results are reported in Table 5.2.

SAXS experiments were performed in the I22 instrument (Diamond light source, Oxford) for samples prepared with 7 kDa SMA-2000P using a q range between 0.007 nm^{-1} and 0.4 nm^{-1}. Samples were positioned in a brass sample holder equipped with channels for the circulation of the water. Temperature was increased from the value of 15 °C up to 45 °C with a use of a water bath to which the channels were connected. Samples were equilibrated for one hour at each temperature. Experimental data are reported in Figure 5.1 B.

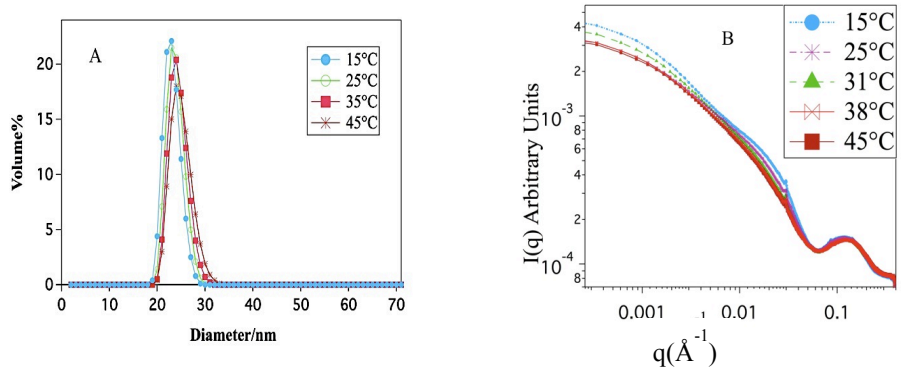

Figure 5.1. A) DLS (A) and SAXS (B) data of SMALPs prepared with 7 kDa SMA-2000P and deuterated DMPC after purification via gel filtration chromatography. *The small peak at q ≈ 0.03Å^{-1} is a detector artefact.*

SANS analysis was performed on the D11 instrument located at the ILL research institute. SMALP samples were prepared with the use of deuterated DMPC in either a deuterated or hydrogenated phosphate buffer. Initial analysis of the samples was performed at 25 °C. Successively, the temperature was raised to 45 °C within a time space of 4 hours. Samples were then analysed on a cooling down process at 35 °C, 25 °C and finally 15 °C. For each data set fitting was performed globally for the two solvent contrasts (0% D_2O and 100%D_2O).

Data were reduced from the initially recorded images following the protocol reported in Chapter 2 Section 2.8.1 and successively fitted using the SAS Analysis package [11] from NIST written in Igor Pro to a model of a core-shell cylinder , the core radius was convoluted by a Shultz distribution to add polydispersity. The model also includes a "face" layer on top and bottom to take into account the phospholipid headgroups. The interactions between discs were fitted using a Hayter Penfold charged sphere approximation. A description of the model and schematic representation can be found in Chapter 2 Section 2.8.2.1.

For fitting of the SAXS data the same core-shell cylinder model was combined to a Shultz sphere model to fit the low q region showing the presence of larger structures. Some of the parameters were calculated or taken from literature and held during the fitting, for instance the water content of head groups within the

faces assumed to be 0.57, value based on the work of Smith et al [12]. Parameters calculated and held during the fitting are reported in Table 5.1.

Parameters	*SANS Value*		*SAXS Value*
Solvents SLD	*Deuterated Buffer*	*Hydrogenated Buffer*	9.4×10^{10} cm^{-2}
	6.29×10^{10} cm^{-2}	-5.67×10^{11} cm^{-2}	
Head groups SLD	1.86×10^{10} cm^{-2}		$11.5\ 10^{10}$ cm^{-2}
Copolymer SLD	1.81×10^{10} cm^{-2}		10.85×10^{10} cm^{-2}
Temperatures	15 °C; 25 °C; 35 °C; 45 °C		15 °C; 25 °C; 31.2 °C; 38 °C; 45 °C;
Salt concentration	0.25 M		0.25 M
Dielectric constant	78		78

Table 5.1. Table summarising values calculated and held during fitting of SAXS and SANS data.

The remaining parameters were fitted and results are reported in Table 5.2. Fitting results for SANS data are summarised in Table 5.3 and a global picture of the SAXS data at different temperatures is reported in Figure 5.1.

	15 °C	*25 °C*	*31 °C*	*38 °C*	*45 °C*
Volume Fraction	3.32×10^{-7} $\pm 0.1\times 10^{-8}$	2.6×10^{-7} $\pm 0.1\times 10^{-8}$	3.8×10^{-7} $\pm 0.1\times 10^{-8}$	$1.8\ 10^{-7}$ $\pm 0.1\times 10^{-8}$	3.7×10^{-7} $\pm 0.1\times 10^{-8}$
Sphere radius (nm)	14.2 ±1	16.8±1	13.1±1	12.6±1	12.1±1
Polydispersity	0.56±0.03	0.5±0.03	0.48±0.03	0.68±0.03	0.61±0.03
SLD sphere (cm^{-2})	9.9× 1010 $\pm 0.1\times 10^{10}$	9.9×10^{10} $\pm 0.1\times 10^{10}$	9.9×10^{10} $\pm 0.1\times 10^{10}$	9.9×10^{10} $\pm 0.1\times 10^{10}$	9.9×10^{10} $\pm 0.1\times 10^{10}$
Volume fraction	0.00016 ± 0.00002	0.00014 ±0.00002	0.00015 ±0.00002	0.00013 ±0.00002	0.00012 ±0.00002
SMALPs core radius (nm)	3.9±0.0.5	3.9±0.05	4.1±0.05	4.3±0.05	4.3±0.05
Radial polydispersity (σ)	0.26±0.005	0.26±0.005	0.28±0.005	0.28±0.005	0.38±0.005
Core length (nm)	2.6±0.05	2.6±0.05	2.6±0.05	2.6±0.05	2.6±0.05
Radial shell thickness (nm)	1.1±0.05	1.1±0.05	1.2±0.05	1.2±0.05	1.2±0.05
Face shell thickness (nm)	1.3±0.05	1.3±0.05	1.3±0.05	1.3±0.05	1.3±0.05
SLD core (cm^{-2})	$8.5\times 10^{10}\pm$ 0.05×10^{10}	$8.5\times 10^{10}\pm$ 0.05×10^{10}	$8.48\times 10^{10}\pm$ 0.05×10^{10}	$8.56\times 10^{10}\pm$ 0.05×10^{10}	$8.56\times 10^{10}\pm$ 0.05×10^{10}
mol% solvent in rim	0.5±0.05	0.5±0.05	0.5±0.1	0.5±0.05	0.5±0.05

Table 5.2. Summary of results of fitting SAXS data of SMALPs prepared with 7 kDa SMA-2000P copolymer and DMPC to the core-shell cylinder model combined to the Shultz sphere model.

The analysis performed with small angle X-ray scattering technique showed an increase in the total diameter between 25 °C and 38 °C rather than between 15 °C and 25 °C, which might be expected considering the DMPC transition temperature to be around 24 °C. The increase in the diameter is likely to be due to the lateral thermal expansion of the phospholipid since the specific volume

change of the copolymer is very small as demonstrated by the analysis performed on the copolymer solutions reported in Chapter 3.

This higher transition temperature might be due to the loss of cooperativity within the phase transition of the boundary lipids in contact with the copolymer as also suggested by Shaw et al. [13] As a consequence the transition temperature of the DMPC packed in the SMALPs structures is increased above the transition temperature of 24 °C detected in vesicles. Face thickness (constituted of DMPC heads) and length of the core of the discs (defined the tails of the DMPC molecules) revealed to be stable over the different temperatures

Solvent penetration within the copolymer belt was found to be constant at a 0.5mol%. Also copolymer penetration within the core was found constant for all the temperature analysed of 50% than average value, coherent with other SAXS experiments performed on same lipids composition (Chapter 4).

Analysis of the results obtained also revealed a decrease of the sphere dimension as the temperature rises in correspondence with the increase of the SMALP diameters. This might be related to the lipids exchange between SMALPs and aggregates of DMPC present in solution, founding supported by the work conducted on the protein-stabilised nanodiscs [14], which revealed nanodiscs to be a very dynamic system with continuous exchange of lipids among the discs.

Analyses on the temperature response of the discs were performed by dynamic scanning calorimetry (DSC) and scattering technique on the protein-stabilised nanodiscs showing this time an upward shift in the phase transition temperature (by about 5 °C) of the DMPC bilayer.
Also the Lipodisq® technology was probed over a range of different temperatures, however for the data reported by Orwick et al it is suggested that the SMA with 3:1 styrene to maleic acid proportion caused the transition temperature to reduce by about 10 °C [15].

Temperature	*DLS Diameter (nm)*	*SAXS Diameter (Core + Shell) (nm)*
15 °C	8.61 ± 0.03	9 ± 0.5
25 °C	9.56 ± 0.03	9 ±0 .5
35 °C	10.31 ± 0.05	9.6 ± 0.5 [a]
45 °C	11.10 ± 0.06	10 ± 0.5

Table 5.3. Summary of diameter values found for the different analysis performed on SMALPs assembled with 7 kDa SMA-2000P copolymer analysed at different temperatures. (a) Actual temperature was 31 °C.

A different behaviour was observed for SMALPs analysed via SANS, (where the sample was heated up from 25°C to 45 °C in 4 hours and then analysed at the temperatures of 45 °C, 35 °C 25 °C and 15 °C in comparison with results obtained with SAXS and DLS analyses.

Indeed, samples showed a decrease in the disc diameter from about 7.6 nm to 5.6 nm between 25 °C and 45 °C. The diameter was found to have similar value at 35 °C and then increases again at 25 ° C and then is stable at 15 °C. Samples analysed at of 25 °C before the experiment on temperature scan and results of the second analysis conducted at 25 °C after the heating were compared. Experimental results of analyses performed at the 25°C before and after the heating completely overlap showing the SMALPs to came back to their original dimensions.
Some of the parameters were calculated or reported from literature values and held during fitting. A summary is reported in Table 5.1.

Results showed an almost complete overlap of the two graphs showing the SMALPs to come back to the original dimension. Results of fitting are summarised in Table 5.4.

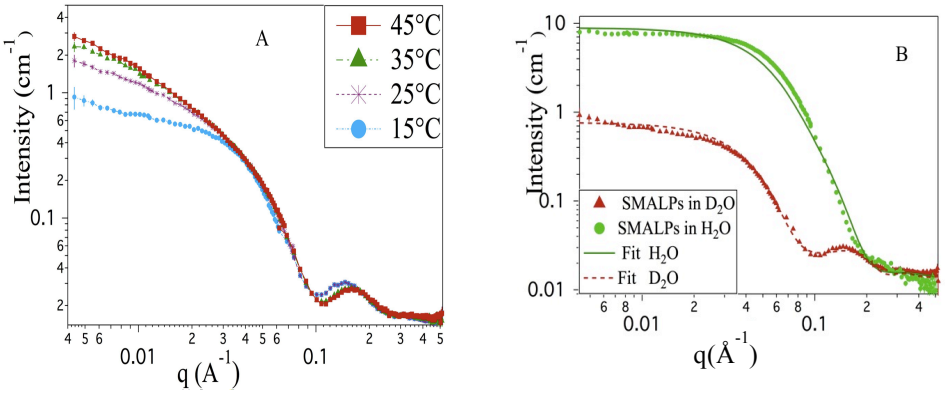

Figure 5.2. A) SANS pattern of SMALPs assembled with 7 kDa SMA2000P copolymer and d-DMPC analysed at different temperatures all in 100% D_2O B) Fitting of data from same sample with two buffer contrasts at 15°C.

	SMALPs Core length (nm)	*SMALPs Diameter (nm)*	*SMALPs Radial Shell Thickness (nm)*	*Copolymer mol% In the core*	*SMALPs mol% Solvent in the rim*
25°C	2.6 ± 0.05	9.4 ± 0.1	0.92 ± 0.02	12%	0.4 ± 0.05
45°C	2.6 ± 0.05	7.8 ± 0.1	1.1 ± 0.02	16%	0.6 ± 0.05
35°C	2.6 ± 0.05	7.8 ± 0.1	1.1 ± 0.02	14%	0.6 ± 0.05
25°C	2.6 ± 0.05	9.4 ± 0.1	0.92 ± 0.02	12%	0.4 ± 0.05
15°C	2.6 ± 0.05	9.2 ± 0.2	0.99 ± 0.02	12%	0.6 ± 0.05

Table 5.4. Summary of principal parameters values from fitting of SANS data of SMALPs prepared with use of 7 kDa SMA-2000P copolymer and d-DMPC.

Solvent penetration in the polymer belt was found to be between 0.4 mol% and 0.6 mol% in good agreement with results from SAXS analyses. Polymer penetration within the core was found to be 12 mol% at the temperatures of 15°C and 25°C, an increase proportional to the raise of the temperature was detected showing a 14 mol% at 35°C and a maximum of 16 mol% at 45°C.

This behaviour might be related to the increased mobility of the carbon chains constituting the core of the SMALPs and lateral expansion with consequently increase of the volume available for the copolymer penetration.

5.2.2 Analysis of SMALPs Assembled with the 6 kDa RAFT Copolymer

Samples prepared with the use of the 6 kDa RAFT copolymer were also analysed via DLS and SANS to investigate their behaviour under different temperatures. As previously reported in Chapter 3, the 6 kDa RAFT copolymer in solution showed to possess unique properties in terms of stability when different important parameters (pH, temperature, salt concentration) were changed. This behaviour was proved to have an impact also on the stability of the SMALPs assembled showing very stable structures in terms of dimensions in all the analyses performed.

DLS experiment was done on a non gel-filtrated solution of SMALPs prepared with the 6 kDa RAFT copolymer and deuterated DMPC in hydrogenated phosphate buffer solution. Solutions were all filtered to avoid contamination from dust particles. Temperature was scanned from 15 °C up to 45 °C leaving the sample to equilibrate for 20 min at each temperature. 7 runs were performed for 11 repeats on the same sample for each temperature. Data were then imported into Igor pro software and fitted to a log normal distribution function to obtain the value of the mean radius of SMALPs. A graph reporting the sample at different temperature is showed in Figure 5.3, results are reported in Table 5.5. Samples showed a constant hydrodynamic diameter value around 15 nm ± 1 nm.

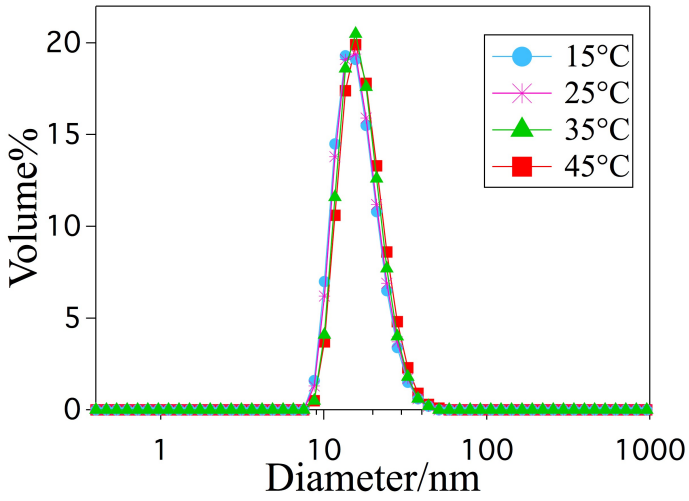

Figure 5.3. DLS experimental data of SMALPs assembled with 6 kDa RAFT copolymer and deuterated DMPC in hydrogenated phosphate buffer solution at four different temperatures.

In order to understand the contributions of the lipids and the copolymer on the SMALPs structure formation a SANS analysis was also performed. Samples were prepared following the procedure reported in Chapter 4 Section 4.2 SMALPs were prepared as follow:

- 6 kDa RAFT + deuterated DMPC in hydrogenated phosphate buffer;
- 6 kDa RAFT + hydrogenated DMPC in deuterated phosphate buffer;

Samples were analysed at the LOQ instrument located in ISIS (Oxford) at 15 °C, 25 °C and 45 °C. Temperature was controlled with the use of two water baths. Figures 5.4 A and B report an example of the behaviour of SMALPs at the three temperatures in two different contrasts. Data were reduced and corrected following the standard protocol and analysed using the SANS Analysis package within Igor pro [11]. Data taken at different solvent contrasts were simultaneously fitted to the same model of a charged core shell cylinder introduced in Chapter 4. Some of the parameter values were calculated or set from literature and are reported in Table 5.1.

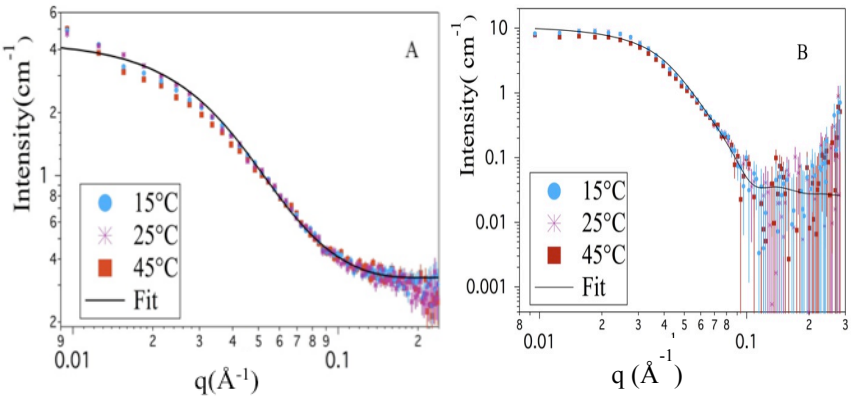

Figure 5.4. A) SANS patterns collected on LOQ instrument of SMALPs constituted of 6 kDa RAFT copolymer and hydrogenated DMPC in 100%D_2O analysed in a range of temperature from 15 °C to 45 °C, B) SANS pattern collected on the same instrument of SMALPs made of deuterated 6 kDa RAFT copolymer and hydrogenated DMPC in 0%D_2O phosphate buffer.

Temperature	*DLS*[a] *Diameter (nm)*	*SANS Diameter (Core + Shell) (nm)*
15 °C	15.23 ± 0.07	13.5 ± 0.2
25 °C	15.45 ± 0.07	13.5 ±0.2
35 °C	16.05 ± 0.07	—
45 °C	16.43 ± 0.07	13.5 ±0.2

Table 5.5. Summary of diameter values obtained with the different analysis performed on SMALPs assembled with 6 kDa RAFT copolymer analysed at different temperatures. (a) Values refer to diameters calculated based on hydrodynamic radius obtained by fitting the experimental data to a lognormal distribution function, ± are standard deviations.

Experimental data from both DLS and SANS analysis showed a SMALPs diameter very stable over the range of temperature studied with only a slight increase of 1 nm in the DLS data. Overall SMALPs assembled with either 6 kDa RAFT and 7 kDa SMA-2000P copolymers showed to be stable on a temperature range from 15 °C to 45 °C. This result well agree with the general behaviour reported for protein stabilised nanodiscs [16] which showed to be stable over a range of temperature from 4 °C to 37 °C. Also the Lipodisq® technology [17] has also been proved to be stable in the range of temperature between 20 °C and 30°C. Compared to the Lipodisqs® that were reported to

considerably alter the DMPC phase transition temperature SMALPs demonstrated a better reproducibility of the natural membrane environment.

5.3 Investigation of SMALPs Stability at Different pHs

SMALPs are assembled through the interaction between the SMA copolymer chains and the lipids in solution. As discussed in Chapter 3 one of the main properties of the copolymers used in this study is their sensitivity to the pH. Indeed, SMALPs have been shown [18, 19] to disassemble at acidic pH and reassemble at pH around 8. This feature is particularly interesting since it allows the controlled dissociation of the SMALPs with the possibility to regenerate the protein containing lamellar membranes, which can then be used for a number of other studies [18]. The present work focuses on the analysis of SMALPs stability at pH higher than 8.

Samples were prepared as reported in Chapter 4 with hydrogenated DMPC assembled with 7 kDa SMA-2000P in deuterated buffer solution at two different pHs. In order to reach the desired pH, samples collected from the gel filtration process and re-concentrated were dialysed against the chosen buffer following the procedure reported in Chapter 4 Section 4.2.

Figure 5.5 reports the fitting of experimental data collected on SANS instrument LOQ. Fitting was done with the core-shell cylinder model introduced in Chapter 4 with IGOR software and results are reported in Table 5.6.

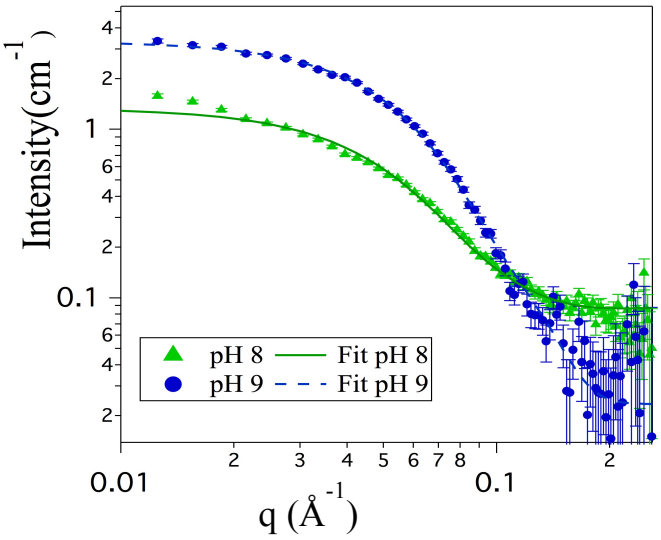

Figure 5.5. SANS patterns of SMALPs composed of 7 kDa SMA-2000P and hydrogenated DMPC in Deuterated phosphate buffer solution analysed at respectively pH 8 and pH 9.

Fitting Parameters	*pH 8*	*pH 9*
Volume fraction	0.003 ± 0.001	0.01 ± 0.001
Core radius (nm)	3.6 ± 0.02	3.6± 0.02
Radial polydispersity (σ)	0.19 ± 0.05	0.19 ± 0.05
Core length (nm)	2.6 ± 0.02	2.6 ± 0.02
Radial shell thickness (nm)	0.9 ± 0.02	0.9 ± 0.02
Face shell thickness (nm)	0.8± 0.02	0.9± 0.02
SLD core (cm^{-2})	-0.12×10^{10} $\pm0.02\times10^{10}$	-0.13×10^{10} $\pm0.02\times10^{10}$
mol% solvent in rim	0.42 ± 0.03	0.83 ± 0.03
Background (cm^{-1})	0.09 ±0.05	0.08 ± 0.05

Table 5.6. Results of fitting of SANS experimental data collected on samples prepared with two different buffer pHs

Comparison of the scattering patterns of samples in the two solutions pHs showed an increase in the intensity as the pH was incremented to the value of pH 9.Also a significant increment was detected in the volume fraction value at pH 9. A higher pH value seemed also to lead to an increment of the solvent penetration in the polymeric belt; this might be due to the increased solubility of

the copolymer whereas other parameters shows not to be affected by the increasing in the pH value.

5.4 Investigation of SMALPs Stability at Different Salt Concentrations

Biological membranes are surrounded by an aqueous solution containing a number of ion species such as Na^+; Cl^-; K^+; Mg^{2+} or Ca^{2+}. The concentration of these ions can be quite different in the inner space or on the outside of the cell. Lipid bilayer act as osmotic barrier between the inner cell and the surrounding, which interaction is subject of numerous researches [20-22]. Indeed ion binding affects the stability and structures of the lipid bilayers but also the way proteins binds and interacts [22, 23].

Samples analysed were prepared following the procedure reported in Chapter 4 with hydrogenated DMPC assembled with 7 kDa SMA-2000P in deuterated buffer solution with two different salt concentrations (200 mM and 50 mM of NaCl). Samples collected from the gel filtration process and re-concentrated were dialysed against the chosen buffer as reported in Chapter 4 Section 4.2.

SMALPs were analysed at the LOQ instrument located in ISIS (Oxford) at the temperature of 25 °C. Figure 5.6 reports the SANS path of SMALPs analysed at two different salt concentrations, both samples are in deuterated phosphate buffer. Data were reduced and corrected following the standard protocol and analysed using the SANS Analysis package within Igor pro [11]. Data taken at different solvent contrasts were simultaneously fitted to the same model of a charged core shell cylinder introduced in Chapter 4. Some of the parameter values were calculated or set from literature and are reported in Table 5.7. Results of fitting data from 50 mM concentration are reported in Table 5.8. Fitting of both set of data with different contrasts showed very closed values as suggested from the graph reported in Figure 5.6 where data of SMALPs in 50 mM NaCl and in 200 mM NaCl buffer partially overlap.

Parameter	*SANS Value*	
Solvents SLD	*Deuterated Buffer*	*Hydrogenated Buffer*
	6.29×10^{10} cm^{-2}	-0.57×10^{10} cm^{-2}
Head groups SLD[12]	1.86×10^{10} cm^{-2}	
Copolymer SLD	1.81×10^{10} cm^{-2}	
Temperature	25 °C	
Salt Concentration	0.25 M; 0.1 M	
Dielectric Constant	78	

Table 5.7. Table summarising values calculated (except for SLD of the face which has ben set from literature) and held during fitting of SAXS and SANS data.

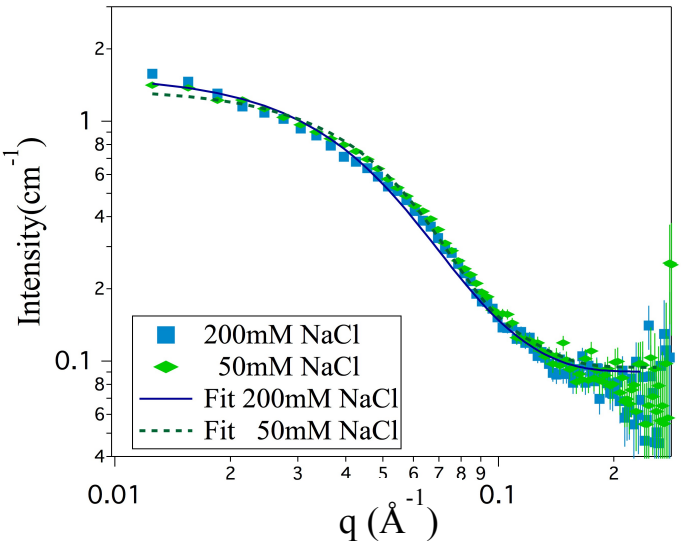

Figure 5.6. SANS pattern of SMALPs assembled with use of 7 kDa SMA-2000P, h-DMPC in deuterated buffers prepared with two different salt concentrations fitted to a core-shell model.

Fitting of the experimental data revealed (example in Figure 5.7) a swelling effect of the increased salt concentration. Indeed whereas diameter and thickness of the SMALPs showed to be stable the polymeric belt revealed an increased thickness.

At the same time a decrease of mol% of copolymer in the core and mol% of solvent in the polymer were detected. These results are in good agreement with what revealed the analysis of copolymers in buffer solutions at different concentrations. Main parameters values from global fitting of SMALPs prepared in hydrogenated and deuterated buffers at 50 mM NaCl concentration and fitting of SMALPs prepared in two different salt concentration in hydrogenated phosphate buffers are reported in Table 5.8.

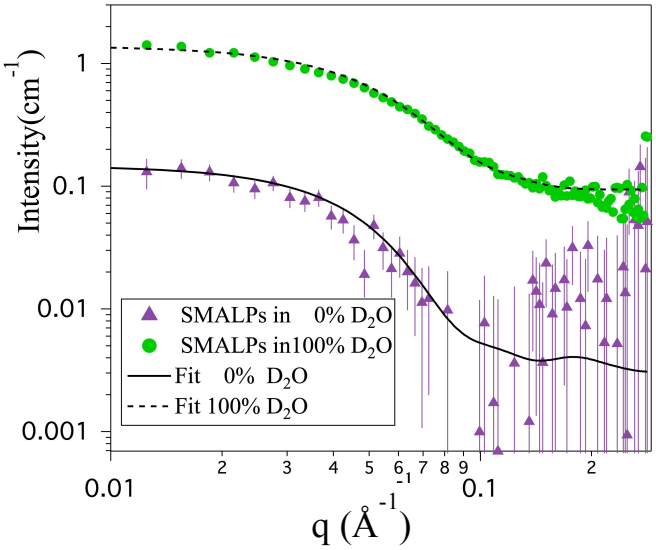

Figure 5.7. SANS patterns of SMALPs composed of 7kDa SMA-2000P and h-DMPC assembled in phosphate buffer with concentration of NaCl of 50 mM in either 100% D_2O or 0% D_2O buffer. Data are fitted simultaneously to a core-shell cylinder model previously introduced.

NaCl Concentration	*SMALPs Core length (nm)*	*SMALPs Diameter (nm)*	*SMALPs Radial Shell Thickness (nm)*	*Copolymer mol% In the core*	*SMALPs mol% Solvent in the rim*
0.25 mM	4.1± 0.05	8.5 ± 0.1	0.6 ± 0.02	7%	0.35 ± 0.05
0.1 mM	4.1± 0.05	8.8 ± 0.1	0.8 ± 0.02	5%	0.29 ± 0.05

Table 5.8. Summary of principal parameters values obtained from fitting of SANS data of SMALPs prepared in buffers with two different NaCl concentrations.

5.5 Effect of Lipid Composition on SMALPs Formation and Stability

5.5.1 Impact of the Tail Length of Phospholipids in Use

The presence of lipids with different chains properties (length or degree of saturation) has shown to be closely related to some biological processes such as the activation of some membrane proteins [24].

One of the main applications of the SMALPs technology is to be used as a model membrane to allow the analysis of the membrane proteins in an environment as close as possible to the natural cell membrane. In order to do that, it is of great advantage to be able to assemble the SMALPs with the use of different phospholipids. Therefore a systematic analysis on the impact of the lipids in use was started in this study with the use of one of the most common phospholipid in the cell membrane the so-called DPPC (1-2 dipalmitoyl-sn-glycero-3-phopshodicholine).

- Materials

Samples were prepared following the procedure reported in Chapter 4 Section 4.2. Copolymer in use was the 7 kDa SMA-2000P. In order to probe the impact on the SMALP structure and assembly of phospholipids with a different tail length samples were prepared with an increased amount of 1-2 dipalmitoyl-sn-glycero-3-phopshodicholine (DPPC) which structure is reported in Figure 5.8 and Figure 5.9 DMPC (structure can be found in Figure 4.2 in Chapter 4) Lipids were purchased either from Sigma Aldrich in case of the hydrogenated form (purity ≥ 99%) or from Avanti Polar Lipids, for the deuterated version (purity ≥ 99%), all were used as received.

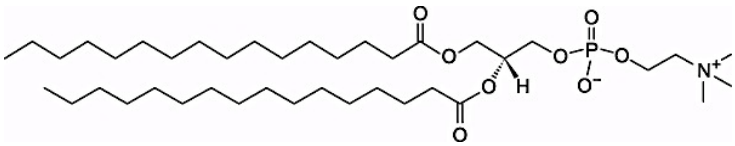

Figure 5.8. Structure of 1 2-dipalmitoyl-sn-glycero-3-phosphocholine (DPPC). M_w 734.039 g/mol.

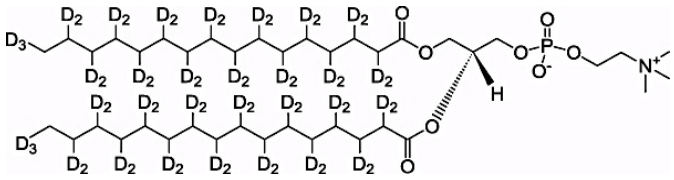

Figure 5.9. Structure of 1 2-dipalmitoyl-d62-sn-glycero-3-phosphocholine (deuterated DPPC). M_w 800.446 g/mol.

Samples were prepared with different DMPC/DPPC proportions and mixing deuterated and hydrogenated lipids with different buffer contrasts in order to better explore the core composition. Data are reported as the wt% of each lipid in the disc. Although preparation of nanodiscs with DPPC contents of 100wt% DPPC was attempted, the highest concentration where stable nanodiscs were observed was 70wt% DPPC.

Analyses of the gel filtration spectra provided a preliminary qualitative investigation of the samples prepared. The graph reported in Figure 5.10 suggests a decrease of interaction between the SMA copolymer and the phospholipids proportionally to the increase of DPPC percentage into the core. Simultaneously, an increase in peak areas relative to larger and smaller structures present in solution is detected.

From the integration of the peak areas the approximate percentage of the copolymer participating to the SMALPs formation was calculated, values are reported in Table 5.9.

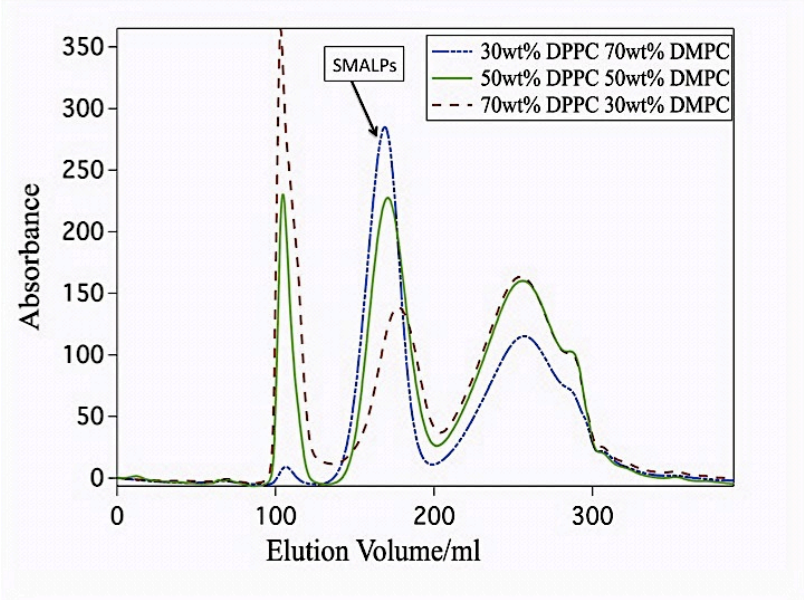

Figure 5.10. Gel filtration paths of SMALPs prepared with increasing percentage of DMPC/DPPC phospholipids.

Sample	*30wt% DPPC + 70wt% DMPC*	*50wt% DPPC+ 50wt% DMPC*	*70wt% DPPC+ 30wt% DMPC*
Copolymer Percentage in SMALPs	*49%*	*31%*	*23%*

Table 5.9. Values of percentage of SMA copolymer contributing to the assembly of SMALP structures calculated from integration of area below peaks identified in the gel filtration graph of three different sample compositions.

This initial analysis suggested that the use of different chain lengths has an impact on the driving forces involved in the assembly process. Formation and stability of SMALPs can be seen as the result of the equilibrium between different forces in act: the hydrophobic attraction forces between the acyl carbon chains that make packing favourable, in addition to the electrostatic repulsion of the heads which makes packing unfavourable, the hydrophobic interaction between the styrene components of the copolymer with the

phospholipid chains, finally the hydrophilic interaction of the hydrophilic components of the copolymer with the surrounding water.

From the analysis of these data an important factor influencing the SMALPs aggregation process is suggested to be the temperature at which sample preparation takes place. Indeed all samples have been prepared at room temperature (approximately 23 °C), which is very close to the main transition temperature of DMPC but far from the transition temperature of DPPC (approximately 41 °C). This causes the DPPC to be in the gel phase with a chain tilt angle of about 32°. This new chain conformation might leave less space for the copolymer penetration into the core. SMA molecules that are not interacting with the hydrophobic tails might tend to interact among each other forming copolymers aggregates instead.

Protein-stabilised nanodiscs assembled with DPPC have been reported instead to be prepared after incubation of DPPC at 38 °C for 4 to 18 hours [25, 26] since the initial state of the lipids-detergent mixture has been found to determine the self- assembly process of nanodiscs [25]. This might also be the reason why the 100wt% DPPC composition did not assemble into SMALPs prepared at 23 °C whereas protein stabilised nanodiscs were able to form after incubation of DPPC at suitable temperature.

DLS analysis was successively performed on all the samples with different DMPC/DPPC ratio. Samples were analysed at 25°C following the same procedure reported in Chapter 4.3.1. A graph of the obtained sizes distribution is reported in Figure 5 11.

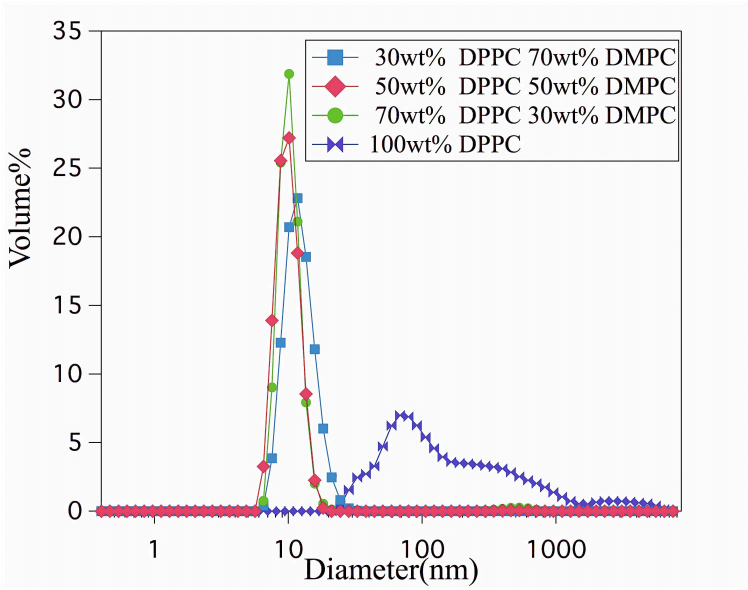

Figure 5.11. DLS path of mixed DPPC/DMPC solutions assembled with 7 kDa SMA-2000P copolymer showing the hydrodynamic diameter of assembled structures at different DPPC/DMPC ratio.

Analysis of gel-filtered solutions via DLS experiments confirmed the different aggregation processes suggested by the observation of gel filtration data. Fitting of experimental curves to a lognormal distribution showed an increase in hydrodynamic diameter as the amount of DPPC increased to the 70wt%DPPC composition, not revealed by later SANS analysis (results are reported in Table 5.10). This might to be due to instability of the samples causing aggregations among the SMALPs. Indeed polydispersity of this particular sample was found to be higher than those at the 30wt%DPPC and 50wt%DPPC compositions. Sample composed of 100wt%DPPC were not suitable for the formation of SMALPs. Indeed DLS analysis confirmed the results suggested by the analysis of the gel filtration chromatography spectrum revealing a very polydisperse sample with a broad distribution of particle sizes of about 100 nm in diameter.

Sample	*30wt% DPPC + 70wt% DMPC*	*50wt% DPPC+ 50wt% DMPC*	*70wt% DPPC+ 30wt% DMPC*	*100wt% DPPC*
Hydrodynamic Diameter	*11.7 ± 0.09*	*9.7± 0.02*	*9.9± 0.01*	_____

Table 5.10. Summary of hydrodynamic diameter values obtained fitting of DLS experimental data to a lognormal function.

Structural analyses were conducted via SANS experiments performed on the LOQ instrument. Sample compositions and fitting of the data are summed up in Table 5.11. In Figure 5.12 are shown examples of SANS data from samples prepared with different DPPC percentages. Data were fitted to the model previously introduced for SMALPs SANS/SAXS analysis (Chapter 2 Section 2.8.3). The SLD of the core was theoretically calculated according to the different percentage of DPPC and assuming the SLD for DPPC and DMPC tails to be equal to the values reported in Table 5.12. However, parameters were then fitted to take into account the copolymer penetration into the core. Also other parameters were calculated and held during the fitting and values are reported in Table 5.12. All the other parameters were fitted and results of principal parameters are reported in Table 5.13.

Sample	*SMALPs Lipids Composition*	*Buffer Contrast*	*Fitting Analysis*
A	1) 30wt% d-DPPC+ 70wt% d-DMPC 2) 30wt% h-DPPC+ 70wt% d-DMPC	1) 32% D_2O 1-2) 0% D_2O	Global Fitting of two buffer contrasts and two lipid contrasts
B	1) 50wt% d-DPPC+ 50wt% d-DMPC 2) 50wt% h-DPPC+ 50wt% d-DMPC	1) 32% D_2O 1-2) 0% D_2O	Global Fitting of two buffer contrasts and two lipid contrasts
C	1) 70wt% d-DPPC+ 30wt% d-DMPC 2) 70wt% h-DPPC+ 30wt% d-DMPC	1-2) 0% D_2O	Global Fitting of two lipid contrasts

Table 5.11. Summary of the different SMALP lipid compositions and contrasts used for SANS analysis performed on LOQ instrument.

Parameter	*SANS Value*	
Solvents SLD	*Deuterated Buffer*	*Hydrogenated Buffer*
	6.29×10^{10} cm^{-2}	-0.57×10^{10} cm^{-2}
**DMPC tails SLD*	h-DMPC	d-DMPC[27]
	_____	7.2×10^{10} cm^{-2}
**DPPC tails SLD*	h-DPPC [28]	d-DPPC [29]
	-0.39×10^{10} cm^{-2}	7.45×10^{10} cm^{-2}
Head Groups SLD[28]	1.86×10^{10} cm^{-2}	
Copolymer SLD	1.8×10^{10} cm^{-2}	
Temperature	25 °C	
Salt Concentration	0.25 M	
Dielectric Constant	78	

Table 5.12. Summary of the various parameters calculated or reported from literature used in the data fitting.

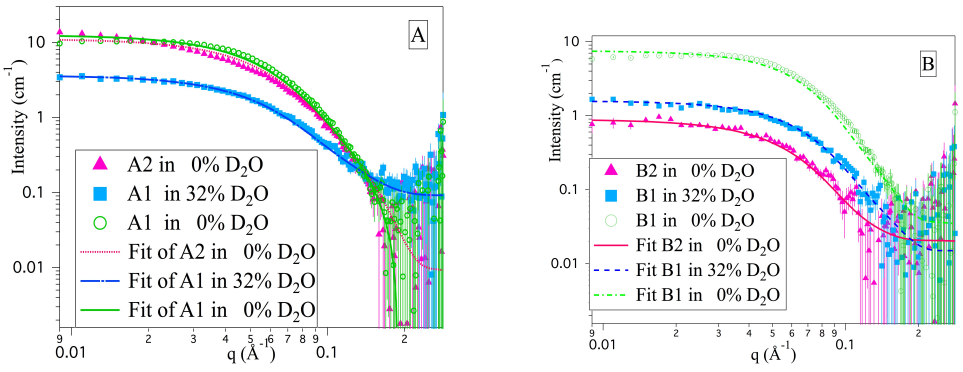

*Figure 5.12. Figure A) Global fitting of SANS data from SMALPs of 30wt% DPPC and 70wt% DMPC prepared in different contrasts. **A1** (30wt% d-DPPC-70wt% d-DMPC) in 0% D_2O and 32% D_2O. **A2** (30wt% h-DPPC-70wt% d-DMPC) in 0% D_2O B) Global fitting of SANS data from SMALPs of 50wt% DPPC. Figure B) 50wt%DMPC prepared in different contrasts, **B1** (50wt% d-DPPC-50wt% d-DMPC) in 0% D_2O and 32% D_2O. **B2** (50wt% h-DPPC-50wt% d-DMPC) in 0% D_2O.*

SMALPs Lipid Compositions	*SMALPs Thickness (nm)*	*SMALPs Diameter (nm)*	*SMALPs Radial Shell Thickness (nm)*	*Copolymer mol% in the core*	*SMALPs mol% Solvent in the rim*
30wt% d-DPPC+ 70wt% d-DMPC / *30wt% h-DPPC+ 70wt% d-DMPC*	4.1 ± 0.2	8.3± 0.2	± 0.02	27%	0.48 ± 0.05
50wt% d-DPPC+ 50wt% d-DMPC / *50wt% h-DPPC+ 50wt% d-DMPC*	4.4 ± 0.2	7.9± 0.2	0.84± 002	15%	0.43 ± 0.05
70wt% d-DPPC+ 30wt% d-DMPC / *70wt% h-DPPC+ 30wt% d-DMPC*	4.5 ± 0.2	8.6± 0.2	0.83± 0.02	13%	0.5± 0.05

Table 5.13. Summary of results of fitting experimental SANS data to a model of a capped core-shell cylinder with a polydisperse core radius.

Assuming that the area of each DMPC molecule [30] within the bilayer to be 0.596 nm^2 and the area of each DPPC molecule within the bilayer at 20 °C to be 0.479 nm^2 [30], then assuming that each sample is composed of the percentage indicated for each lipid components it is possible to calculate the number of DMPC and DPPC molecules contained in each bilayer leaflet, results are summarised in Table 5.14.

SMALPs Lipids Composition	*Overall Bilayer Size (nm^2)*		**DMPC molecules in each bilayer leaflet*	**DPPC molecules in each bilayer leaflet*
	Min	*Max*		
30wt% DPPC+ 70wt% DMPC	38	48	90	60
50wt% DPPC+ 50wt% DMPC	30	38	50	80
70wt% DPPC+ 30wt% DMPC	36	45	40	130

*Table 5.14. Table summarising the overall bilayer size and the average number of DMPC and DPPC molecules in each different sample compositions. * Indicates average values.*

Comparing the values reported in Table 5.14 to the value reported in Chapter 4 for a sample composed of only DMPC and assembled with the same SMA (approximately 70 DMPC molecules in the leaflet bilayer for SMALPs with an overall bilayer area between 40 nm^2 and 50 nm^2) an increase in the total number of phospholipid molecules in the core was noticed. This is probably due to the smaller area per molecule occupied by the DPPC phospholipids compared to the DMPC dimensions. The same results were also found for protein-stabilised nanodiscs [26]. Although DPPC is a larger molecule, the fact that it is in the solid state at 25 °C (where these measurements were made) results in a smaller molecular area than that of DMPC at the same temperature. Indeed, DMPC is above its chain melting transition, meaning the disordered tail regions occupy more space in the bilayer.

The increases in the thickness of the discs associated with the increased amount of DPPC is in accordance with results found in similar analyses performed on the protein stabilised nanodiscs [26] and is within the range of values found for DPPC lipid bilayers [31]. The increase in the thickness is within the order expected of 0.4-0.5 nm due to the difference in chain length between DMPC and DPPC. The values reported in Figure 5.13, showing the trend of core length as function of DPPC content, refer only to the SMALPs core associated with the chain length, i.e. the phospholipid heads and hydration water are not included in the dimension reported. The thickness of the face layer (8 ± 0.2 nm),

representing the region occupied by the phospholipid heads, was also found to be in good agreement with literature reported values [28, 30].

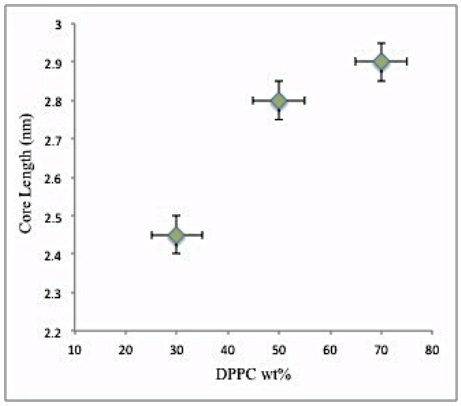

Figure 5.13. Plot of SMALPs core length as a function of DPPC weight percentage used in SMALPs preparation. Dimension reported refers only to the tails of the phospholipids corresponding to the core dimension in the model in use.

5.5.2 Effect of Using a Mixture of Charged and Uncharged Lipids

Work presented so far involved the use of uncharged zwitterionic phospholipids such as DMPC and DPPC. However it was demonstrated that among the numerous lipids composing the cell membrane [32], an important role is played by anionic lipids such as DMPG, which carry a net negative charge [33]. The presence of phosphatidylglycerol phospholipids varies considerably depending on the particular membrane. For instance, a very high percentage is found in bacterial membranes [32] while, even if such lipids are not that abundant in eukaryotic membrane, their presence was found in mitochondria and blood cells [34].

Among the phosphatidylglycerol (PG) class the 1,2 dimyristoyl-d54-sn-glycero-3-phosphoglycerol (sodium salt) DMPG molecule was selected. This molecule possesses the same chain length as the DMPC molecule and differs only in the

head group structure. It is also characterised by a very similar main transition temperature (23 °C) at the particular salt concentration and pH conditions analysed here [35]. This allowed the impact of the charge to be evaluated by keeping constant all other parameters. SMALPs were therefore prepared from a mixture of DMPC and DMPG phospholipids following the sample preparation procedure reported in Chapter 4.2.

The SMALPs assembled with different proportion of DMPC and DMPG in a phosphate buffer solution with pH 8 and NaCl concentration of 200 mM were analysed via DLS and SANS experiments in order to be able to investigate the impact of the charge on the assembly process and stability of the system.

- Materials

Samples were prepared following the procedure reported in Chapter 4 Section 4.2. The copolymer used was the 7 kDa SMA-2000P. In order to probe the impact on the SMALP structure and assembly of phospholipids with charged heads, samples were prepared with an increasing proportion of 1,2-dimyristoyl-*sn*-glycero-3-phosphoglycerol (sodium salt) (DMPG) the structure of which is reported in Figure 5.14 and the tail deuterated version in Figure 5.15, DMPC (structure in Figure 4.1 in Chapter 4). Lipids were purchased either from Sigma Aldrich in case of the hydrogenated form (purity ≥ 99%) or from Avanti Polar Lipids, for the deuterated version (purity ≥ 99%) all used as received.

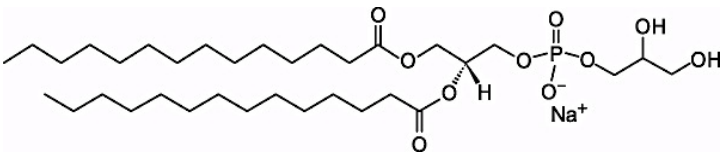

Figure 5.14. Structure of 1,2 dimyristoyl-sn-glycero-3-phosphoglycerol (sodium salt) (DMPG). M_w= 688.85.

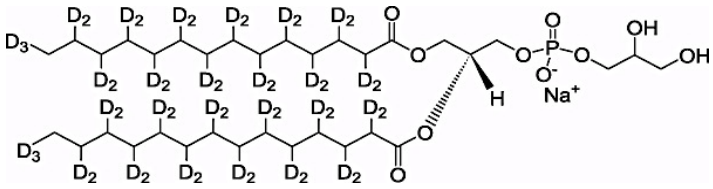

Figure 5.15. Structure of 1,2 dimyristoyl-d54-sn-glycero-3-phosphoglycerol (sodium salt) (d-DMPG); M_w= 743.178.

Analysis of the gel filtration spectra of SMALPs assembled with different DMPC/DMPG percentages (Figure 5.16) revealed a significant decreasing of cooperation between lipids and SMA. Indeed integration of the area below each peaks showed that only 14% of the total copolymer in solution is taking part to the SMALPs formation. Results of integrations performed are summarised in Table 5.15.

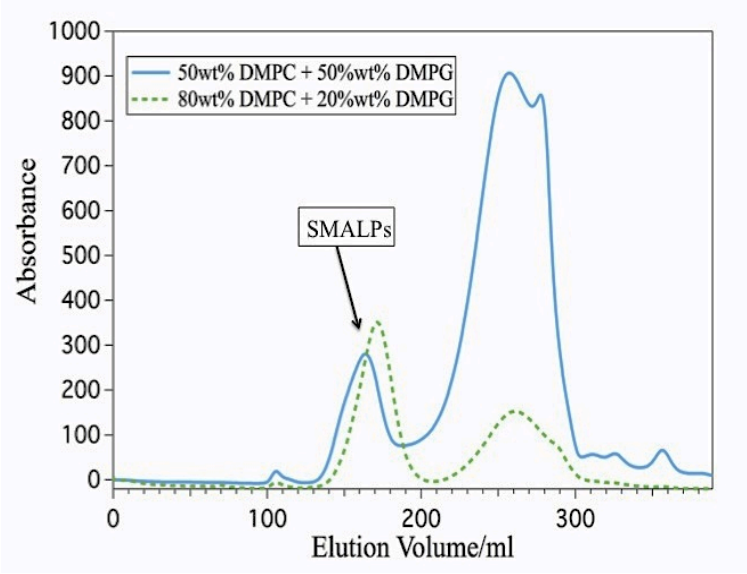

Figure 5.16. Gel filtration paths of SMALPs prepared with increasing percentage of DMPC/DMPG phospholipids.

Sample	*20wt% DMPG + 80wt% DMPC*	*50wt% DMPG+ 50wt% DMPC*
Copolymer Percentage in SMALPs	*56%*	*14%*

Table 5.15. Values of percentage of SMA copolymer contributing to the assembly of SMALP structures calculated from integration of area below peaks identified in the gel filtration graph of two different samples composition.

DLS analysis was successively performed on all the samples with different DMPC/DMPG ratio. Samples were analysed at 25 °C following the same procedure reported in Chapter 4.3.1. A graph of the obtained sizes distribution is reported in Figure 5 17.

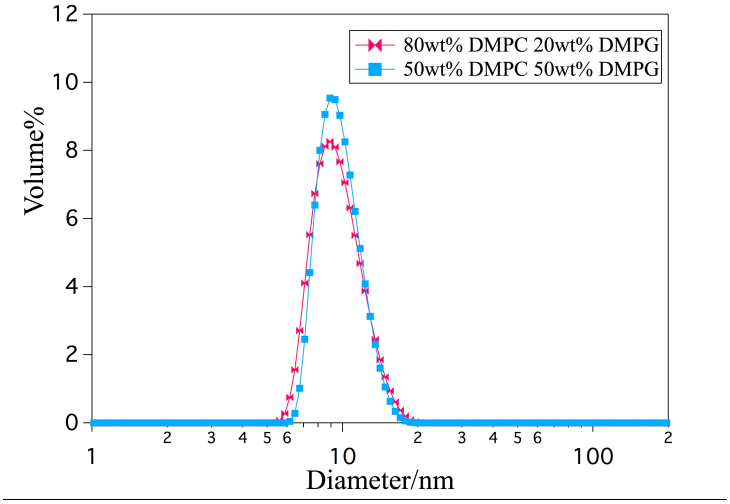

Figure 5.17. DLS patterns of SMALPs in phosphate buffer solution composed of a mixture of DMPC and DMPG phospholipids.

Structural analyses were conducted via SANS experiments performed on the D11 instrument at the ILL research centre. Sample compositions and fitting of the data are summed up in Table 5.14. Data were fitted to the model previously

introduced for SMALPs SANS/SAXS analysis (Chapter 2 Section 2.8.3). However the code was modified in order to fit the SLD of the faces giving a value, which also includes possible contributes from the solvent molecules.
Fitting of the experimental data at different contrasts are shown in Figure 5.18.
The SLD of the core was calculated according to the different percentage of DMPG and assuming the SLD for DMPC and DMPG to be equal to the values reported in AppendixA4 however, parameters were fitted to take into account the copolymer penetration into the core. Also other parameters were calculated and held during the fitting and values are reported in Table 5.17. All the other parameters were fitted and results of principal parameters are reported in Table 5.18. A complete table with all the calculated fitting values for all the contrasts in use is reported in Appendix A4.

Sample	*SMALPs Lipids Composition*	*Buffer Contrast*	*Fitting Analysis*
A	1) 80wt% d-DMPC+ 20wt% d-DMPG 2) 80wt% h-DMPC+ 20wt% d-DMPG	1-2) 100% D_2O 1) 32% D_2O 1) 0% D_2O	Global Fitting of three buffer contrasts and two lipids contrasts
B	50wt% d-DMPC+ 50wt% d-DMPG 50wt% h-DMPC+ 50wt% d-DMPG	0% D_2O	Global Fitting of one buffer contrasts and two lipids contrasts

Table 5.16. Summary of the different SMALP lipid compositions and contrasts used for SANS analysis performed on LOQ instrument.

Parameter	*SANS SLD Value*	
Solvents SLD	*Deuterated Buffer* 6.29×10^{10} cm^{-2}	*Hydrogenated Buffer* -5.67×10^{11} cm^{-2}
DMPC, DMPG tails SLD [28]	h-DMPG/h-DMPC -0.42×10^{10} cm^{-2}	d-DMPG/d-DMPC 7.2×10^{10} cm^{-2}
Head Groups SLDs [28]	DMPC 1.86×10^{10} cm^{-2}	DMPG 3.2×10^{10} cm^{-2}

Table 5.17. Summary of the various parameters calculated or reported from literature used in the data fitting.

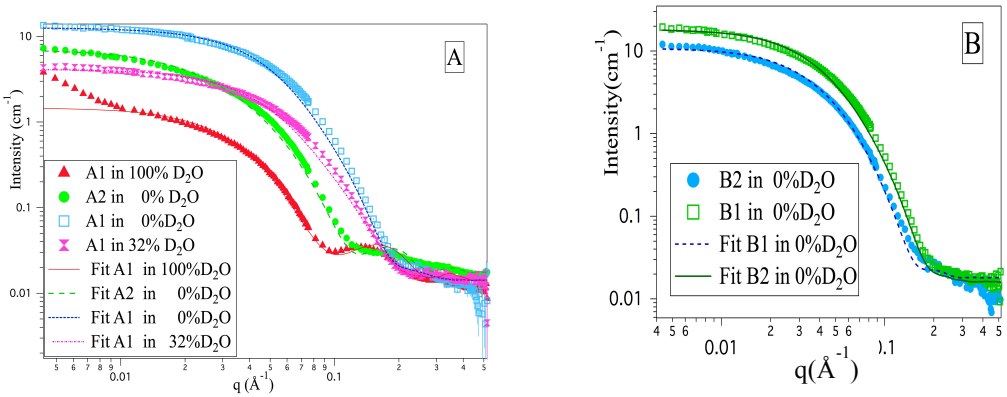

Figure 5.18. SANS patterns of SMALPs in three different buffer contrasts and two lipid compositions.

The results obtained from fitting of SANS scattering data (summarised in Table 5.18) showed that the assembled SMALPs possess a phospholipid core characterised by an average core diameter of 7.4 ± 0.2 nm indicating an overall bilayer size between 38 nm^2 and 48 nm^2 for samples prepared with 80 wt% DMPC and 20 wt% DMPG. Increasing the amount of DMPG to a 50wt% of the

total composition led to the formation of slightly larger SMALPs with an overall core surface area between 45 nm^2 and 64 nm^2.

This could be related to the increased repulsion forces between phospholipids head groups when negatively charged lipids are incorporated. Indeed, lipid areas for DMPG molecules were found in previous studies of molecular structures to be larger than the DMPC molecules, due to the repulsive electrostatic interaction among the charged head groups [36].

SMALPs Lipids Composition	*SMALPs Thickness (nm)*	*SMALPs Total Diameter (nm)*	*SMALPs Face Shell Thickness (nm)*	*SMALPs Radial Shell Thickness (nm)*	*SMA mol% in the core*	*Solvent mol% in the rim*
80wt% d-DMPC+ 20wt% d-DMPG	4.3 ± 0.1	9.4 ± 0.1	0.8 ± 0.05	0.9 ± 0.05	18%	0.48 ± 0.05
80wt% d-DMPC+ 20wt% h-DMPG						
50wt% dDMPC+ 50wt% d-DMPG	4.6 ± 0.1	9.5 ± 0.1	1.0 ± 0.05	0.97 ± 0.05	8%	0.33 ± 0.05
50wt% d-DMPC+ 50wt% h-DMPG						

Table 5.18. Summary of main structural parameters found from fitting of SANS data of SMALPs assembled with different DMPC/DMPG proportion.

The total SMALPs thickness showed an increase with the increased DMPG percentage in the sample, however the actual core constituted of the phospholipid tails was found to be constant at a value of 2.6 ± 0.1 nm whereas the increase in the total value is due to the thickness of the faces of the discs constituted by phospholipids heads. This apparent increase might relate to the different arrangement of the polymer around the SMALPs. Indeed it was also

found a consistent decrease of the copolymer penetration into the core at the highest DMPG percentage.

Overall SMALPs composed of mixtures of DMPC and DMPG seemed to possess a thicker copolymer belt region wrapped around the core and correspondingly a much lower copolymer penetration within the core. This was particularly observed in the case of SMALPs composed of 50wt% d-DMPC and 50wt% d-DMPG, where a copolymer mol% into the core of about 8.6% was found compared to the 12mol% found for SMALPs composed of only DMPC. This new arrangement of the polymeric belt might be related to the potential interaction of the hydrophilic part of the copolymer with the negatively charged headgroups on the faces of the discs.

Moreover assuming that the area of each DMPC molecule [30] within the bilayer to be 0.596 nm^2 and the area of each DMPG molecule [37] within the bilayer at 27 °C to be 0.62 nm^2 then assuming that each sample is composed of the indicated lipid composition it is possible to calculate the number of DMPC and DMPG molecules contained in each bilayer. The results are summarised in Table 5.19.

SMALP Lipid Composition	*Overall Bilayer Size (nm^2)*		*DMPC molecules in each bilayer leaflet*	*DPPC molecules in each bilayer leaflet*
	Min	*Max*		
80wt% DMPC+ 20wt% DMPG	38	48	58	14
50wt% DMPC+ 50wt% DMPG	45	64	46	44

Table 5.19. Summary the overall bilayer size and the average number of DMPC and DPPC molecules for different sample compositions.

Previous studies have shown that DMPG behaviour is strongly dependent on the solution pH and salt concentration [35, 38]. Therefore interesting future work could be analysing this system changing those parameters.

5.6 Conclusions

The present chapter covers quite a broad structural investigation on the SMALPs. It can be divided into two fundamental sections. In the first section investigation was carried out on the stability and structural changes in SMALPs when changes were made to important physical chemical properties of the solutions. Results suggested a good structural stability of SMALPs at a temperature range between 15 °C and 45 °C.

Measurements at different pH and salt concentrations also revealed that SMALP samples prepared using DMPC under standard conditions can then be dialysed against the desired pH or salt concentration buffer solution with no loss of structural stability nor change in the dimensions. However it has been found that increasing the pH of the phosphate buffer results in an increase of the solvent penetration into the copolymer belt region. This behaviour might be related to an increased solubility of the copolymer, which consequently causes a rearrangement of the copolymer around the disc.

The second part of the chapter was dedicated to probing the impact of the lipid composition to the formation and stability of SMALPs. Work aimed to analyse the effect of the chain length revealed the successfully assembly of SMALPs with the use of mixture of DMPC and DPPC but not pure DPPC.
SANS data analysis revealed an increase in the length of the core caused by an increased percentage of DPPC in solution that expands the structure dimension. This phenomenon is likely to be connected to the difference in the tail lengths and it is in agreement with previously published literature on protein-stabilised nanodiscs [26]. Although good results have been obtained with the analysis performed, further investigation could be done with DPPC/DMPC mixtures at a temperature above the main transition temperature of DPPC. Indeed it has been showed that the lipid phase in which the protein stabilised nanodiscs are

assembled has an impact on the formation and also stability in terms of size of the supports [39, 40].

SMALPs prepared with a mixture of DMPC and DMPG phospholipids were also analysed via SANS and DLS experiments with the aim to investigate the impact of the charged headgroups of DMPG on both the assembly process and the stability of the SMALPs. Different percentages of DMPC/DMPG molecules were assembled into the SMALPs, showing an increased diameter likely to be connected to the increase in area per molecule of the DMPG phospholipids. SMALPs assembled with this new lipid composition offer a medium for investigation of the impact of the use of larger lipids area on the protein. Indeed it has been found that DMPG may play a role in regulating protein translocation [41] but also modulating bacterial membrane permeability [42] and facilitating protein folding [43].

5.7 References

1. Brown, D.A. and E. London, *Functions of lipid rafts in biological membranes.* Annu Rev Cell Dev Biol, 1998. **14**: p. 111-36.
2. Pike, L.J., *Lipid rafts: bringing order to chaos.* J. Lipid Reseach., 2003. **44**(4): p. 655-667.
3. Kraft, M.L., *Plasma membrane organization and function: moving past lipid rafts.* Molecular biology of the cell, 2013. **24**(18): p. 2765-8.
4. Simons, K. and D. Toomre, *Lipid rafts and signal transduction.* Nature reviews. Molecular cell biology, 2000. **1**(1): p. 31-9.
5. Kiselev, V.Y., et al., *Lateral dynamics of charged lipids and peripheral proteins in spatially heterogeneous membranes: comparison of continuous and Monte Carlo approaches.* J Chem Phys, 2011. **135**(15): p. 155103.
6. Capelluto, D.G.S. and SpringerLink (Online Service), *Lipid-mediated protein signaling*, in *Advances in experimental medicine and biology,*2013, Springer,: Dordrecht ; New York. p. 1 online resource.
7. Suzuki, K.G., *[Mechanisms for signal transduction in lipid rafts of cell plasma membranes].* Seikagaku. The Journal of Japanese Biochemical Society, 2013. **85**(1): p. 34-7.
8. Lee, A.G., *Lipid–protein interactions in biological membranes: a structural perspective.* Biochim. Biophys. Acta, Biomembr., 2003. **1612**(1): p. 1-40.
9. Killian, J.A., *Hydrophobic mismatch between proteins and lipids in membranes.* Biochim. Biophys. Acta, 1998. **1376**(3): p. 401-416.
10. Jiménez-Monreal, A.M., et al., *Influence of the Physical State of the Membrane on the Enzymatic Activity and Energy of Activation of Protein Kinase C α†.* Biochem., 1999. **38**(24): p. 7747-7754.
11. Kline, S.R., *Reduction and analysis of SANS and USANS data using IGOR Pro.* J Appl Crystallogr, 2006. **39**: p. 895-900.

12. Smith, M.B., et al., *Neutron reflectometry of supported hybrid bilayers with inserted peptide.* Soft matter, 2010. **6**(5): p. 862-865.
13. Shaw, A., et al., *Phospholipid phase transitions in homogeneous nanometer scale bilayer discs.* FEBS Lett., 2004. **556**(1-3): p. 260-264.
14. Nakano, M., et al., *Static and dynamic properties of phospholipid bilayer nanodiscs*, in *Journal of the American Chemistry Society* 2009. p. 8308-8312.
15. Orwick, M.C., et al., *Detergent-Free Formation and Physicochemical Characterization of Nanosized Lipid–Polymer Complexes: Lipodisq.* Angewandte Chemie International Edition, 2012. **51**(19): p. 4653-4657.
16. Rasmussen, T.E., *Application of Nanodiscs for Studies of Model Membranes Organisation and Dynamics* . in *Department of Physics and Chemistry and Department of Biochemistry and Molecular Biology.* 2010, Univestiy of Southern Denmark.
17. Yu, D., *Biophysical Studies Of Styrene-maleic Acid Copolymer Stabilised Membrane Mimentics*. 2013, University of Connecticut.
18. Jamshad, M., et al., *Surfactant-free purification of membrane proteins with intact native membrane environment.* Biochemical Society Transactions, 2011. **39**(3): p. 813.
19. Lin, Y., *Over-expression and Biophysical Characterisation of Membrane Proteins Solubilised in a Styrene Maleic Acid Polymer*, 2011, University of Birmingham.
20. Binder, H. and O. Zschörnig, *The effect of metal cations on the phase behavior and hydration characteristics of phospholipid membranes.* Chem. Phys. Lipids, 2002. **115**(1-2): p. 39-61.
21. Pandit, S.A., et al., *Molecular dynamics simulation of a dipalmitoylphosphatidylcholine bilayer with NaCl.* Biophys. J., 2003. **84**(6): p. 3743-50.
22. Cevc, G., *Membrane electrostatics.* Biochim. Biophy. Acta Biomem., 1990. **1031**(3): p. 311-382.
23. Ohki, S. and K. Arnold, *A mechanism for ion-induced lipid vesicle fusion.* Colloids Surf., B, 2000. **18**(2): p. 83-97.
24. Lee, A.G., *How lipids affect the activities of integral membrane proteins.* Biochim. Biophy. Acta Biomem., 2004. **1666**(1-2): p. 62-87.

25. Bayburt, T.H., et al., *Self-Assembly of Discoidal Phospholipid Bilayer Nanoparticles with Membrane Scaffold Proteins.* Nano Lett., 2002. **2**(8): p. 853-856.
26. Denisov, I.G., et al., *Thermotropic phase transition in soluble nanoscale lipid bilayers.* J Phys Chem B, 2005. **109**(32): p. 15580-8.
27. Gerelli, Y., et al., *Lipid Rearrangement in DSPC/DMPC Bilayers: A Neutron Reflectometry Study.* Langmuir, 2012. **28**(45): p. 15922-15928.
28. Wadsater, M., et al., *Aligning nanodiscs at the air–water interface, a neutron reflectivity study.* Langmuir, 2011. **27**: p. 15065-15073.
29. Clifton, L.A., et al., *Asymmetric phospholipid: lipopolysaccharide bilayers; a Gram-negative bacterial outer membrane mimic.* J. Royal. Soc. Interf., 2013. **10**(89).
30. Nagle, J.F. and S. Tristram-Nagle, *Structure of lipid bilayers.* Biochim. Biophys. Acta, 2000. **1469**(3): p. 159-195.
31. Tristram-Nagle, S. and J.F. Nagle, *Lipid bilayers: thermodynamics, structure, fluctuations, and interactions.* Chem. Phys. Lipids, 2004. **127**(1): p. 3-14.
32. Dowhan, W., *Molecular basis for membrane phospholipid diversity: Why are there so many lipids?*, in *Annual Review of Biochemistry*1997. p. 199-232.
33. Zhao, W., et al., *Role of phosphatidylglycerols in the stability of bacterial membranes.* Biochimie, 2008. **90**(6): p. 930-938.
34. Uran, S., et al., *Analysis of phospholipid species in human blood using normal-phase liquid chromatography coupled with electrospray ionization ion-trap tandem mass spectrometry.* J. Chromatogr. B, 2001. **758**(2): p. 265-275.
35. Lamy-Freund, M.T. and K.A. Riske, *The peculiar thermo-structural behavior of the anionic lipid DMPG.* Chem. Phys. Lipids, 2003. **122**(1–2): p. 19-32.
36. Pan, J., et al., *Molecular structures of fluid phase phosphatidylglycerol bilayers as determined by small angle neutron and X-ray scattering.* Biochim. Biophys. Acta, Biomembr., 2012. **1818**(9): p. 2135-2148.

37. Marra, J., *Direct measurement of the interaction between phosphatidylglycerol bilayers in aqueous electrolyte solutions.* Biophys J, 1986. **50**(5): p. 815-825.
38. Winther;, L.R., *The Phase Transition of DMPG and its Dependence on pH*, 2008, Niels Bohr Institute; Copenhagen University.
39. Bayburt, T.H. and S.G. Sligar, *Membrane protein assembly into Nanodiscs.* FEBS Lett., 2010. **584**(9): p. 1721-1727.
40. Bayburt, T.H., et al., *Self-Assembly of Discoidal Phospholipid Bilayer Nanoparticles with Membrane Scaffold Proteins.* Nano Lett., 2002. **2**(8): p. 853-856.
41. De Vrije, T., et al., *Phosphatidylglycerol is involved in protein translocation across Escherichia coli inner membranes.* Nature, 1988. **334**(6178): p. 173-175.
42. Nikaido, H. and M. Vaara, *Molecular basis of bacterial outer membrane permeability.* Microbiological Reviews, 1985. **49**(1): p. 1-32.
43. Shoemaker, S.D. and T. Kyle Vanderlick, *Intramembrane electrostatic interactions destabilize lipid vesicles.* Biophys J, 2002. **83**(4): p. 2007-2014.

6

6 Conclusions and Proposed Future Work

6.1 Conclusions

In the work detailed in this thesis, an in depth structural analysis of a new class of support for membrane proteins studies was undertaken in the present work. SMALPs (also known as copolymer-stabilised nanodiscs) were structurally characterised by means of small angle X-ray and neutron experiments in conjunction with DLS, TEM and Cryo-TEM experiments.

Initial analyses were focused on the already successful formulation [1]. SMALPs were assembled with a 7kDa SMA-2000P copolymer and DMPC phospholipids in a phosphate buffer solution containing a concentration of 200 mM NaCl and at a pH value kept around 8. It was found that the structures possess nanometre sizes with a diameter around 8 nm ± 2 nm and thickness of approximately of 5 nm ± 1 nm. SANS and SAXS studies revealed a strong interaction between the hydrophobic acyl chains of the phospholipids and the copolymer wrapped around the SMALPs. Experimental results suggest that the hydrophobic part of the copolymer that penetrates the nanodiscs core was found between 15 and 20mol% of the total core.

All experiments, performed with the use of freshly prepared samples, throughout three years showed coherence in the dimensions and general stability of SMALPs.

The assembly process was found to be regulated by the cooperation process between quantities of phospholipids (calculated to be approximately 140 DMPC molecules per bilayer) and the SMA copolymer.

An important part of this project was dedicated to the understanding of the role played by the copolymer belt in the size and stability of the SMALPs (Chapter 3 and Chapter 4). The architectural characteristics of the copolymer were investigated in order to understand the key factor that plays a crucial role in SMALPs formation. The analysis performed on different copolymers showed that optimal results were obtained with the use of SMA with a 2:1 styrene to maleic acid total molar ratio and a low molecular weight. SMAs with the optimal 2:1 ratio but high molecular weight (110 kDa or 63 kDa) were not suitable to form SMALPs. A less predominant presence of semi alternating units (SSM/MSS) within the copolymer architecture was found seemingly to lead the to the formation of more stable structures. The 7 kDa SMA-2000P commercial copolymer proved to give the most reproducible results together with the 6 kDa RAFT copolymer which was a perfectly alternating copolymer possessing also a small tail of only styrene (SSS).

In addition the 6kDa RAFT copolymer was found to possess the unique characteristic of entirely contribute to the SMALPs formation with no free copolymer left in solution after the assembly process takes place. This represents a great advantage from point of view of the structural analysis of the SMALPs since no further purification is needed. Consequentially there is no loss of material during the gel filtration process and a better control of the concentration and composition of the structures formed.

The second part of the project was focused on the analysis of the SMALPs behaviour when environmental conditions were changed (Chapter 3 and Chapter 5). The stability of the SMALPs samples was investigated from 5 °C up to 45 °C in preparations using either 7 kDa SMA- 2000P copolymer or the 6 kDa RAFT copolymer combined with DMPC phospholipids. A separate analysis was also performed on the copolymer solutions at the same set of temperatures via DLS and SANS/SAXS experiments.

Copolymers were analysed in phosphate buffer solution at the same pH and salt concentration used in the SMALPs formulation. Data collected revealed a good stability of structures formed in solution by the SMA alone over a broad range of temperatures (15 °C to 45 °C). This stability of the copolymers is believed to influence the stability of SMALP structures, which kept their structural dimensions over a range of different temperatures. These results are particularly important for instance in case of storage of the SMALPs encapsulated membrane proteins at low temperature (fridge) but also give the chance to analyse the membrane proteins not only at room temperature but for instance at the average body temperature of 37°C with no modification of the dimensions of the support in use.

Finally attention was focused on the SMALPs lipid components (Chapter 5). After the initial characterisation performed on samples assembled with the use of only DMPC phospholipids, SMALPs were analysed with DMPC combined with longer acyl chains (DPPC) and DMPC combined with charged heads (DMPG). Results showed that is possible to create SMALPs combining different chain length and it is also possible to insert phospholipids with negatively charged heads without affecting their structural stability.

6.2 Current Projects and Proposed Future Work

Since the introduction of the SMALPs technology in 2009, more and more research groups showed interest in the use of these supports for membrane proteins studies. SMALPs have already been proved to be able to encapsulate and maintain the structures of *Bacteriorhodopsin* (bR) and PagP proteins [1]. The group of Gulati et al. recently successfully extracted and encapsulated molecules of ABC transporters with the use of the SMALP technology [2]. Not only did they show the capability of SMALPs to extract and preserve the structural integrity of ABC transport proteins but they also demonstrated the stability with temperature from 10°C to 90°C. Also the recent work of Paulin and Jamshad [3] showed the capacity of SMA copolymer to encapsulate

membrane proteins involved in the cell division process from the membrane of the *Staphylococcus aureus*.

The work presented in this project probed the stability of the SMALPs structures over different temperatures, salt concentrations and pHs. The results obtained could be integrated with further investigations on the stability of SMALPs at freezing temperature useful for the storage of membrane proteins usually kept at temperatures around -20 °C, or to determine the stability of SMALPs towards freeze drying for long term storage of supported membrane proteins.

Concerning the SMALPs stability at different temperatures, experiments performed using SANS showed that SMALPs prepared with both polymers are stable when analysed for 4 hrs at temperatures of 15 °C, 25 °C, 35 °C and 45 °C. An interesting experiment that could be add to these set of data is reported in the thesis of Diane Yu from the Connecticut University [4]. In this project Lipodisq® structures are analysed at different temperatures with 48 hours DLS experiments in order to identify a temporal frame in which the Lipodisq® are stable as platform for membrane proteins studies at a specific temperature.

Although the models used in this study are good enough to investigate important structural parameters further modelling may be performed to better characterise the SMALPs structures. For instance the model in use to probe the possible presence of a curvature even if enabled some initial analysis being based on complicated mathematical equations is very difficult to use and needs to be implemented to give the possibility of further analyses.

Although in the present study attention was focused on the SMA copolymer preliminary experiments suggest (data not shown) that other polymers could possess the capability to assemble with phospholipids to form copolymer-stabilised nanodiscs. In particular in the group of Professor Karen Edler a new project has just started involving the use of poly(styrene-co-dimethyl propylamine) (SMI). This copolymer appears to be suitable for assembly of

SMALPs at acidic pHs covering the range between 3 and 7 which might be useful in experiments where low pH is required. Further analysis of the copolymer structure, changing the hydrophobic/hydrophilic components as well as external conditions such as pH and salt concentration of the buffer solution will contribute to the full understanding of the system and its application.

Concerning reproduction of the natural membrane protein environment, previous work has shown the complexity of this system, since cell membranes contain not only presence range of different phospholipids but also species such as cholesterol. Cholesterol plays a major role in regulating the membrane properties such as the fluidity and in modulating the membrane proteins functions [5, 6]. Future experiments should therefore explore the effects of the presence of cholesterol molecules within the SMALP core together with new combination of lipids. Experiments have also already been performed to investigate the temperature stability of the DMPC/DPPC and DMPC/DMPG compositions. Analysis of these data will contribute to complete the work on the different lipids composition presented in Chapter 5.

6.3 References

1. Knowles, T.J., et al., *Membrane Proteins Solubilized Intact in Lipid Containing Nanoparticles Bounded by Styrene Maleic Acid Copolymer.* JACS communications, 2009. **131**(22): p. 7484-7485.
2. Gulati, S., et al., *Detergent-free purification of ABC (ATP-binding-cassette) transporters.* Biochemical Journal, 2014. **461**(2): p. 269-278.
3. Paulin, S., et al., *Surfactant-free purification of membrane protein complexes from bacteria: application to the staphylococcal penicillin-binding protein complex PBP2/PBP2a.* Nanotechnology, 2014. **25**(28): p. 285101.
4. Yu, D., *Biophysical Studies Of Styrene-Maleic Acid Copolymer Stabilised Membrane Mimetics*, 2013.
5. de Meyer, F. and B. Smit, *Effect of cholesterol on the structure of a phospholipid bilayer.* Proceedings of the National Academy of Sciences, 2009. **106**(10): p. 3654-3658.
6. Brown, D.A. and E. London, *Structure and Function of Sphingolipid- and Cholesterol-rich Membrane Rafts.* Journal of Biological Chemistry, 2000. **275**(23): p. 17221-17224.

Appendices

Appendix A1

Pringle Model

The math for this model was derived by Matthew Turner and his PhD student Alex Rautu and successively used to write the model in Igor code by Andrew Jackson.

It includes a form factor of a hyperbolic paraboloid, expressed through Equation A.1 using cylindrical coordinates in which:

$z=r^2\alpha-\beta\cos 2\theta$, with $|\alpha|<|\beta|$ being the two respective curvatures. A schematic representation of the model is given in Figure A1.

$$\frac{I(q)}{I(o)} = \int_0^{2\pi} d\varphi \sin\varphi \operatorname{sinc}^2\left(\frac{qd\cos\varphi}{2}\right)\left[\left(S_0{}^2 + C_0{}^2\right) + 2\sum_{n=1}^{\infty} S_n{}^2 + C_n{}^2\right] \quad \textit{Equation A.1}$$

Where C_n and S_n are defined by :

$$C_n = \int_0^R r dr \cos(qr^2\,\alpha\cos\varphi) J_n(qr^2\beta\cos\varphi) J_{2n}(qr\,\mathrm{sen}\varphi) \quad \textit{Equation A.2}$$

$$S_n = \int_0^R r dr \sin(qr^2\,\alpha\cos\varphi) J_n(qr^2\beta\cos\varphi) J_{2n}(qr\,\mathrm{sen}\varphi) \quad \textit{Equation A.3}$$

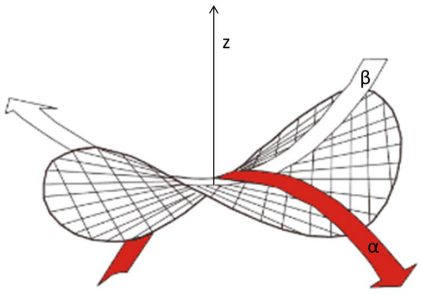

Figure A.1. Schematic representation of the saddle surface reproduced in the model.

Since this was a preliminary analysis, the structure factor was not included in the model. However fitting of the data was very difficult due to the complexity of the model, which required forcing many of the parameters in order to get

sensible fitting results. Nonetheless it was possible to obtain physically meaningful results for some of the data analysed in particular results for the SANS data 80wt% d-DMPC 20wt% d-DMPG in hydrogenated phosphate buffer solution are reported in Table A.1. However, values for the two curvature terms were both essentially zero suggesting that it is possible to approximate the system to a flat disc. Given the complexity of this model, and the high computational demands fitting to this model was also abandoned as the data could be adequately fitted to the flat disc model.

Model Parameter	*Fitting of Experimental Data*
α (rad)	0
Background (cm^{-1})	0.00862
β (rad)	0
Radius (nm)	4.3
Scale	0.012
SLD Pringle (cm^{-2})	6.63×10^{-10}
SLD Solvent (cm^{-2})	-0.57×10^{-10}
Thickness (nm)	3.1

Table A.1. Table summarising results of fitting experimental SANS data collected in D11 instrument (ILL, Grenoble) to the "Pringle model" described above.

Appendix A2

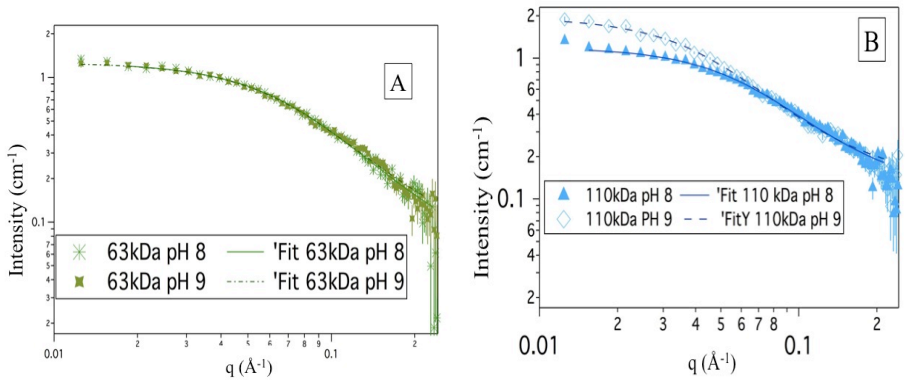

Figure A.2. SANS data of A) 63 kDa SMA in phosphate buffer solution with 200mM NaCl respectively at pH (empty green stars) 8 and 9 (filled green stars) B) 110 kDa SMA in phosphate buffer solution with 200 mM NaCl respectively at pH 8 (empty blue triangles) and pH 9 (filled blue triangles) all curves are fitted to a Debye model (continuous and dotted lines).

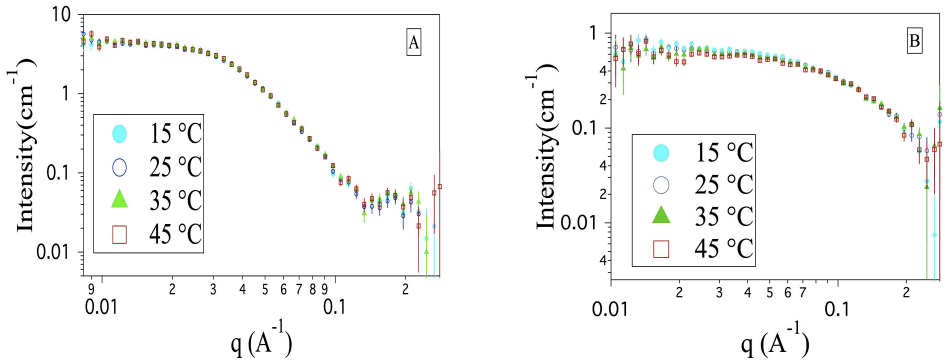

Figure A.3. SANS data of 6kDa RAFT copolymer solution (A) and 7kDa SMA-2000P copolymer solution (B) collected at different temperatures on LOQ instrument.

Appendix A3

Calibration graph derived from UV-Vis absorption measurements for a range of copolymer solution concentrations, used to determine copolymer concentration after gel filtration. The copolymer used to make the calibration graph was the commercial copolymer SMA2000P (7kDa Mw) measured using a 1cm wide cuvette. Absorbance shown is at a wavelength of 254nm Error bars were too small to be visible in the graph.

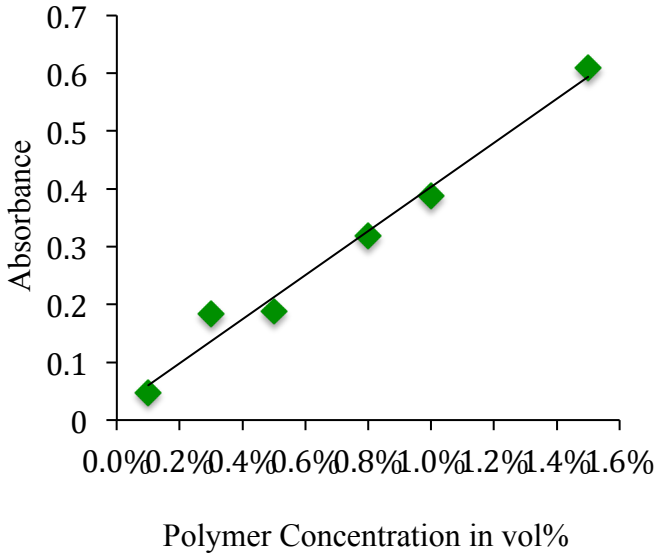

Figure A.4. Calibration curve of Absorbance of different copolymer concentrations.

Appendix A4

Lipid Composition		*SLD X-ray* (cm^{-2})	*SLD Neutrons* (cm^{-2})
100wt% h-DMPC	*tails*	9.4×10^{10}	-0.43×10^{10}
100wt% d-DMPC	*tails*	___	7.4×10^{10}
100wt% h-DMPC *100wt% d-DMPC*	*heads*	1.86×10^{10}	11.5×10^{10}
100wt% h-DPPC	*tails*	___	-0.39×10^{10}
100wt% d-DPPC	*tails*	___	7.45×10^{10}
100wt% h-DPPC *100wt% d-DPPC*	*heads*	___	1.86×10^{10}
100wt% h-DMPG	*Tails*	___	-0.45×10^{10}
100wt% d-DMPG	*Tails*	___	7.4×10^{10}
100wt% h-DMPC *100wt% d-DMPG*	*heads*	___	3.2×10^{10}
80wt% d-DMPC *20wt% d-DMPG* *80wt% d-DMPC* *20wt% h-DMPG*	*heads*	___	2.11×10^{10}
50wt% d-DMPC	*heads*	___	2.53×10^{10}

50wt% d-DMPG *50wt% d-DMPC* *50wt% h-DMPG*			
80wt% d-DMPC *20wt% d-DMPG*	*tails*	___	7.40×10^{10}
80wt% d-DMPC *20wt% h-DMPG*	*tails*	___	5.83×10^{10}
50wt% d-DMPC *50wt% d-DMPG*	*tails*	___	7.40×10^{10}
50wt% d-DMPC *50wt% h-DMPG*	*tails*	___	3.48×10^{10}
30wt% d-DPPC *70 wt% d-DMPC*	*tails*	___	7.43×10^{10}
30 wt% h-DPPC *70 wt% d-DMPC*	*tails*	___	5.07×10^{10}
50 wt% d-DPPC *50 wt% d-DMPC*	*tails*	___	7.43×10^{10}
50 wt% h-DPPC *50 wt% d-DMPC*	*tails*	___	3.51×10^{10}
70 wt% d-DPPC *30 wt% d-DMPC*	*tails*	___	7.44×10^{10}
70 wt% h-DPPC *30 wt% d-DMPC*	*tails*	___	1.95×10^{10}
All DPPC/DMPC proportions	*heads*	___	1.86×10^{10}

Table A.2. Scattering length densities of lipids used.

Buffer Composition	*SLD X-ray (cm^{-2})*	*SLD Neutrons (cm^{-2})*
0% D_2O	9.4×10^{10}	-0.57×10^{10}
32% D_2O	___	1.62×10^{10}
60% D_2O	___	3.54×10^{10}
100% D_2O	___	6.29×10^{10}

Table A.3. Scattering length densities of the different buffer contrasts used.

Copolymer	*SLD X-ray (cm^{-2})*	*SLD Neutrons (cm^{-2})*
6 kDa RAFT	10.9×10^{10}	1.89×10^{10}
6 kDa RAFT Deuterated	___	5.27×10^{10}
7 kDa SMA-2000P	10.7×10^{10}	1.81×10^{10}

11 kDa	10.5×10^{10}	1.78×10^{10}
33 kDa	10.9×10^{10}	1.58×10^{10}
63 kDa	10.7×10^{10}	1.81×10^{10}
110 kDa	10.7×10^{10}	1.81×10^{10}

Table A.4.Scattering length densities of the copolymers used.